Nancy-Université
Université Henri Poincaré

AVERTISSEMENT

Ce document est le fruit d'un long travail approuvé par le jury de soutenance et mis à disposition de l'ensemble de la communauté universitaire élargie.

Il est soumis à la propriété intellectuelle de l'auteur. Ceci implique une obligation de citation et de référencement lors de l'utilisation de ce document.

D'autre part, toute contrefaçon, plagiat, reproduction illicite encourt une poursuite pénale.

➢ Contact SCD Nancy 1 : theses.sciences@scd.uhp-nancy.fr

LIENS

Code de la Propriété Intellectuelle. articles L 122. 4
Code de la Propriété Intellectuelle. articles L 335.2- L 335.10
http://www.cfcopies.com/V2/leg/leg_droi.php
http://www.culture.gouv.fr/culture/infos-pratiques/droits/protection.htm

Ecole Doctorale RP2E
Ressources, Produits, Procédés et Environnement

Thèse
présentée pour l'obtention du titre de

Docteur de l'Université Henri Poincaré
en Géosciences

par
Léonid SEROV

Métallogenèse de l'uranium dans la région de Litsa (Péninsule de Kola, Russie)

Soutenance publique le 24 juin 2011

Membres du jury:

Président	: **Olivier VANDERHAEGHE,** *Professeur, G2R-CREGU, Nancy*
Rapporteurs	: **Tapani RÄMÖ,** *Professeur, Université d'Helsinki* **Didier BEZIAT,** *Professeur, Université de Toulouse*
Directeurs de thèse	: **Michel CUNEY,** *Directeur de Recherche CNRS, G2R–CREGU, Nancy* : **Anne-Sylvie ANDRE-MAYER,** *Maître de conférences-HDR,G2R-CREGU, Nancy*
Examinateur	: **Laurent BAILLY**, *Ingénieur de recherche, BRGM, Orléans*
Invités	: **Marc BROUAND,** *Ingénieur, AREVA NC – BG Mines* **Elena AFANASIEVA,** *Ingénieur, VSEGEI, St Petersbourg, Russie* **Yury MIRONOV,** *Head of the Department of uranium geology and radioecology, VSEGEI, St-Petersbourg, Russie*

ACKNOWLEDGEMENTS

This thesis was financed by AREVA NC and carried out partly in G2R laboratory of the «University of Henri Poincaré» (UHP - Nancy, France) and partly in Uranium deposits department of «A.P. Karpinsky All Russia Geological Research Institute» (VSEGEI – Russia, St-Petersburg).

There are quite a few persons, who participated, supported and significantly contributed to this project, which I would like to thank.

Michel CUNEY, my director of the thesis, for inspiration, sharing experience and guidance. **Anne-Sylvie ANDRE-MAYER**, my co-director of the thesis, for her comprehensive contribution, encouragement and patience.

Tapani RÄMÖ and Didier BEZIAT, reviewers of my thesis, for the honor of examining this research.

AREVA NC:

Claude CAILLAT - for invitation over this project and his concern of it. **Philippe KISTER** and **Patrick LEDRU** - for participating the field trips and valuable directions. **Jean-Pierre MILESI** and **Marc BROUAND** - for considerable assistance and useful advices.

G2Riens et Cregusiens:

Michel CATHELINEAU - for his cordiality and support. **Pierre SCHUMACHER** - for his infinite favour and improving my French. **Olivier VANDERHAEGHE** - for numerous tutorials with valuable instructions. **Julien MERCADIER** - for his significant contribution and reliability. **Askar MUNARA** and **Rakhim UTEYEV**, my favourite Kazakhs, for being near.

Marc LESPINASSE, **Bernard POTY**, **Marie-Christine BOIRON, Judith SAUSSE**, **Cedric DEMEURIE**, **Cedric CARPENTIER**, **Jerome STERPENICH**, **Isabelle DUHAMEL**, **Jeremy NETO**, **Laurent RICHARD, Oliviers: CARDON**, **PIERRON**, **BELCOURT**, **Jessica BONHOURE**, **Sandrine CINELU**, **Alham IBRAHIM**, **Ambrose KIPROP**, **Isseini MOUSSA**, **Wilfried TOE**, **Philippe LACH**, **Vincent GIRARD**, **Stephane RENARD**, **Stephanie FLEURANCE**, **Karine PISTRE**, **Apolline LEFORT** – for various sorts of help and sympathy.

Christine LEONARD, **Patrick LAGRANGE**, **Marie-Odile CAMPADIEU** and **Laurence MOINE** – for administrative assistance and amiability.

CRPG-CNRS:

Etienne DELOULE, **Michel CHAMPENOIS** and **Denis MANGIN** – for implementation of geochronological studies and affability.

VSEGEI:

Yury MIRONOV – for disciplinary arrangements and strategic advices. **Elena AFANASIEVA** and **Aleksandr LIPNER** – for the whole Kola Peninsula experience and support. **Vladimir LOBAEV** – for introduction to PhD, Frnace and Nancy life.

Vitaly MIKHAILOV, **Vladimir FUKS**, **Vladimir CHERNOV**, **Aleksey PUGOVKIN**, **Igor MAL'KOV**, **Aleksandr LODYGIN**, **Svyatoslav ENGALYCHEV**, **Elena SMIRNOVA** and others – for various usefull assistance and affinity.

Besides I would like to thank **Vyacheslav GOLUBEV** and **Aleksandr EMETZ**, CREGU collaborators, for valuable advices. And **Aleksandr SHURILOV**, whose thesis I consider to be the master example of research and which I tried to follow.

Finally I want to thank **my family** and **my friends**, for their belief and patience.

And most of all **DINA**, my «fulcrum» wife, for her thorough devotion, faith and love.

Merci beaucoup !

ABSTRACT

The Litsa district is one of the most interesting areas of the Kola Peninsula with respect to uranium metallogenesis. Presenting all the features of uraniferous province, it endured a protracted geological history with several successive uranium enrichments. There are over 30 uranium occurrences and manifestations, totally estimated at 102,000 tons in Speculative Resources (IAEA nomenclature), with an average grade of Uranium 0.01%. They occur at different stratigraphic levels of the geological succession in the district: Archean, Paleoproterozoic, Mesoproterozoic and Paleozoic. Uranium content in the geological formations gradually increases during the geological evolution of the Litsa district from Archean to Paleozoic. The most abundant and probably prospective for the economic-grade uranium mineralization is Paleozoic pitchblende vein type, located around the Litsa-Araguba granitoid complex, where favorable protoliths, structures and epigenetic processes are encountered.

Key words: Uranium, Litsa district, Kola Peninsula, Occurrences, Metallogenesis.

RESUME

L'objectif de la thèse de Léonid Sérov est de caractériser les conditions de genèse des différents types de minéralisations uranifères observées dans la région de Litsa-Araguba en spécifiant les impacts relatifs des processus magmatiques et hydrothermaux sur les enrichissements en uranium successifs observés depuis l'Archéen jusqu'au Calédonien dans le socle ou dans les granitoïdes.

Les travaux géologiques de terrain (structurales, géophysiques, etc…) couplés à des études pétrographiques, géochimiques et géochronologiques ont permis de mettre en évidence trois grands groupes de minéralisations.

- **Les minéralisations archéennes** (2,75-2,65 Ma) à uranium, thorium et REE sont associées à des **pegmatoïdes archéennes** résultant de la fusion partielle d'un socle préexistant. L'anomalie de Dikoe est associée à un enrichissement en muscovite conséquent alors que l'anomalie de Skalnoe est caractérisée par des signatures pétrographiques et géochimiques similaires à celles des anomalies paléoprotérozoïques. Les datations U/Pb sur uraninite donnent des pages de 1825±20 et 1827±98 Ma, plus jeunes que celles attendues, ce qui semble être à relier à des processus magmatiques et métamorphiques plus récents. Les âges obtenus sur les roches encaissants (U/Pb sur zircons) donnent des âges de 2465±130 Ma pour les cœurs de zircons et de 2115±56 Ma pour les bordures.
- **Les minéralisations paléoprotérozoïques** (2.2-2.1 Ga) sont concentrées dans des **veines de granites pegmatoïdiques encaissées dans des gneiss**. Les études pétrographiques et géochimiques traduisent des phénomènes d'albitisation et de dequartzification. Les âges obtenus sur l'anomalie de Namvara (U/Pb) sur uraninite sont de 2185±81 Ma, en accord avec les hypothèses paléoprotérozoïques.
- **Les minéralisations uranifères** de type Litsvskoe **sont polyphasées :**

o La phase d'enrichissement la plus ancienne (1.75-1.65 Ga) sous forme d'uraninite est à associé à des processus de migmatisation de métasédiments riche en aluminium.

o Des minéralisations disséminées associées à des dykes mafiques s'exprime sous forme de brannérite et de minéraux riches en uranium et REE, datée par Rb-Sr à 1 Ga.

o La minéralisation la plus importante et la plus récente est Paléozoïque, datée par U/Pb sur pechblende à 455±6 Ma. Elle est à relier à des processus hydrothermaux.

Mots clefs : Uranium, District de Litsa, Péninsule de Kola, métallogénie

CONTENT

Figure captions

PART 1.

PART 2.

PART 3.

Table captions

GENERAL INTRODUCTION

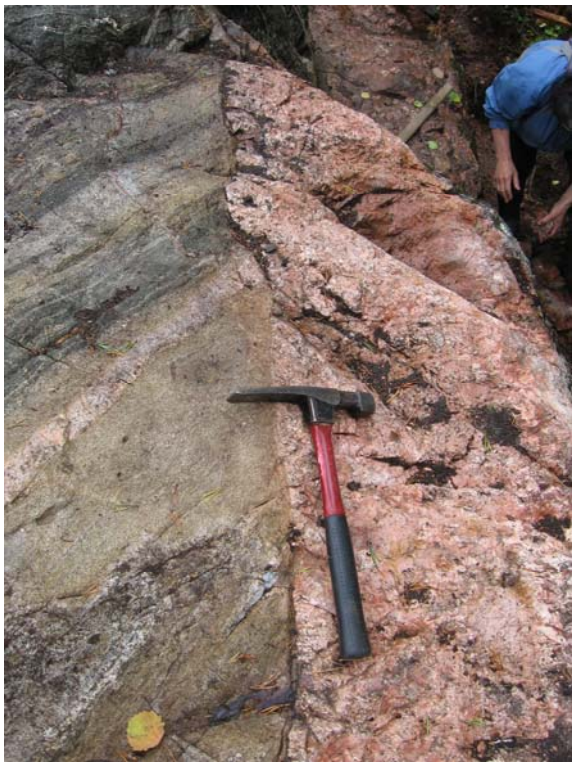

The aim and the main objectives of the study

The principle aim of this thesis is to characterize the conditions of uranium metallogenesis within the Litsa district with a special emphasis on the processes (magmatic and epigenetic) responsible of uranium enrichment, tectonic units controlling its localization, and relations between these circumstances and geological evolution of the area, and thus, defining exploration criteria for the discovery of uranium deposits in this and similar areas.

The major objectives are to study lithogeochemical, mineralogical, structural, geochronologic and other characteristics of the different types of uranium mineralization within the Litsa district in order to answer the specific questions:

- What are the petrogeochemical and mineralogical characteristics of the Archean-Paleoproterozoic basement formations hosting the uranium mineralization?
- What are the petrogeochemical and mineralogical characteristics of the granitoids which intrude the basement? What is their potentiality to represent a uranium source?
- What is the type of the different alterations which affect the basement formations and the Litsa-Araguba granitoids? What are their origins and their possible role in the genesis of the uranium mineralization?
- What are the temporal relations between basement rocks, granitoids intruding this basement, alterations, sedimentary cover and the various types of mineralization observed in this area?
- Is there any relation between the Mesoproterozoic sedimentary formation and the uranium mineralization of the district?
- What are the main processes (magmatic and/or epigenetic) leading to such uranium enrichment observed in the district?

Above mentioned objectives and comparison with other uraniferous provinces allow to establish the genetic model for uranium abundance within the Litsa district.

Methodology

The present research was carried out in G2R laboratory of the «University of Henri Poincaré» (UHP - Nancy, France) and uranium deposits department of «A.P. Karpinsky All Russia Geological Research Institute» (VSEGEI – Russia, St-Petersburg). The following activities were accomplished:

- Bibliographic studies of the published and archive data;
- Field works in the Litsa district;
- Geochemical analyses of the samples;
- Petrographical and mineralogical studies;
- Isotopic geochronological analyses;
- Interpretation and statistic analyses of the satellite images;
- Writing and design of the manuscript;

Bibliographic studies

Geological aspects of the Kola Peninsula are sufficiently studied by many researchers, generally due to the presence of exceptional geological conditions and economic valuable (up to unique) deposits and within this area. Among them the studies of *Scheglov* (1993) and *Glebovitsky* (2005) should be mentioned. They highlight the principle stages of geological evolution, especially in terms of the continental riftogenesis and relevant magmatism, and were considerably used in this thesis.

The neighborhood of the Litsa district with the Pechenga Ni ore region causes the existence of numerous data, obtained since the first third of the 20th century. The special uranium investigations here were provided since 1950-s, mainly by *«Nevskgeologia»* forces, including airborne and ground geophysical surveys, drilling and trenching. These data are mostly unpublished and presented only in archives, it was under top-secret stamp until recently. Also because of the long storage and disturbance of the 1990-s the primary information, especially the drill-core, is lost. The main open publication devoted to uranium occurrences of the Litsa district belongs to *Savitskii et al*. (1995). The description of Mesoproterozoic sediments and uranium manifestations within them was disclosed by *Negrutza et al*. (1994). These publications, as well as accessible archive data of *«Nevskgeologia»*, were also decidedly helpful for this thesis.

Besides above mentioned publications the data of AREVA NC and *«Novaya Lekhta»* collaboration was used, particularly the geophysical maps and satellite images.

Field works

Three field trips were accomplished in the framework of this research in 2006, 2007 and 2008. They were organized and provided by uranium deposits department of VSEGEI under the guidance of A. Lipner and E. Afanasieva. The director and co-director of this thesis (M. CUNEY and A.-S. ANDRE-MAYER) and also AREVA NC specialists (C. CAILLAT, P. KISTER and P. LEDRU) participated and significantly contributed to these works. Most of the uranium objects were visited and sampled, besides the representative outcrops of the Litsa-Araguba granitoids and Sredny-Rybachy sedimentary basin were studied.

The materials and data obtained during field works (structural observations, mapping, photographing and sampling) present the major part of this thesis, mainly in Part 2, devoted to the description of the uranium occurrences.

Analytical studies

The complex of various analyses for the samples from the Litsa district was provided during this research.

Geochemical composition of the host rocks was studied using ICP-AES&MS in CRPG-CNRS and VSEGEI laboratories (the analytical procedure and the standarts used are described in *Carignan et al., 2001)* and statistically processed using *Lithogeochemistry 1.0 beta* and *Microsoft Excel 2003*. ICP-MS was also used to determine the REE distribution in uranium oxides.

Petrographical studies of the samples were carried out by optic observations (transmitted and reflected light) using *Polam P312, Leica DM 2500 P and Olympus BX51* and other microscopes, the images were taken by integrated digital cameras and edited with *Adobe Photoshop CS* and *COREL DRAW X3.*

Chemical composition of uranium and accessory minerals were studied using scanning electronic microscope (SEM) *Hitachi FEG S-4800* (UHP – Nancy, France) and microprobes (EMP): *CAMECA SX 100* (UHP – Nancy, France), *CamScan MV 2300* (VSEGEI – St-Petersburg, Russia). The back scattered electron microscopic images (BSEM) were taken using these devices also.

U-Pb isotopic composition of the uranium oxides and zircons was measured by Secondary Ion Mass Spectrometry (SIMS) using *CAMECA IMS-3F, IMS 1270* (CRPG-CNRS – Nancy, France) and *SHRIMP-II* (VSEGEI – St-Petersburg, Russia), the Concordia diagrams were built using *ISOPLOT* software (Ludwig, 1999).

Design of the manuscript

The text of the manuscript was written with *Microsoft Word 2003* and compiled with *Adobe Acrobat Professional 7.0*. All figures of the thesis (performed using the published and archive materials and the data, obtained during present research) were designed using *Mapinfo 8.0 SCP*, *Adobe Photoshop CS* and *COREL DRAW X3* softwares. Tables and some diagrams were compiled using *Microsoft Excel 2003*.

Terminological aspects

Some aspect concerning the terminological differences between Russian (Soviet) and Western geological schools should be emphasized.

The first aspect concerns geochronological scale, which is not similar in Russian and Western geological literature and in particularly the subdivision of Archean and Proterozoic, the presence of local (for the eastern part of the Fennoscandian shield) stratigraphic units and contradictions between the traditional scheme and newly obtained isotopic constraints. The general chronostratigraphic scale with time limits and correlation between Russian and International stratigraphic units is presented in Table 1.

Tableau 0.1. General chronostratigraphic scale of Precambrian (correlated with the International) (*after Glebovitsky and Shemyakin; 1996, Mitrofanov and Negrutza; 2002*)

Acrothemne	Eontheme	Eratheme/System	Local subdivision	Limits, Ma	International unit
PROTEROZOIC PR	Upper PR_2	*Vendian* V	Upper *V_2*	620±50	Neoproterozoic
			Lower *V_1*	650±50	
		Riphean R	Upper *R_3*	1000±50	
			Middle *R_2*	1350±50	Mesoproterozoic
			Lower *R_1*	1650±50	
	Lower PR_1 (*Karelian*, K)	Upper K_2	*Vepsian Vp*	1800	Paleoproterozoic
			Kalevian Kl	1920	
			Ludicovian Ld	2100	
		Lower K_1	*Jatulian Jt*	2300	
			Sariolian Sr	2400	
			Sumian Sm	2500	
ARCHEAN AR	Upper AR_2 (*Lopian*, L)	Upper L_3		2800	Neoarchean
		Middle L_2		3000	Mesoarchean
		Lower L_1		3200	
	Lower AR_1 (*Saamian*, S)			3600	Paleoarchean

The second aspect is connected with classification of the occurrences by uranium content, since the majority of the uranium occurrences in the Litsa district are not sufficiently studied for Identified Resource evaluation including Reasonably Assured Resources according the IAEA classification system. The grade of the occurrences in better case can be estimated in Inferred (Speculative) Resources only. Thus, the information is sometimes controversial and the same occurrences are ranged as ore-showing or as deposits in different reports.

In present thesis the following classification of uranium occurrences is used:

Anomaly – mineralized spot of small size (few meters) with uranium content below 300 ppm.

Ore-showing – extended U-mineralized zone with average uranium content over 300 ppm and evaluated or presumed resource less 5000 t.

Deposit – evaluated occurrence with resource over 5000 t for 300 ppm uranium cross-cut.

Also different units are used for radiometric measurements. In Russia the most common is micro-Roentgen per hour (μR/h) measured by radiometer, while in France - counts per second (cps) by scintillometer. The direct correlation between Roentgen en cps is not so easy. IAEA indicate a correlation between Roentgen en the content of K, U and Th at 1m from the ground: 1% K = 1.505 μR/h, 1 ppm U = 0.653 μR/h, 1 ppm Th = 0.287 μR/h.

The both devices were used during the field trips provided in the framework of this thesis with the prevalence of radiometer. μR/h units are also common for archive data and reports.

Besides, there are different approaches to the origin of uranium enriched granitoid formations in the granite-gneiss domes. Either intrusive emplacement, or in-situ partial melting, or high-temperature metasomatosis can been proposed. In such cases the neutral terminology is used as much as possible in the present thesis.

And finally there are some linguistic problems caused by translation and transliteration of the names from Cyrillic to Latin alphabet. They mainly concern toponyms, which give the names to geological units and occurrences. Often coming from aboriginal languages (Saamian, Karelian etc.) these names can be transliterated differently and this often occurred in various publications. Nevertheless in this thesis the most common variants are used, translated using the appropriate linguistic rules.

Structure of the manuscript

The manuscript of the thesis consists of present general introduction, three parts, and general conclusion. Each part starts with its own introduction, contains several paragraphs with necessary illustrations (figures and tables) and finishes with conclusions.

Part 1 is devoted to general review of the studied area. The information, concerning its geographical and administrative location is given in the beginning. The position of the Litsa district in regional geotectonic environment and the description of main tectonic units are disclosed in the first paragraph. The second paragraph reveals metallogenic potential of the district, while the third one presents metallogenic preconditions and features of the uranium mineralization.

Part 2 describes the geological settings, the field observations for each uranium occurrence and brings re-interpreted ore-showing maps of the uranium occurrences of the Litsa district.

Part 3 focus on the petrogeochemical, mineralogical and geochemical characteristics and brings geochronological constraints on the uranium occurrences.

Part 4 considers the principle stages of geological evolution of the district and relevant uranium enrichment processes. The genetic model of the occurrences within the Litsa district is established there.

General conclusion summarizes the main results of the studies and mentions unsolved problems, proposing additional investigations.

PART 1.

REGIONAL GEOLOGICAL REVIEW AND METALLOGENIC POTENTIAL OF THE LITSA DISTRICT

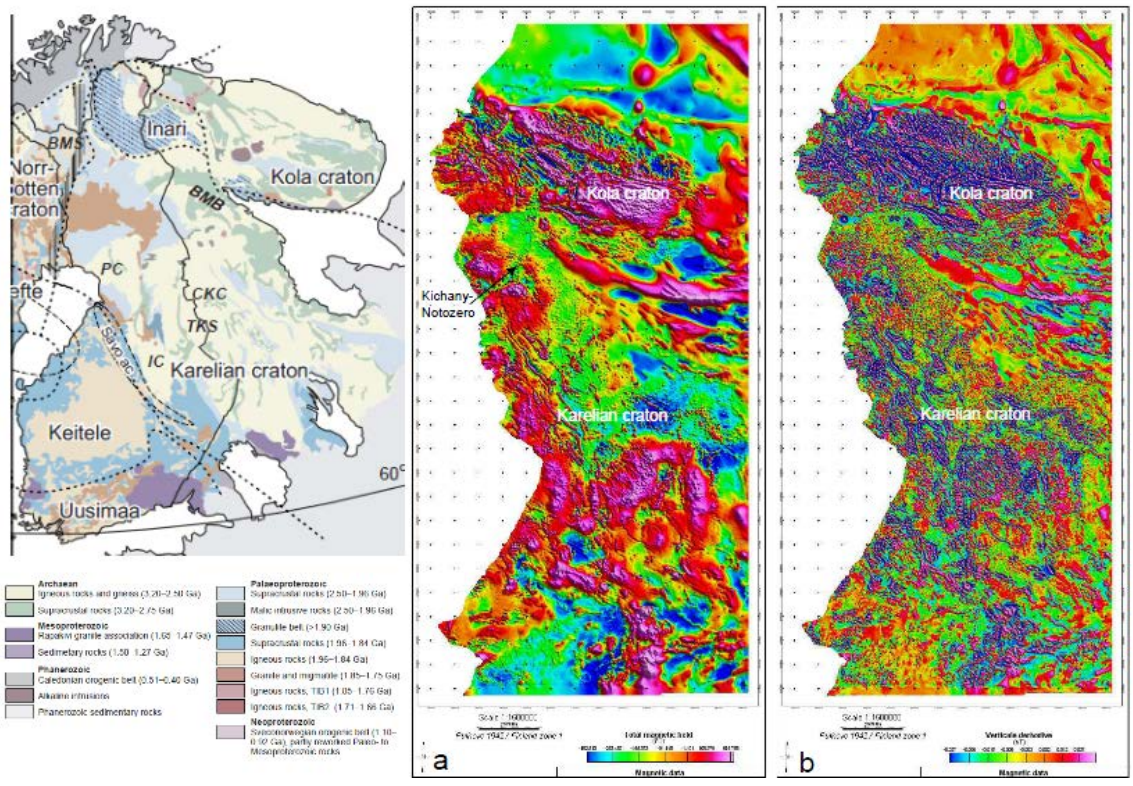

Introduction

The Litsa district is situated on the north-west of the Kola Peninsula, close to the state border with Norway and Finland. The administrative center of the region – Murmansk (population 300 000) is about 60 km to the east, besides there are two medium towns (Zapolyarny and Pechenga) and several small settlements within the area, mainly of a mining and military purpose. Zapolyarny (population 17 000) is a satellite town for Pechenga-Nikel' mining complex (the filial of the Noril'sk Nickel' enterprise) and is connected with Murmansk by a highway and a single track railroad.

Geographically the district includes the basins of Pechenga, Titovka, Zapadnaya Litsa and Ura rivers. The «Litsa» is a common toponym for several objects in the area. The climate is subarctic, softened by Gulfstream current. The average summer temperature is +9 – +14ºC, in winter -9 – -14ºC. Besides there are polar days and nights in summer and winter respectively. The relief is undulating (hills up to 400 m), the landscape is presented by tundra, forest and swamp, pergelisol is absent. The territory is irregularly and rather poorly outcropped for about 2% (Figure 1.1).

Over 30 uranium occurrences and manifestations were discovered within the Litsa district; they will be described in part 2 of the thesis. And this part is devoted to the general geological review (geotectonic position, characteristics of the main tectonic units) and metallogenic potential (description of metallogenic preconditions and features) of the studied area. The certain geological, petrogeochemical and mineralogical features, concerning the uranium occurrences, will be given in the part 2 and 3 as well.

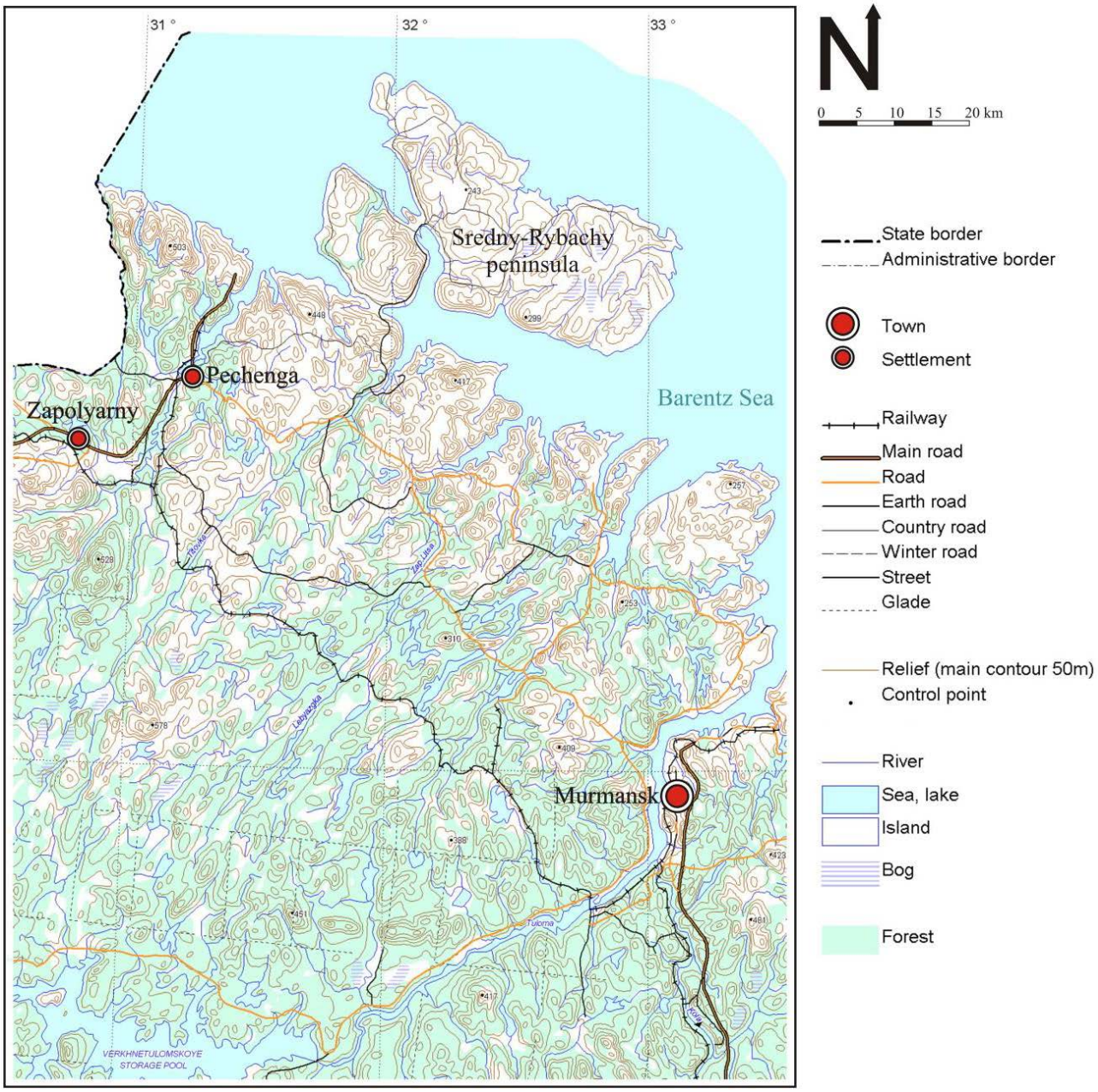

Figure 1.1. Topographical map of the Litsa district (after published topographical maps).

1.1. Geotectonic position of the Litsa district

Geotectonicaly the Litsa district belongs to the North-Eastern part of the Fennoscandian shield, which represents the oldest Earth crust and had endured the complex geological evolution from Archean to Late Paleozoic. The evolution of the Fennoscandian shield is defined by progressive cratonization with multiple riftogenic events, brought to the destruction, transformation and complication of the Earth crust. The major feature of the Fennoscandian shield's structure is its zoning, which appears the "rejuvenation" of the geological formations and riftogenic events in north-east – south-west direction *(Scheglov, 1993)*. The present erosive level shows the following sequence of principal tectonic units, distinguished by the composition, structure and the character of geological evolution (from NE to SW):

- Archean-Early Proterozoic Kola-Karelian domain (megablock);
- Early Proterozoic Svecofennian domain (megablock);
- Late Proterozoic Goth-Dalslandian domain (megablock);

On the west the Fennoscandian shield is framed by Norway Caledonian domain, which is considered to be a huge thrust upon Pre-Cambrian basement, and the Pre-Cambrian prominences among Caledonides - to be a tectonic windows in overlapping Caledonian allochton (Figure 1.2).

Between Kola-Karelian and Svecofennian domains there is Raahe-Ladoga zone, which is reliably distinguished on the territory of Finland as a structure between Archean and Proterozoic crust. In comparison with Svecofennian domain, which is relatively homogeneous, the Kola-Karelian is divided into several provinces: Kola, Belomorian and Karelian. They display differences and are usually described separately.

The Litsa district is located in the North-Western part of Kola province, characterized by complex mosaic-block constitution. By geological and geophysical data the certain elements of this province are singled out. These are the Central-Kola, Murmansk and Inari blocks of mainly granite-gneiss composition and extended Voron'ya-Kolomozersk supracrustal greenstone belt, separating the first two blocks. Besides, there is Pechenga riftogenic structure, which is a North-Western part of Pechenga-Varzuga riftogenic belt, crosscutting the whole Kola province in SE-NW direction (Figure 1.2).

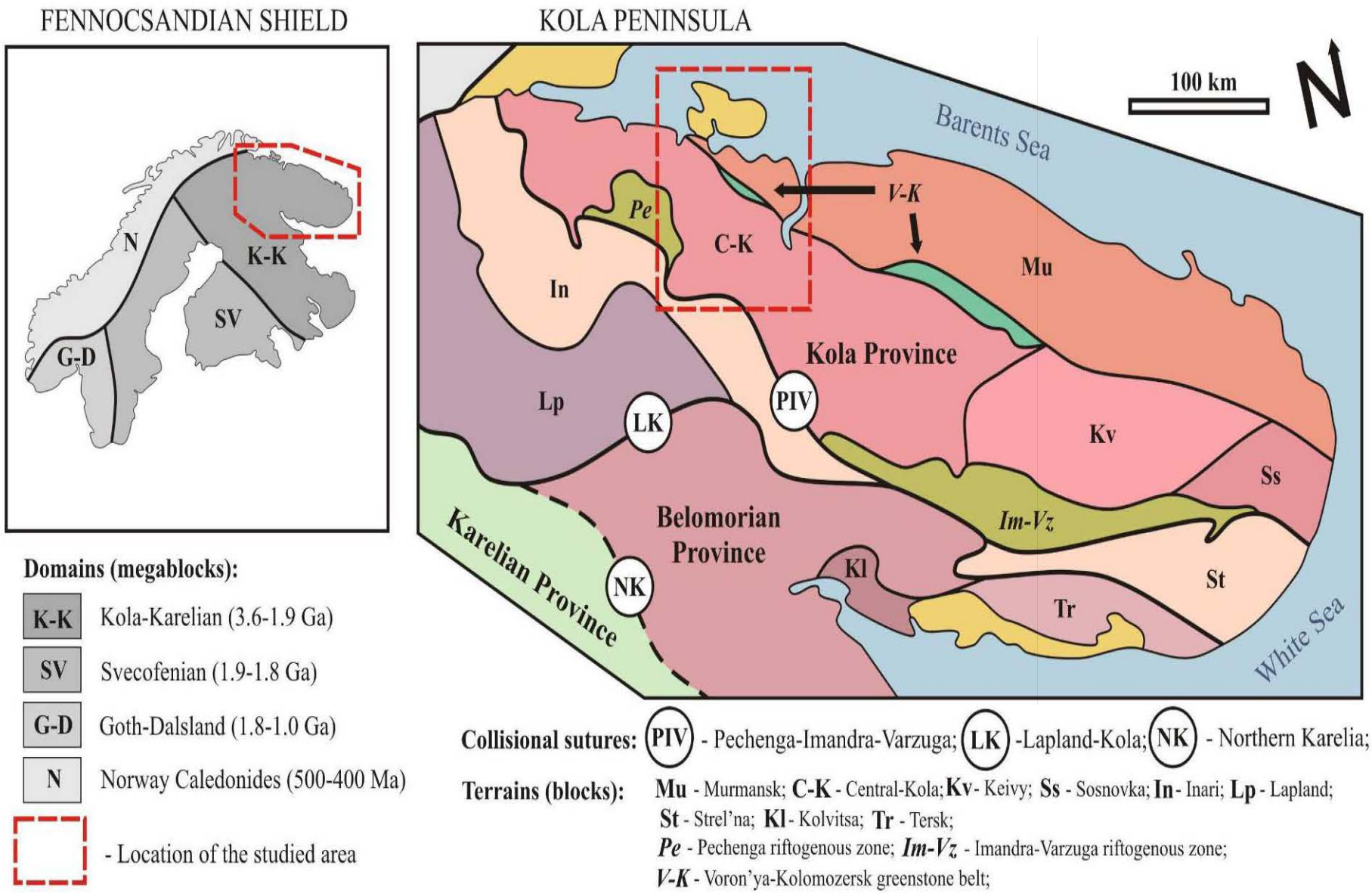

Figure 1.2. Geotectonic position of the Litsa district *(after Scheglov, 1999; Balagansky, 2001 and Glebovitsky, 2005).*

Also there are two transverse superimposed tectonic zones: Barents Sea and Litsa-Araguba, distinguished in the area (Figure 1.4)

1.1.1. Central-Kola block

In this block the Archean complexes are presented by repeatedly and dissimilarly (from high temperature amphibolite to granulite facies) metamorphosed paragneiss and crystalline schist of the Kola series and also orthometamorphic rocks of various composition: TTG and granite-gneiss formations, which are identified as a primary continental crust *(Vetrin; 1984)*. All of them occur in united geological structures and are jointly migmatized and deformed, which makes difficult the study of their interrelations. Meanwhile the second ones are considered to be the basement for the first ones.

The Kola series can be divided into two suites, by their bedding in the anticline folds and the drilling data. The Lower suite is presented by homogenous biotite and pyroxene gneiss (probably metamorphosed volcanic andesite-dacite rocks) and the Upper suite – by biotite-garnet-sillimanite gneiss with interlayers of ferrigenous quartzite and high aluminous schist. The section of the Kola Superdeep Borehole (SD-3 - Figure 1.4) reveals that the Kola series are developed from the depth of 6,842 km to 12,262 km with five sedimentary megarhythms in its consequence. The ground geophysical surveys in the region determined the seismic border (the passage from high to low velocity medium) on the interval of 12-18 km, which can be considered as a bed of the Kola series stratum. Thus, its total thickness on the level of contemporary erosion is not less than 6 km *(Glebovitsky, 2005)*.

The isotopic dating of these rocks (in the section of SD-3) indicates their crystallization in the interval of 2933-2832 Ma (Table 1.1).

Nowadays several cycles of deformation and metamorphism are distinguished within Central-Kola terrain *(Dobrzhinetskaya; 1978)*. The early cycle is synchronous with granulite facies metamorphism of moderate pressure and accompanied by two stages of folding. The late – by five stages of folding, during which the major regional isoclinic folds of north-western strike were developed. These deformations were attended by secondary metamorphism from granulite to amphibolite facies. On the whole the degree of metamorphism of the district is increasing from north-east to south-west, with temperature variation from 650 ºC to 800ºC and pressure – from 4-5 to 6-7 kbar *(Dobrzhinetskaya; 1978)*.

1.1.2. Murmansk block

Murmansk block is extended from the White Sea to the Sredny-Rybachy peninsula for 600 km with the width of 60-70 km, blowing out in north-western direction (Figure 1.2). Its southern border is presented by a system of deep faults, which had been traced by geophysical data to the depth of 35-40 km, dipping to N-E. On the north it is bounded by «Karpinsky» fault in the aquatory of the Barents Sea.

The block is built up with TTG, granite-gneiss, plagiogranite and migmatite formations. Also the relicts of supracrustal formations, presented by cristalline schist, biotite-amphibole gneiss and amphibolite, are marked and could be confronted with the volcanic-sedimentary rocks of Vorn'ya- Kolomozero greenstone belt. All these formations are metamorphosed all over the extent of the block in the high temperature amphibolite facies. The age of the migmatite-granite complex is estimated by Sm-Nd method as 2.68-2.94 Ga *(Timmerman and Daly; 1995)* and by U-Pb method (with zircons from different generations) as 2.85 Ga *(Puchkarev et al.; 1979)*. The last number is interpreted as an age of metamorphism and migmatization.

The typical feature of this tectonic unit is combination of circular and semi-circular lineaments, which can be interpreted as thrusts. The linear schistosity traces the displacement zones, along which the Murmansk block formations thrust upon the Voron'ya-Kolomozero zone *(Glebovitsky; 2005)*.

1.1.3. Inari block

This block borders upon the Central-Kola block with a system of thrusts (Figure 1.4) and is built up with granite-gneiss, amphibole, biotite gneiss and migmatite of undifferentiated Kola-Belomorian complex. This terrain doesn't play any significant role in the uranium metallogeny of the district.

1.1.4. Voron'ya-Kolomozero zone

This sutural structure results of the thrusting of the Murmansk block over the Central-Kola block with a major north-western strike and north-east dip (Figures 1.2 Figure 1.2. **Geotectonic position of the Litsa district** ***(after Scheglov, 1999; Balagansky, 2001 and Glebovitsky, 2005).***and 1.4). According to the seismic and gravimetric data, this zone is traced to a depth of 35-40 km and reaches Moho surface. It has a thickness about 10-15 km. The gravimetric and magnetometric fields in this structure are characterized by a sequence of local linear ΔT and

Δg maximum and minimum (Figure 1.8 and Figure 1.9) which are caused by basic intrusions and areas of the pegmatoidic granite and quartz-feldpathic metasomatite respectively. Some researchers consider this greenstone belt to be a protorift structure *(Savitskii et al.; 1995)*.

The most complete sequence of volcanic-sedimentary formations can be observed in the Polomo-Porosozero structure far to the east of the Kola Peninsula from the Litsa district. And within the studied area this greenstone belt is presented by its fragment - Uraguba structure.

Here the sedimentary stratum is presented by basal conglomerate and metamorphosed turbidite, the volcanic rocks – by sequence of komatiite, tholeite and andesite-dacite. The pyroxene komatiite formations compose most part of the section, they form consistent layers with a thickness of 60-200 m and are presented by coarse, fine and irregular grained amphibolite. The intense deformation of these rocks leads to total disappearance of the primary texture.

The supracrustal complex of Voron'ya-Kolomozero belt is metamorphosed in the high temperature grade of amphibolite facies. It has been sufficiently studied geochronologically (Table 1.1.1) to confront the geological events with the time scale (Glebovitsky; 2005):

2.92-2.87 Ga – komatiite-tholeitic volcanism;

2.87-2.88 Ga – basalt-andesite-dacite volcanism;

2.88-2.79 Ga – sedimentation;

2.7-2.65 Ga – late kinematic intrusions, metamorphism of amphibolite facies, REE pegmatite formation;

Thus, the duration of the Voron'ya-Kolomozero belt development was about 200-250 Ma.

1.1.5. Pechenga zone

Pechenga zone is a north-eastern sequel of the regional Pechenga-Imandra-Varzuga riftogenous belt (Figure 1.2). It is nearly isometric: 70 x 45 km, and has asymmetric internal structure. The presence of volcanic rocks and dykes to the north indicates that the dimension of this structure was much bigger. In its southern frame, there are fragments of Archean greenstone belt, which means, that the rift inherited this linear structure *(Scheglov; 1993)*.

The northern boundary is stratigraphic with basal conglomerates or overlaying volcanic rocks, and the southern – with granitic domes of Proterozoic age. The thickness of the zone increase from north to south and in this direction increases also the grade of metamorphism.

The deep structure and stratigraphy of the Pechenga zone was studied by many researchers, due to its exceptional role in non-radioactive metallogeny of the Kola Peninsula. The world famous Cu, Ni and PGE bearing intrusions with an age of 1.85 Ga are located within the section of this zone, where over six rhythms of volcanic and synchronous intrusive magmatism, separated by periods of terrigenous or carbonate sedimentation, were distinguished *(Gelbovitsky; 2005)*. According to geochronological data, the total term of Pechenga structure formation is over 650 Ma. It starts with the stratified basic intrusions of an age of 2505-2490 Ma *(Vetrin; 2000)*, than their erosion and burial with terrigenous formations. The approximate (Rb-Sr bulk) age of the final acid volcanism is in the period of 1.85-1.76 Ga *(Balashov; 1996)*.

The orogenic stage of the Pechenga rift development was attended by penetration of the Litsa-Araguba complex intrusions along north-eastern deep faults, which play an exceptional role in the localization of the most uranium occurrences of the district.

1.1.6. Litsa-Araguba granitoid complex

The intrusions of this complex are traced from south-west to north-east within deep faults of the same strike, fixing Litsa-Araguba regional tectonic zone (Figure 1.2). They occur as 6 individual plutonic bodies (Litsa, Lebyazhka, Nyaljavr, Portlubol, Uraguba and Araguba), extending over 80 km along this zone. This granitoidic plutons, dated at 1762±9 Ma (Svecofennian) (Savitskii et al., 1995) inherited the granite-gneiss domes of the suggested Late Archean – Paleoproterozoic age. They migmatize the hosting gneiss of the Kola series, possibly playing an important role in the formation of the rich uranium occurrences in the Litsa district.

The dimensions of the plutons increase southward from 4 x 4 km to up to 30 km in diameter. In the same direction the constitution of the massifs simplifies and the density of veins decreases. The multiphase composition of the complex is presented by the following constituents: I – quartz diorite and granodiorite; II – porphyric biotite granite; III – fine and medium grained leucogranite; and veins of porphyric granite, aplite, pegmatite, diorite and diabase.

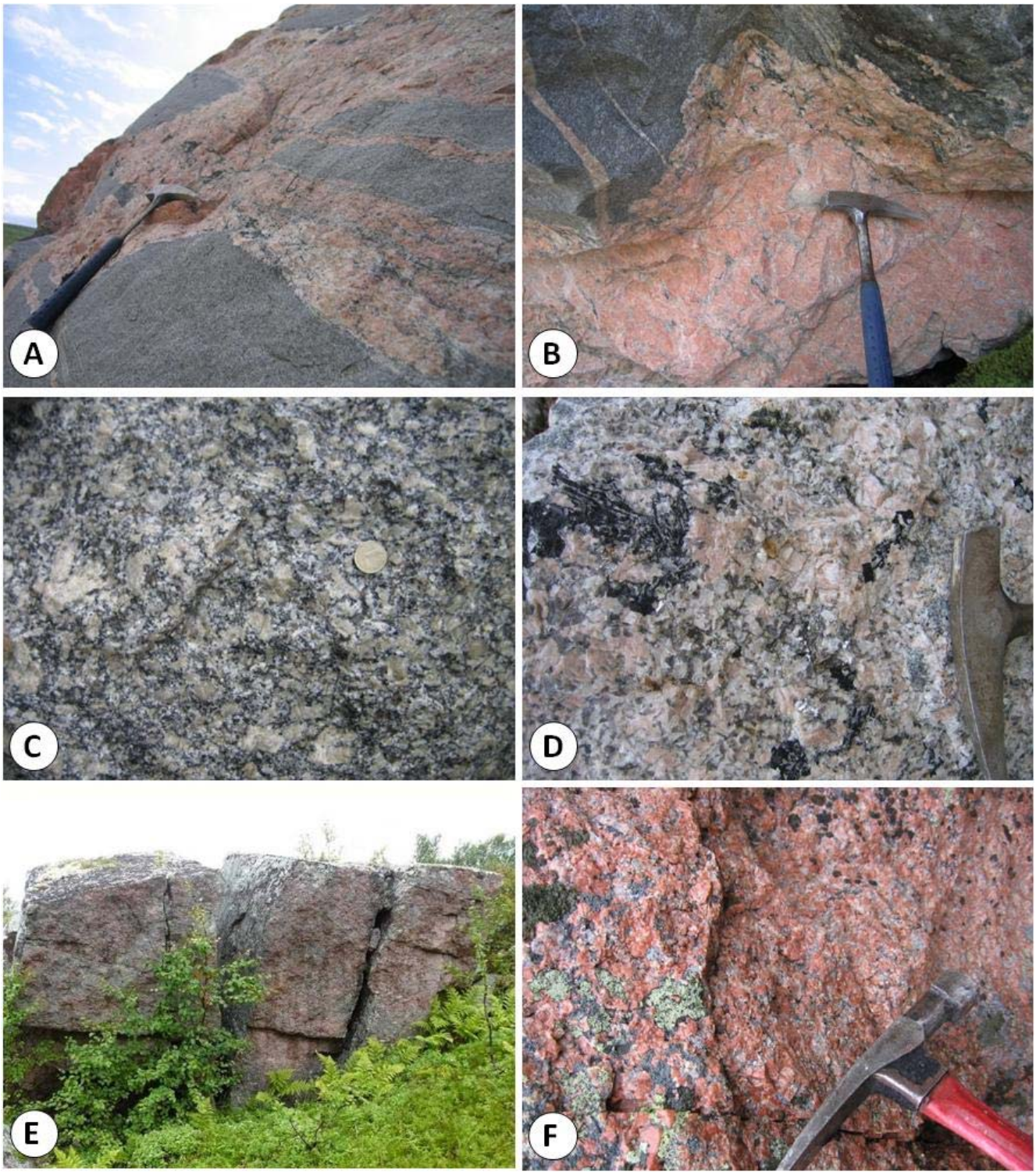

Figure 1.3. A and B. Contact between gneisses of the Kola suite and the Portulobsk granite belonging to the Late Paleoproterozic Litsa-Araguba set of intrusions, **C.** Inner part of the Portulobsk granite massif, feldspar prophyry facies (Field stop Litsa-Araguba_71), **D.** Detail of a facies of the Late Paleoproterzoic Portulobsk granite intrusion, tourmaline and muscovite bearing (Field stop Litsa-Araguba_70, up to 40 mrph), **E.** General overview on the outcrop of Uraguba massif, **F.** Granular texture of the Lista granite [sample 133b].

The Portulobsk massif was visited during the July 2006 field works (see field stops Litsa-Araguba 70 and 71):

- the contact of this massif with enclosing rocks (field stop 70) is characterized by abundant granitic dykes (<1 m wide) either concordant with the enclosing gneisses or clearly crosscutting them and forming pods (Figure 1.3 A and B). Several generations of dykes were observed. These dykes display a strong heterogeneity of textures, colour, and mineralogy: from aplitic to pegmatitic, from white to dark pink and they contain quartz, K-feldspar, and/or muscovite and/or biotite, and/or schorlite, and/or sulphides (Figure 1.3D). Note the presence of a two mica leucogranite (sample 70-2);

- the inner part of the massif (field stop 71) consists in grey porphyritic granite containing K-feldspar megacrysts up to 5 cm long (Figure 1.3C) and biotite. Both plagioclase (zoned) and orthoclase are present. Muscovite was not observed. This type of granite represents about 25% of the Litsa-Araguba massif

- Measured radioactivity on outcrops varies between 30 and 40 mrh, i.e. slightly higher than the background values of the Kola suite gneisses (<30 mrh) and comparable to the biotite-rich selvages. Representative samples of the different facies have been collected for whole rock uranium and thorium geochemical analyses.

The interest of such intrusions is their presence close to the richest uranium occurrences (eg. Litsa, Beregovoe, <2 km). Their age, 1762±9 Ma (Svecofennian) (Savitskii et al., 1995), is comparable (although slightly younger) to the age of uraninite in the surrounding migmatised biotite gneiss (1850-1750 Ma in the Litsa occurence), suggesting a possible genetic link between the emplacement of these granitic intrusions and the migmatisation of the host gneisses.

At a regional scale, migmatisation of aluminous U-rich metasediments, such as those of the Kola series, can generate peraluminous melt, which usually form good source rock for uranium (i.e. showing high uranium content, with uranium in leachable minerals like uraninite). It is possible that the Litsa-Araguba granitic intrusions partly derives from the melting of such sediments and could constitute an additional source for uranium. Petrographical studies and whole rock geochemistry on this granite will be described in part 2, in order to precise the nature of the magmatism (peraluminous or high-K calcalkaline granitoids) and its potential as an uranium source for vein-type deposits.

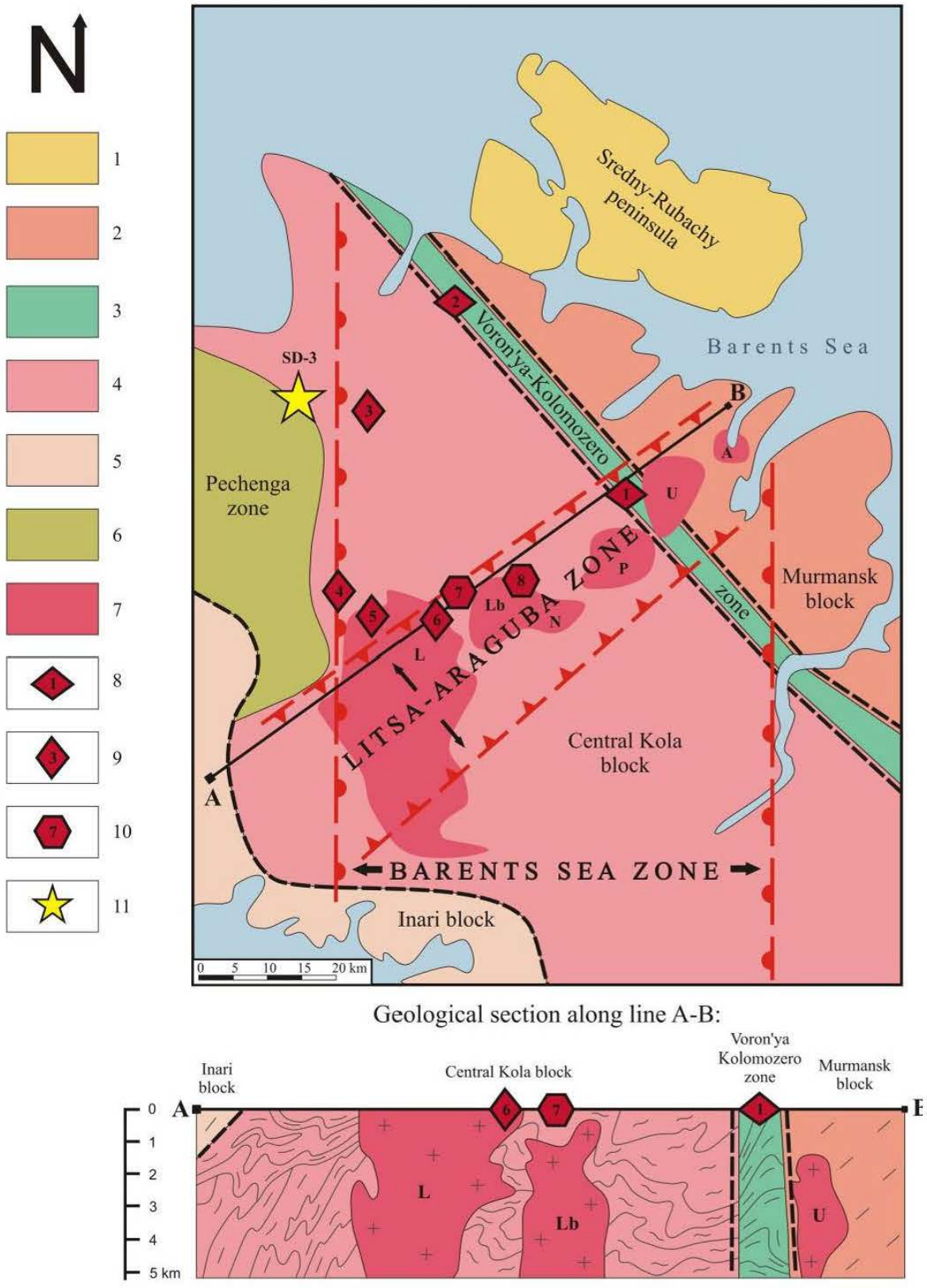

Figure 1.4. The tectonic map of the Litsa district. *(Modified after Mikhailov and Afanasieva; 2007).* 1.Mezoproterozoic sediments; 2. TTG, orthogneiss and supracrustals (2.5-3 Ga); 3. Volcanic-sedimentary formations (2.9-2.6 Ga); 4. Paragneiss, crystalline schist, TTG and granite-gneiss formations (2.9-2.8 Ga); 5. Granite-gneiss, amphibole, biotite gneiss and migmatite (2.7-2.0 Ga); 6. Rift related magmatic-volcanic-sedimentary formations (2.5-1.7 Ga); 7. Litsa-Araguba granitoids complex (1.76 Ga): L-Litsa, Lb-Lebyazhka, N-Nyaljavr, P-Portubol, U-Uruguba, A-Araguba massifs; 8-10- Uranium occurrences: 8-Archean (2.75-2.65 Ga), 9-Proterozoic (2.2-2.1 Ga), 10- Paleozoic (400-300 Ma), (1-Dikoe, 2-Skal'noe, 3- Polyarnoe, 4- Namvara, 5-Cheptjavr, 6- Javr, 7- Litsevskoe, 8- Beregovoe); 11- Kola Superdeep Borehole SD-3.

As most of uranium occurrences are related to the massifs of Litsa-Araguba granitoid complex, it presents a certain interest for its geochemical and mineralogical characteristics, which are described thereafter.

11 samples were studied with ICP-AES, MS analyses, optic and electronic microscopy.

The average composition of major elements in the samples is close to the clarke values: SiO_2=71%; Al_2O_3=14%; TiO_2=0.22%; Fe_2O_3=1.94%; MnO=0.03%; MgO=0,65%; CaO=1,25%; Na_2O=4,1%; K_2O=4,15% and P_2O_5=0.11% (Table 2.5.2.1).

The Th/U ratio for the most of the samples is between 4 and 1, and in some of them the thorium content predominates the uranium one leading to Th/U > 4.

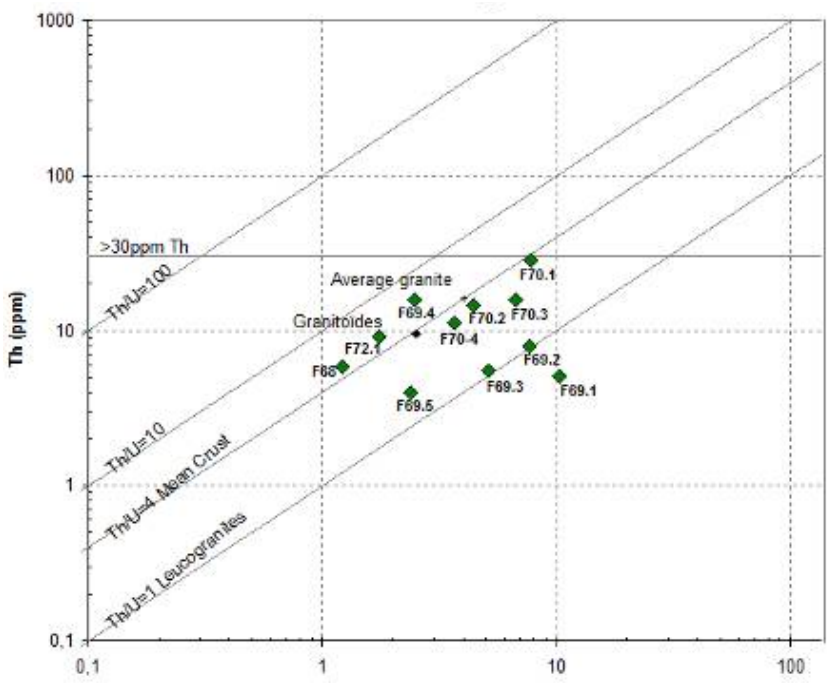

Figure 1.5. Th=f(U) diagram for the Litsa-Araguba granitoïds

The optic observations revealed various alterations, which affect the Litsa-Araguba granitoids, i.e. intensive chloritization of biotite, muscovitization, clay alterations and sericitization of plagioclase (Figure 1.5).

The total REE content in the Litsa-Araguba granitoids varies from 36 to 120 ppm, with maximum value 653 ppm (sample 70.1). Almost all samples have pronounced negative Eu anomaly, except 69.1 and 69.3 (Figure 1.6).

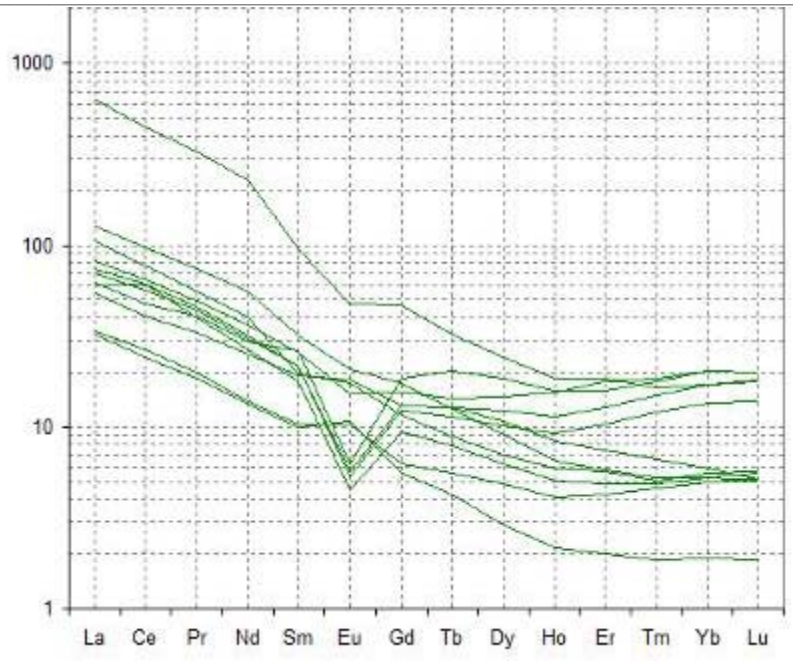

Figure 1.6. REE Spectra of Litsa-Araguba granitoids.

A - Macroscopic image of the sample F69.1

B - Macroscopic image of the sample F69.3

C - Macroscopic image of the sample F70.1

D - Macroscopic image of the sample F70.3

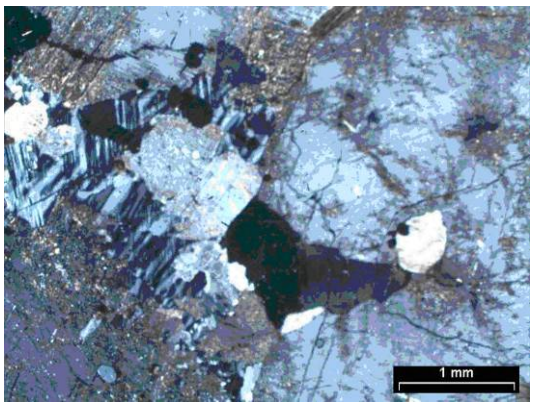

E – General view on the granite [sample F69.1] (transmitted light, crossed nicols, x50);

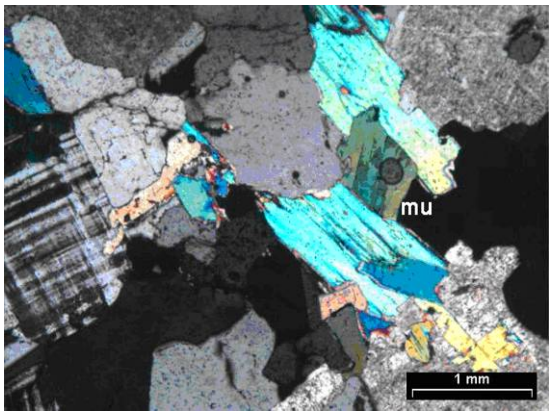

F – Muscovitization [sample F69.3] (transmitted light, crossed nicols, x50);

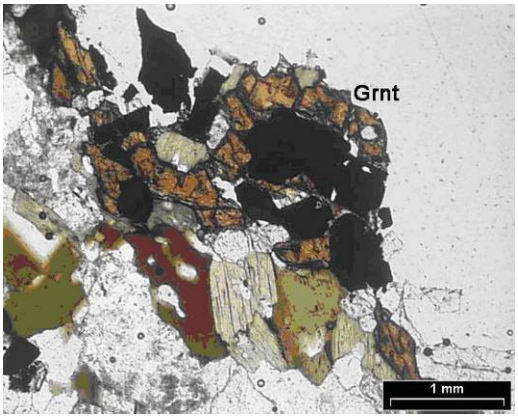

G – Metamorphic garnet grains[sample F70.1] (transmitted light, parallel nicols, x50);

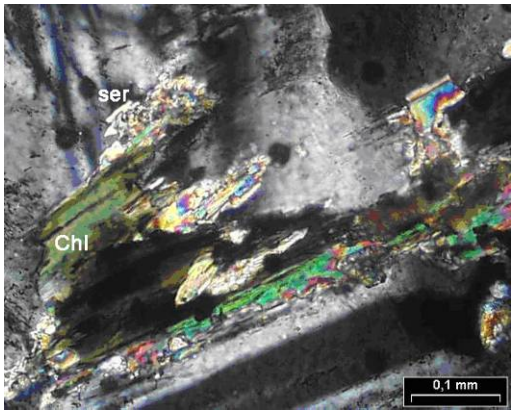

H – Chloritization, sericitization [sample F70.3] (transmitted light, crossed nicols, x500);

Figure 1.7. Petrographical characteristics of the Litsa-Araguba granitoid complex.

1.1.7. ***Sredny-Rybachy sediments (see part 2.3. for more details).***

The Mesoproterozoic-Neoproterozoic (Upper Riphean-Vendian) weakly metamorphosed sediments are developed on the North of the district and build up the Sredny-Rybachy Peninsula. They overlie the eroded Archean basement with a sharp structural-stratigraphic unconformity. The Upper Riphean part of the sequence consists of the arkose and siltstone of Kil'din series, which are overlain with quartz sandstone of Volokovaya series with boulder conglomerate in the bed (*Negrutza et al.; 1994*). The series are divided on certain suits, according to their composition, transgressive-regressive sequence, grade of clasts and foliation.

The upper suits of the Kil'din series and the conglomerate-breccia of the Volokovaya series base are phosphate-bearing (up to 10-12 wt% of P_2O_5) and are considered by some researchers *(Negrutza et al.; 1994)* to be a part of Barents Sea phosphorite basin. It presents syngenetic manifestations of titanium and phosphorus; the last ones are accompanied by uranium-bearing phosphate minerals (francolite).

Due to its discordant relation with the Archean-Proterozoic basement and the presence of unconformity related uranium occurrences in Tersky block of the Kola Peninsula (Figure 1.2), this area also presents a scientific interest for such occurrences.

1.1.8. Barents Sea zone

This submeridian regional superimposed structure (Figure 1.4) is actually a northern extremity of regional Ladoga-Barents Sea zone, which extends for 900 km from the North to the South through Kola, Belomorian and Karelian provinces of the Fennoscandian shield with a width of about 40-50 km *(Afanasieva et al.; 2004)*.

It was developed during Paleoproterozoic (Early Karelian) epoch of the protoactivization *(Kazansky; 1988)* and after geophysical data presents a linear belt of the crust extension with the relevant swell of the Moho surface. In gravimetric field, this zone stands out for its anomalies with sharp gradient drops.

The specific features of the Ladoga-Barents Sea zone, as the major uranium-bearing structure of the Litsa district, are: the wide spread of ductile-brittle deformations (with mylonites and cataclasites), the intensive and repeated (mainly linear) granitization processes and occurrence of quartz-feldspathic metasomatic bodies *(Savitskii et al.; 1995)*.

The granitization processes are irregularly distributed in space and time (2.5-1.8 Ga) and are accompanied with significant uranium and REE occurrences, where they are mostly apparent. Such occurrences are connected with pegmatite and silicious-alkaline metasomatite.

1.1.9. Litsa-Araguba zone

The Litsa-Araguba regional tectonic zone is considered to be the main uranium-bearing structure in the studied area. According to some researches *(Kazansky; 1984)* its development was associated with the Paleoproterozoic (Late Karelian) protoactivization epoch. After geophysical data this is a linear zone of the horizontal displacement of the upper (up to 15 km) crust and concerned warping of the Moho surface.

The specific features of the Litsa-Araguba zone are: the wide development of cataclasite and mylonite; the occurrence of six massifs chain of the Litsa-Araguba granitoid complex and associated migmatization; intense and repeated manifestation of the magnesian-alkaline and alkaline metasomathosis of the sodic line *(Savitskii et al.; 1995)*.

Table 1.1. Isotopic dating of various formations in the Litsa district.

ROCK	AGE (Ma)	METHOD	REFERENCE
Tonalite gneiss of the Kola series (SD-3: 9745 m)	2933±54	U-Pb	*Bibikova et al.; 1993*
Tonalite gneiss of the Kola series (SD-3: 11943-11950 m)	2835±5	U-Pb	*Kola Superdeep…; 1998*
Tonalite gneiss of the Kola series (SD-3: 11762-11770 m)	2832±6	U-Pb	*Kola Superdeep…; 1998*
Granite-gneiss (Voron'ya-Kolomozero)	2810±13	Sm-Nd	*Timmerman and Daly; 1995*
Granite-gneiss (Voron'ya-Kolomozero)	2850±30	U-Pb	*Puchkarev et al.; 1979*
Meta-andesite (Voron'ya-Kolomozero)	2930±90	Pb-Pb	*Ovchinnikova et al.; 1985*
Komatiite (Voron'ya-Kolomozero)	2802±67	Sm-Nd	*Vrevsky; 2000*
Andesite-dacite (Voron'ya-Kolomozero)	2870±40	U-Pb	*Kudryashev et al.; 1998*
Plagiomicrocline granite (Voron'ya-Kolomozero)	2760±13	U-Pb	*Kudryashev, Gavrilenko; 2000*
Pegmatite (Voron'ya-Kolomozero)	2730±15	Rb-Sr	*Pushkarev et al.; 1978*
Ni-bearing gabbro-wehrlite (Pechenga)	1982±8	U-Pb	*Smol'lin et al.; 1999*
Gabbro-norite (Pechenga)	2505±16	U-Pb	*Amelin et al.; 1995*
Granite (Litsa-Araguba)	1762±9	U-Pb	*Vetrin et al.; 2000*
Granite (Litsa-Araguba)	1760±20	U-Pb	*Puchkarev et al.; 1995*

Table 1.2. Radioactive elements distribution in the Litsa-Araguba granitoid complex *(after Afanasieva et al.; 2007).*

Sampling area	Rock	Amount of samples	U (ppm)	Th (ppm)
Lebyazhka massif	Porphyroid granite	24	3.2	35
N-W Litsa massif	Porphyroid granite	40	4.1	44
S-E Litsa massif	Porphyroid granite	22	5.5	?
Lebyazhka and Litsa massifs	Granodiorite	33	4.1	28
Lebyazhka and Litsa massifs	Granite	53	3.6	42
Lebyazhka and Litsa massifs	Porphyroid granite	28	3,5	?
Western Litsa massif	Porphyroid granite	33	6.1	27.4
Smaller Uraguba massif	Granite, granodiorite	21	6.6	52.4
Greater Uraguba massif	Granite, granodiorite	22	4.3	35
Portlubol massif	Granite, granodiorite	26	3.8	31

1.2. Metallogenic potential of the Litsa district

The uranium ore potential of the whole Litsa district is estimated at 102,000 tons in Speculative Resources (IAEA nomenclature), with an average grade of uranium 0.01%. This estimation has been done for all the occurrences together, i.e. individual resources per occurrence are not determined, except the Litsa occurrence, which is the largest and richest one (up to 3 wt% of uranium for pitchblende vein occurrence), but remains uneconomic (<2,870 t of uranium at 0.05 wt% of uranium on average in Prognosticated Resources).

The potential of the Litsa district consists of the complex of various preconditions and features of uranium mineralization, which can be subdivided into several groups. The first major group is geological, which include: structural, lithological and hydrothermal-metasomatic preconditions. Geophysical preconditions are also very important, mainly because of the overlapping Quaternary formations; they consist of magnetic, gravimetric and radiometric fields. Radiogeochemical preconditions are presented by intensively differentiated areas with contrasted uranium distribution.

The local radioactive anomalies, the aero-gamma spectrometric haloes of anomalous uranium concentration, uranium occurrences and manifestations compose the complex of features, which are described in part 2.

1.2.1. Structural preconditions

Structural preconditions play an exceptional role in the spatial localization of the uranium mineralization. They include various permeability zones, such as deep faults with ductile-brittle deformations, which perform favorable conditions for ore-bringing systems and ore-localizing settings. These are the block-separating north-western deep faults and interfaced faults of North-Eastern strike, controlling the granitoid massifs placement. Such faults are apparent on satellite images and also in geophysical fields.

The interpretation of satellite images and posterior statistic spline analysis allow distinguishing the most permeable plots within Litsa district.

The interpretation (Figure 1.8) was executed, using the LANDSAT-7 (USA) satellite image (chanel 4), and based on two principles: deduction («from general to particular») and conformality (geomorphological units are conformal to the relevant geological structures). The lineaments are classified on three groups: circular, orthogonal (N-S and E-W strike) and diagonal (N-E and S-W strike).

Within the Litsa district the large circular structure is deciphered; it is orientated in latitudinal direction and has the dimension of 100 x 90 km, the factor of ellipticity 0.8. This unit corresponds to the Central-Kola uplifting, confirmed by geophysical data, and is connected with the intrusions of Proterozoic granitoids.

The orthogonal lineaments trace the submeridian deep fault zones of Barents Sea zone and latitudinal seams of Voron'ya-Kolomozero greenstone and Pechenga riftogenous zones. Among diagonal lineaments the north-eastern direction predominates, fixing the Litsa-Araguba tectonic zone and interfacing faults.

The spline analysis of permeability consists of counting the quantity of differently orientated lineaments along the grid and thus revealing the most permeable plots (Figure 1.9). The major role in uranium occurrences localization belongs to diagonal, mainly North-Eastern, zones of permeability, which correspond to the common direction of fault zones in the area.

1.2.2. Geophysical preconditions

Geophysical preconditions generally present the behavior of magnetic, gravimetric and gamma fields.

The magnetic field has a complex morphology with significant drops of T parameter: combination of sharp positive anomalies of north-western direction, separated by north-eastern negative anomalous sectors (Figure 1.10). They correspond to the zones of deep faults and the areas of different geological formations. The basic rocks of the Pechenga and Voron'ya-Kolomozero zones together with the Litsa-Araguba granitoids are characterized by clear positive magnetic field.

The magnetic field and its vertical derivative illustrate a regional structural pattern of the Kola craton. EW to NW-SE trending structural discontinuities, marked by few stretched magnetic anomalies, separate different blocks of the Kola Peninsula that have contrasted magnetic properties (blocks I and II in Figure 1.11). The southern limit could correspond to the Paleoproterozoic suture zone. The vertical derivative shows a strong EW to NW-SE fabric that is attributed to the main regional foliation, parallel to the main lithological discontinuities. This fabric is offset by two main structures, trending NE-SW (structures I and II in Figure 1.15) and cross cut by Paleozoic carbonatite and alkaline intrusions among which the Apatity intrusion.

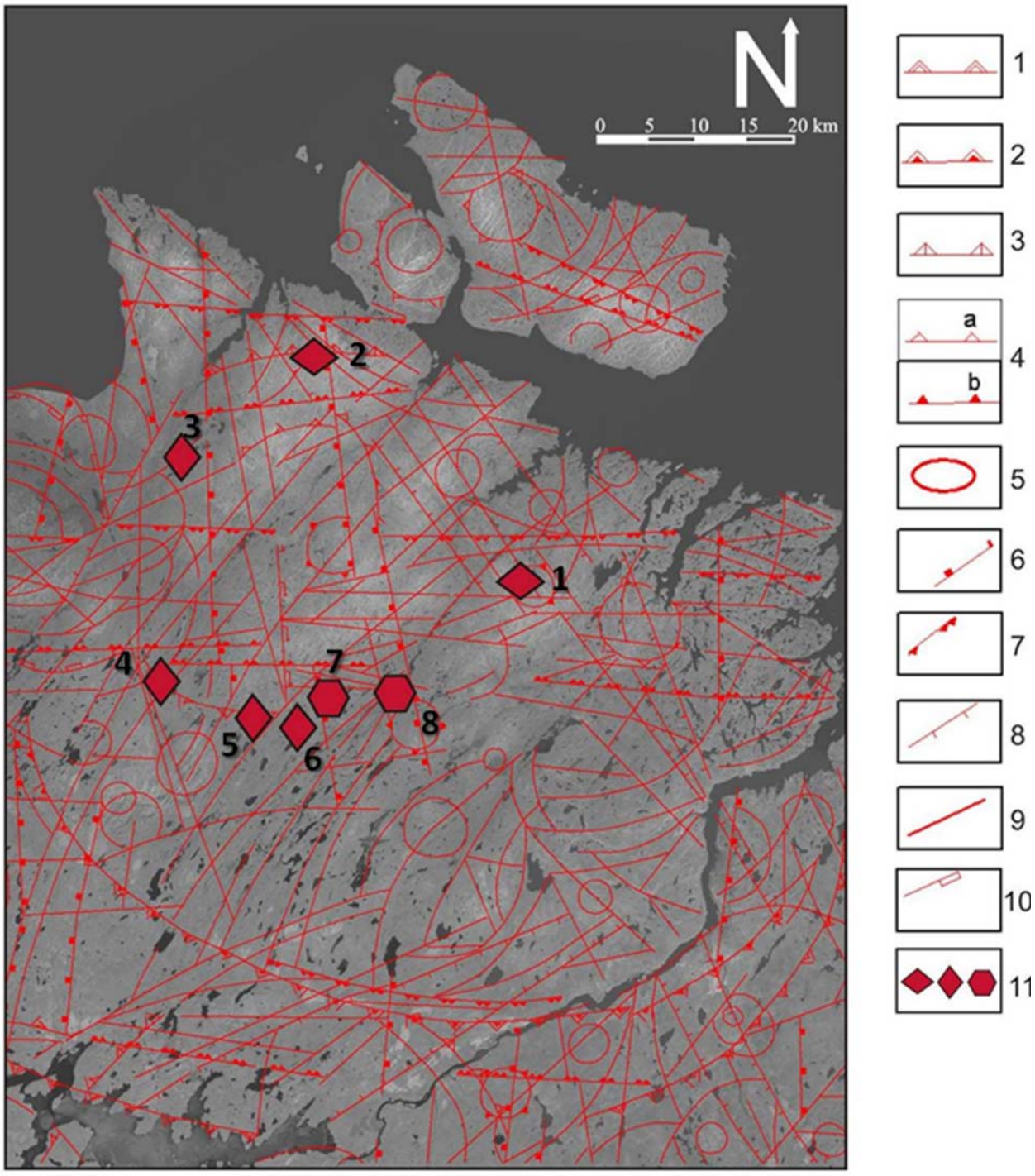

Figure 1.8. Satellite image interpretation map of the Litsa district. *(after Pugovkin; 2007).* 1- internal parts of the dome uplifts; 2- external parts of the dome uplifts; 3- 1st order granite-gneiss domes; 4- 2nd order granite-gneiss domes: a- with outcropped substratum; b- with non-outcropped substratum; 5- uncertain genesis structures; 6- longitudinal fault zones; 7- latitudinal fault zones; 8- diagonal fault zones; 9- other dislocations; 10- platform superimposed depressions; 11- Uranium occurrences.

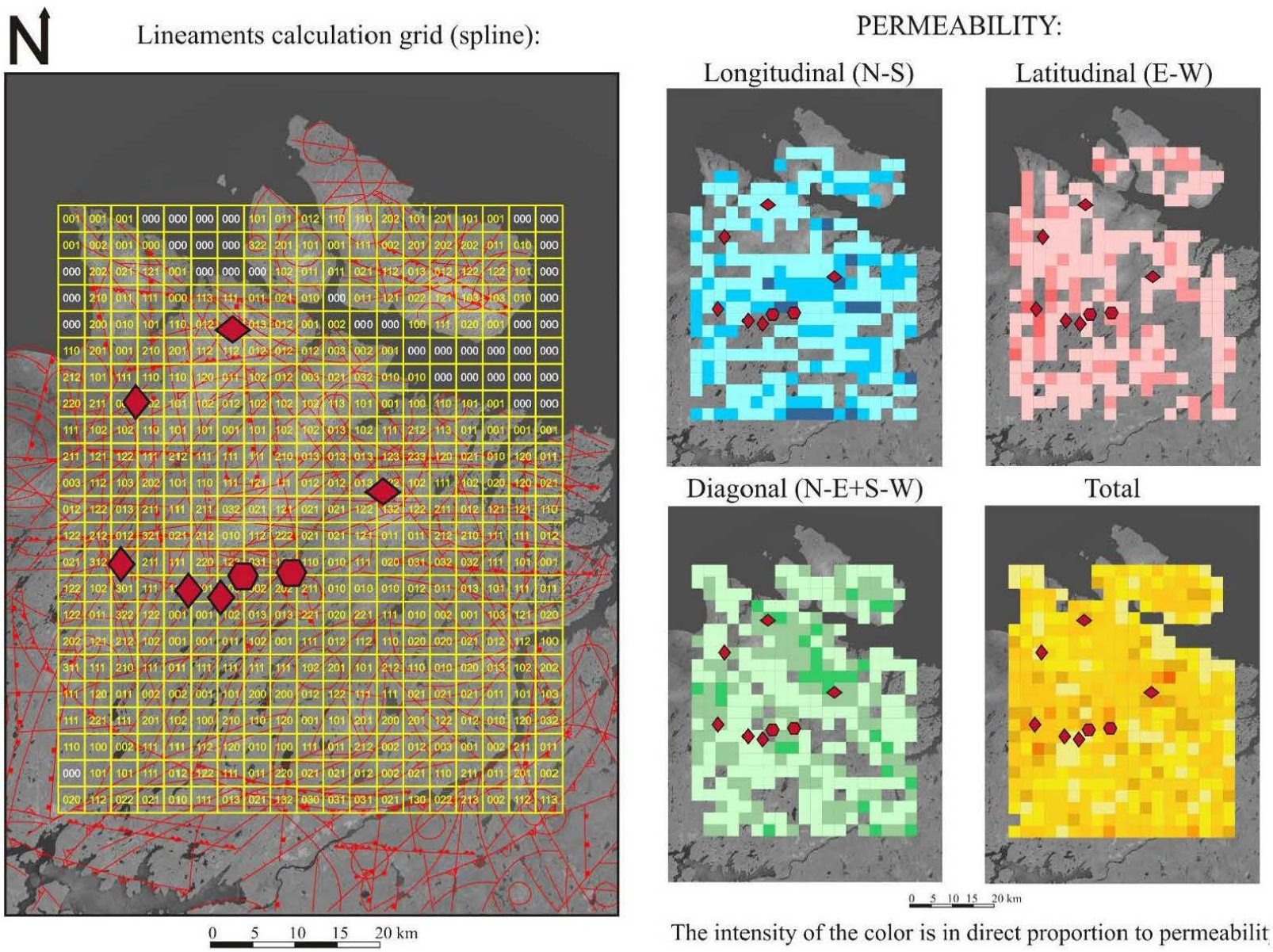

Figure 1.9. The spline analysis of permeability in the Litsa district.

The structural and metamorphic elements have been observed in the periphery of the Litsa granitoids. The host rocks mainly consist of migmatitic paragneisses (metapelites and shales) and orthogneisses mainly derived from granitic rocks. Alternation between these sedimentary and magmatic-derived gneisses suggests original intrusive contacts between granites and pelitic rocks in many places. Contacts are often sharps and a dense network of granitic and pegmatitic veins is observed near the contact within the sedimentary rocks. Basic dykes are locally observed, cross cutting both sedimentary and magmatic formations, prior to migmatisation.

The main foliation, synchronous of the migmatisation, is trending NW-SE and steeply dipping at the regional scale. It probably corresponds to the main fabric observed on the vertical derivative of the magnetic field (Figure 1.16). This foliation is affected by folding of several wavelength and amplitude. Mesoscopic folds are often marked by the intrusion of pegmatites within the axial planes attesting of a progressive deformation during the migmatitic-magmatic evolution. This tectonic evolution is considered to be of Archean age although reworking during the Paleoproterozoic events is locally suspected.

In the vicinity of the Litsa granites, intense deformation trending NE-SW may be observed with the granite marked by an intense foliation. Granitic veins are foliated with the host paragneiss and are cross cut by pegmatitic veining that is also foliated. These textural relationships may attest of a progressive deformation event synchronous of the granitic intrusion. These structures are parallel to the NE-SW structure visible on the aeromagnetic maps (Figure 1.16).

The gravimetric field of the Litsa district is less differentiated. The rocks of the Murmansk and Central-Kola blocks display mainly average value of gravity. The sharp positive anomaly in the western side coincides with the Pechenga riftogenous zone with wide development of basic volcanic formations (Figure 1.10).

The total radioactivity of the surface in subarctic regions is reduced, because of the overlapping glacial formations, spodosol soils and marshes, where the content of U (Ra), Th and K is 0.25-0.8 ppm, 2.0-4.0 ppm and 0.5-1.5% respectively. Nevertheless The average content of radioactive elements within the Litsa district is slightly heightened: U(Ra) up to 3 ppm, Th up to 15 ppm with the background content of K up to 3%. The gamma-radiation exposure rate of the Litsa district displays distinct anomalous sector (up to 15 μR/h), where the most of the occurrences are located (Figure 1.11).

1.2.3. Radiogeochemical preconditions

The radiogeochemical differentiated areas are characterized by disturbed primary-constitutional uranium distribution, which indicates the processes of its remobilization. The radiogeochemical differentiation is conditional on epigenetic redistribution of uranium as a result of post-magmatic and hydrothermal transformations of the rocks.

Within the Litsa district there are several areas of contrast uranium distribution. The first is connected with the migmatization fields around Litsa-Araguba granitoid complex, the second one coincides the Vorn'ya-Kolomozero zone (Figure 1.13).

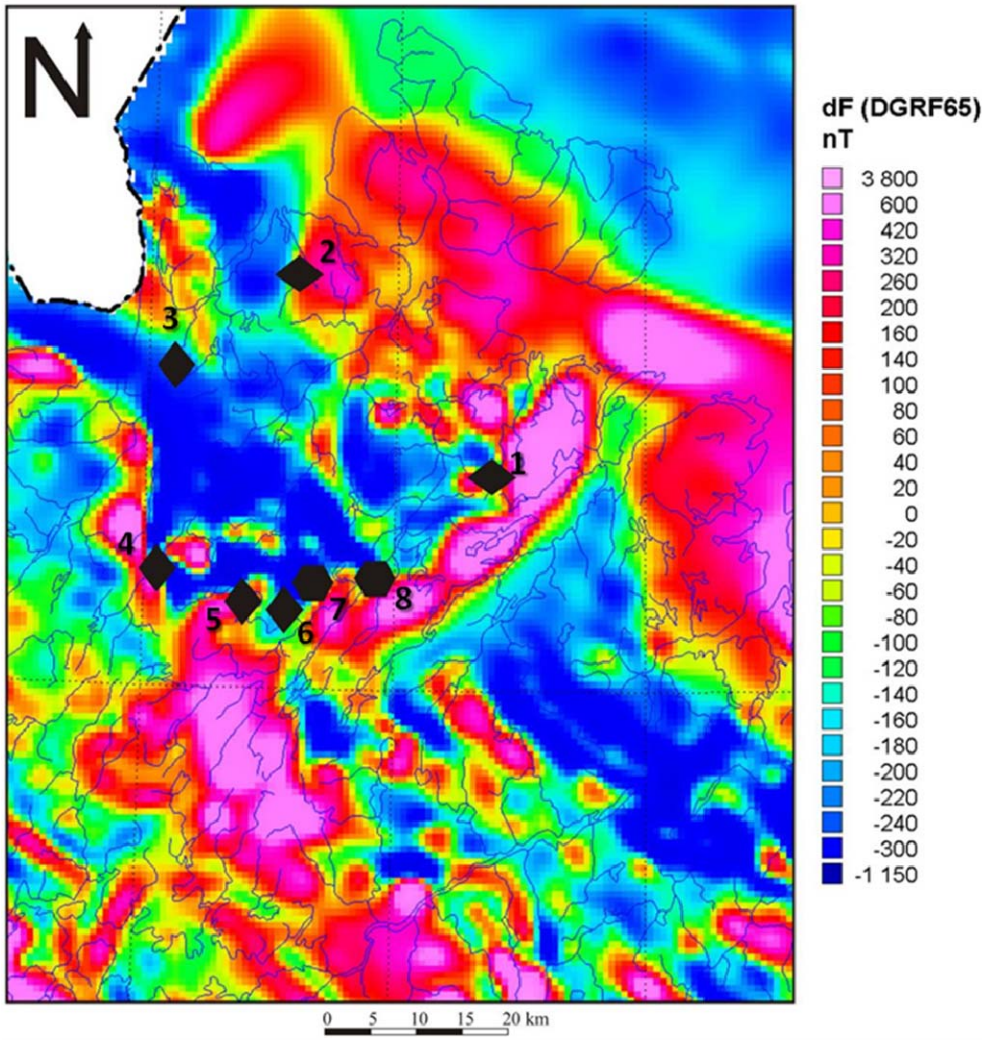

Figure 1.10. Aeromagnetic field map of the Litsa district. *(after Korhonen, Zdanova et al.; 2000).* Uranium occurrences: 1-Dikoe, 2-Skal'noe, 3- Polyarnoe, 4-Namvara, 5- Cheptjavr, 6- Javr, 7- Litsevskoe, 8- Beregovoe.

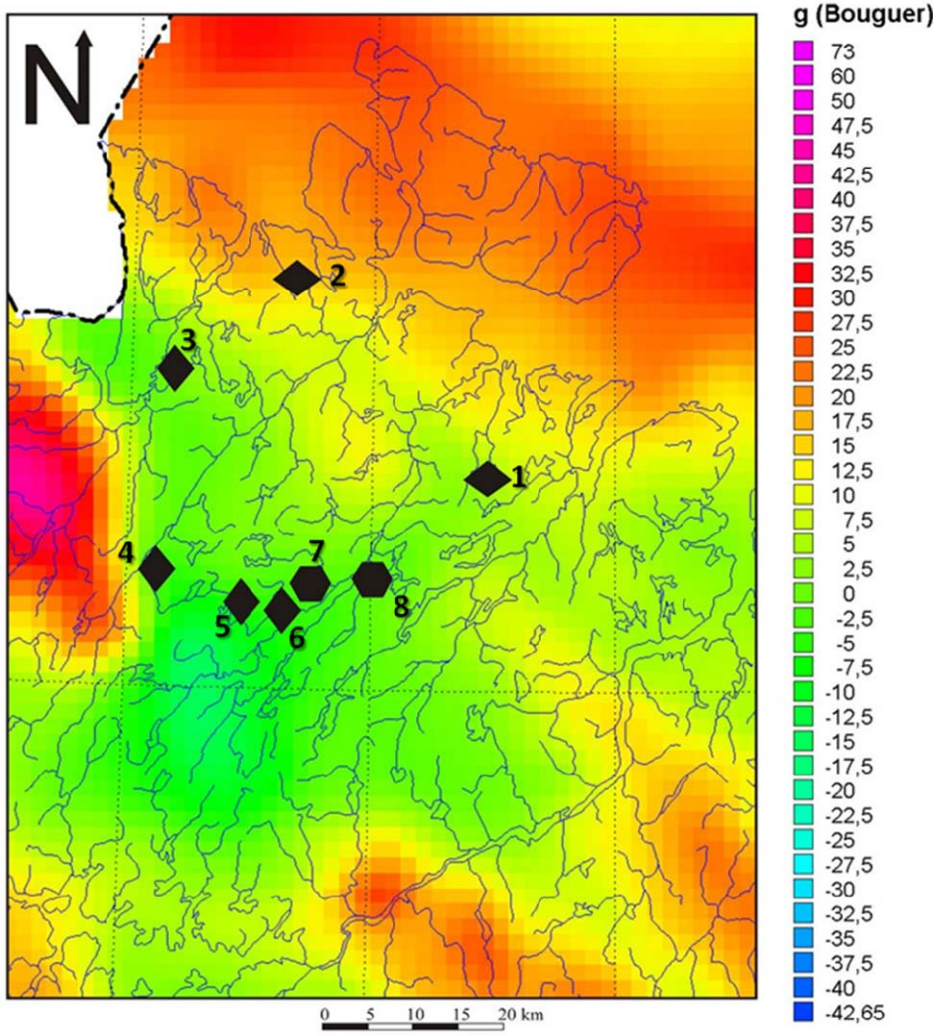

Figure 1.11. Gravimetric field map of the Litsa district. *(after Korhonen, Zdanova et al.; 2000).*

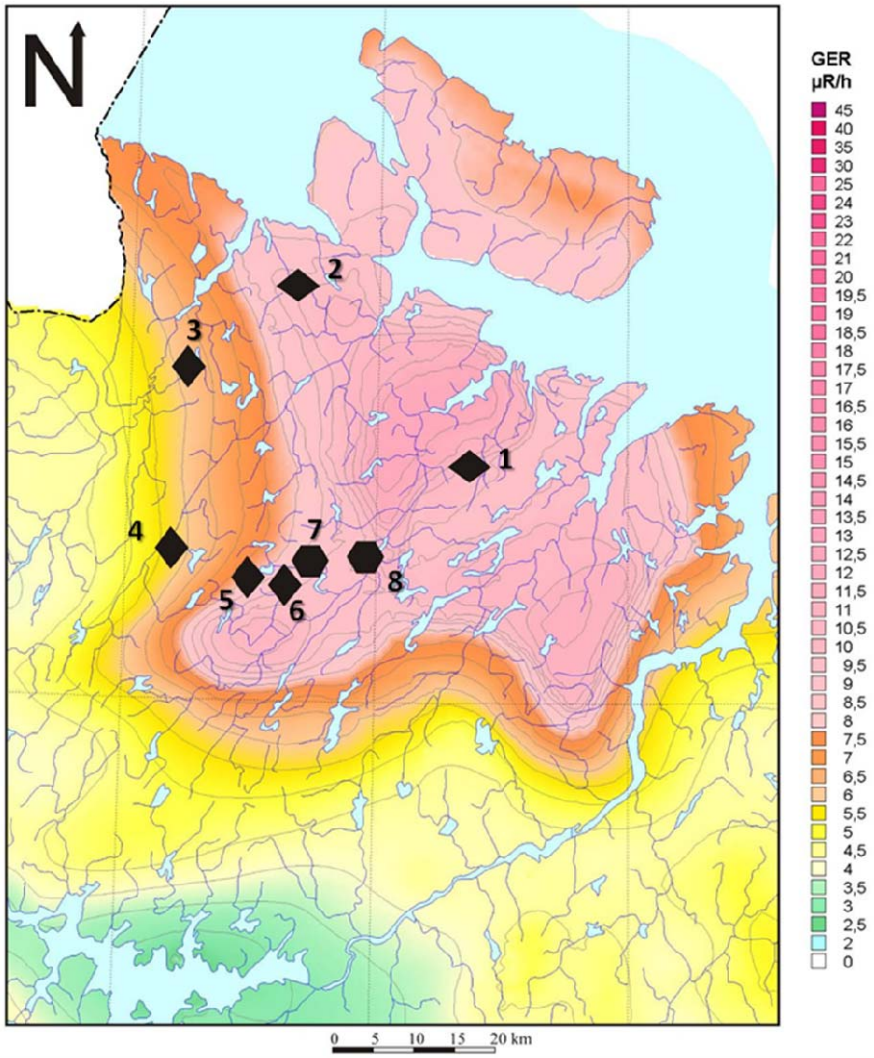

Figure 1.12. Gamma field map of the Litsa district *(after airborne radiometric surveys; 1970-91).*

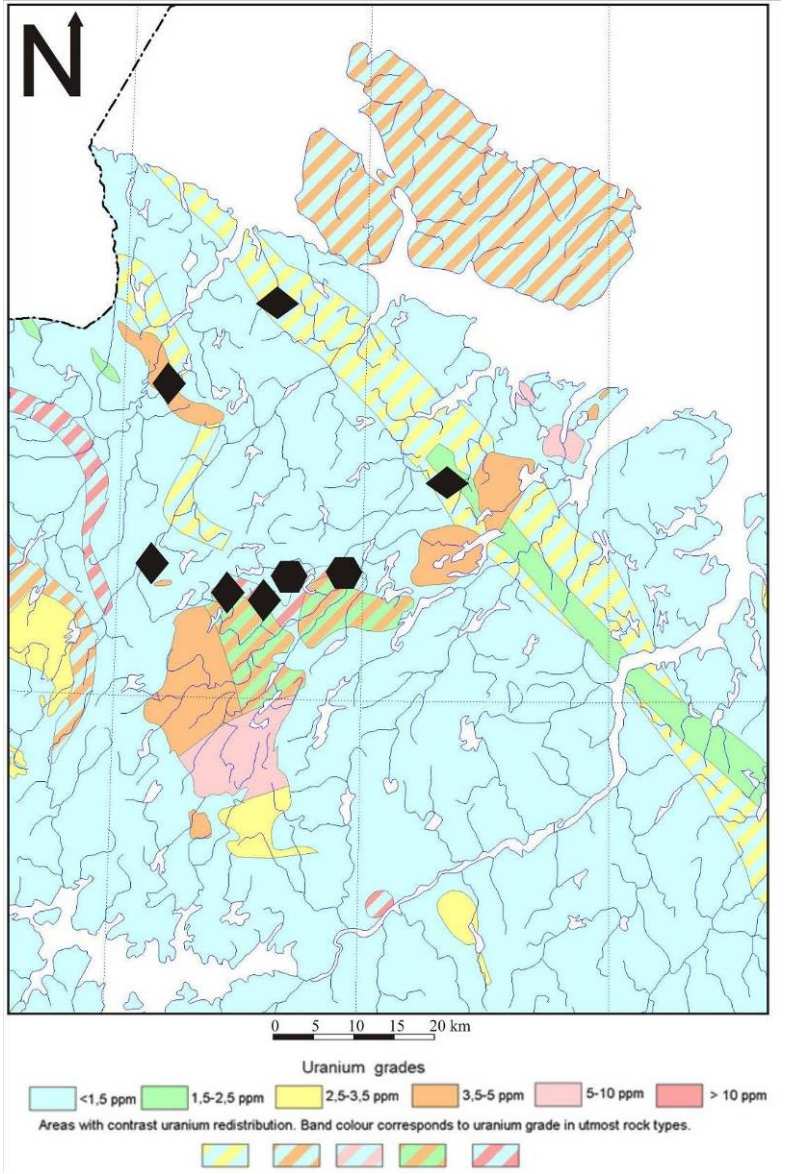

Figure 1.13. Radiogeochemical map of the Litsa district. *(after VSEGEI, Nevskgeologia, Sevzapgeologia)*

1.3. Tectonic evolution of the Litsa district in the framework of the Kola and Karelian craton.

The previous local geophysical informations can be reinterpreted at the Karelia and Kola craton scale. A preliminary look at the aeromagnetic surveys provides some guidelines for understanding the significance of some of the main structural trends and relations between structures and metamorphism provides insights on the tectonic evolution (Figure 1.14, Figure 1.15 and Figure 1.16).

The Kola craton is considered to be an Archean basement that has been reactivated during the Svecofennian orogeny, Paleoproterozoic terranes being accreted on its southern margin within the Belomorian Mobile belt.

The magnetic field and its vertical derivative (Figure 1.16) illustrate a regional structural pattern different of the Karelian craton. EW to NW-SE trending structural discontinuities, marked by few stretched magnetic anomalies, separate different blocks of the Kola Peninsula that have contrasted magnetic properties (blocks I and II in Figure 1.16a). The southern limit could correspond to the Paleoproterozoic suture zone. The vertical derivative shows a strong EW to NW-SE fabric that is attributed to the main regional foliation, parallel to the main lithological discontinuities. This fabric is offset by 2 main structures, trending NE-SW (structures 1 and 2, Figure 1.16a) and cross cut by Paleozoic carbonatite and alkaline intrusions among which the Apatity intrusion (Figure 1.16).

The structural and metamorphic elements have been observed in the periphery of the Litsa granitic body that is dated around 1,700 Ma. The host rocks mainly consist of migmatitic paragneisses (metapelites and shales) and orthogneisses mainly derived from granitic rocks. Alternation between these sedimentary and magmatic-derived gneisses suggests original intrusive contacts between granites and pelitic rocks in many places. Contacts are often sharps and a dense network of granitic and pegmatitic veins is observed near the contact within the sedimentary rocks (Figure 1.17a and b). Basic dykes are locally observed, cross cutting both sedimentary and magmatic formations, prior to migmatisation.

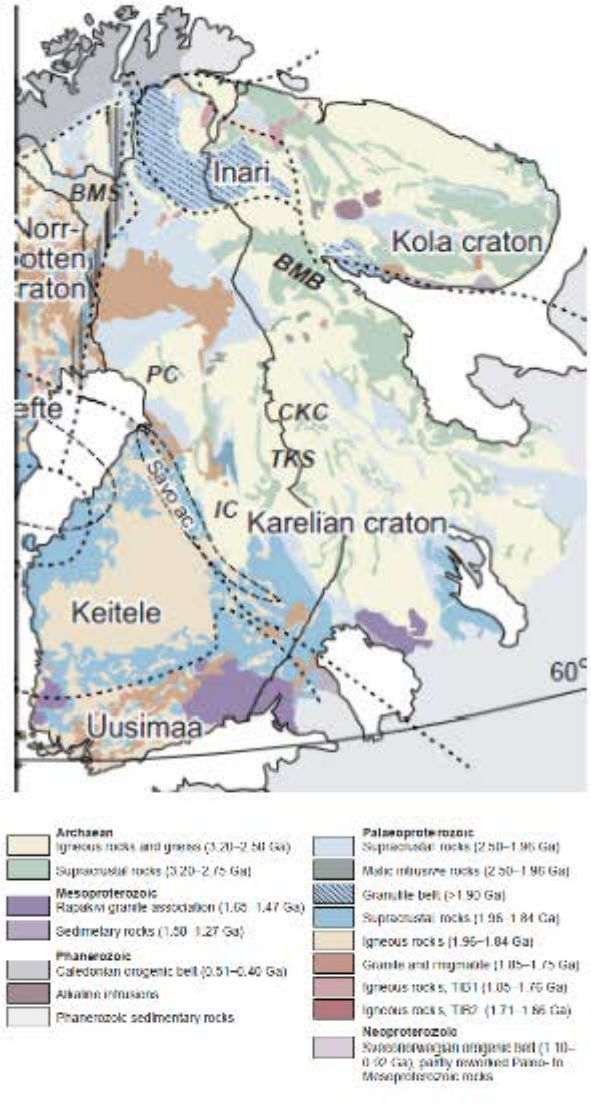

Figure 1.14. Main orogenic provinces of the Svecofennian shield (BMB: Belomorian Mobile belt).

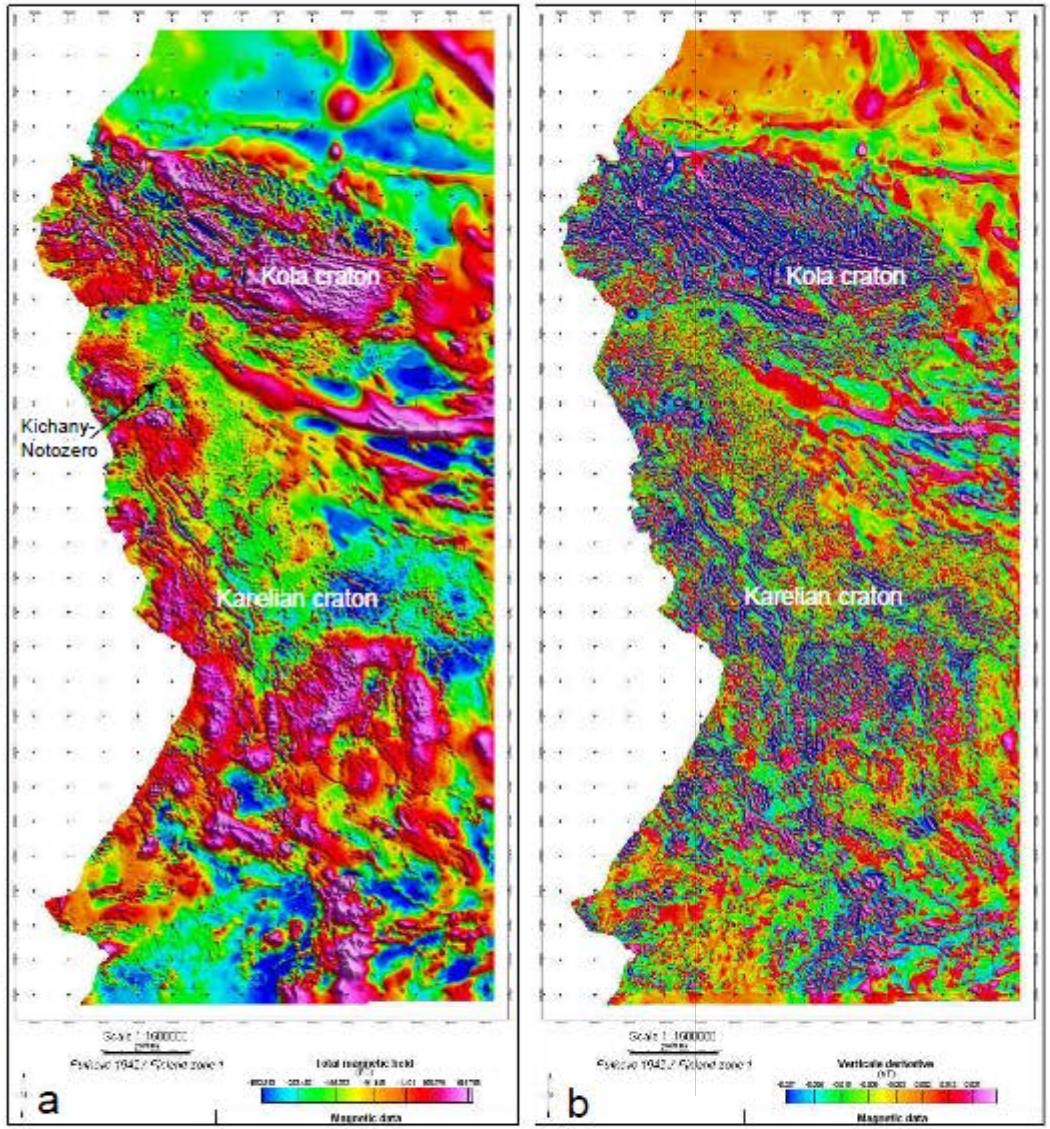

Figure 1.15. Aeromagnetic maps of the Karelian craton and Lapland-Kola orogen a: Total Magnetic field; b: First vertical derivative of the total Magnetic field

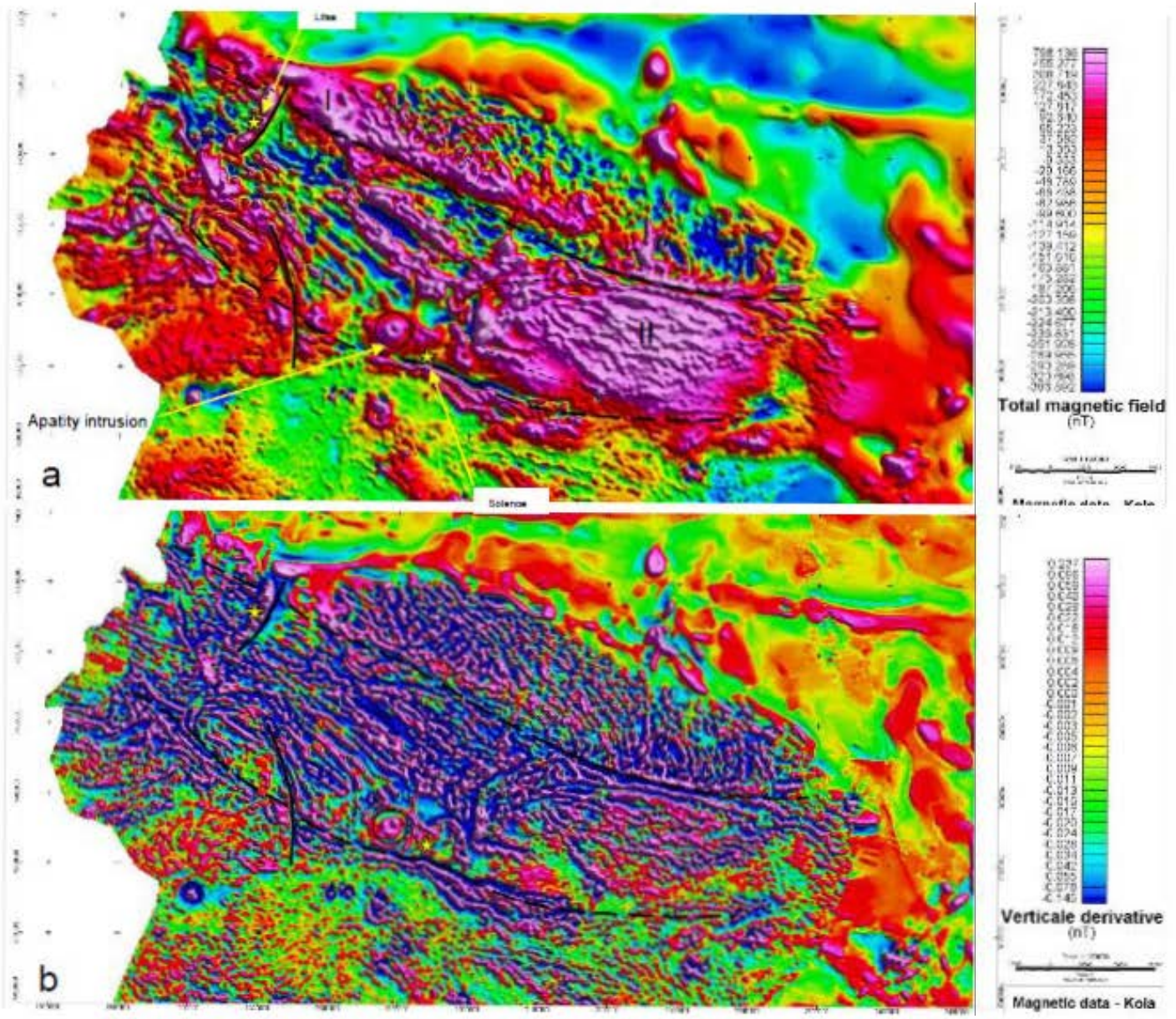

Figure 1.16. Aeromagnetic maps of the Kola block a. Total magnetic field, b. First vertical derivative of the magnetic field in the Kola Peninsula.

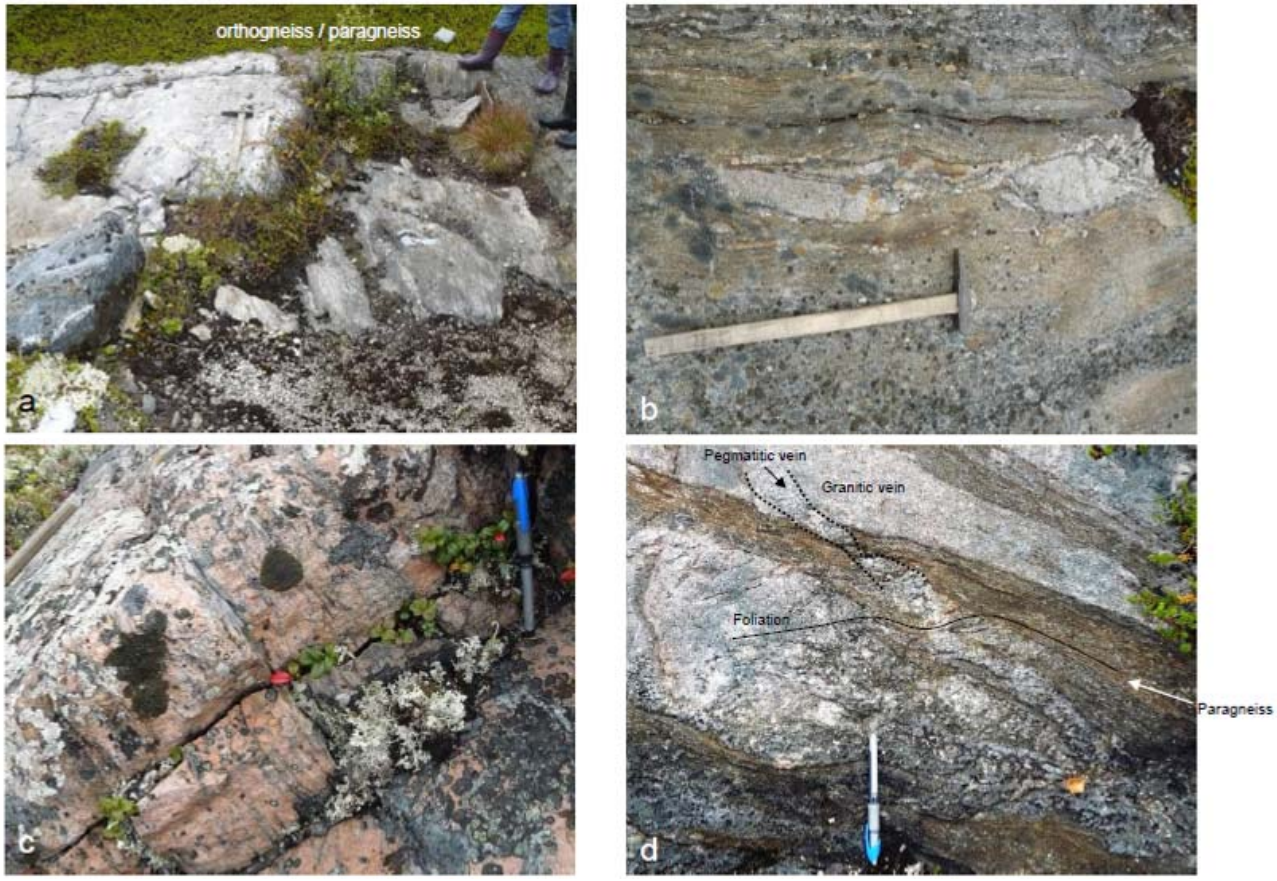

Figure 1.17. Gneiss sequence in the Kola Peninsula and relationships with granitic intrusion. **a.** Contact between orthogneiss and paragneiss. **b.** Pre-tectonic granitic, aplitic and pegmatitic veining near the contact rocks of the Litsa granite. **c.** Foliated granite on the Northern margin of the Litsa granite. **d.** Pegmatitic vein crosscutting a granitic vein within the host rocks of the Litsa granite.

1.4. Conclusions

The Litsa district presents an area of the oldest continental crust of the North-Eastern part of the Fennoscandian shield, which have endured a protracted geological evolution from Archean to Paleozoic and characterized by complex mosaic-block constitution.

It displays all features of a uraniferous province with over 30 uranium occurrences and manifestations, totally estimated at 102,000 tons in Speculative Resources (IAEA nomenclature), with an average grade of uranium 0.01%.

Most of uranium occurrences are situated within the Central-Kola block, built with repeatedly and dissimilarly metamorphosed paragneisses and crystalline schists of the Kola series (2.9-2.8 Ga), and in the Voron'ya-Kolomozero zone, suturing the Central-Kola and Murmansk blocks, where the occurrences are associated with uranium-bearing pegmatoids (2.7-2.65 Ga).

The Litsa-Araguba regional tectonic zone, established during the Paleoproterozoic protoactivization epoch, is traced with a chain of Litsa-Araguba granitoid complex massifs (1.7 Ga), which migmatize the host gneisses and are characterized with heightened uranium content (more than 5 ppm).

Besides there is a submeridian regional superimposed Barents Sea zone, also developed during Paleoproterozoic, with wide spread of ductile-brittle deformations and the intensive and repeated granitization processes.

The described geological units and tectonic structures, responsible for localization of uranium occurrences, are distinctively marked in geophysical fields and present the zones of permeability for uranium migration and the barriers for its localization.

PART 2.

GEOLOGICAL SETTINGS, FIELD OBSERVATIONS AND RE-INTERPRETED ORE-SHOWING MAPS OF THE URANIUM OCCURRENCES OF THE LITSA DISTRICT

Introduction

Litsa district endured several successive uranium enrichments from Archean to Paleozoic, which lead to the formation of more than 30 uranium occurrences and manifestations of different types (Figure 2.1). The distinction of uranium mineralization types is debatable, due to insufficient scrutiny and the different approaches to this problem. Thus, the Russian geologists *(Savitskii et al.; 1995)* refer to the “metasomatic” classification of the uranium occurrences, distinguishing:

1. REE-Th-U mineralization in pegmatoidic granite and quartz-feldspathic metasomatite (Dikoe and Skal'noe ore-showings);
2. Uranium mineralization in aplogranite chlorite-albite metasomatite and albitite (Polyarnoe, Namvara, Cheptjavr and Javr ore-showings);
3. Uranium mineralization in albite-hydromica-chlorite metasomatite (Litsevskoe and Beregovoe ore-showings);

Besides, they mention REE-P-U mineralization in terrigenous rocks (Sredny-Rybachy Peninsulas).

Meanwhile, the studies provided in the framework of this thesis, casted several doubts on such approach, revealing some differences between the occurrences belonging to the same type, according to the mentioned classification.

Consequently, the worthwhile approach is to describe the uranium mineralization in terms of its age (from the oldest to the youngest), citing the data of the previous researches and precising the features, obtained during the recent field works and analytical studies.

Still there are some peculiarities of such approach, concerning the polycyclic genesis of some occurrences. Particularly, the Litsevskoe ore-showing, as the most distinctive and representative in the district, display several stages of uranium enrichment, and will be described according to the most significant stage of uranium mineralization, in the paragraph, devoted to Paleozoic enrichment.

All the data of this part are compiled from Savitskii et al. (1995), Afanasieva (2007) and Kister et al. (2007), and field observations (field works, 2006-2007-2008) (Figure 2.2).

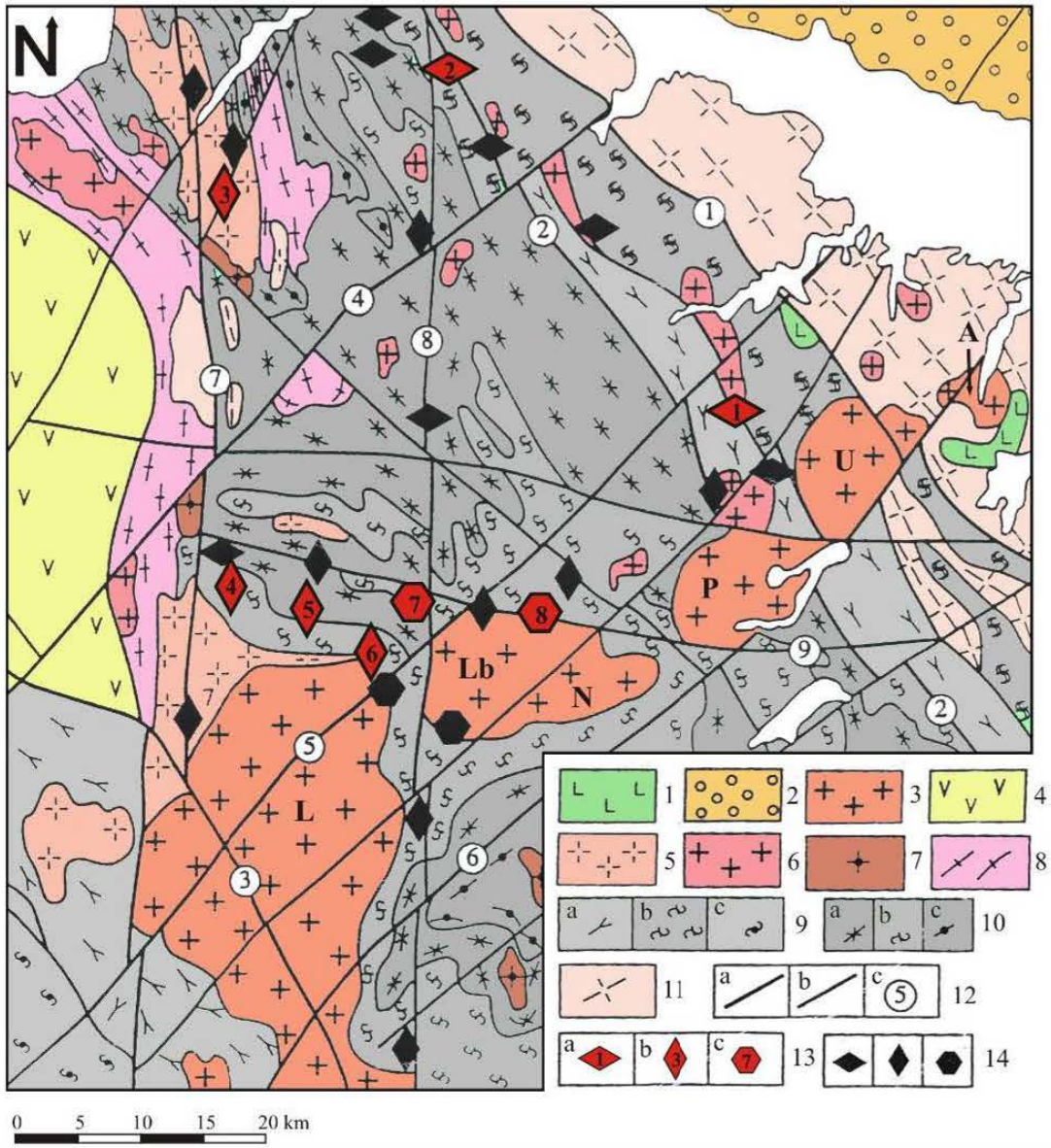

Late Proterozoic:
1 - Murmansk gabbro-dolerite and dolerite complex;
2 - conglomerate, sandstone and siltstone of Kil'din series;

Early Proterozoic:
3 - Litsa-Araguba granitoid complex (L - Litsa, Lb - Lebyazhka, N - Nyaljavr, P - Portlubol', U - Uraguba, A - Araguba massifs);
4 - Pechenga series: volcanic-tuffogenous-sedimentary rocks;
5 - Kaskeljavr grainite complex;

Late Archean:
6 - Voron'ya metasomatic granite complex;
7 - Tuloma anatectic granite complex;
8 - Porojarvi diorite-plagiogranite complex;
9 - Tundra series: a - amphibole, b - biotite and two-mica, c - undifferentiated gneiss and schist;
10 - Kola series: a - aluminous, b - garnet-biotite and amphibole-biotite, c - amphibole and pyroxen gneiss and schist;

Early Archean:
11 - Barents Sea tonalitic gneiss and plagiogranite complex;

Tectonic elements:
12 - Faults: a - I-st order; II-nd order; c - numbers and names (1 - North Kola, 2 - Uraguba, 3 - Porojarvi, 4 - Titovka, 5 - Litsa, 6 - Araguba, 7 - Nyasyukk-Kuchintundra, 8 - Urdozero, 9 - Cheptjavr);

Uranium occurrences:
13 - Major occurrences of different type: a - Archean in pegmatite and quartz-feldspathic metasomatite, b - Proterozoic in alcaline metasomatite, c - Paleozoic in pitchblende veins; (1 - Dikoe, 2 - Skal'noe, 3 - Polyarnoe, 4 - Namvara, 5 - Cheptjavr, 6 - Javr, 7 - Litsevskoe, 8 - Beregovoe);
14 - Other occurrences and manifestations of these types;

Figure 2.1. Geological map of the Litsa district. *(after Savitskii et al.; 1995)*

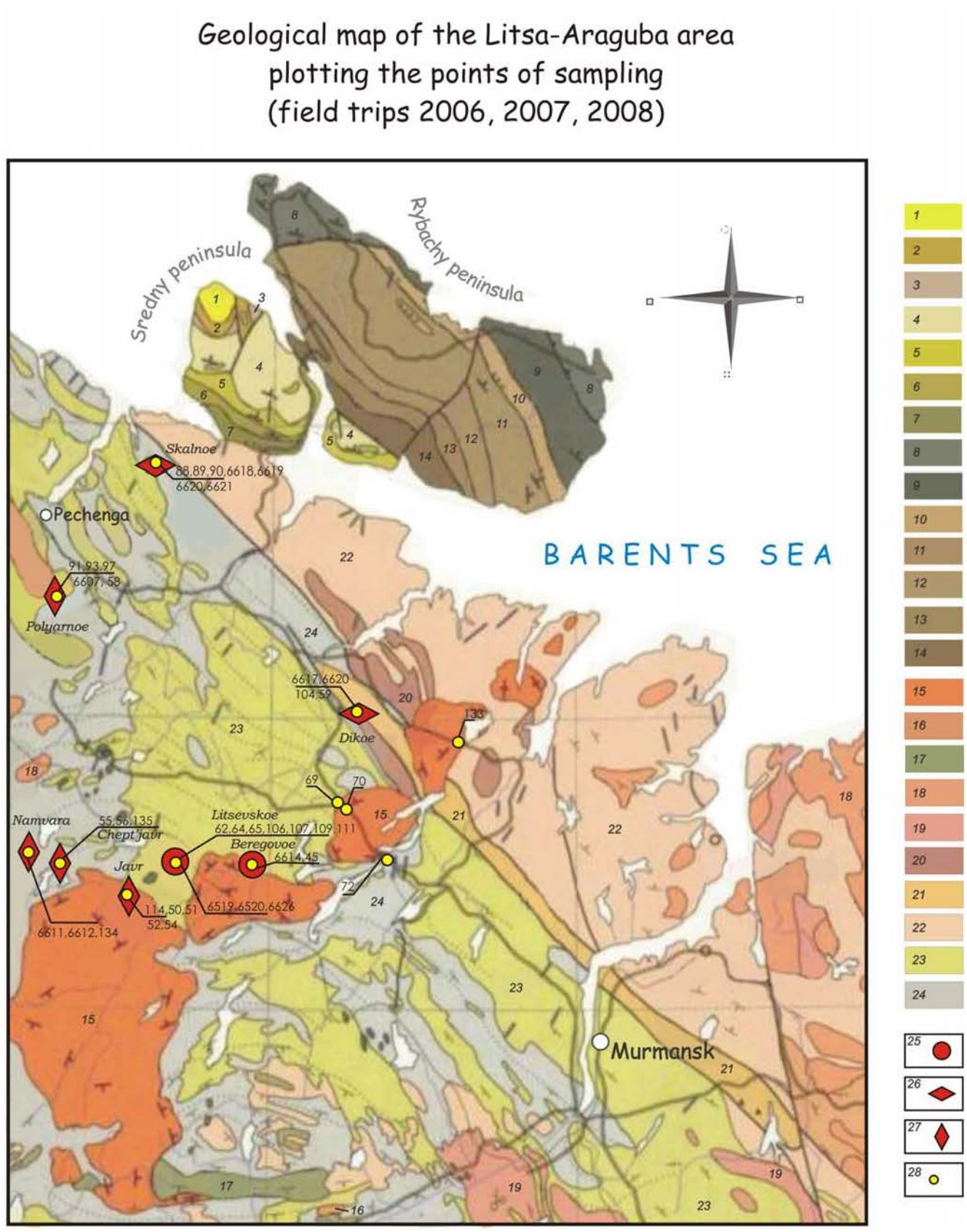

Figure 2.2. Location of the different field stops from the field work of 2006, 2007 and 2008. The sample numbers have been located. 1-14: Sedimentary formations of Riphean; 15-24: Basement formations; 25-27: Uranium occurrences; 28: points of sampling.

2.1. Archean occurrences

The oldest uranium mineralization in the Litsa district is connected with Archean pegmatoidic rocks (2750-2650 Ma - *Anderson; 1990*). Several uranium occurrences and manifestations of this type are located mainly in the central sector of the Voron'ya-Kolmozero tectonic zone (Figure 1.4). It is bounded by the Northern-Kola fault to the north-east and by the Uraguba fault to the south-west (Figure 2.1).

The Voron'ya-Kolmozero zone is mostly composed of biotite and two-mica gneisses, arbitrarily referred to the Upper Archean Tundra series, which occur together with amphibole gneiss and amphibolite crumpled into a system of intricate folds with a dominant north-western strike. These folds have a limb distance of 3-4 km and are accompanied by narrow (200-300 m) sub-concordant fault-related fold zones, where most of the uranium-bearing granitoid vein-like bodies are located.

The Tundra series are uniformly metamorphosed under the conditions of the disthene-muscovite facies (*Belyaev et al.; 1977)*. With this background there are local linear zones of the middle-temperature retromorphic alteration, namely, silicification zones with muscovite-sillimanite veinlets and nests.

The uranium anomalies are controlled by the linear north-west striking zones of boudinage and granitoid injections. The zones are up to 20-25 km long and 1-2 km wide and present areas with of uranium-bearing pegmatoidic granite and quartz-feldspathic metasomatite, dated by K-Ar method on biotite at 2750±50 Ma (*Anderson; 1990*). They are preferentially situated in the cores or bends of the anticline folds and may occupy about 30-40% of the exposed rocks. The contacts with the hosting gneiss are concordant and sharp, but occasionally uranium-bearing granitoid lenticular bodies are crosscutting them.

As a rule, the average background uranium content in the Late Archean gneiss and granitoid is below 2.5 ppm. The uranium-bearing lenses and nests contain more than 0.1 wt % of uranium. The enriched zones are usually several meters in size and occupy about 20-30% of the pegmatoidic granite and quartz-feldspathic metasomatite total volume.

The most representative ore-objects of this type are Dikoe and Skalnoe ore-showings, but there are also numerous manifestations of the same type extended within the Voron'ya-Kolmozero tectonic zone over a long distance, also beyond the Litsa district.

2.1.1. Dikoe ore-showing

The Dikoe ore-showing was discovered as a result of airborne surveys, performed in 1961, and revealed several radioactive anomalies, which were explored in 1970 by the «Nevskgeologia»: drilling along 5 profiles, developing ground geophysical surveys (scale 1:50,000 and 1:10,000) and trenches (Figure 2.3).

It is located in the junction of Litsa and Uraguba faults within the southern exocontact of Voron'ya granitoid complex, regionally in the intersection of the Litsa-Araguba and the Voron'ya-Kolmozero tectonic zones (Figures 1.4 and Figure 2.3).

Two areas of vein-like pegmatoidic granite and quartz-feldspathic metasomatite bodies with anomalous radioactivity (100-2700 μR/h) were revealed in the sector. They have the 1 x 5 and 1.5 x 6 km dimensions and the north-west orientation (315-320°). Geological and radiometric surveys provided in these areas discovered over 400 uranium-bearing bodies of the same strike located in the fault-related fold zones and mainly concordant with the strongly deformed biotite and two-mica gneiss of the Tundra series. The majority of these bodies have vein and lenticular shape and a maximum extension of 250 m with 15 m thickness. They are confined to the cores and limbs of the thin isoclinic anticlines, complicated by the lengthwise faults with the zones of cataclasis and intensive tectonic schistosity. The background uranium content in these rocks is 8.5 ppm. The anomalous radioactivity is commonly connected with biotite and biotite-muscovite selvages at the margin of quartz-feldspathic veins (Figure 2.4).

From 5 to 12 lenses and nests with uranium grade over 0.01 wt % were defined in each of these bodies. Their maximum length reaches 40 m and thickness of 2 m. Within them, there are lenses with uranium grade over 0.03 wt % (up to 0.2 wt %) with sizes up to 25 x 1.5 m *(Savitskii et al.; 1995)*. The uranium mineralization of such nest-like and lenticular discontinuous distribution was traced by drilling to a depth of 40 m (Figure 2.5).

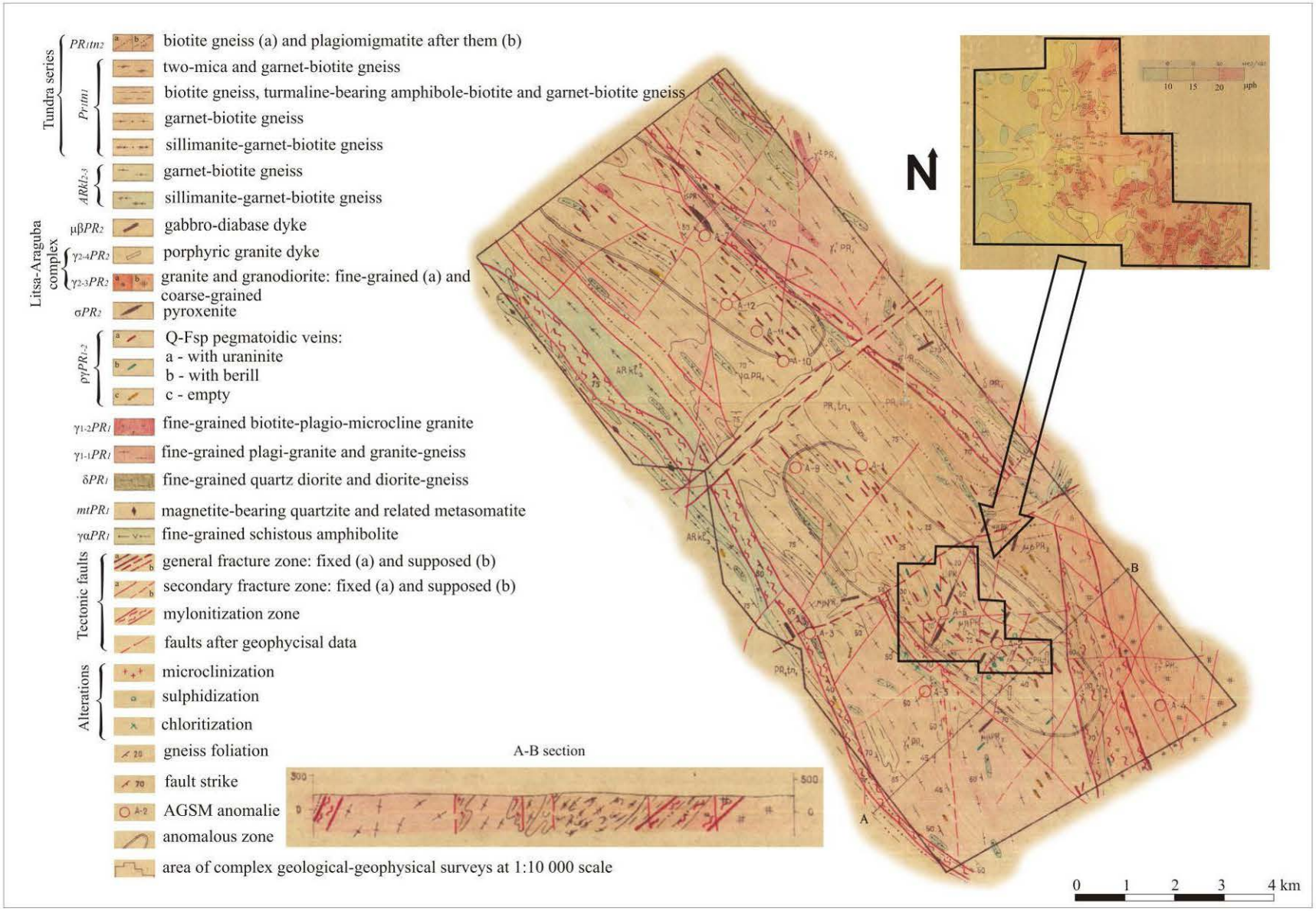

Figure 2.3. Geological map of the Dikoe ore-showing area (inserted geological cross section and radiometric map of the most anomalous zone) *(after «Nevskgeologia»; 1975).*

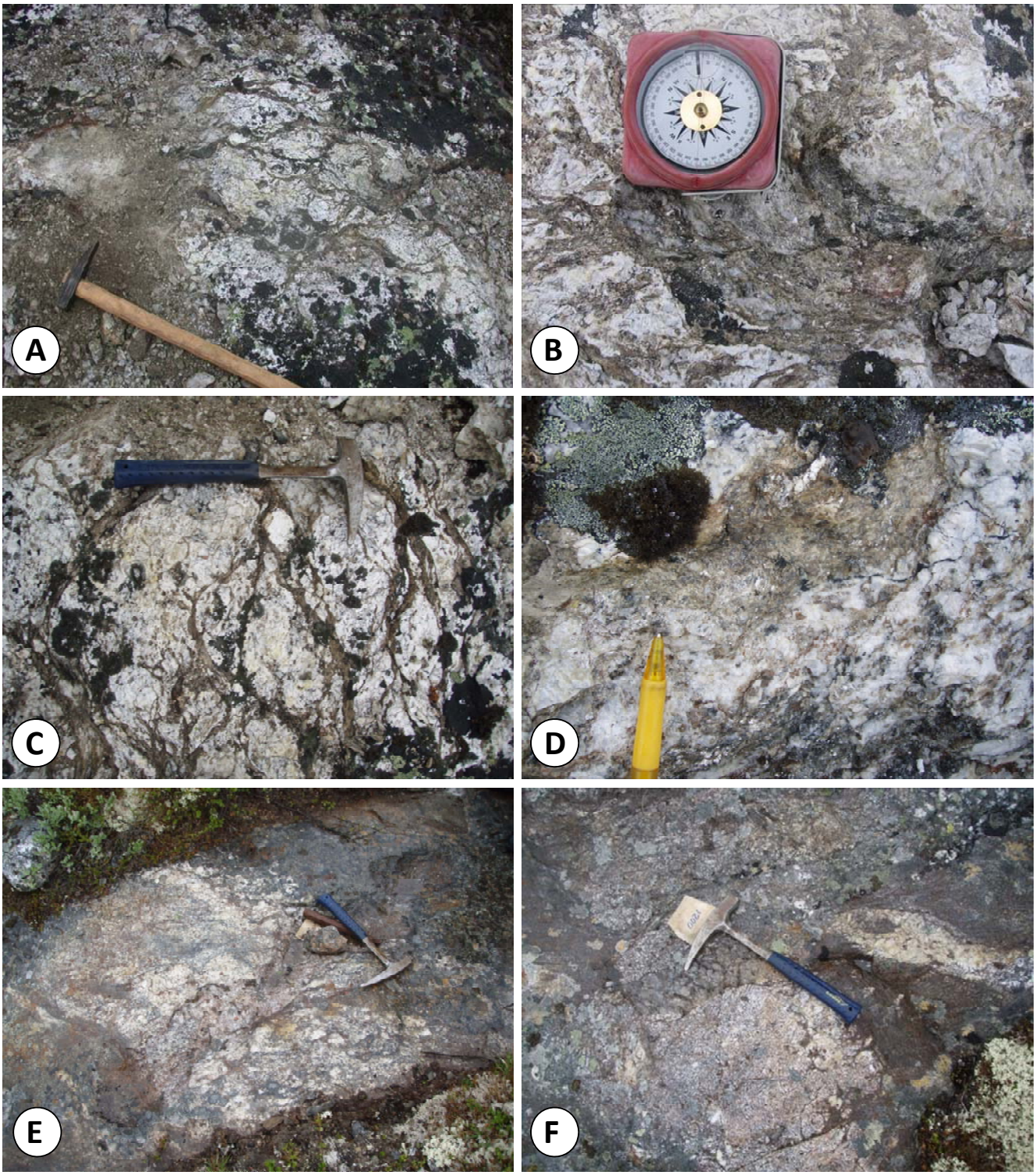

Figure 2.4. A. E. and F. general view on the rocks with anomalous radioactivity (2700 μR/h) **B.** fringes of biotite and biotite-muscovite composition around the quartz-feldspathic clusters [sample 59]; **C and D.** anastomosing muscovite-bearing fractures crosscutting a radioactive Archean granitoid (Dikoe_104). Muscovite replaces biotite. Outcrop up to 400 cps.

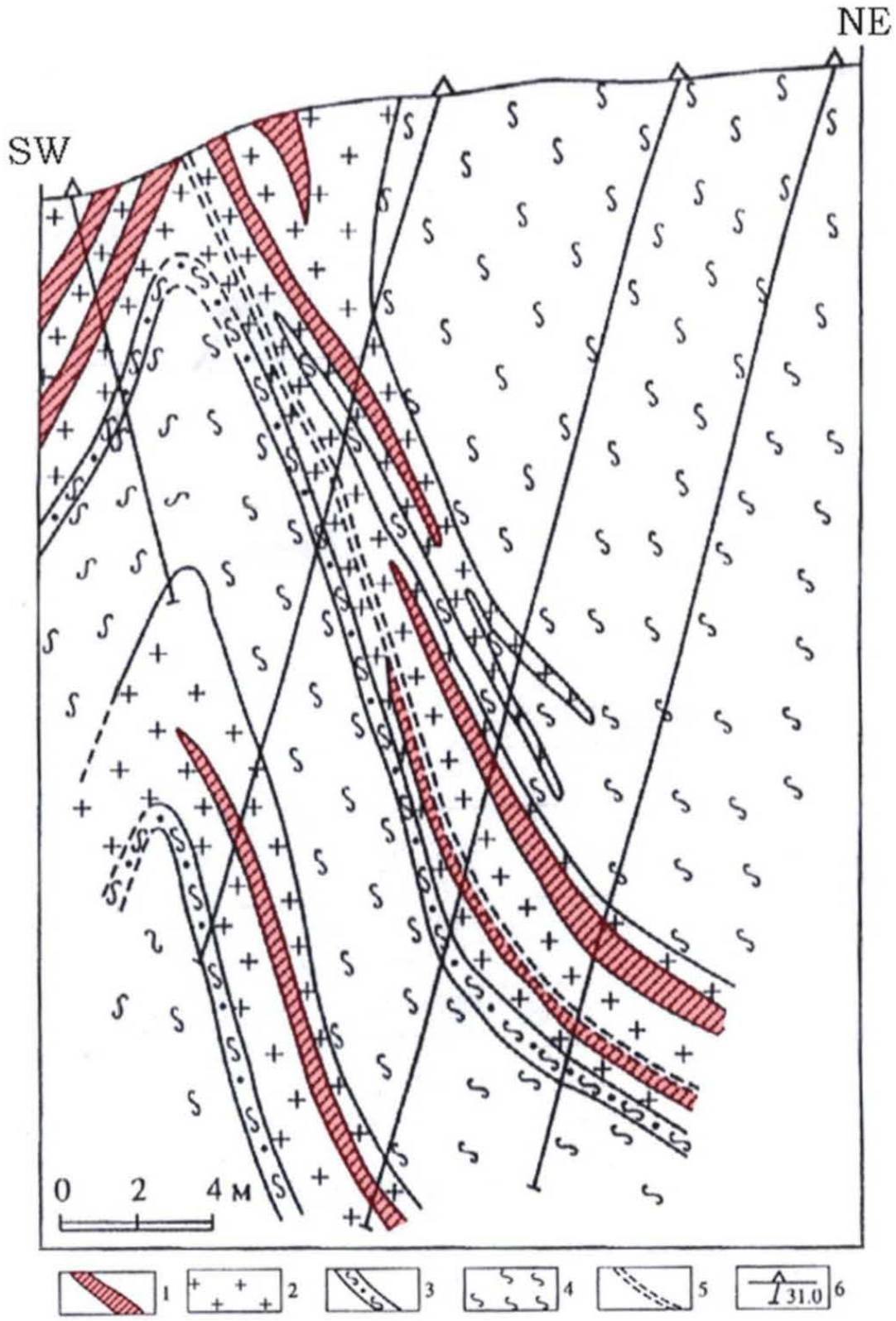

Figure 2.5. Geological section of the Dikoe ore-showing central sector. *(modified from «Nevskgeologia» and «VSEGEI»).* **1.** Ore bodies (quartz-feldspathic metasomatite with U-grade > 0.03%; **2.** Pegmatoidic granite with U-grade (0.005-0,02%; **3.** Porphyroblastic biotite gneiss; **4.** Migmatized biotite and garnet-biotite gneiss; **5.** Mylonite suture; **6.** Drill holes.

2.1.2. Skalnoe ore-showing

The Skalnoe ore-showing was discovered by «Nevskgeologia» in 1980. Various ground surveys (geological and geophysical on a scale of 1:50,000 and 1:10,000) following the airborne gamma-spectrometric anomalies were provided in the area.

Regionally it is located in the intersection of the Voron'ya-Kolmozero tectonic zone and Ladoga-Barents Sea zone (Figure 1.4), the structural control is conditioned by the junction of submeridian Urgozero and north-western Uraguba faults (Figure 2.1).

Over 600 radioactive anomalies were discovered in the area, most of them can be grouped in five zones of anomalous radioactivity (Figure 2.6). The maximum radioactivity (up to 1500 μR/h) was recorded in zones II and III. The anomalies are connected to quartz-feldspathic metasomatite and pegmatoidic bodies (Figure 2.7) striking north-west and concordant or subconcordant with enclosed migmatized biotite and garnet-biotite gneiss, containing interlayers of amphibole gneiss, schist and amphibolite. Cataclasis and superimposed silicification, muscovite, quartz-muscovite and biotite-muscovite alterations are observed in these rocks.

The uranium grade varies from 0.11 wt % to 0.24 wt % and up to maximum of 0.39 wt % *(Afanasieva et al.; 2007)*.

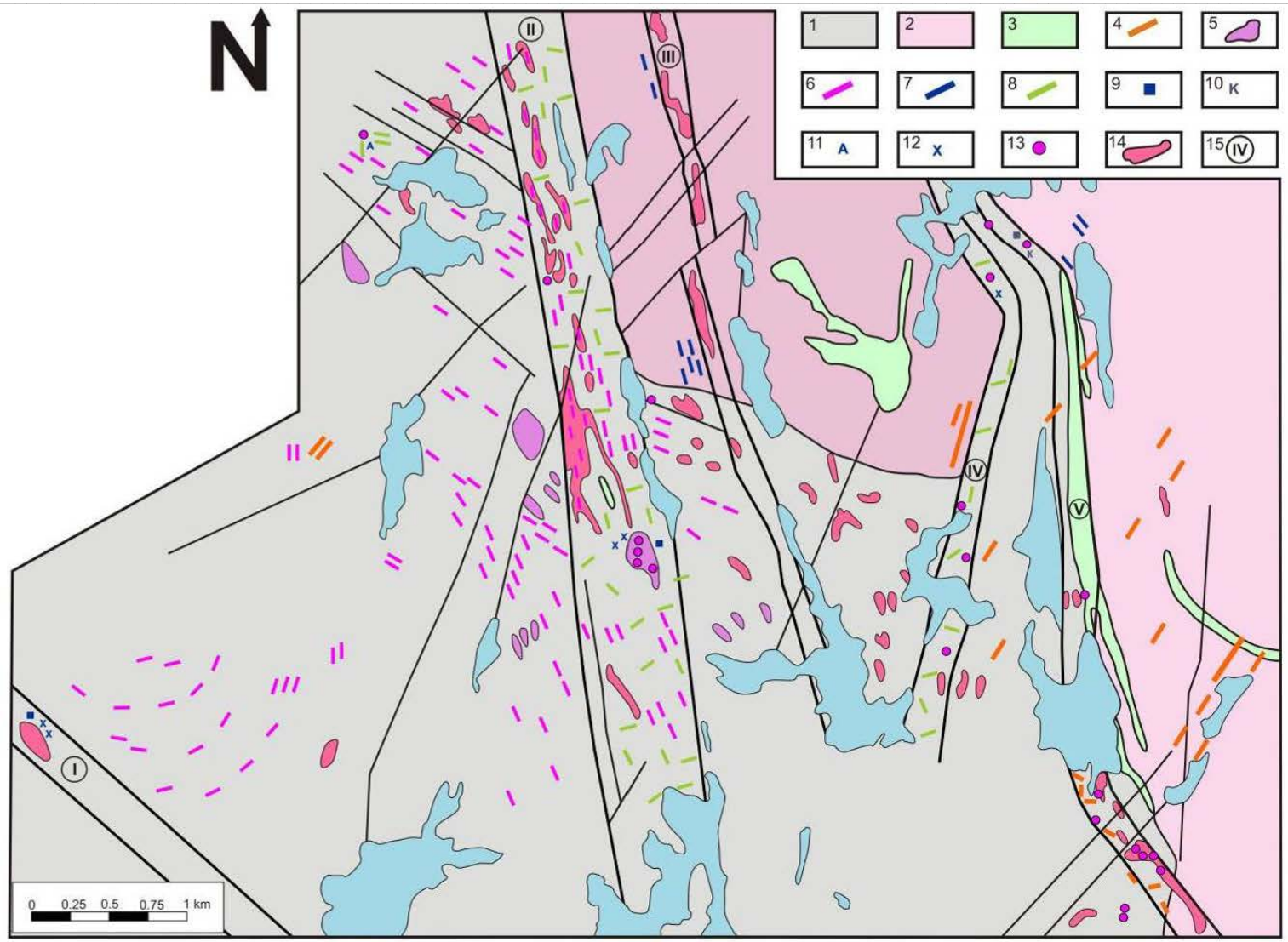

Figure 2.6. Geological map of the Skalnoe ore-showing area (modified after Nevskgeologia). 1. Migmatized garnet-biotite gneiss, 2. Plagiogranite, 3. Amphibolite, 4. Dolerite, gabbro-dolerite, 5. Quartz-plagioclase metasomatite (on a map scale), 6. Quartz-plagioclase metasomatite (out of the map scale), 7. Quartz-microcline-plagiocalse metasomatite (out of the map scale), 8. Greisenization, 9. Sulphidization, 10. Carbonatization, 11. Albitization, 12. Chloritization, 13. Anomalies > 1000 μR/h; 14. Anomalous groups, 15. Anomalous zone numbers.

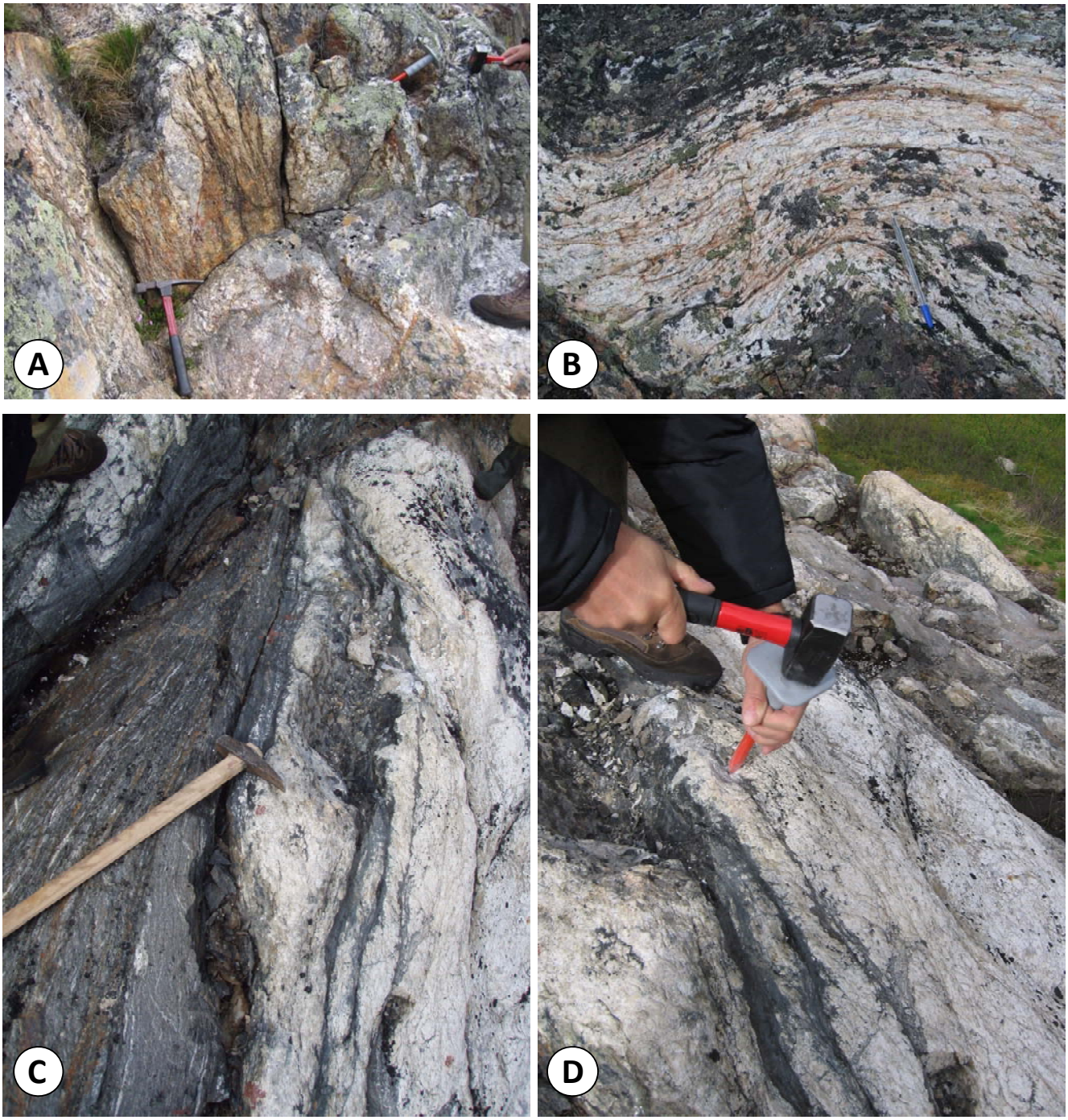

Figure 2.7. Uranium-bearing rocks of the Skalnoe ore-showing. **A.** Outcrop 90 showing intrusive quartz-feldspar pegmatoid dyke < 1m wide with quartz-boudinage structures. **B.** Granitoid vein, boudinated and subconcordant with the host gneiss**; C.** Outcrop 89 at Skalnoe showing the sharp contact between vein-like intrusion of quartz-feldspar granitoid (right) and the darker fine grained mylonitic gneisses (left) where coarse grained bitotie restite occur and **D.** Radioactive granitoid vein-like body (up to 1000 µR/h in biotite rich layers).

.

2.2. Paleoproterozoic occurrences

The uranium occurrences of this age are located within the Ladoga-Barents Sea tectonic zone (2200-2100 Ma – *Anderson; 1984*) (Figure 1.4).

The host rocks are represented by migmatized biotite, garnet-biotite and amphibole-biotite gneiss and schist of the Kola series, which are deformed in a system of linear submeridian folds with a limb distance of several kilometers. The uranium occurrences are usually associated with the exocontacts of the Kaskeljavr granite massifs and are also confined to the intersection of regional sublongitudinal faults and interfaced north-eastern striking faults.

The ore-bearing structures are distinctly marked in geophysical fields *(Savitski et al., 1985)* and present steeply dipping mylonite and cataclasite submeridian zones, injected with veins of pegmatoidic, aplite-pegmatoidic granite and quartz-plagioclase-microcline metasomatite (2450-2150 Ma; *Anderson; 1984*). The thickness of such zones is up to 500-700 m, and more than a half of them are occupied by granitoidic bodies. These rocks are cut by Paleoproterozoic concordant and transverse mafic dykes (1860±30 Ma; *Sabotovich; 1987*) and also by the Paleozoic lamprophyre dykes. The intensive mylonitization and cataclasis within described tectonic zones is accompanied by the wide development of quartz-sericite and quartz-chlorite-sericite sheared rocks, microcline and chlorite-albite metasomatite, and also albitite, dated by Rb-Sr and U-Pb method at 2200±200 Ma (*Vinogradov et al.; 1984*).

Most of the uranium occurrences are concentrated in the pegmatoidic granite veins and quartz-feldspathic metasomatite, which suffered superimposed chlorite-albite alterations. The mineralized zones are oval-shaped and extend in submeridian direction for 1.0-1.5 km with several hundred meters wide. They contain lens-shaped ore bodies up to 400-500 m long and 10-15 m thick with average uranium grade between 0.02 and 0.2 wt % *(Savitskii et al.; 1995)*.

The most representative occurrences of this type are: Polyarnoe, Namvara, Cheptjavr and Javr ore-showings, besides there are about 10 similar manifestations observed in the Litsa district.

2.2.1. Polyarnoe ore-showing

The Polyarnoe ore-showing was discovered by «Nevskgeologia» as a result of following airborne gamma-spectrometric anomalies. In 1970 it was intensively explored with various ground geological and geophysical surveys (scale 1:50,000 to 1:2,000) with drilling along 7 profiles (40 drill holes), outcropping and trenching.

The Polyarnoe ore-showing is situated located in the western flank of Ladoga-Barents Sea regional tectonic zone, close to the western exocontact of Paleoproterozoic Kaskeljavr granite complex, at the junction of Nyasyukk-Kuchintundra submeridian fault with the interfaced north-east striking fault (Figure 2.1).

The rocks enclosing the ore-showing consist of migmatized and aluminous gneiss of the Kola series, metamorphosed to the amphibolite facies. The rocks are deformed into longitudinal steeply deeping isoclinal folds 500-700 m wide. The fold cores are injected with vein-like lense-shaped bodies of pegmatoidic granite, quartz-feldspathic metasomatite and microclinite, developed after them (Figure 2.8). The metasomatite replace up to 30% of the granite volume. The pegmatoidic bodies are surrounded by porphyroblastic gneiss, where porphyroblasts are made of microcline (Figure 2.9).

The cores of the anticlines are crosscut with the zones (200-300 m) of cataclasis, mylonitization and intensive tectonic schistosity, steeply dipping to the east. Up to 70% of the thickness of these zones is made of quartz-chlorite-albite metasomatite, considered to be a result from retromorphosis to the low grade metamorphic conditions, corresponding to the formation of siliceous-potassic metasomatite *(Vingradov et al.; 1984)*. Sometimes superimposed carbonate alteration with sulphides is observed; the Pb-Pb age of galena is dated at 380±20 Ma *(Savitskii et al.; 1995)*. All the preceding rocks are cut by mafic dykes of Paleoproterozoic Nyasyukk complex.

The ore-bodies are located mainly in the inner parts of the cataclastic and mylonitic zones, they consist of chlorite-albite metasomatite and albitite with uranium grade 0.01-0.08 wt %. The shape of the bodies is complex, but on the whole is lense-like, with the thickness from 3-5 to 40-50 m. Within them there are more enriched lenses (1.0 x 7.0 m) with uranium grade up to 0.2 wt % *(Savitskii et al.; 1995)*. The extension of the ore-bodies was traced by drilling to a depth of more than 200 m (Figure 2.10).

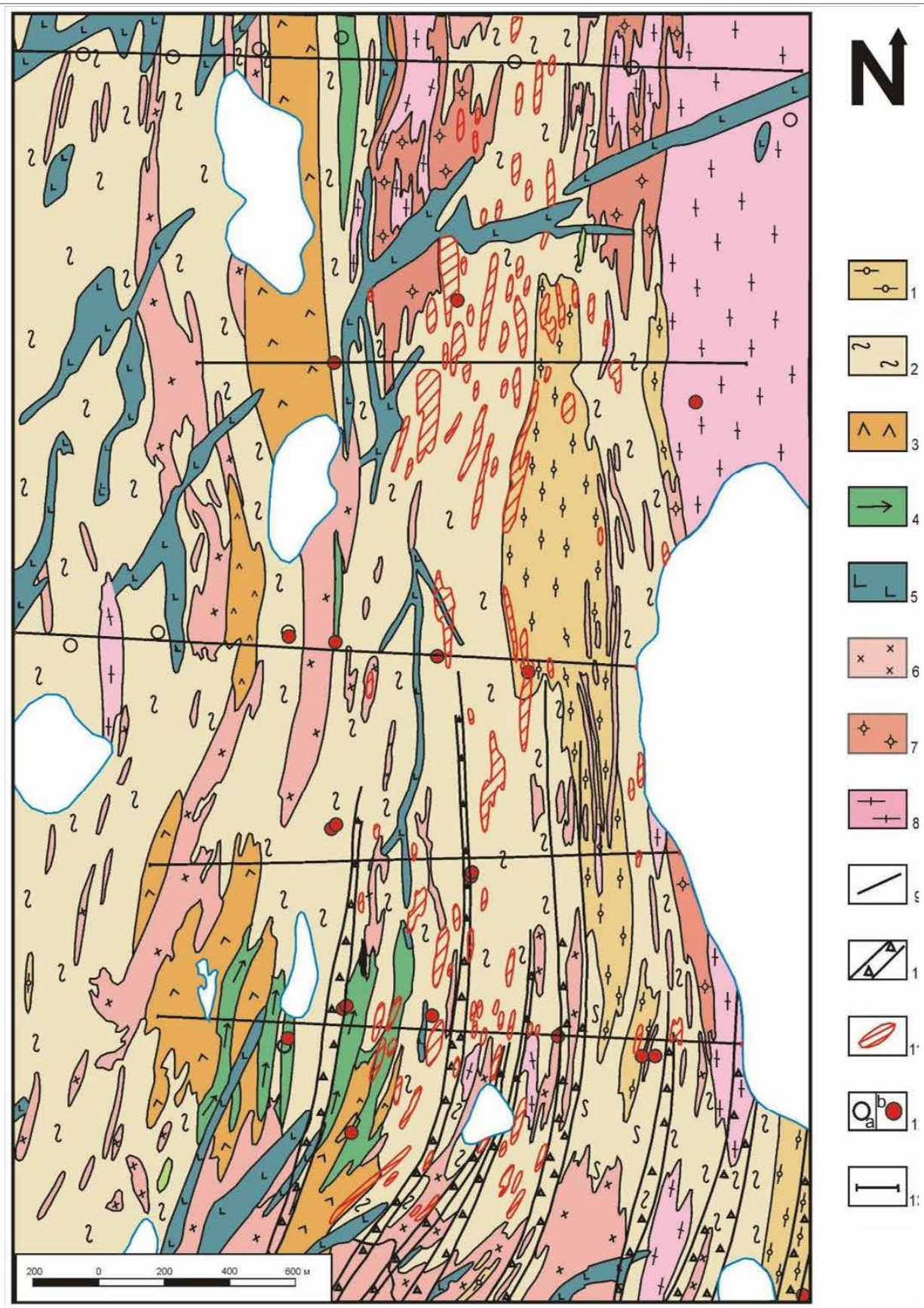

Figure 2.8. Geological map of the Polyarnoe ore-showing area (modified from *«Nevskgeologia»; 1970).* 1. Migmatized garnet-biotite gneiss; 2. Migmatized biotite gneiss; 3. Amphibole and biotite-amphibole gneiss; 4. Amphibolite; 5. Gabbro and gabroo-dolerite; 6. Granite and pegmatite; 7. Porphyroblastic leucocratic microcline granite; 8. Plagioclase and microcline-plagioclase granite and migmatite; 9. Faults; 10. Mylonite and cataclasite zones; 11. Projections of the mineralized zones; 12. Drill holes: regular (a) and with intervals of U > 0.01 wt% (b); 13. Drilling profiles.

It is important to emphasize, that the field observations, provided in the framework of present study, had not detected the described neither chlorite-albite metasomatites nor albitites in the outcrops of the ore-showing. These types of alterations were discovered in the drill core, which is not remained today (Figure 2.9).

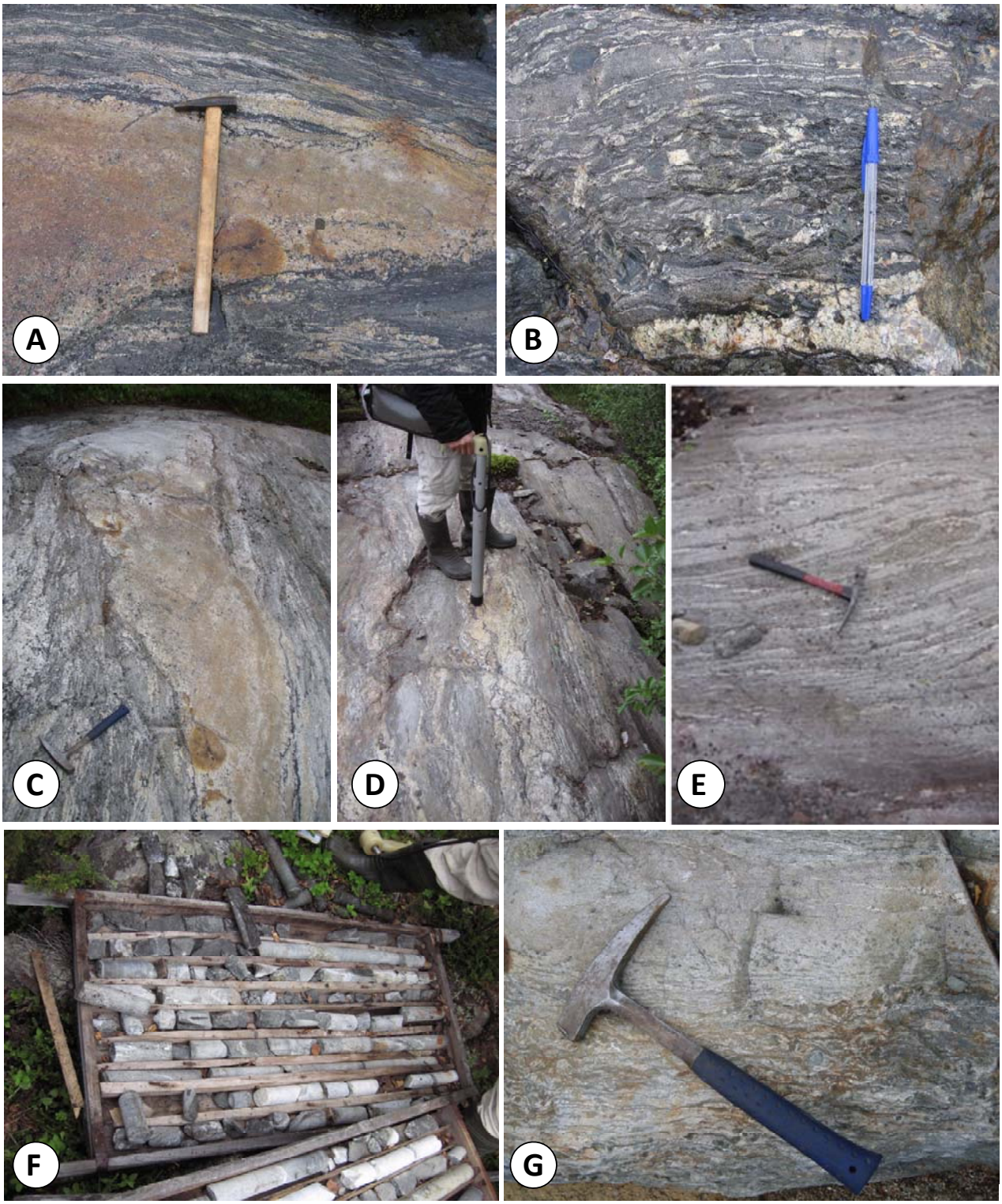

Figure 2.9. Uranium-bearing rocks of the Polyarnoe ore-showing. **A.** Oxidized granitoid vein boudinated and subconcordant with the enclosing biotite-rich gneiss [samples 58-1, 58-2]; **B, E and G.** Migmatized gneiss of the Kola series; **C and D.** Radioactive Early Paleoproterozic granitoid vein-like body, boudinated and subconcordant to the NW striking gneisses of the Kola Suite. Up to 250 cps in the bitote-rich oxidizd zones (Polyarnoe_97); **F.** Drill-hole section preserved in the Polyarnoe occurrence.

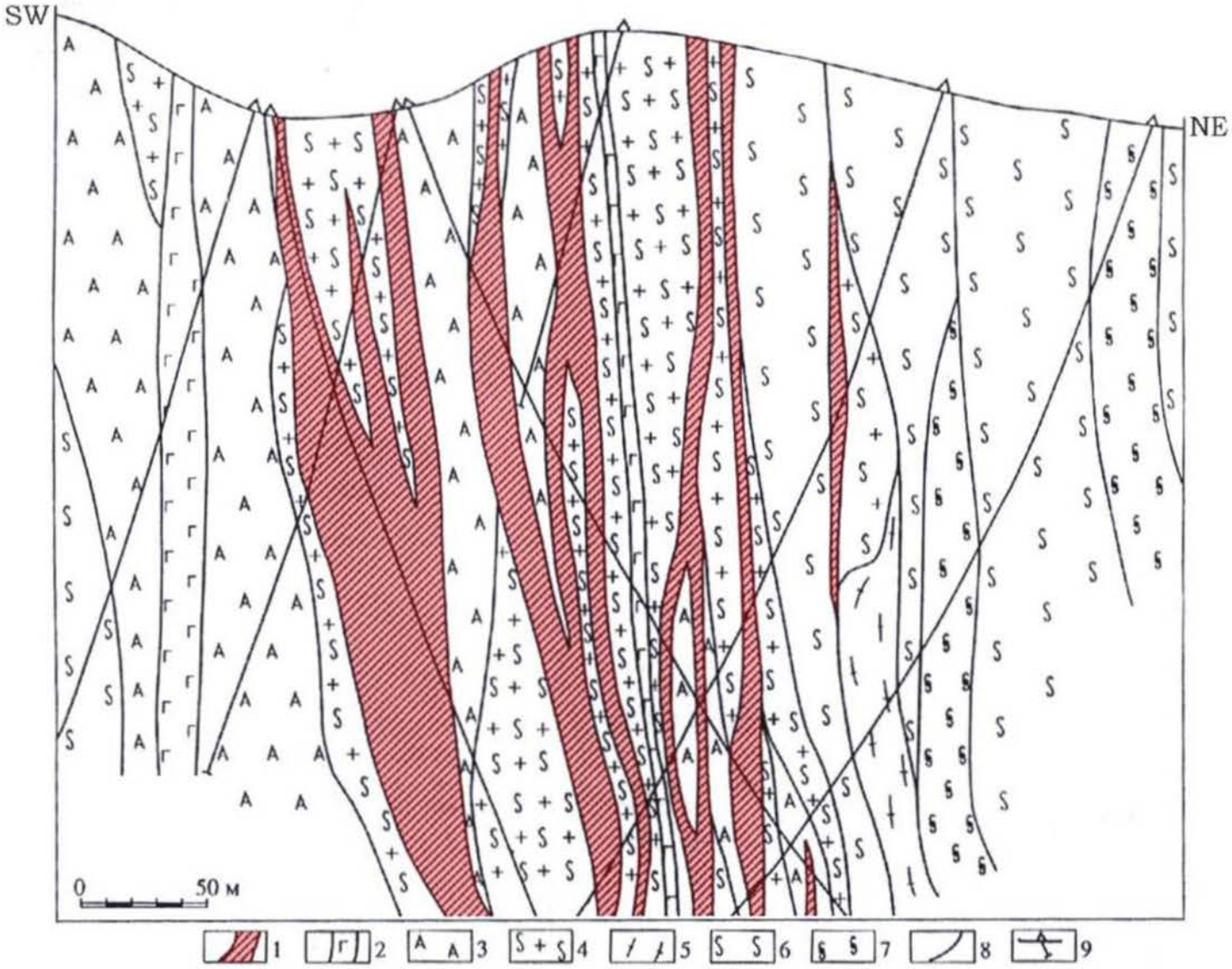

Figure 2.10. Geological section of the Polyarnoe ore-showing central sector *(after «Nevskgeologia» and «VSEGEI»).* 1. Ore-bodies (albite-chlorite metasomatite and albitite with U-grade >0.03%; 2. Gabbro-dolerite and gabbro (Nyasyukk complex; 3. Quartz-chlorite-albite metasomatite; 4. Stripe granitic migmatite after biotite gneiss; 5. Plagio-microcline granite-gneiss; 6. Migmatized biotite gneiss and schist; 7. Migmatized garnet-biotite gneiss and schist; 8. Mylonite and cataclasis suture; 9. Drill holes.

2.2.2. Namvara ore-showing

The Namvara ore-showing was discovered in 1977 by «Nevskgeologia» as a result of radiometric surveys on a scale of 1:25,000. Several trenches, 11 drill holes (to a depth of 75-145 m), electric and magnetic exploration (100 x 20 m grid) were executed in this area.

Regionally it belongs to the Ladoga-Barents tectonic zone (Figure 1.4) and is situated in the north-western limb of Namvara anticline; structurally it is controlled by the submeridian East-Pechenga fault zone (Figure 2.11).

The rocks of Namvara anticline are represented by intensively migmatized biotite gneisses with the interlayers of garnet-amphibole and garnet-kyanite gneisses, sometimes enriched with graphite and sulphides. A sericitic alteration is observed in these rocks. The leucosome of the migmatite has the composition of anatectic plagiogranite.

Within the longitudinal tectonic zone (450-500 m wide) the rocks are intensively foliated with a general 320-325° strike with wide development of mylonite and cataclasite. The foliation is complicated with synfolded faults parallel to its axis; along them the bodies of pegmatoidic plagiogranite with high radioactivity (up to 3700 cps) are located. According to the reports of «Nevskgeologia» the granite displays albite and microcline alteration.

The dimension of the ore-showing is 650 x 450 m, while most of mineralized spots are localized within the 45 x 3 m stripe. The uranium anomalies correspond to mylonitic or cataclasitic zones, strongly oxidized by weathering (Figure 2.12), and are located in layered bodies of migmatite, pegmatoidic veins with associated biotite-enriched selvages.

The uranium grade varies between 0.01 and 0.34 wt %. One of the drill holes intersected 3 intervals with uranium grade 0.01-0.027 wt % on the depth of 39-42 m *(Afanasieva et al.; 2007)*.

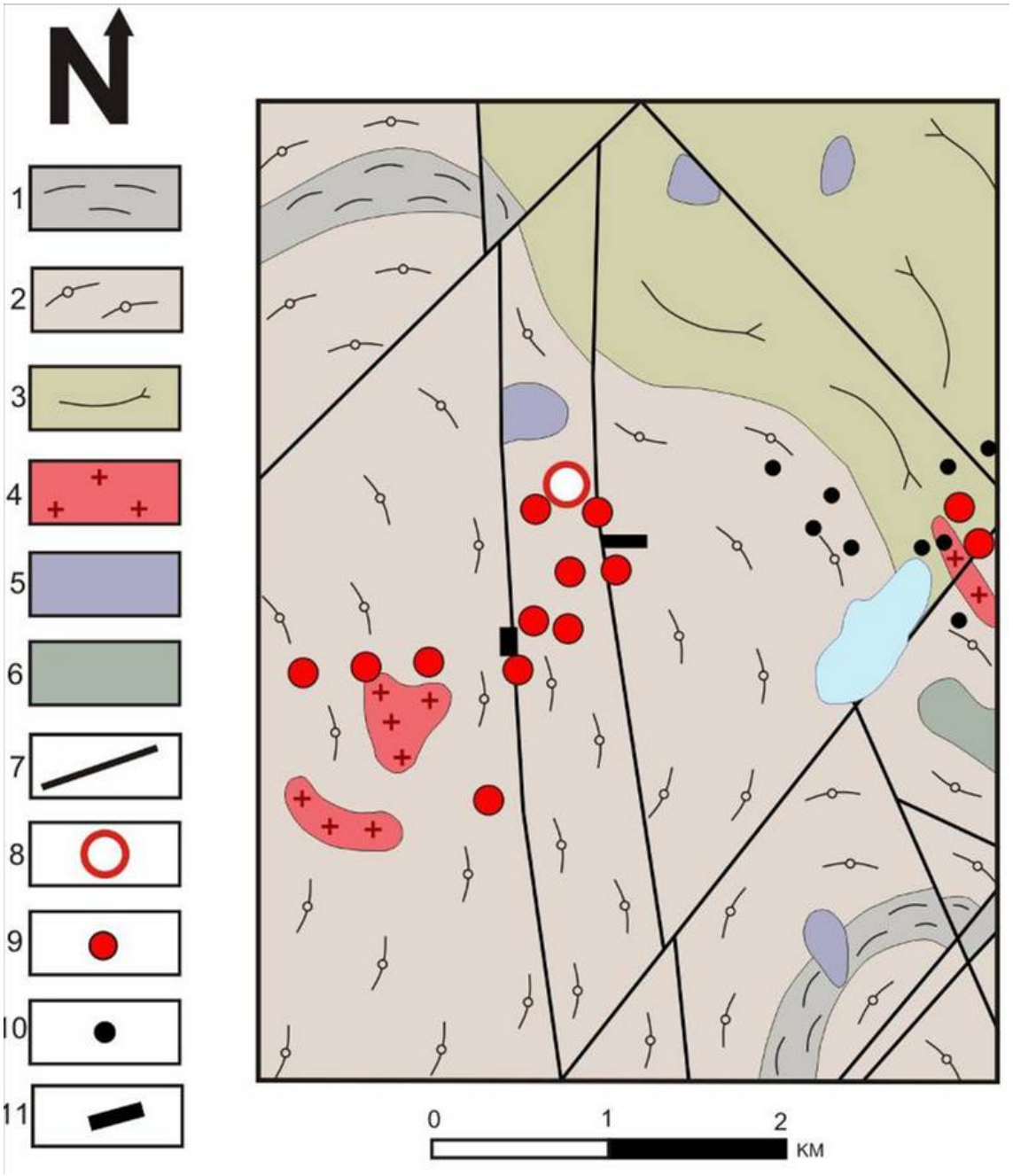

Figure 2.11. Geological map of the Namvara ore-showing area (modified after *Kondakov; 1974).* 1. 1-3 Kola series (Ar2). 1. Biotite gneiss and schist; 2. Garnet-amphibole gneiss and schist; 3. Amphibole, biotite-amphibole gneiss and schist; 4. Late Archean plagioclase and microcline-plagioclase granite; 5. Gabbro, gabbro-norite; 6. Metaolivinite; 7. Faults; 8. Namvara occurrence; 9. Radioactive anomalies; 10. Drill holes; 11. Trenches.

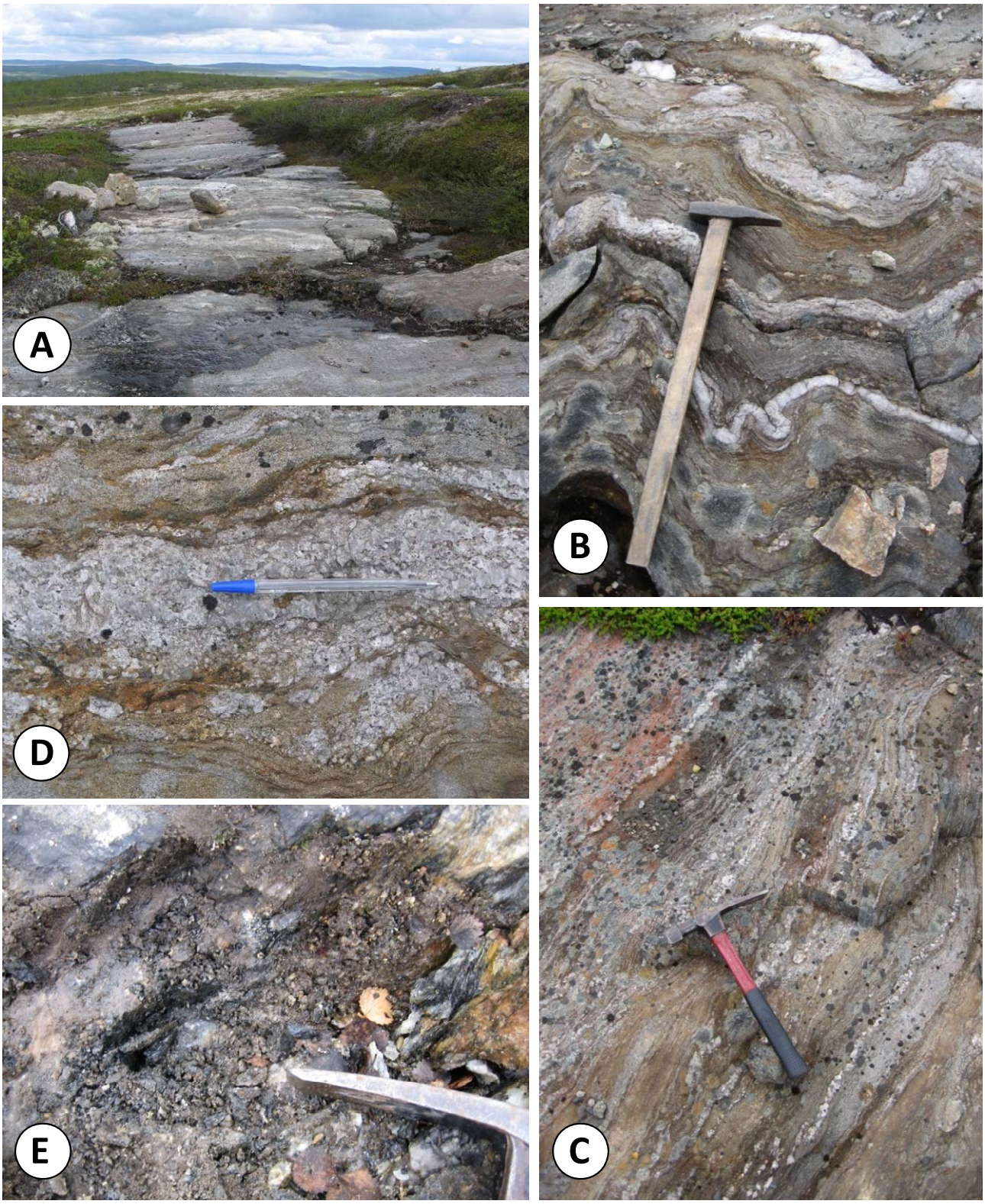

Figure 2.12. The uranium-bearing rocks of the Namvara ore-showing. **A.** General view on the trench; **B and C.** Foliated migmatized hosting gneiss [sample 134a]; **D and E.** Oxidation and alteration.

2.2.3. Cheptjavr ore-showing

The Cheptjavr ore-showing was discovered by «Nevskgeologia» in 1974. It was explored by complex geological-geophysical surveys (scale 1:10,000): radiometric, electric and magnetic, spur gamma-survey and drilling (14 drill holes).

It is located in the northern exocontact of Litsa massif with migmatized biotite gneiss of the Kola series (Figure 2.1), penetrated by Archean diorite and Paleoproterozoic pegmatoidic plagiogranite. The structural control corresponds to the Cheptjavr latitudinal fault zone. This regional zone has an important significance for uranium localization in the district and was revealed by structural geophysical surveys, satellite image interpreting and in some places traced by drilling. Within Cheptjavr fault zone the rocks are intensively fractured and often brecciated with superimposed processes of feldspatization, chloritization, silicification and biotite enrichment *(«Nevskgeologia»; 1976)*.

44 anomalies were revealed in the area of the ore-showing. They are confined within silicified pegmatoidic granite with cataclasis, biotite gneiss and Litsa-Araguba granite. The maximum radioactivity (up to 2300 μR/h) occurs in structures (diaclases), mainly oriented in 60° and enriched in biotite (Figure 2.13, Figure 2.14). The average uranium grade is 0.045 wt % *(Afanasieva et al.; 2008)*.

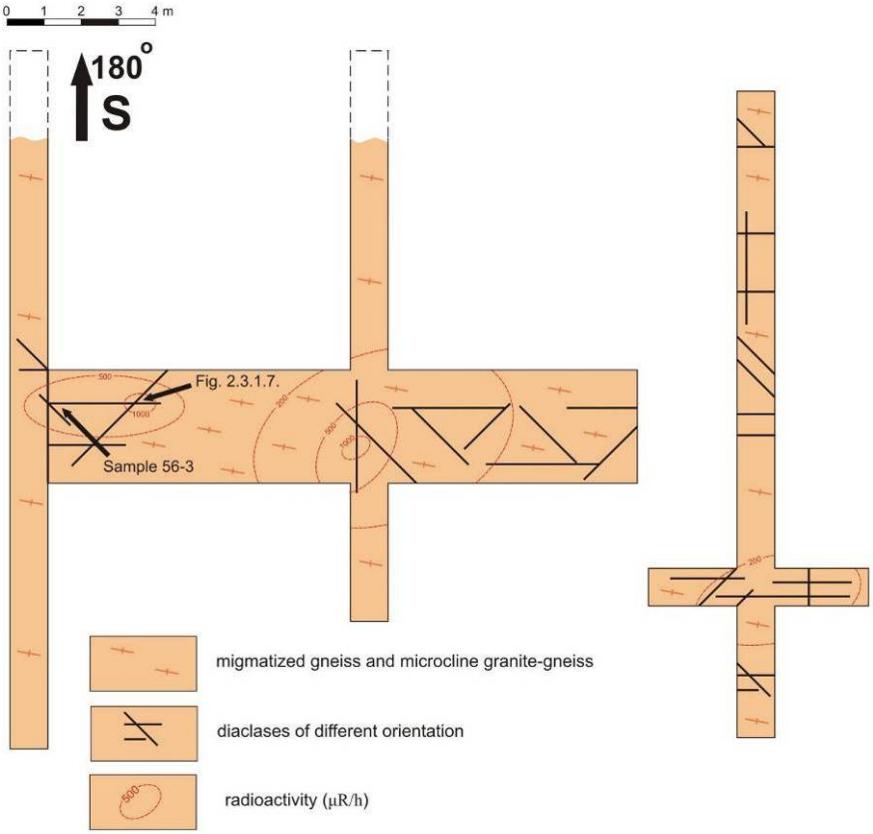

Figure 2.13. Scheme of the trenches in the Cheptjavr ore-showing *(compiled after field work 2007).*

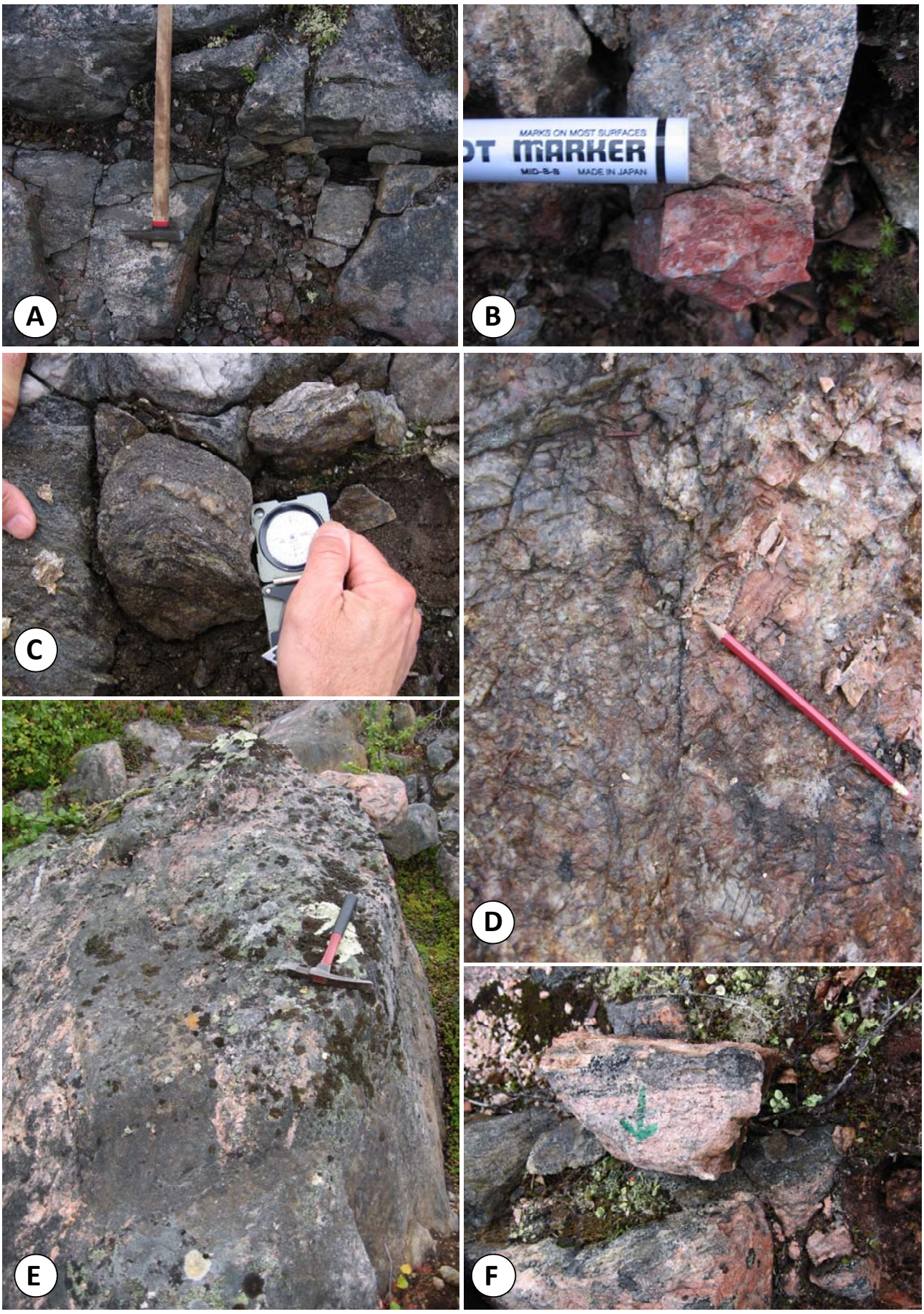

Figure 2.14. Uranium-bearing rocks of the Cheptjavr ore-showing. **A.** Structures enriched in biotite with anomalous (600 μR/h) radioactivity; **B.** Microcline vein in the migmatite.

2.2.4. Javr ore-showing

The Javr ore-showing was discovered in 1955 as result of accompanying exploration during the geological surveys (scale 1:200,000 and 1:10,000). In 1974 the forces of «Nevskgeologia» provided several geological and detailed radiometric surveys (0.5 x 1 m grid), hand drilling and trenching.

Regionally it is situated at the intersection of the Litsa-Araguba with the Ladoga-Barents Sea tectonic zones, in the northern exocontact of the Litsa massif with the gneiss of the Kola series (Figure 2.1).

Several anomalies were discovered in the sector of the ore-showing. The uranium mineralization is associated with tectonic fractures in the fragmentation zones of the microcline granite, close to the contact with the migmatized biotite gneiss. The fractures have submeridian and sublatitudinal orientation and are filled with the clastic material, cemented by quartz and fluorite. The microcline granite is remarkable for its heightened radioactivity (40-100 μR/h), which reaches anomalous values (up to 1000 μR/h) in the intersection of the differently orientated structures (Figure 2.15). In such knots the enrichment in biotite, up to monomineralic biotite aggregates, is observed.

The average uranium grade is 0.04-0.05 wt % with a maximum of 0.103 wt % *(«Nevskgeologia»; 1957).*

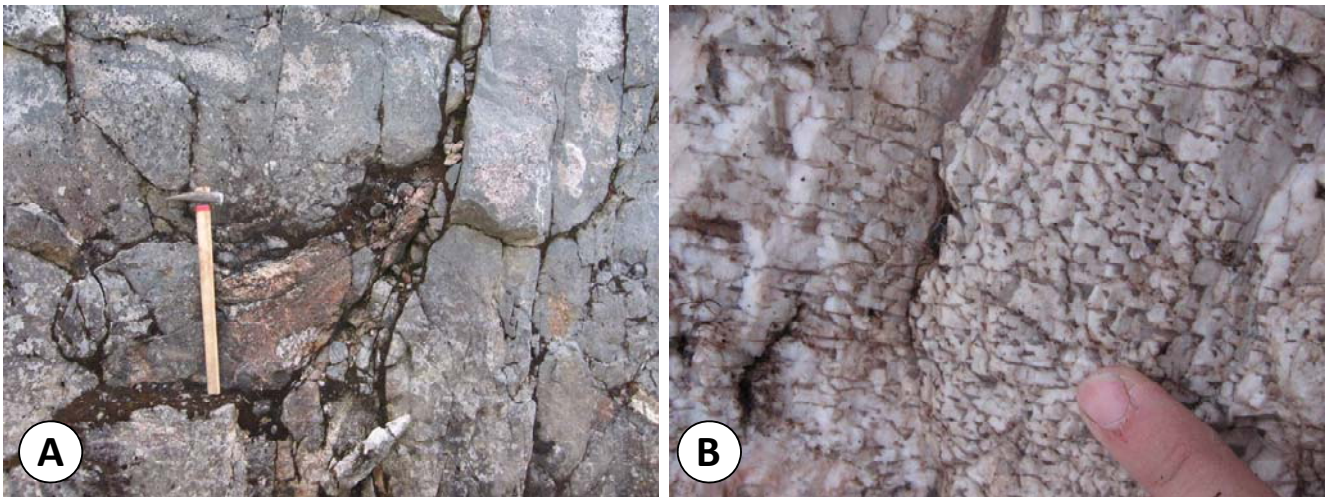

Figure 2.15. The uranium-bearing rocks of the Javr ore-showing. **A.** Anomalous radioactivity (up to 1000 μR/h) at the junction of the differently orientated structures, filled with up to monomineralic biotite aggregates; **B.** Microcline granite with heightened (40-100 μR/h) radioactivity.

2.3. Neoproterozoic occurrences

The REE-P-U mineralization is located in Mezoproterozoic - Neoproterozoic (Riphean - Vendian) terrigenous sediments within Sredny-Rybachy Peninsulas. They are associated with phosphate-bearing arkose sandstones and siltstones of the Kil'din series and conglomerate-breccia of the Volokovaya series.

Kil'din series present a transgressive-regressive sequence and consist of 5 suits (Figure 2.16). Pyaryajarvi suit (pr) – the basal stratum, discordant with the Late Archean basement (plagio-microcline granite and pegmatite), which displays no significant features of weathering along the unconformity surface. Palvi (pl) and Poropelon (pp) suits, which correspond to the transgressive maximum. Then Zemlepakhti (zm) suit littoral and Karujarvi (kr) suit of drying lagoon facies sediments.

Volokovaya series formations of Kuyakan (kk) and Puman (pm) suits trangressively and unconformably overlay the Zemlepakhti and Karujarvi suits, and continually pass to the Rybachy series: Motka (mt), Lonsk (ln), Pereval (pv) and May (m) suits.

The phosphate-bearing sediments are developed within the area of about 200 km^2 and their total thickness is 25-35 m. The phosphorus occur in disk-shaped nodules or clastic-concretions 0.5 x 0.7 cm. P_2O_5 grade varies between 0.5 and 6 wt %. Within phosphate-bearing horizons there are interlayers with an average uranium grade of 0.005-0.008 wt %, which contain lens-bodies up to 1.5 x 200 m with maximum uranium grade of 0.01 wt %. Besides uranium the nodules display the presence of REE (up to 0.35 wt %), Y (up to 0.4 wt %), Pb (up to 0.07 wt %) and Sr (up to 800 ppm) *(Negrutza et al.; 1981)*.

The uranium and accompanying elements are concentrated in francolite ($Ca_5[PO_4,CO_3]_3F$), which occur in the nodules as a fine-grained or cryptocrystaline aggregates. Besides francolite the uranium-bearing Sr-Ba-apatite and complex phosphate minerals of variable composition, albite, chlorite, rutile and pyrite are observed *(Negrutza et al.; 1981)*.

The Pb-Pb age of phosphate nodules formation was estimated at 830±70 Ma, and their genesis is considered to be syn-sedimentary. Negrutza and co-authors suppose the local source of the components, probably within the Litsa granitoids.

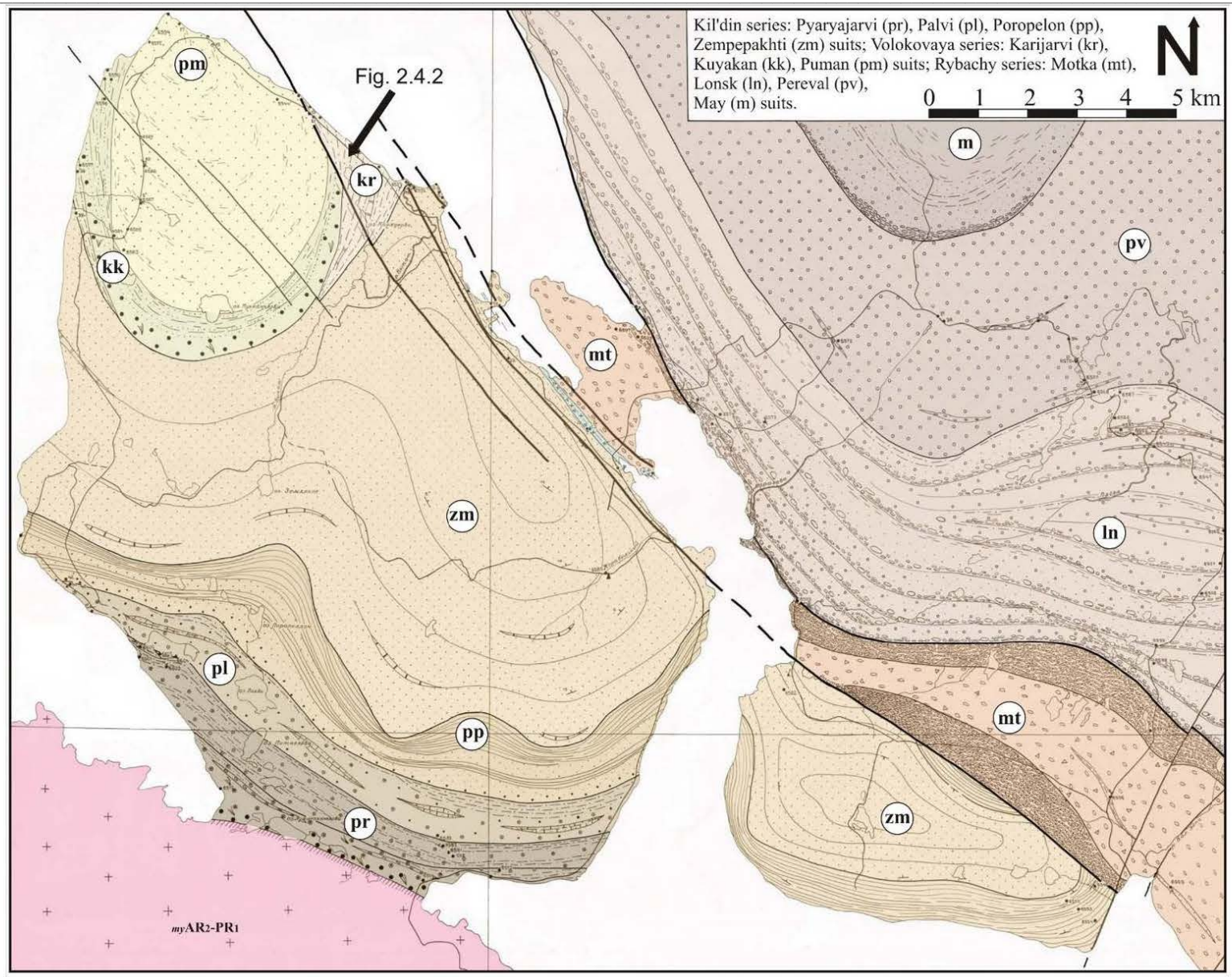

Figure 2.16. Geological map of the Sredny-Rybachy Peninsulas *(after Afanasieva et al.; 2007)*.

During the field work, provided in the frame of present study, no significant increase of radioactivity was observed in siliciclastic sediments of Sredny-Rybachy Peninsulas. Within the fine-grained siltstones the oxidized horizons were observed. They are partly reduced (along subvertical fractures), probably by diagenetic fluids, deriving from the enclosing reduced sediments of dark green color with pyrite (but no organic matter has been observed on the field and in thin sections). They are immature, although partly deposited in a continental environment: ripple marks, mud-cracks, etc. The presence of oxidized sediments is scarce, restricted to a few (0.1-1 m thick) horizons intercalated within the predominantly reduced sedimentary pile (Figure 2.17).

The reduced and immature character of the Riphean sediments in the Sredny-Ribachy Pensinsula constitutes unfavorable conditions to generate oxidized acid brines able to leach and transport uranium, as found in the Athabasca Basin *(Kister et al.; 2007)*. Besides they don't display other important geological preconditions, like graphite-bearing formations in the basement, leaching and strong alteration of the sedimentary cover.

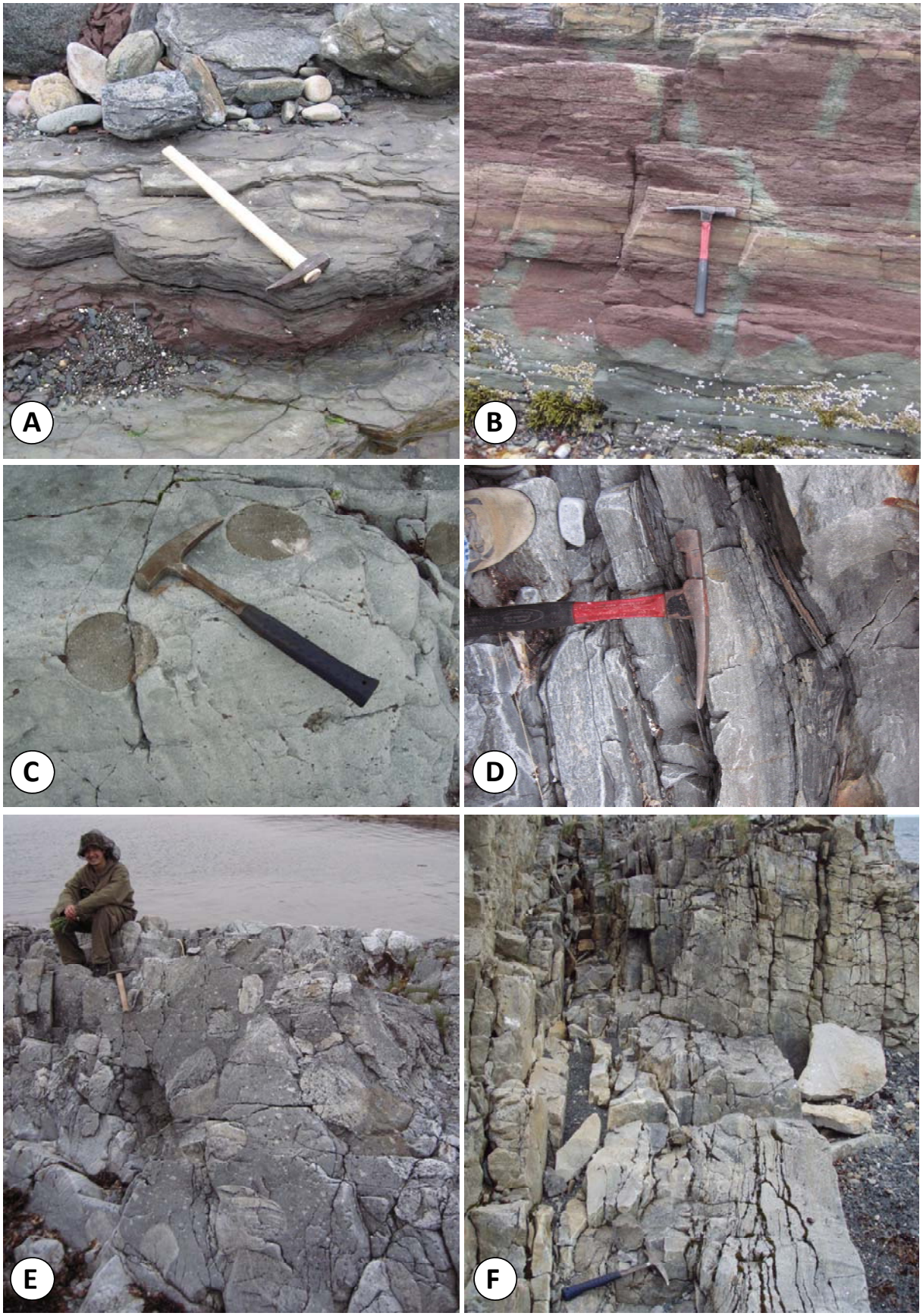

Figure 2.17. Mesoproterozoic sediments of the Sredny-Rybachy Peninsulas. **A.** Karujarvi suit siltstone; **B.** partly reduced oxidized horizon; **C.** dropstone observed in sandstone; **D.** siltstone, **E.** conglomerate; **F.** fault affecting the Kurujavri and Puman series.

2.4. Paleozoic occurrences

The major ore-showing in the district Litsevskoe and related occurrences of this type are mainly concentrated in the axial sector of the Litsa-Araguba regional tectonic zone (Figure 1.4).

Most of the occurrences occur within the exocontact of the Litsa and the Lebyazhka massifs and are mainly located in biotite and sillimanite-biotite gneiss of the Kola series, migmatized by the granite. The average uranium content in the migmatized rocks is 2.4-2.9 ppm and thorium content is 18-26 ppm.

The uranium mineralization is controlled by the zones of intensive fracturing and brecciation, filled with albite-hydromica-chlorite metasomatite *(Savitskii et al.; 1995)*. Alteration zones have a thickness up to 40-50 m and contain ore-bodies occurring as gently dipping lenses and stockworks. Their length reaches tens of meters and their thickness is measured from several centimeters up to 30 m. The uranium grade in the ore-bodies varies from 0.01 wt % up to 0.1 wt %; thorium – from 0.005 wt% to 0.01 wt %.

As it was mentioned above, the Litsevskoe ore-showing is the most significant occurrence of this type and age. It is considered to be a small deposit with the prognostic reserves of 2,869 tons *(Afanasieva et al.; 2007)*. Besides Litsevskoe there are several occurrences (Beregovoe ore-showing and others) of this type observed in the district.

2.4.1. Litsevskoe ore-showing

The Litsevskoe ore-showing was discovered in 1962. In 1973-1974 it was explored by «Nevskgeologia» with various geological and geophysical surveys, abundant drilling and trenching. It is situated at the north-eastern exocontact of the Lebyazhka massif at the intersection of the Litsa and Cheptjavr faults within migmatized gneiss of the Kola series (Figure 2.1), deformed into sublatitudinal folds with limbs dipping at 50-60°. The folds are intersected by concordant and transverse tectonic faults, filled with cataclasites and breccias (Figure 2.20), sometimes with fragments of arkoses and conglomerates (presumably of Riphean age) *(Savitskii et al., 1995)*. These faults have a thickness from 3-5 m up to 30 m and steeply dipping: the north-eastern faults dip to the north-west; the submeridian ones to the south. From field work observations, provided in the framework of this thesis, several types of anomalies were discovered in the sector of the Litsevskoe ore-showing, which presumably correspond to different stages of uranium enrichment, as discussed thereafter.

- Anomalies, associated with migmatization processes (Paleoproterozoic event), were observed in the host gneiss, which presents the former sediments of variable nature: pelite (now biotite-gneiss), arkose (now feldspar-gneiss) and sandstone (now quartzite). They are migmatized to various degrees. Evidence of partial melting, such as leucosome veins (Figure 18), can be observed in biotite-rich gneiss, and absent in quartz-rich layers, which have gradual contacts with the melted parts. The highest radioactive anomalies (up to 1500 μR/h) are associated with dislocated biotite enriched gneiss, which have an average radioactivity of 30-40 μR/h, and uranium content between 3 and 123 ppm (Th: 24-46 ppm). The radioactivity of surrounding quartz-feldspathic gneisses is below 20 μR/h linked to an uranium content of 2.5-2.9 ppm and a thorium one of 18-26 ppm.

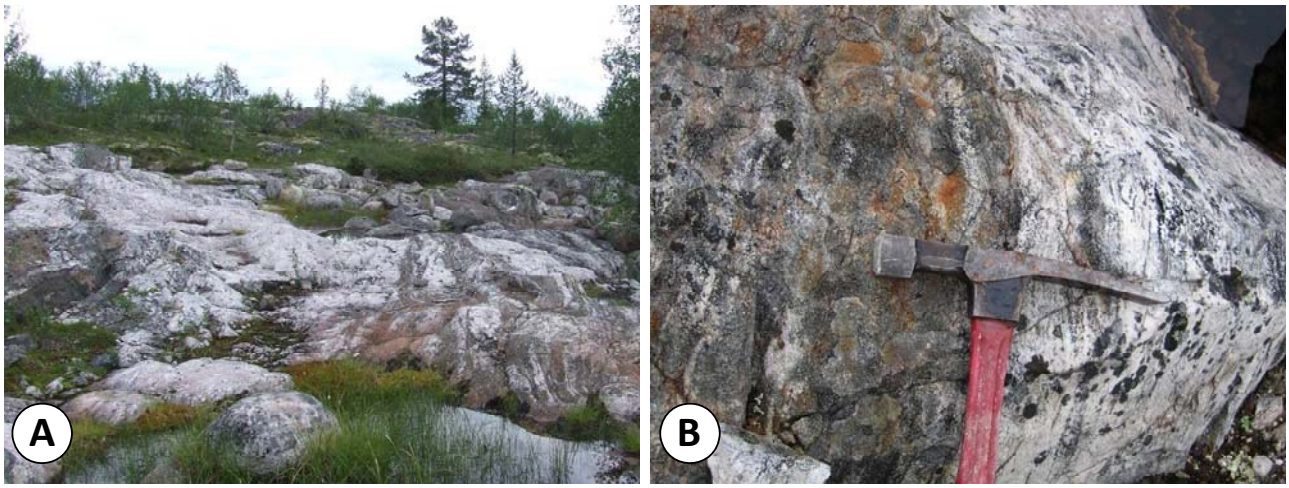

Figure 18. Host rocks of the Litsevskoe ore-showing with **A.** general view on the outcrop of the host gneisses; **B.** migmatized biotite-rich gneiss layer containing quartz-felspathic leucosomes.

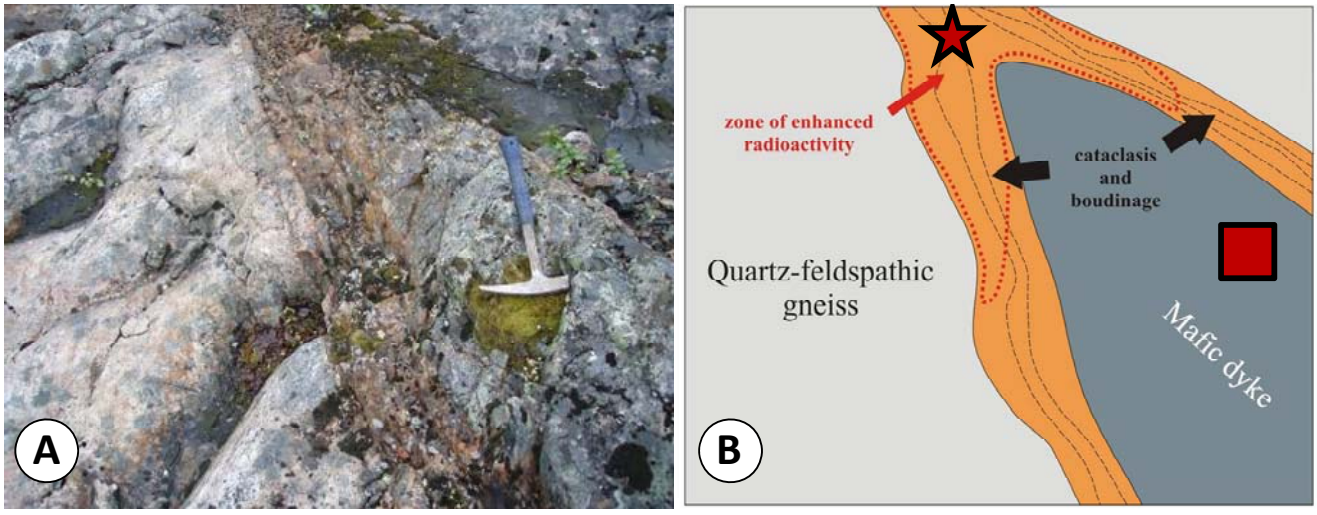

Figure 2.19. A. Photograph and **B.** Scheme showing a NS striking mafic dyke crosscutting NE striking quartz-feldpsar gneisses. The dyke is characterized by fish-like structures, suggesting a syntectonic emplacement, and by cataclased-oxidized boundaries along which, radioactivity increases (>50 μR/h), especially in the stressed nod (top of the photograph, up to 40 μR/h). Field stop Litsa_106. The star and the square indicate respectively the samples 106.2 and 106.5.

- Highly radioactive anomalies were observed along fine-grained mafic dyke, striking at north-west (345-350°) orientation and crosscutting the host gneiss of the Kola series. They are up to 40 meters long with a thickness 0.2-2 m and are displaced by north-eastern faults. The contacts with the hosting gneiss are sheared and oxidized (Figure 2.19), they display anomalous radioactivity of 250-400 μR/h, up to 1200 μR/h in some local spots.

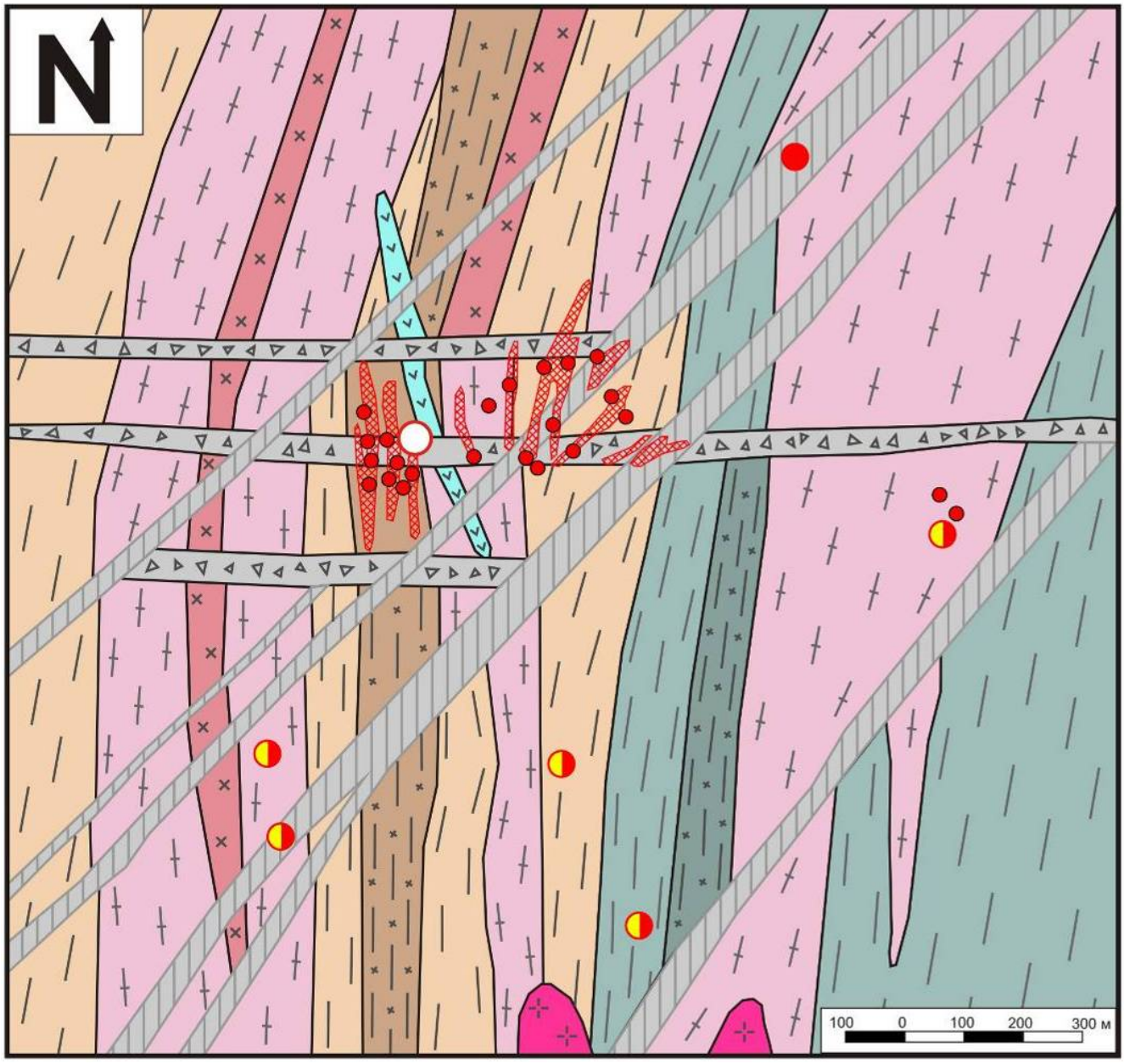

Figure 2.20. Geological map of the Litsevskoe ore-showing area. *(modified after Gromov).* **1.** Biotite gneiss; **2.** Altered biotite gneiss and aplite-pegmatoid granite; **3.** Leucogranite-gneiss; **4.** Cordierite-biotite; garnet-biotite and sillimanite-biotite gneiss; **5.** Altered silica-alumina gneiss and aplite-pegmatoid granite; **6.** Aplite-pegmatoid granite; **7.** Plagio-microcline porphyroblastic granite; **8.** Mafic (dolerite) dyke; **9.** Cataclasis zone; **10.** Breccia zone; **11.** Projections of the ore-bodies; **12.** Litsevskoe occurrence; **13.** Anomalies: U (A) and U-Rn (B); **14.** Drill holes with U > 0.05 wt %.

- The third type of anomalous radioactivity is connected with pitchblende vein within the quartz-muscovite coarse-grained vein, crosscutting biotite-gneisses. The quartz-muscovite vein is non radioactive, 20-30 cm thick and 20 m long. It is striking north-east (60°) and has a subvertical dip. The pitchblende vein is located in the center and has the same orientation; it is 2 cm thick and has a radioactivity over 3000 μR/h (Figure 2.21).

Figure 2.21. A. Photograph and **B.** Scheme of outcrop Litsa_111 showing a subvertical, NE-striking, 20 cm wide, quartzfeldpsar± muscovite vein (outcropping over 22m), which crosscuts NW-striking biotite-rich gneisses. A pitchblende vein, <1 cm thick, NE striking, has outcrops within the felsic dyke over 1.5 m (black and yellow line). Pitchblende vein of the Litsevskoe ore-showing. **C.** Pitchblende vein within quartz-muscovite vein; **D.** Pitchblende with hexavalent uranium minerals [sample 65.1].

According to the previous researches, all discovered ore-bodies are located in the albite-hydromica-chlorite metasomatite, filling the fault and breccia zones, observed within the area of 1.5 km *(Savitskii et al.; 1995)*. Generally, they have a stockwork shape with a complicated internal pattern, located at a depth of 60-150 m. and sometimes rarely they have been traced down to a depth of 250 m. Besides, there are independent lens-like ore-bodies (5-6 x 100-200 m.) located at a depth of 180-200 m. (Figure 2.22). The mineralized bodies are crosscutting the migmatized gneisses and are sub-horizontal. The uranium grade in these bodies varies from 0.01 wt % to 0.4 wt %, with an average value of 0.05 wt %.

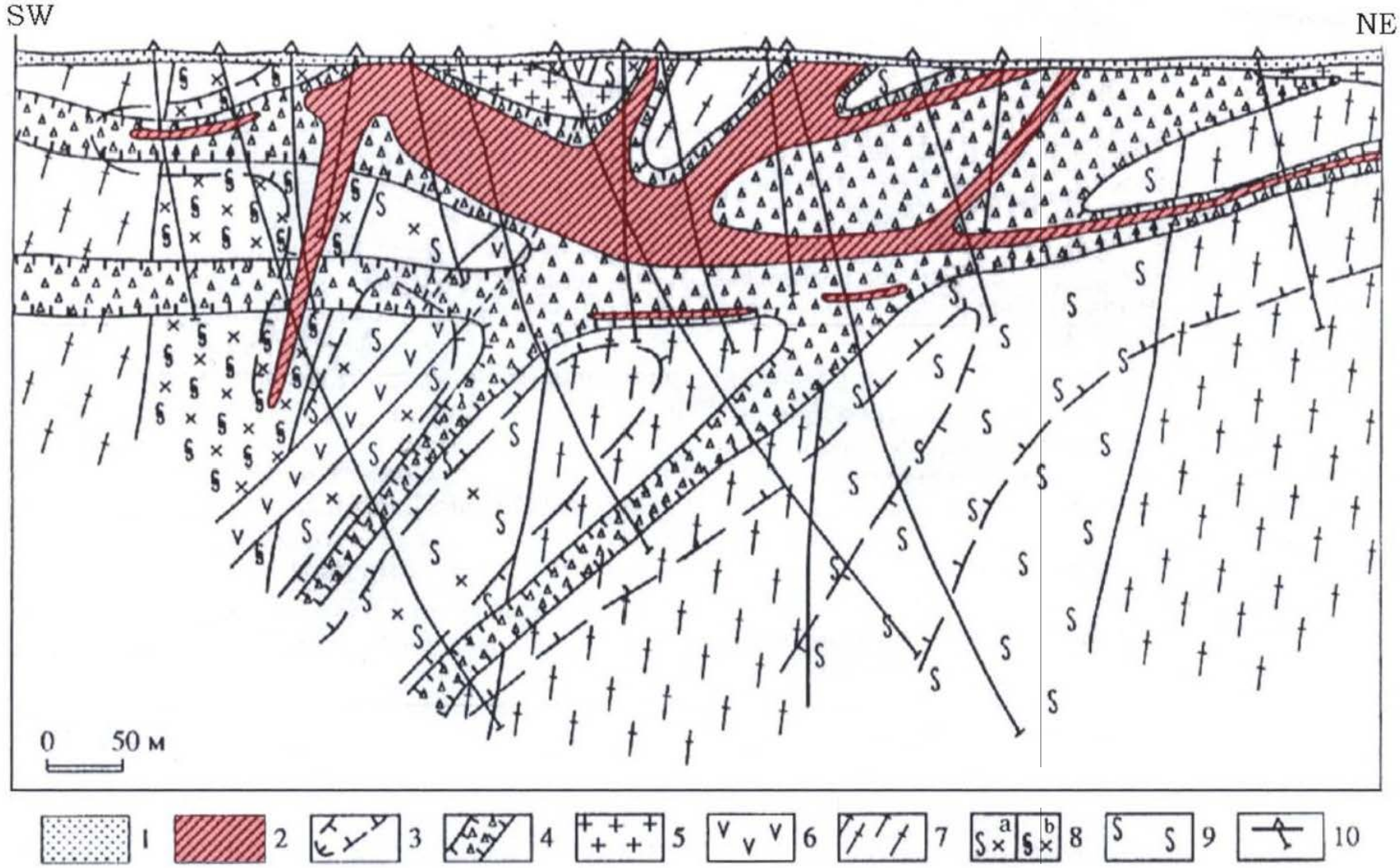

Figure 2.22. Geological section of the Litsevskoe ore-showing central sector. *(after «Nevskgeologia» and «VSEGEI»).* **1.** Moraine; **2.** Ore-bodies (albite-hydromica-chlorite metasomatite and albitite with U-grade > 0.3%; **3.** Boundaries of the metasomatic alteration zone; **4.** Breccias and cataclasis zone; **5.** Leucocratic porphyric granite (Lista-Araguba complex); **6.** Meta-dolerite and gabbro-dolerite; **7.** Intensively migmatized biotite gneiss and granite-gneiss; **8.** Aplite-pegmatoidic injections in biotite (a) and garnet-biotite (b) gneiss and schist; **9.** Migmatized biotite gneiss; **10.** Drill holes.

2.4.2. Beregovoe ore-showing

The Beregovoe ore-showing was discovered by «Nevskgeologia» in 1974. Several detailed geological and geophysical surveys, including drilling and trenching were performed in the area.

It is located at the northern exocontact of Lebyazhka massif among the the Kola series gneisses (Figure 2.1). Regionally it belongs to the intersection of the Litsa-Araguba tectonic zone and the Cheptjavr fault zone. The structural control corresponds to the junction of sub-latitudinal and north-eastern faults.

The host rocks are presented by migmatized biotite, garnet-biotite and two-mica gneiss, crosscut by basic dykes, with intensive hydrothermal-metasomatic alterations. The alteration zone was traced on the surface for more than 800 m and to the depth of 240-400 m. The main process is chloritization; besides, hydromica, carbonate and local albite alterations are recorded (Figure 2.23).

The uranium mineralization was intersected by 5 drill holes, it is concentrated in bed and lens shaped bodies up to 10-20 x 2-2.5 m long and with an average uranium grade of 0.018 wt %. There are also more enriched (up to 0.138-0.2 wt %) and smaller (1.1 x 0.1 m) lenses, intersected by the drill holes *(Afanasieva et al.; 2007)*.

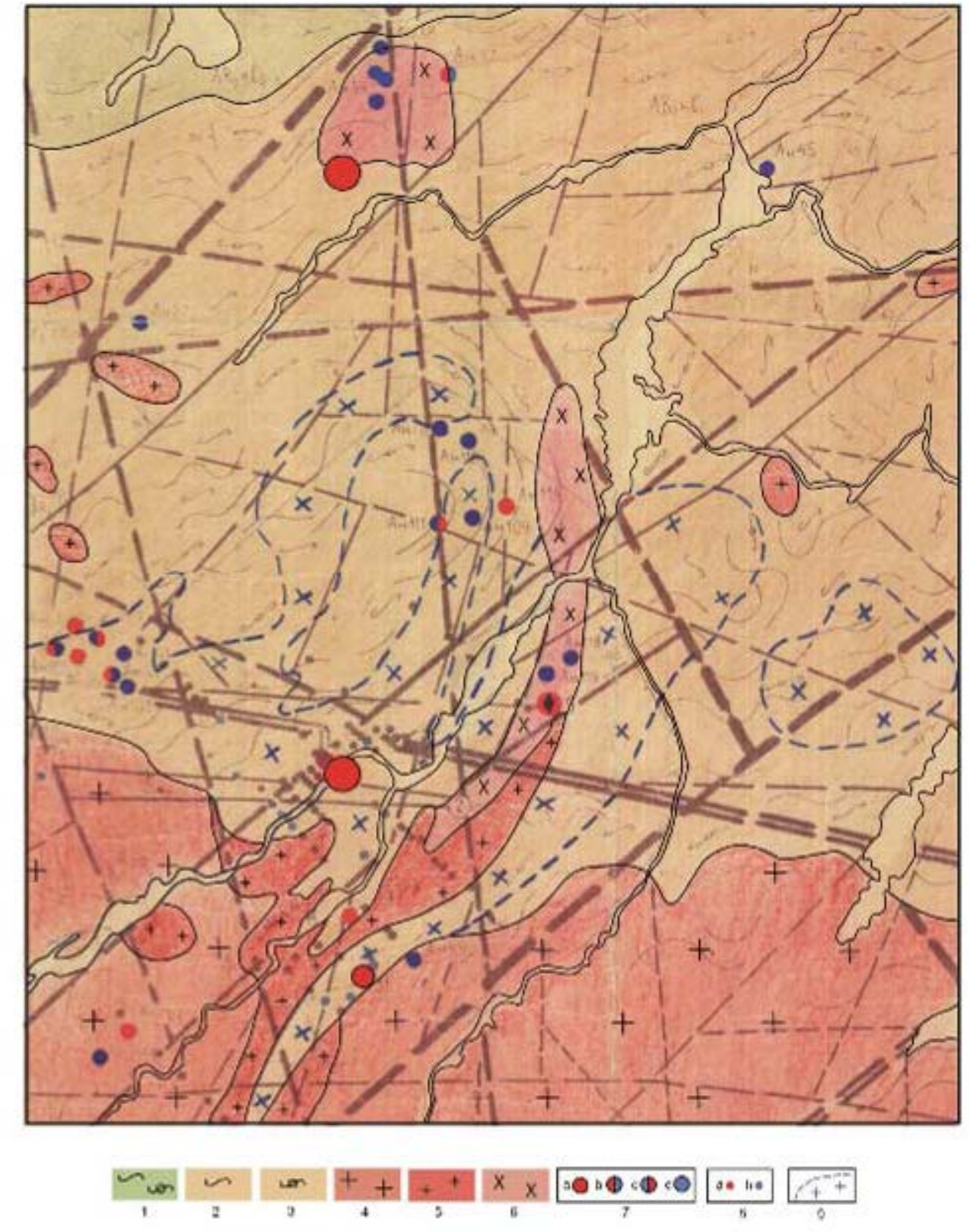

Figure 2.23. Geological map of the Beregovoe ore-showing area. 1. Biotite, garnet-sillimanite-biotite gneiss and amphibolite with interbeds of amphibole-magnetite rocks; 2. Migmatized biotite gneiss; 3. Biotite, garnet-biotite, staurolite-biotite, sillimanite-biotite, cordierite-biotite gneiss; 4. Poprhyraceous and porphyroblastic plagio-microcline granite veins of fine-grained granite and pegmatite; 5. Fine-grained leucocratic biotite-plagio-microcline granite; 6. Aplite-pegmatoid microcline-plagio-granite; 7. Anomalies: Th/U<1 (a), Th/U=1-2 (b), Th/U=2-3 (c), Th/U>3 (d); 8. Anomalies in boreholes: U>0.05% (a), U<0.03% (b); 9. Migmatite after microcline-plagioclase granite.

PART 3.

PETROLOGICAL, MINERALOGICAL, GEOCHEMICAL CHARACTERISTICS AND GEOCHRONOLOGICAL CONSTRAINTS OF THE URANIUM OCCURRENCES OF THE LITSA DISTRICT

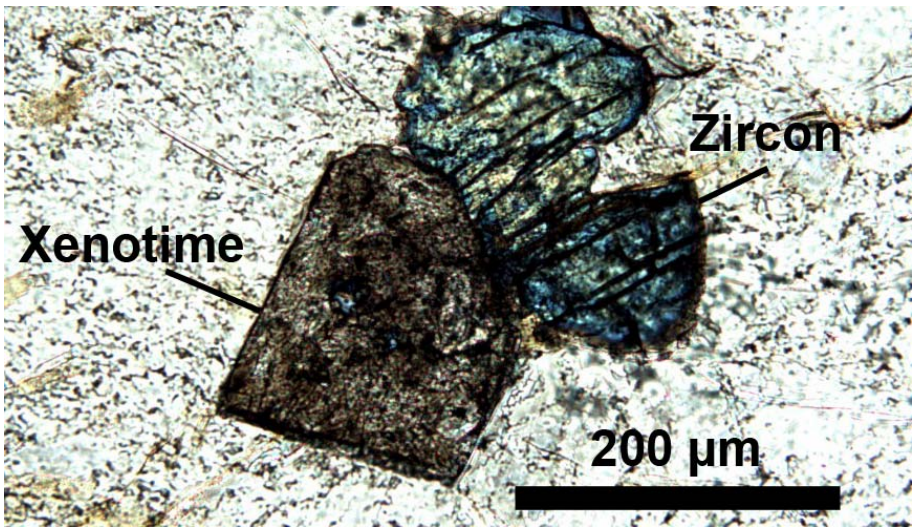

Introduction

Based on the field studies and sampling described in part 2, each occurrences has been studied in a petrological, geochemical, mineralogical and geochronological point of view.

The main objectives of these studies are to:

- Decipher the geochemical characteristics of the uranium occurrences,
- Link the obtained geochemistry with petrological and mineralogical observations,
- Describe the REE content and pattern in each type of uranium occurrence,
- Establish new geochronological constraints on this uranium metallogenic district.

All these data will help to understand the successive geological processes leading to uranium enrichment in the upper crust that will be discuss in part 4.

3.1. Geochemical analyses and mineralogical analyses

ICP-MS and ICP-AES analyses of the Litsa uranium occurrences are presented in Table 3.3, Table 3.4 and Table 3.5). Whole-rock samples have been analyzed at the SARM laboratory (CRPG, CNRS, Nancy, France) using the Carignan et al. (2001) methodology and standards and at the VSEGEI (Saint Petersbourg, Russia) facilities.

Geochemical results will be discussed using AB and QP chemical-mineralogical diagrams of Debon and Lefort (1988). The parameters Q=Si/3-(K+Na+2Ca/3), P=K-(Na+Ca), A=Al-(K+Na+2Ca) and B=Fe+Ti+Mg are calculated in thousands of cations from the major element contents. The average composition of reference rocks have been reported in the diagrams: gb = gabbro; mgb = monzogabbro; mz = monzonite; mzdq = quartz monzodiorite; dq = quartz diorite; s = syenite; sq = quartz syenite; to = tonalite; gd = granodiorite; ad = adamellite; gr = granite (data from Debon and Le Fort, 1983). The rock sample REE concentrations are normalized to the chondrite values from Anders and Grevesse (1989) and plotted as comparative REE patterns.

The binary diagram Th vs. U (in part per million) will be used to characterize the fractionation of the element and their possible leaching or enrichment during alteration processes. All these discriminant diagram are presented in detail in annexe 1.

The mineralogical observations done on specific samples of each occurrence will be used to interpret the observed patterns in these mineralogical-chemical diagrams. The mineralogical studies have been performed both in the G2R and the VSEGEI laboratories.

3.1.1. Archean occurrences

The study of petrographical, geochemical and mineralogical characteristics of the host rocks was based on 17 samples using transmitted and reflected optic microscopy, ICP-AES, MS analyses, SEM and microprobe observations.

The geochemical compositions of the sampled rocks show strong differences which will be explained both by chimico-geochemical diagrams and the mineralogy of the rocks (Table 3.3).

On A vs B diagram (Figure 3.1), the both A and B parameters vary from 16 to 220. The increase of A parameter is conditional on increase of the muscovite content and decrease of feldspar component. The B parameter is related to the content of mafic minerals (mainly biotite) and reaches a maximum value up to 3000 for the sample 89b – biotite enriched migmatitic gneiss from the Skal'noe ore-showing. On the whole, the majority of the samples are located in the fields of peraluminous rocks.

On Q vs P diagram (Figure 3.2), the Q parameter vary from 40 up to 307, which is induced by enrichment in quartz, while sample 59 with the lowest value confirms the quartz dissolution in this rock and the muscovite enrichment. P parameter varies from -145 to 33, corresponding to comparative enrichment in K-feldspar and muscovite. Some figurative points are located along subalkaline trend.

The Th/U ratio, figure 3.3., in most of the samples is below 1, in such way, that the altered and mineralized samples are more enriched with both of the elements.

The microscopic studies of the samples from the Dikoe ore-showing confirmed the intensive development of muscovitization processes, which were observed during the field works as muscovite-bearing shear zones with anomalous radioactivity (Figure 3.4). Thin section displays pleochroic haloes around uranium minerals in almost monomineralic muscovite aggregate. Progressive development of albitization (right) in a plagioclase with local sericite dust have been observed (Figure 3.4.D). Zircons, xenotime and tourmaline are ubiquitous accessory minerals and express within the muscovite-rich shear zone (Figure 3.4. G and H). Acicular brown rutile needles have been observed and have to be related with the chloritization of biotite (Figure 3.4.F).

Figure 3.5. shows the petrological and mineralogical characteristics of the Skalnoe occurrence. Outcrop 88 show the folding and shearing in quartz-feldspar granitoid (Figure 3.5.A). Various rock sections in this outcrop reveal silicification along the muscovite-rich shear zones (Figure 3.5.B). Perthitic feldspar with a sigmoidal shape surrounded by micro-granular quartz and muscovite clusters and albitized microcline crystal surrounded by orthoclase and recrystallized patches of quartz have been observed (Figure 3.5. C and D).

Outcrop 89 at Skalnoe (Figure 3.5.E) expresses a sharp contact between vein-like intrusion of quartz-feldspar granitoid (right) and the darker fine grained mylonitic gneisses (left) where coarse grained biotite restite occur. Nematoblastic texture have been observed (Figure 3.5.G) with muscovitization of biotite and recrystallized feldspar and quartz grains with ternary junctions (Figure 3.5.H).

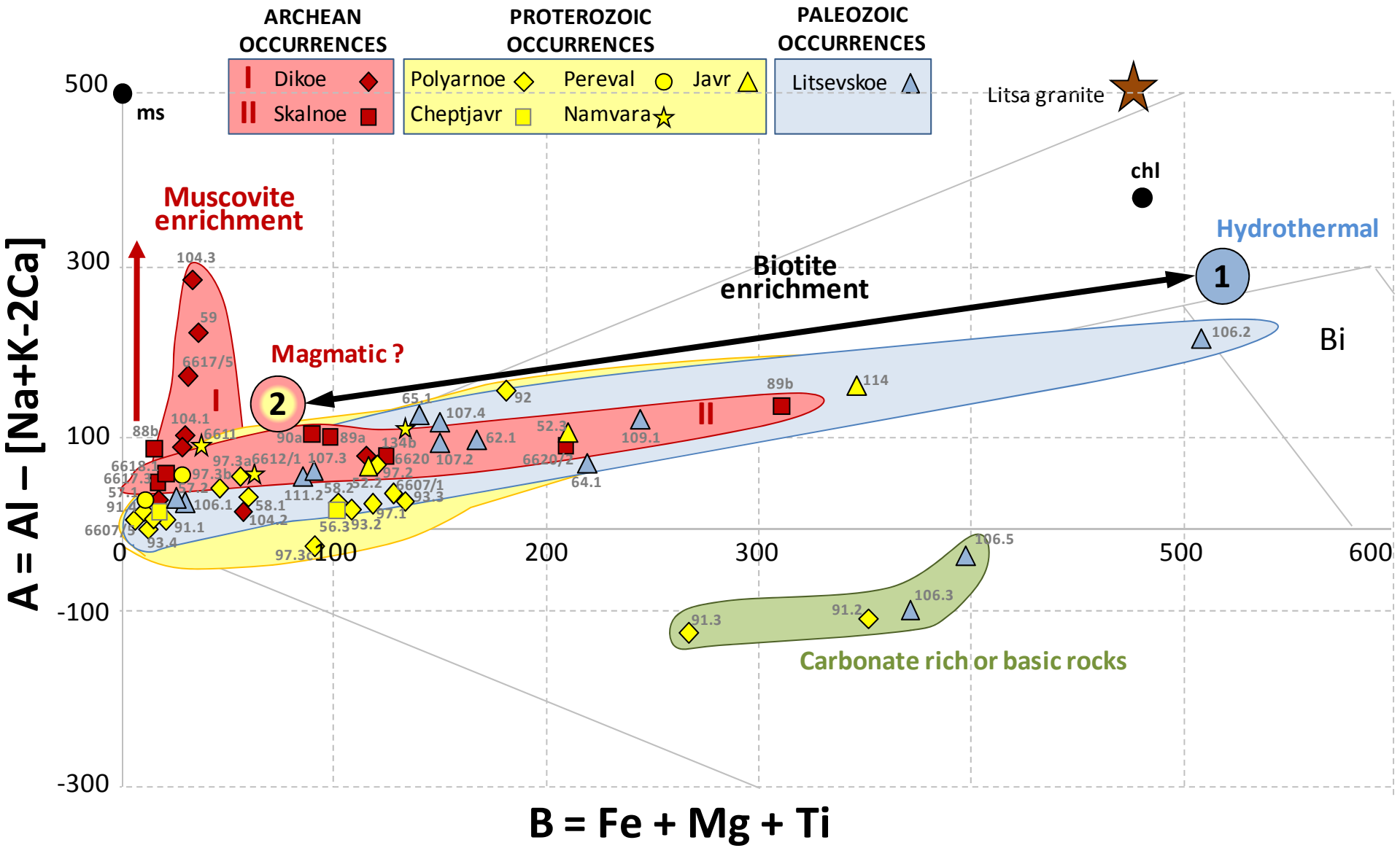

Figure 3.1. Variation in the peraluminous index A with the fractionation parameter B (coloration index) for each individual samples of the Litsa uranium occurrences (diagram from Debon and Lefort, 1988). The A and B parameters are calculated in thousands of cations.

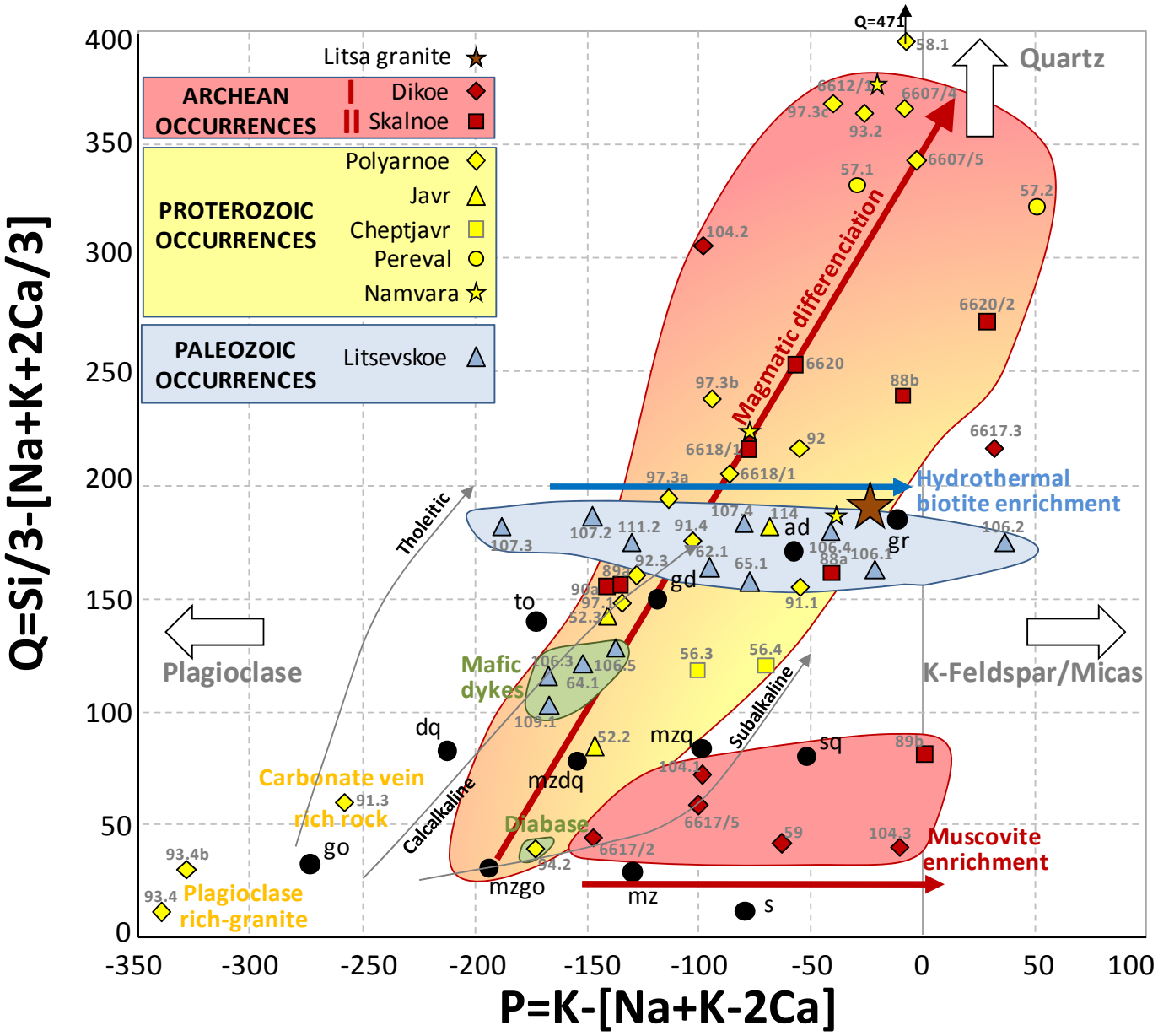

Figure 3.2. Variation of P versus Q parameters for each individual samples of the Litsa uranium occurrences (diagram from Debon and Lefort, 1988). The Q and P values are calculated in thousands of cations. Rock composition references are indicated: mz = monzonite; mzq = quartz-monzonite; mzdq = quartz monzodiorite; dq = quartz diorite; s = syenite; sq = quartz syenite; to = tonalite; gd = granodiorite; ad = adamellite; gr = granite.

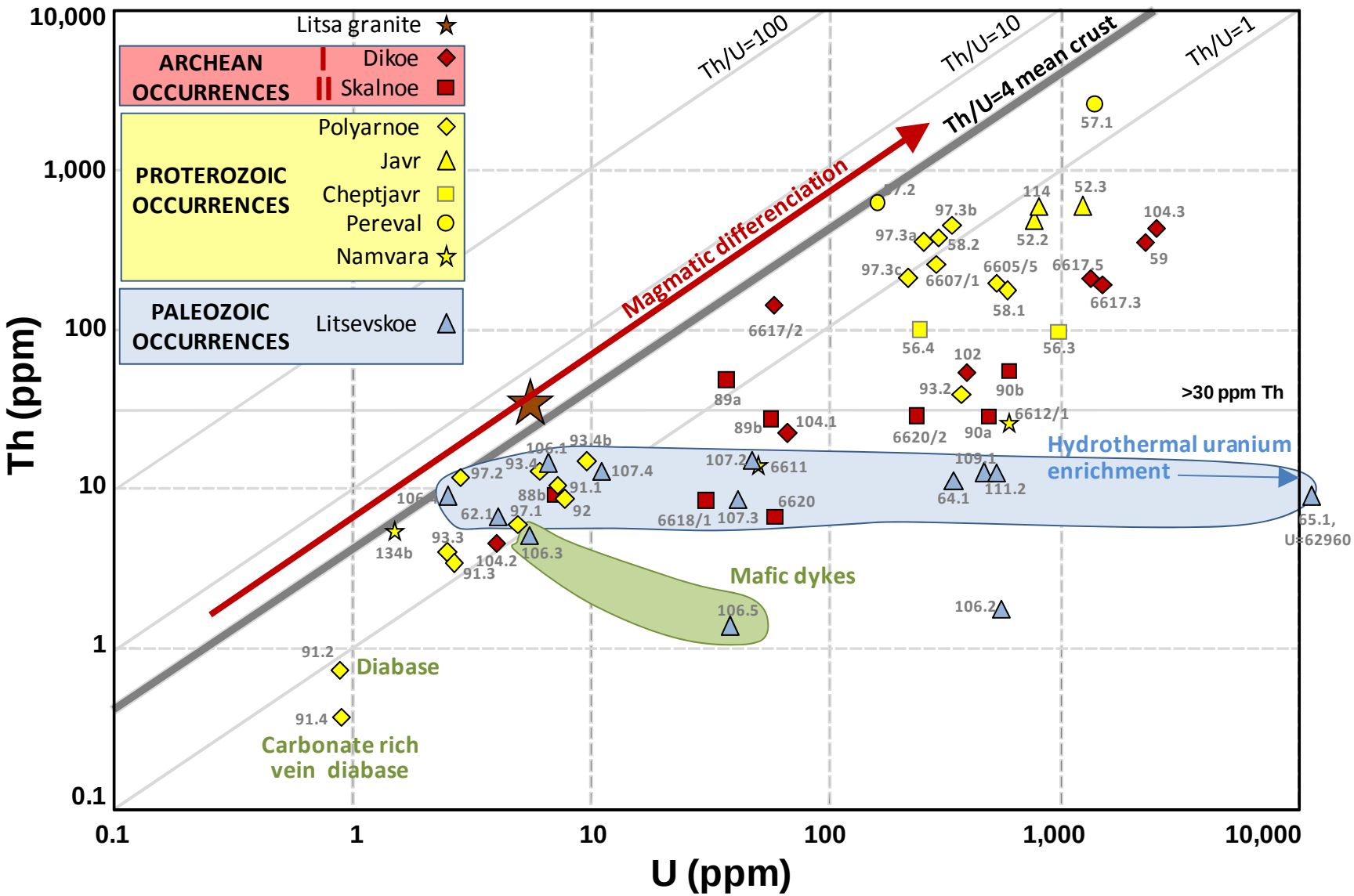

Figure 3.3. U versus Th contents (ppm) for each individual samples from the Litsa uranium occurrences. Th/U ratios of the mean crust and leucogranites are also represented.

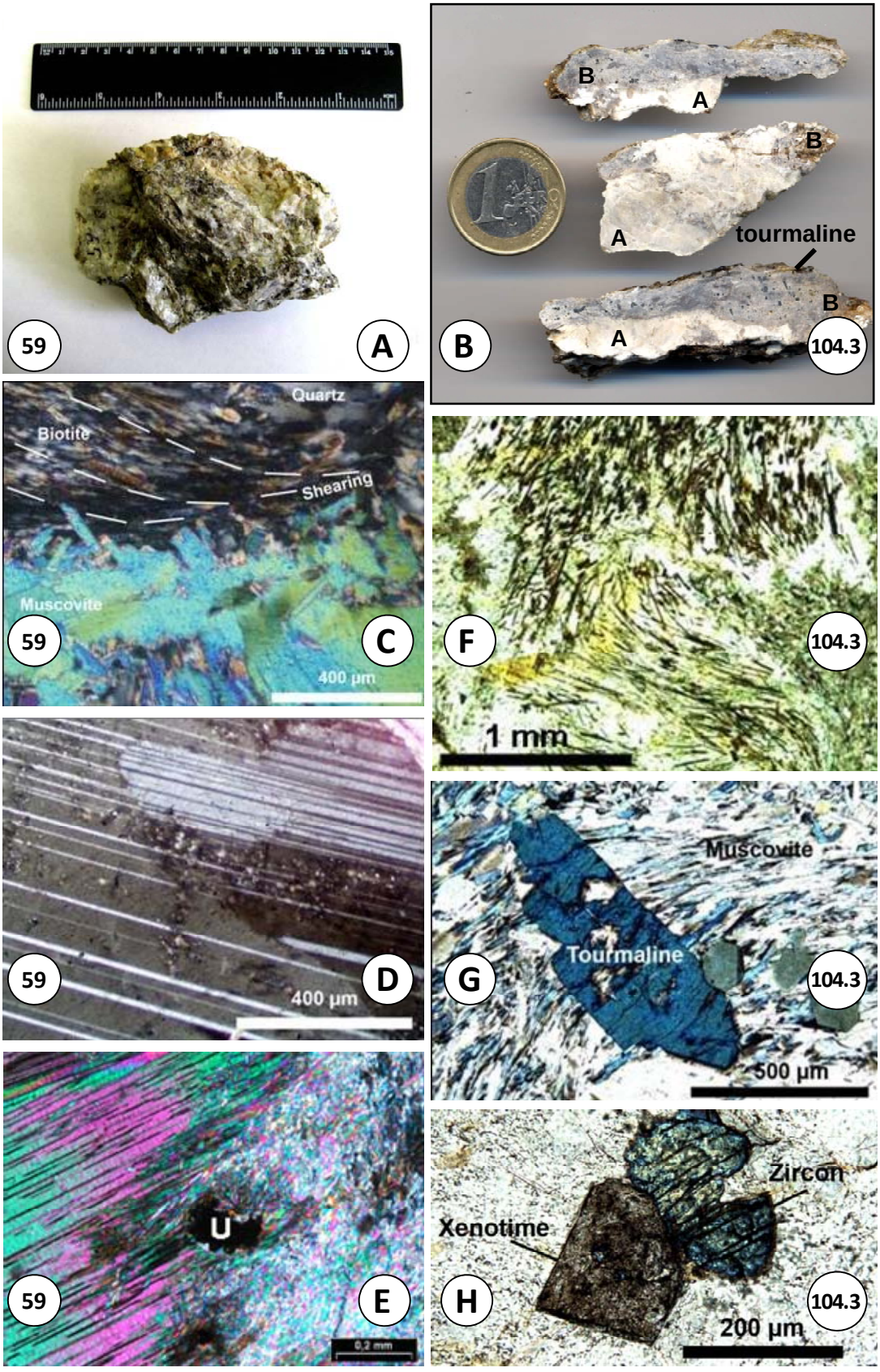

Figure 3.4. Petrographical and mineralogical characteristics of the mineralized pegmatoid from the Dikoe ore-showing. **A. and B.** Macroscopic image of the sample 59 and 104.3 respectively; **C.** Shear zone showing biotite muscovitization and disappearance of quartz; **D.** Progressive development of albitization (right) in a plagioclase with local sericite dust; **E.** Pleochroic haloes around uraninite**; F.** Acicular brown rutile needles issued from the Chloritization of biotite; **G.** Green to bluish tourmaline crystals within muscovite-rich shear zone; **H.** Zircon and xenotime preserved crystals within the muscovite-rich shear zone.

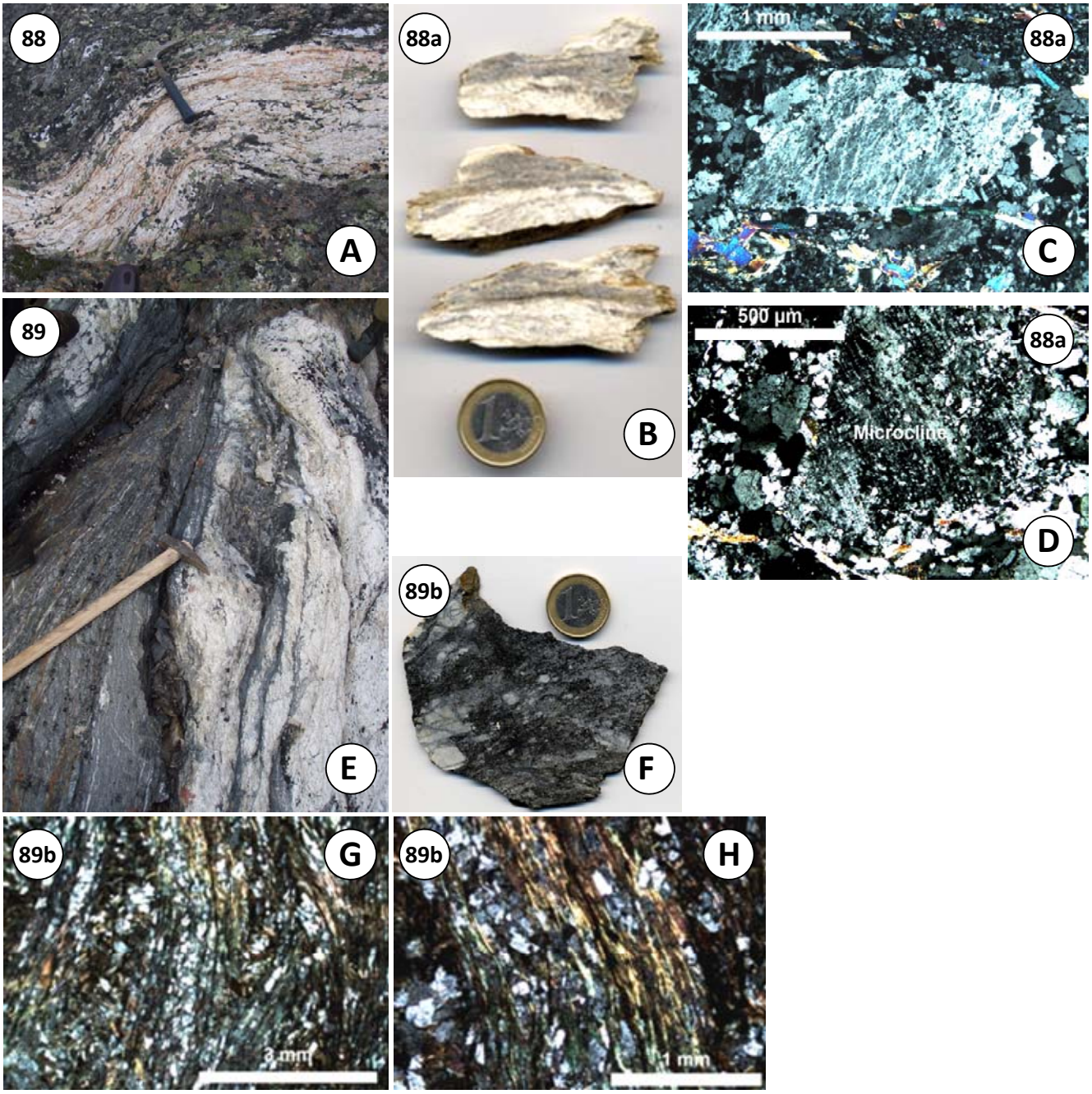

Figure 3.5. **A.** Skalnoe outcrop 88 showing folding and shearing in quartz-feldspar granitoid of the Skalnoe ore-showing; **B.** Various rock-sections of sample 88a extracted from this outcrop revealing silicification along the muscovite-rich shear zones; **C.** Perthitic feldspar with a sigmoidal shape surrounded by micro-granular quartz and muscovite clusters; **D.** Albitized microcline crystal surrounded by orthoclase and recrystallized patches of quartz. **E.** Outcrop 89 at Skalnoe showing the sharp contact between vein-like intrusion of quartz-feldspar granitoid (right) and the darker fine grained mylonitic gneisses (left) where coarse grained biotite restite occur. **F.** Picture of the rock section from the migmatized paragneiss at Skalnoe; **G.** Nematoblastic texture of biotite; **H.** Closer view showing muscovitization of biotite and recrystallized feldspar and quartz grains with ternary junctions.

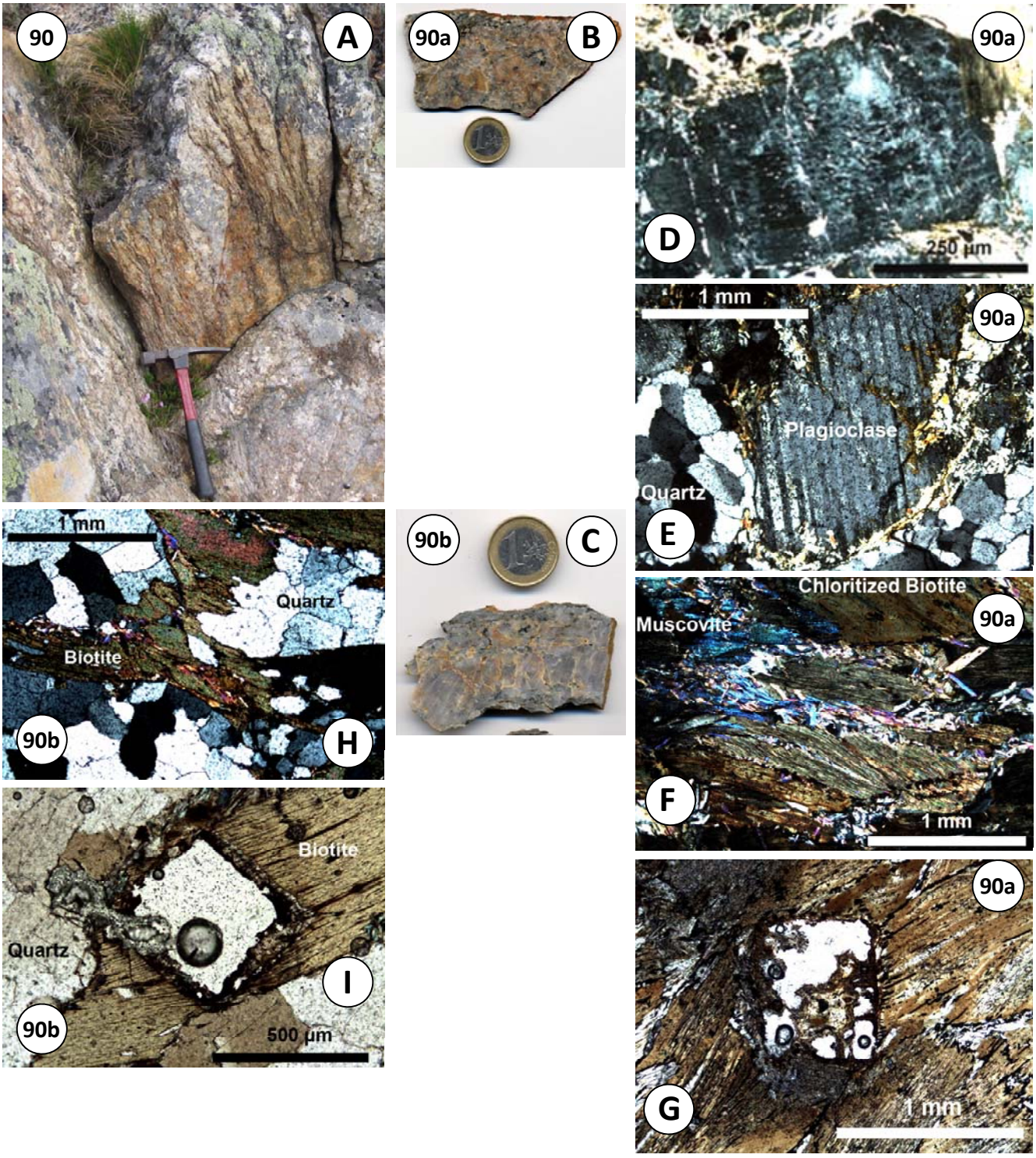

Figure 3.6. A. Outcrop 90 – Skalnoe showing intrusive quartz-felspar pegmatoid dyke <1m with quartz-boudinage structures. **B.** Rock section of sample 90a strongly cataclased feldspar and quartz with interstitial biotite schlierens and boxwork filled by hexavalent uranium minerals; **C.** Rock section of the sample 90b, more silicified than the 90a; **D.** Perthitic feldspar, **E.** Plagioclase enclosed in the biotite-rich restite; **F.** Muscovitization of chloritized biotite; **G.** Cubic boxwork in biotite selvage; **H.** Quartz recrystallization and altered biotite; **I.** Boxwork surrounded by a pleochroic halo in biotite.

3.1.2. Proterozoic occurrences

28 samples from Paleoproterozoic occurrences were studied with transmitted and reflected optic microscopy, ICP-AES, MS analyses, SEM and microprobe observations.

The geochemical compositions of the sampled rocks show strong differences linked to their variable nature which will be explained both by chimico-geochemical diagrams and the mineralogy of the rocks (Table 3.3).

On A vs B diagram (Figure 3.1), the A parameter varies from - 117 to 160. The negative values of A parameter belongs to diabases (sample 91.2) and carbonate vein with sulphides (sample 91.3) from the drill core, discovered in the Polyarnoe ore-showing. The maximum value of B parameter 367 corresponds to mineralized granite sample 114 from the Javr ore-showing, which is utterly enriched in biotite. Thus, most of the samples are weakly peraluminous and are located close to the eutectic point of quartz, K-feldspar and plagioclase. The biotite enrichment trend observed for this Proterozoic samples can be explained both by magmatic or hydrothermal process.

On Q vs P diagram (Figure 3.2), the Q parameter vary from 41 up to 470, indicating enrichment in quartz, and P parameter – from -256 to 35, corresponding to comparative enrichment in K-feldspar and muscovite. On the whole all figurative points depart from the average granite composition, being either enriched in quartz and K-feldspar (samples 58-1, 58-2, 6607/1 from Polyarnoe and 6612/1 from Namvara ore-showing), or depleted in them. The trend observed within this diagram can discriminate the process of biotite enrichment which seems to be linked to a magmatic one (Figure 3.1 and Figure 3.2). The depleted P and Q samples are linked to albitization process (93.4b and 93.4) or to carbonate veins (91.3).

The average content of thorium in the samples is about 300 ppm, which indicates high temperature processes. Uranium tends to increase more rapidly, than thorium, leading to Th/U ratio as low as 0.1.

The optic observations of the thin sections from the Polyarnoe ore-showing revealed the constant association of the uranium minerals with zircons in biotitic stripes, mainly orientated along the schistosity of the gneiss. Biotite crystals are often dark with constant interference, which indicates the enrichment with Fe. Among alteration processes, observed in thin sections, the most remarkable is muscovitization of the gneiss.

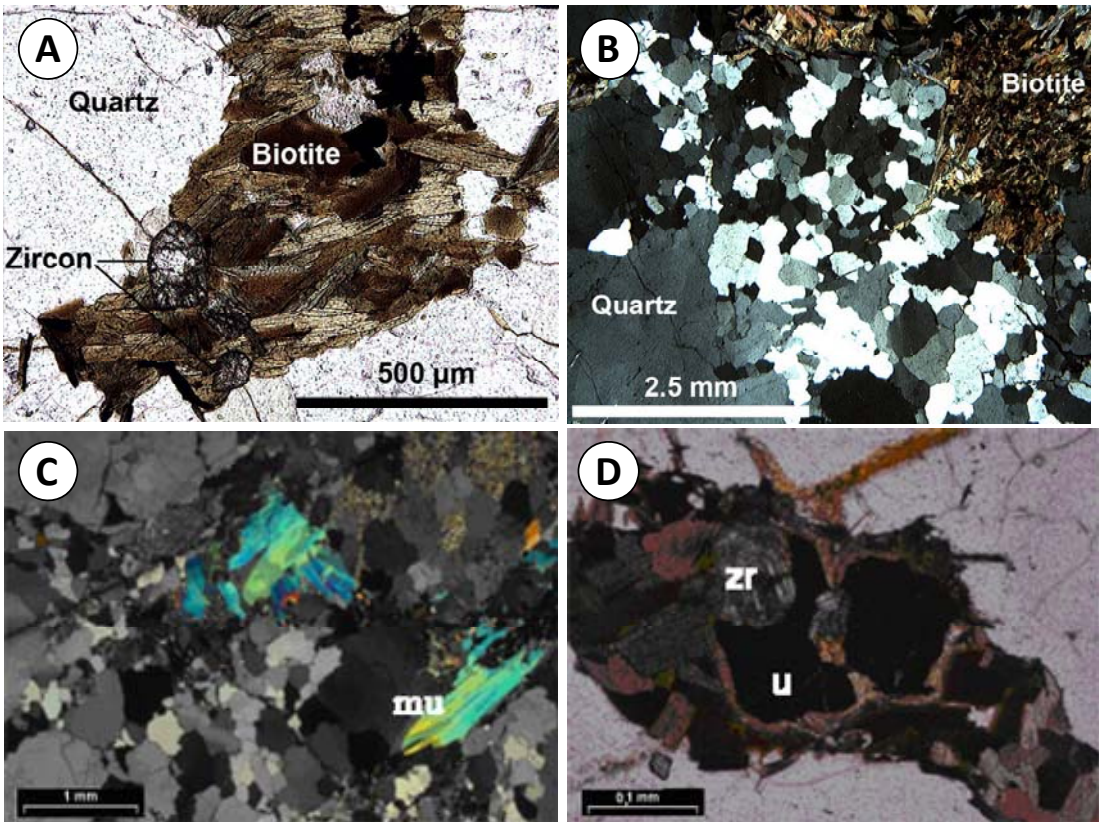

Figure 3.7. A. Biotite selvage with zircon and opaque minerals [sample 58-1]; B. Quartz and biotite in Polyarnoe pegmatite [sample 58-1]; **C.** muscovitization of the gneiss, **D.** Uranium associated with zircon in biotite.

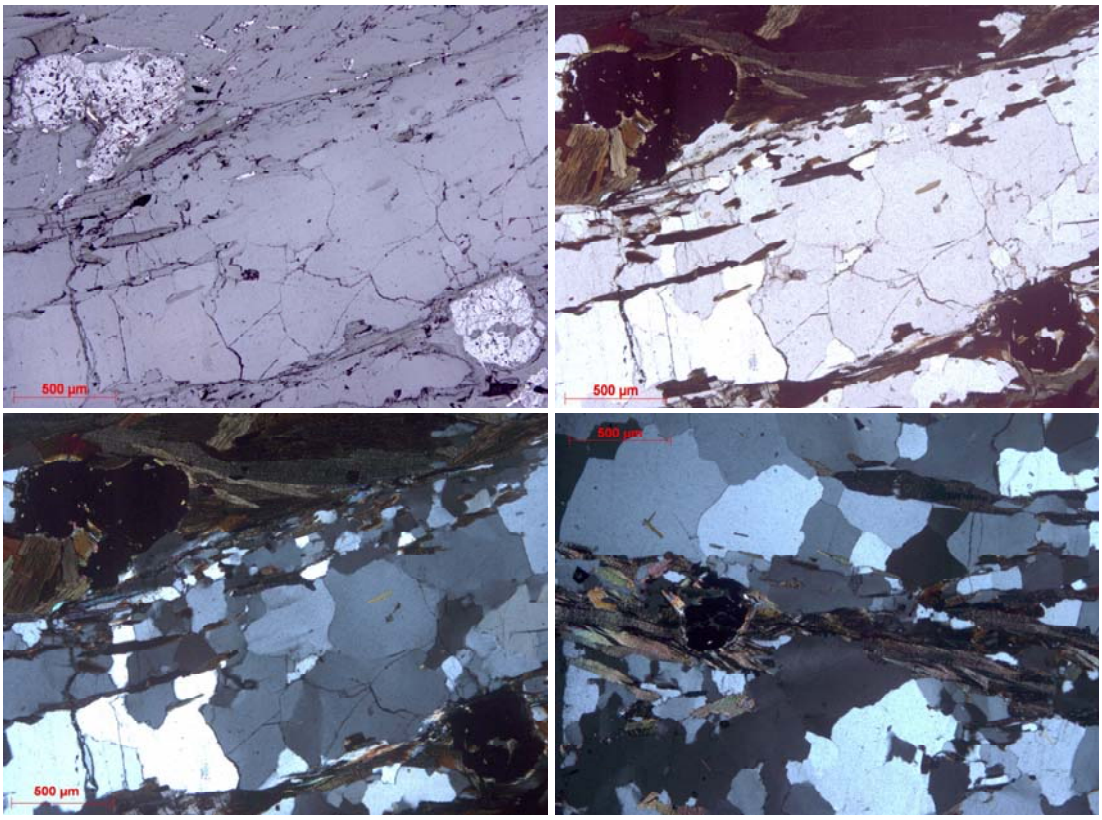

Figure 3.8. Uraninite crystals associated with chloritized biotite in Namvara gneiss.

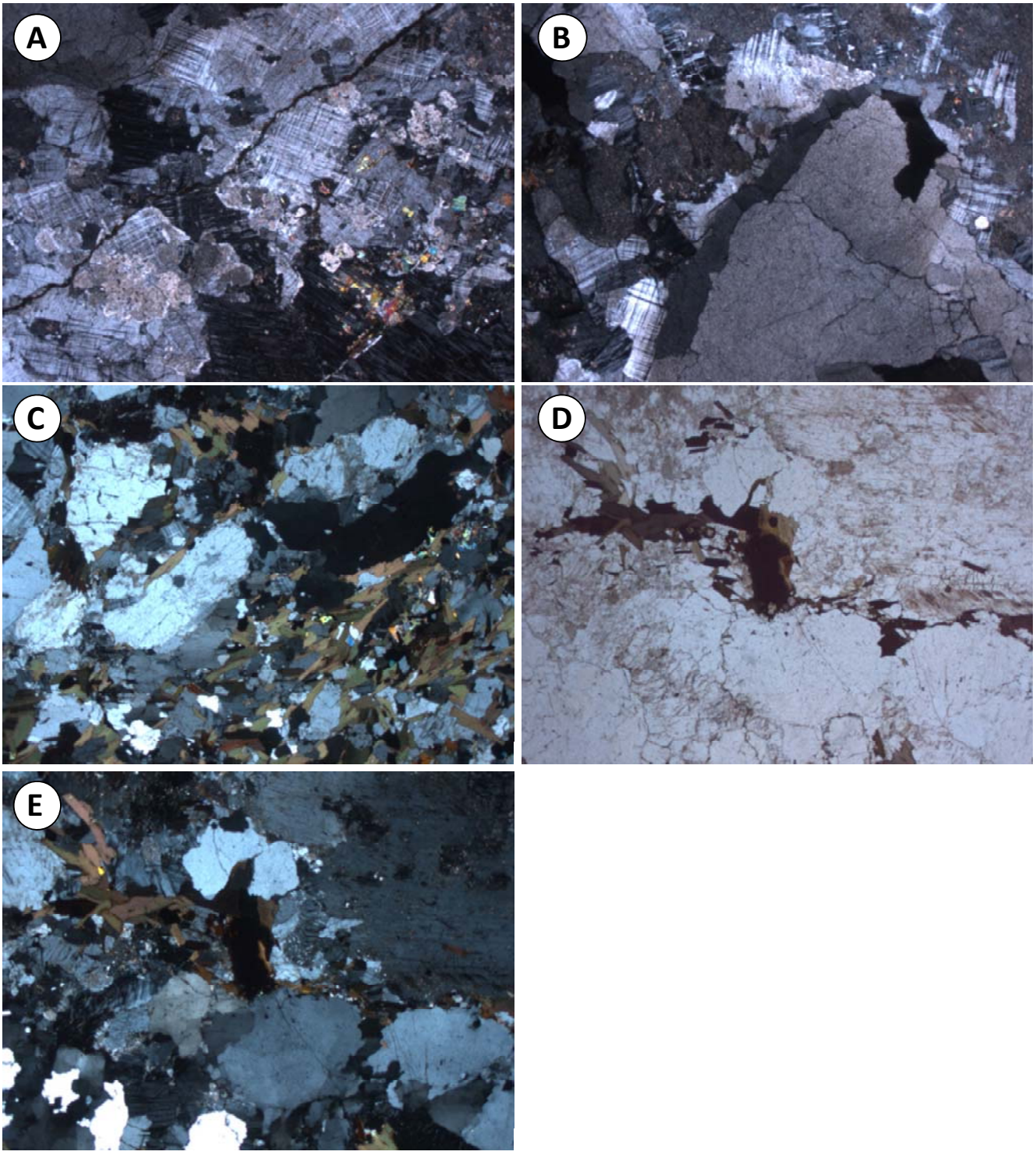

Figure 3.9. Petrographical characteristics of Cheptjavr occurrence. **A** and **C**. Microcline pattern in granite; **B**. and **D.** Uraninite crystal in biotitic stripe of the granite; **E.** Chloritization of biotite in granite.

3.1.3 Paleozoic occurrences

14 samples from the Litsevskoe and Beregovoe ore-showings were chosen for petrographical, geochemical and mineralogical studies, including transmitted and reflected optic microscopy, ICP-AES, MS analyses, SEM and microprobe observations.

The geochemical compositions of the sampled rocks show strong differences linked to their variable nature which will be explained both by chimico-geochemical diagrams and the mineralogy of the rocks (Table 3.5).

The preceding approach of typification, due to the extent of alteration and uranium content was also used for the samples to single out: non-altered, altered and mineralized samples (green, yellow and red symbols diagrams). Sample 65-1 is a pitchblende vein and its presence on A vs B and Q vs P diagram should not be considered.

On A vs B diagram (Figure 3.1), the A parameter varies from -36 (sample F106.5 – mafic dyke) to 222 (sample 106.2 – altered mafic dyke, see Figure 2.19), which is caused mainly by increase of the muscovite content and decrease of feldspar component. The B parameter is related to the content of mafic minerals (mainly biotite) and reaches a 522 value for sample 106.2.

On Q vs P diagram (Figure 3.2), the Q parameter vary from 21 up to 212, which is induced by enrichment in quartz, and P parameter – from -194 to 38, corresponding to comparative enrichment in K-feldspar and muscovite. The variation in the P parameter is linked to the variation in the biotite content and the horizontal trend observed may be linked more to hydrothermal process than to the magmatic one observed in Archean and Paleoproterozoic occurrences.

The low thorium content indicates low temperature processes, while the uranium content reaches 62900 ppm (sample 65.1), so that Th/U ratio is << 0.1 and this fact also indicate much more hydrothermal uranium enrichment.

The microscopic studies of the samples from the Litsevskoe ore-showing revealed the following sequence of hydrothermal alterations. The first stage consists of chloritization (from partial to full replacement), so that ferruginous chlorite inherits the shape of the biotite crystals. The second stage entails quartz dissolution and the voids are filled with cryptocrystallic chlorite, sericite and seldom albite. During the final stage the quartz and plagioclase are replaced by chlorite and pseudomorphic sericite (Figure 3.10 to 3.12).

The development of all these stages of alterations can be seldom observed at the same time. More often some of the stages are missing or weakly revealed.

Besides described alterations, the development of hydromica and clay minerals occur in the rocks. They are filling fractures and are developed after plagioclase. The X-ray analysis determined albite phase with illite, clinochlore and other silicate minerals in the studied samples (Table 3.1).

Table 3.1. Results of X-ray analysis of the samples from Litsevskoe occurrence.

No	Main phases and their number from JCPDS	Probable phases and admixtures and their number from JCPDS
1	Illite (No 26-911), Chlorite (clinochlore) (No 29-701), Quartz (No 33-1161), Albite (No 20-554)	P-Chernovite Y $(As;PO)_4$ (No 26-999) Magnetite (No 25-1376) Willemite Zn_2SiO_4 (No2-1412)
2	Illite (No 26-911), Chlorite (clinochlore) (No 29-701), Quartz (No 33-1161), Albite (No 20-554)	Clinochrysotile (No 27-1276)
3	Chlorite (clinochlore) (No 29-701), Quartz (No 33-1161)	

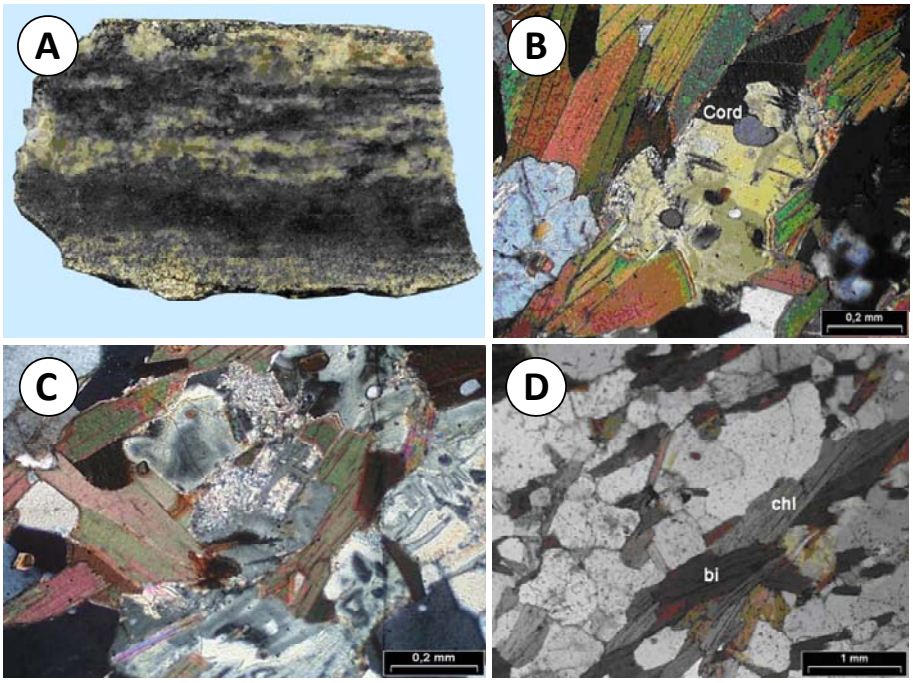

Figure 3.10. Petrographical characteristics of the sample 62.1 from the Litsevskoe ore-showing. **A.** Macroscopic image of the sample 62.1 (migmatized biotite-cordierite gneiss); **B.** Idiomorphic cordierite; **C.** Chloritized biotite; **D.** Hydromica alterations.

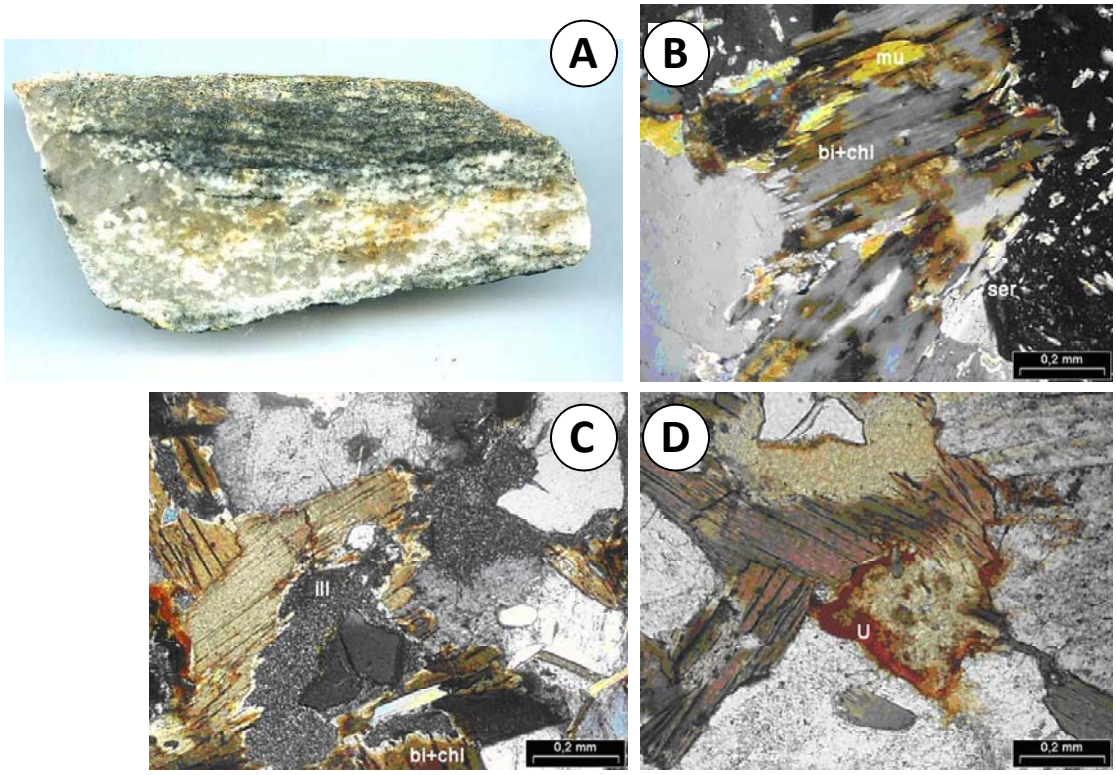

Figure 3.11. Petrographical characteristics of the sample 64.1 from the Litsevskoe ore-showing. **A.** Macroscopic image of the sample 64.1 (biotite-rich gneiss from the 1500 μR/h zone); **B.** Chloritized biotite, muscovite and sericite; **C.** Illite between chloritized-biotite; **D.** Hexavalent uranium minerals.

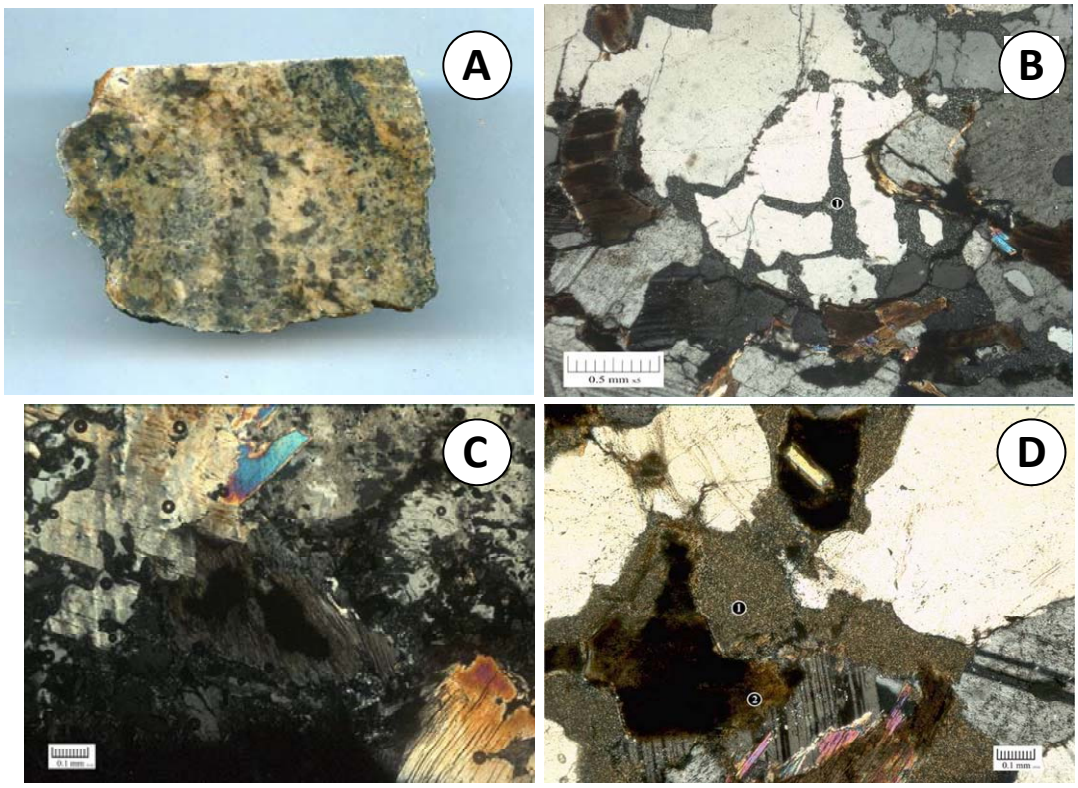

Figure 3.12. Petrographical characteristics of the sample 65.2 from the Litsevskoe ore-showing. **A.** Macroscopic image of the gneiss near the contact with pitchblende vein); **B.** Illite (1) in fractures; **C.** Muscovitization; **D.** Montmorillonite (1) and chamosite (2).

3.2. Uranium and accessory mineralization

3.2.1. Archean occurrences

The uranium-bearing formations within the Voron'ya-Kolmozersk zone display the presence of various accessory and radioactive minerals. The previous researchers distinguished two major types of uranium mineralization: monazite-zircon-uraninite and molybdenite-thorite-uraninite types (*Savitskii et al.; 1995*). Besides they mention hexavalent uranium minerals and the following accessories: magnetite, ilmenite, infrequently apatite or tourmaline.

The optic and SEM observations, provided in the framework of this thesis, confirmed the presence of uraninite crystals associated with accessory zircon or monazite (Figure 3.13A and B). They occur as euhedral inclusions in the silicate minerals, mainly muscovite, with pleochroic haloes around them (Figure 3.4). Besides uraninite, there is coffinite, forming irregular inclusions or fringes (Figure 3.13D). Several REE-bearing and tantalum-niobium minerals were observed (Figure 3.13E and F). The chemical composition of the described minerals is presented in Table 3.6.

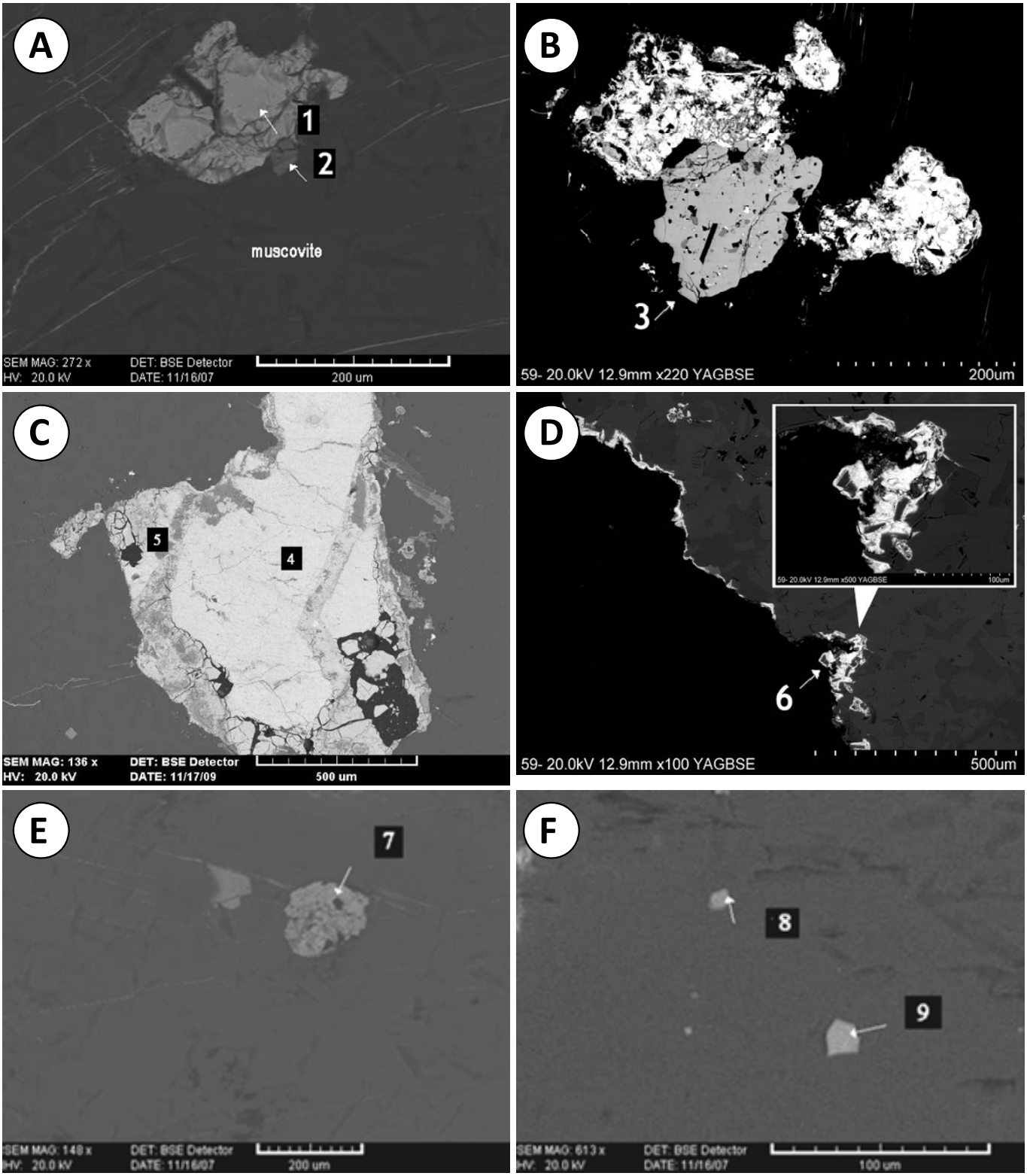

Figure 3.13. Radioactive and accessory minerals of the Archean (Dikoe and Skal'noe) occurrences *(BSEM images; the numbers correspond to semi quantitative SEM-EDS determination, see table X). A.* Uraninite (1) and zircon (2) in muscovite [sample 59]; B. Monazite (3) and uraninite[sample 59]; C. Altered uraninite (4,5); D. Coffinite (6) fringe on a silicate mineral (muscovite) [sample 59]; E. Xenotime (7); F. Pyrochlore type minerals (8,9) [sample 59]

Detailed microprobe analyses of the crystal zones for the sample 59 revealed minerals deriving from the alteration of uranium minerals (Figure 3.14).

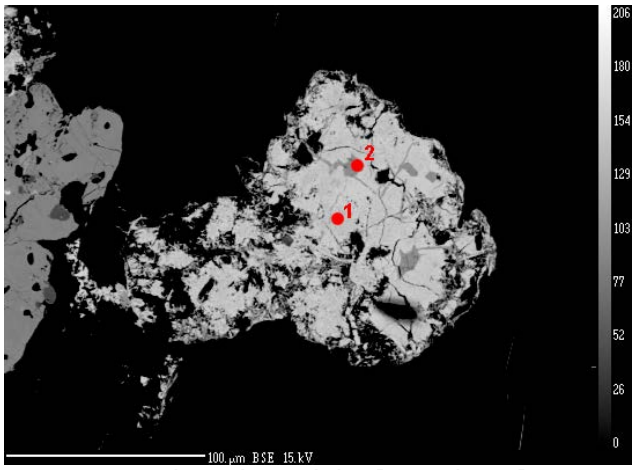

A – Altered uraninite [sample 59];

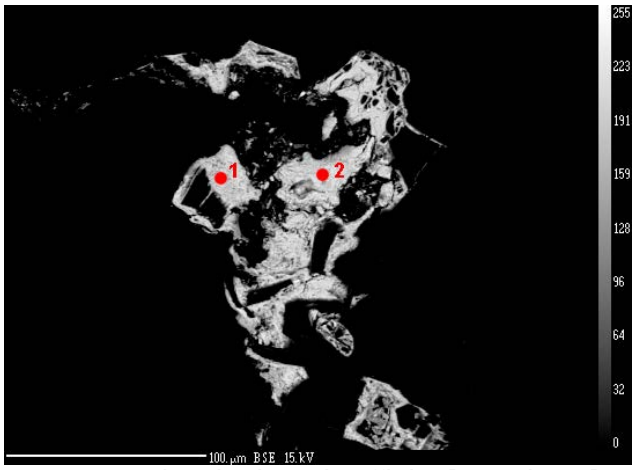

B – Metamicte hydrated coffinite [sample 59];

Element\Point	1	2
Oxide		
Al2O3	0,08	0,43
SiO2	10,81	12,26
K2O	0,87	0
SO2	0,05	0
CaO	0,44	1,04
V2O3	0,01	0
FeO	0	0,56
ZrO2	0	0
PbO	30,89	1,26
UO2	47,99	12,54
Na2O	0,05	0
MgO	0,02	0
TiO2	0	0
MoO3	0,01	0
La2O3	0,01	0,08
ThO2	0,10	32,98
MnO	0	0
Y2O3	0,44	12,95
Ce2O3	0,10	1,73
P2O5	0	2,77
Nd2O3	0,004	0,74
Dy2O3	0,03	2,10
Ta2O5	0	0,03
SeO2	0,06	0
Total	92,85	81,46

Element\Point	1	2
Oxide		
Al2O3	3,49	1,65
SiO2	17,29	16,01
K2O	0,48	0,87
SO2	0	0,02
CaO	5,33	6,68
V2O3	0,01	0
FeO	0,26	0,12
ZrO2	0	0
PbO	0,17	0,86
UO2	47,20	67,14
Na2O	1,26	0,05
MgO	0,04	0,17
TiO2	0	0,014
MoO3	0	0
La2O3	0	0
ThO2	0	0
MnO	0,04	0
Y2O3	0,12	0,07
Ce2O3	0	0
P2O5	0,10	0,21
Nd2O3	0,02	0
Dy2O3	0	0,08
Ta2O5	0,21	0,01
SeO2	0	0
Total	76,01	93,95

Figure 3.14. Microprobe analyses of the uranium minerals from the Dikoe ore-showing. Detection limits are presented in Annexe 3.4

3.2.2. Proterozoic occurrences

The host rocks of the uranium mineralization of Paleoproterozoic age contain a significant portion of accessory minerals, mainly zircon and monazite, which are concomitant to the uranium minerals. Besides monazite and zircon, there are apatite, titanite, ilmenite, allanite, REE-bearing and chalcogenic minerals. The radioactive mineralization is presented by uraninite, brannerite, seldom pitchblende (*Savitskii et al.; 1995, Afanasieva et al.; 2007*) and hexavalent uranium minerals.

Some BSEM images of these minerals are shown on Figure 3.15 and their chemical composition – in Table 3.7. The uraninite crystals are idiomorphic and reach 0.5 mm in size, they are mostly associated with accessory zircon in biotite aggregates among quartz-feldspathic matrix (Figure 3.7). They are almost unaltered and present constant chemical composition (Figure 3.17.), while monazite displays evident dissolution (Figure 3.17G). Zircon often contains micro inclusions of uranium-rich phases and brannerite is mostly subreplacing ilmenite (Figure 3.17C, E).

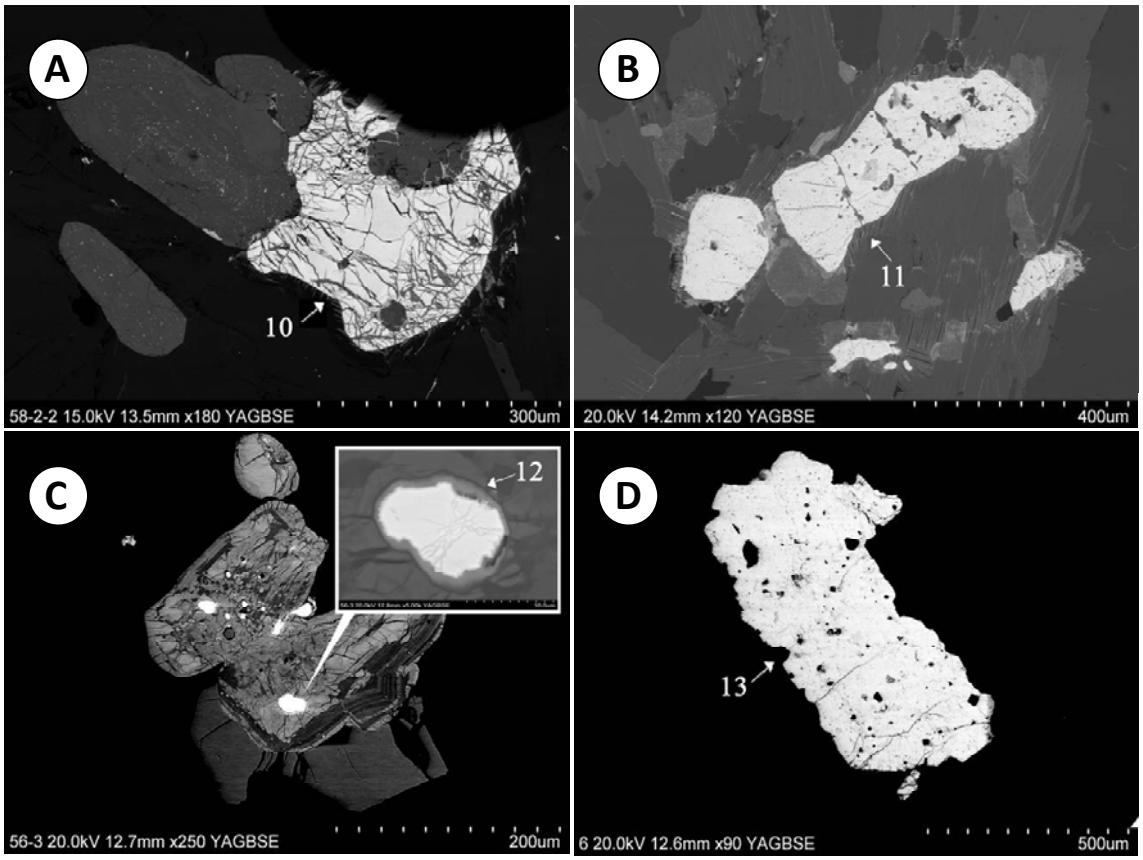

Figure 3.15. Radioactive and accessory minerals of the Paleoproterozoic (Polyarnoe, Namvara, and Cheptjavr) occurrences (BSEM images; the numbers correspond to semi quantitative SEM-EDS determinations). A. Uraninite (10) and zircon [sample 58-2]; B. Uraninite (11) [sample 134a]; C. Uranium oxide inclusion (12) in zircon [sample 56-3]; D. Uraninite (13) [sample 56-3].

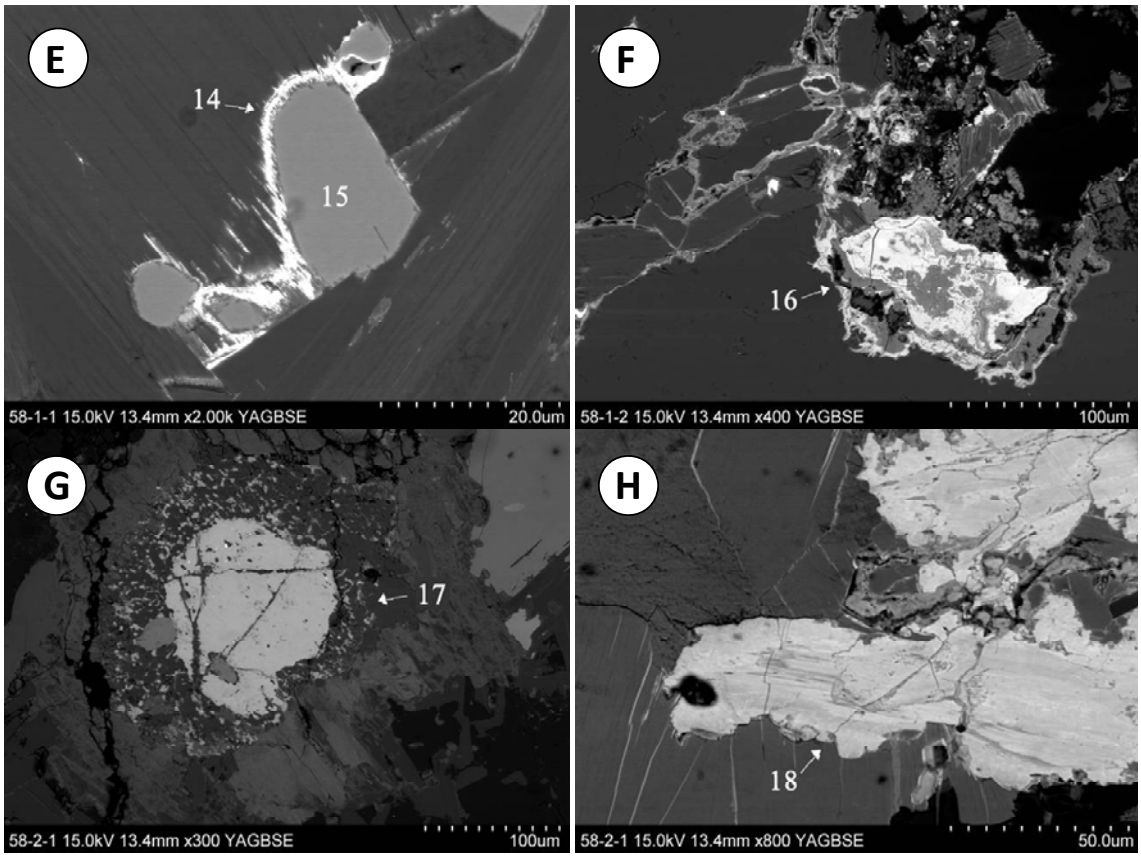

Figure 3.15 (suite). Radioactive and accessory minerals of the Paleoproterozoic (Polyarnoe, Namvara, and Cheptjavr) occurrences *(BSEM images; the numbers correspond to semi quantitative SEM-EDS determinations).* **E.** Brannerite (14) and ilmenite (15) [sample 58-1]; **F.** Xenotime (16) [sample 58-1]; **G.** Monazite (17) [sample 58-2]; **H.** Allanite (18) [sample 58-2].

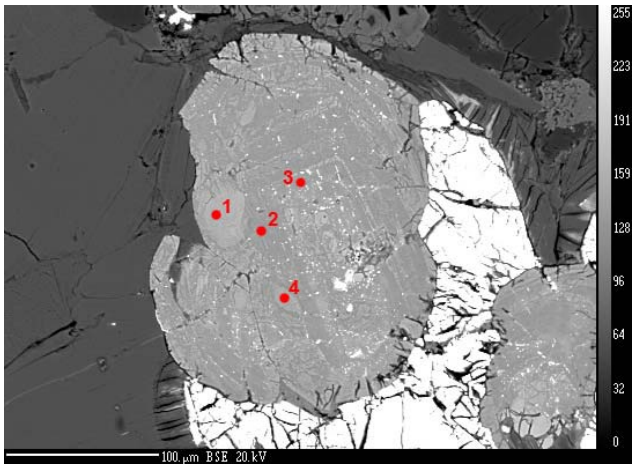

A. Zircon [sample 58-2];

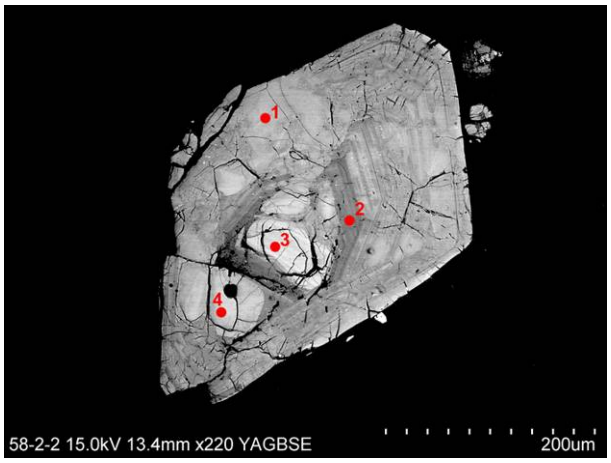

B. Zircon [sample 58-2];

Element \Point	1	2	3	4
Oxide				
Al2O3	0,26	0,53	0,74	0,80
Na2O	0	0,02	0	0,20
SiO2	30,99	29,76	26,80	29,57
K2O	0,01	0,28	0,27	0,14
P2O5	0	0	0,02	0,20
CaO	1,36	1,92	2,69	3,49
FeO	0,97	1,45	1,51	1,27
Y2O3	0	0	0,23	0,11
ZrO2	60,28	53,11	44,78	51,53
HfO2	1,96	1,58	1,47	1,36
PbO	0,04	1,40	4,09	0,14
UO2	0,18	1,60	3,9	1,87
ThO2	0,003	0	0	0,01
TiO2	0,10	0,10	0,06	0,01
Gd2O3	0,04	0,14	0,11	0,15
Dy2O3	0,02	0,03	0,10	0,1
Er2O3	0,01	0,10	0,06	0
Yb2O3	0,07	0,08	0,08	0,16
SO3	0,05	0,51	1,12	0,04
Total	96,28	92,54	88,03	90,96

Element \Point	1	2	3	4
Oxide				
Al2O3	0,35	0,84	0,28	0,16
Na2O	0	0,45	0	0
SiO2	31,06	31,77	31,24	31,69
K2O	0,01	0,03	0,09	0,03
P2O5	0,04	0	0	0,02
CaO	1,45	2,62	0,45	0,87
FeO	1,15	1,23	0,45	1,00
Y2O3	0	0	0,04	0
ZrO2	60,15	54,43	63,76	63,36
HfO2	1,67	1,89	1,24	1,58
PbO	0,02	0,01	0	0,005
UO2	0,20	0,68	0,19	0,14
ThO2	0	0,05	0,06	0
TiO2	0,01	0,06	0,06	0,004
Gd2O3	0	0,06	0,02	0,01
Dy2O3	0	0	0,09	0
Er2O3	0,05	0	0	0
Yb2O3	0	0,11	0,07	0
SO3	0	0,05	0,13	0,06
Total	96,17	94,30	98,17	98,98

Figure 3.16. Microprobe analyses of the zircons from the Polyarnoe ore-showing. Detection limits are presented in Annexe 3.4

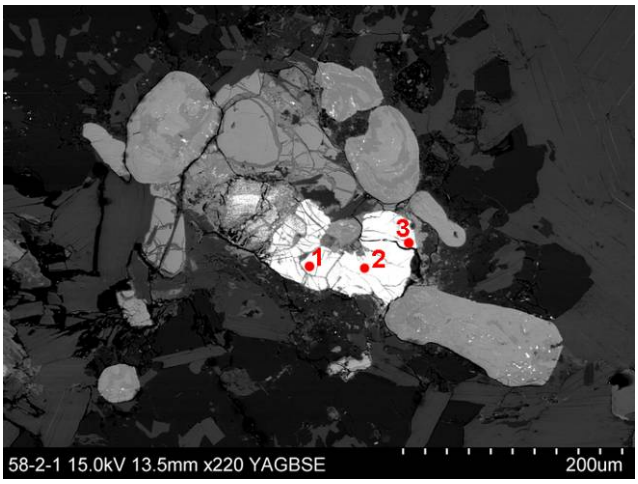

A. Uraninite [sample 58-2];

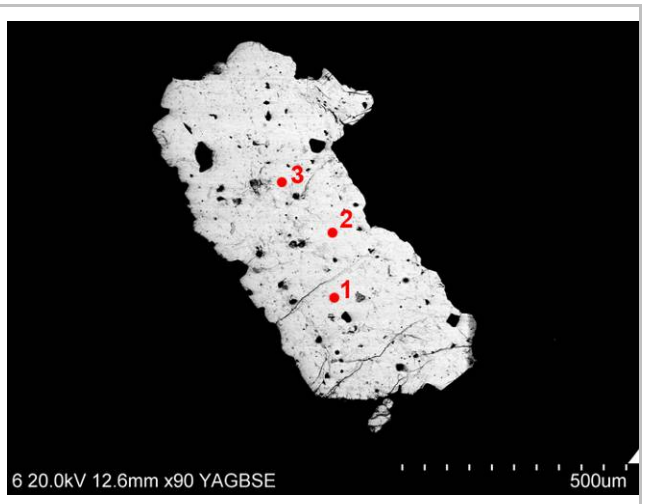

B. Uraninite [sample 56-3];

Element\Point	1	2	3
Oxide			
Al2O3	0,33	1,26	1,12
SiO2	2,04	2,42	1,66
K2O	0,18	0	0,25
SO2	0,48	1,19	0,82
CaO	0,78	2,55	1,67
V2O3	0	0	0
FeO	5,14	6,65	7,01
ZrO2	0,30	0,20	0,05
PbO	8,46	8,46	6,84
UO2	56,91	61,14	44,57
Na2O	0,06	0,31	0,29
MgO	0,01	0,37	0,49
TiO2	0,14	0,070	0,17
MoO3	0,001	0	0,02
La2O3	0	0	0
ThO2	10,32	8,58	11,00
MnO	0	0,01	0
Y2O3	0,54	0,60	0,24
Ce2O3	0,09	0	0,13
P2O5	0,16	0,02	0
Nd2O3	0,69	0,02	0,16
Dy2O3	0,29	0,12	0,08
Ta2O5	0	0	0
SeO2	0,10	0	0,05
Total	87,01	93,97	76,61

Element\Point	1	2	3
Oxide			
Al2O3	0	0	0
SiO2	0	0,05	0
K2O	0,26	0,23	0,26
SO2	0,03	0	0
CaO	0,40	0,45	0,4
V2O3	0	0	0,10
FeO	0,12	0,15	0
ZrO2	0	0	0
PbO	18,51	18,78	19,11
UO2	66,14	67,44	66,96
Na2O	0,13	0,11	0,07
MgO	0,005	0	0
TiO2	0	0	0,06
MoO3	0	0	0
La2O3	0	0	0
ThO2	5,31	5,69	5,62
MnO	0	0,19	0
Y2O3	3,11	1,95	1,95
Ce2O3	0,17	0,04	0
P2O5	0,10	0	0
Nd2O3	0,06	0,10	0,18
Dy2O3	0,31	0,34	0,14
Ta2O5	0	0	0
SeO2	0	0,03	0
Total	94,65	95,54	94,83

Figure 3.17. Microprobe analyses of the uraninites from the Polyarnoe and Cheptjavr ore-showings. Detection limits are presented in Annexe 3.4

3.2.3. Paleozoic occurrences

As it was mentioned in the introduction the uranium mineralization of these occurrences is polychronic. The oldest uranium mineralization (1750-1650 - *Anderson, 1983*) is presented by uraninite (Figure 3.19), included in the chloritized biotite in host gneiss. The main Paleozoic mineralization is represented by pitchblende (Figure 3.19B,C), which make up to 1 cm thick vein (sample 65.1 – Figure 2.4, Figure 3.18). The pitchblende is massive and occupies the central zone of the veinlet. The hexavalent uranium minerals are presented by uranophane, which is often replacing pitchblende with complex shaped boundaries and containing inclusions of radiogenic galena *(Afanasieva et al.; 2007)*, and uranophane-II, which is younger and is commonly crosscutting the older one (Figure 3.19). Besides uraninite, pitchblende and hexavalent uranium minerals the brannerite was observed in some samples (Figure 3.19D).

The disseminated radioactive mineralization from the mafic dykes is represented by brannerite and REE-U-bearing minerals, which could not be determined by semi-quantitative analyses (Figure 3.19F, G).

Accessory minerals in the biotite gneisses are presented by zircon, altered monazite, ilmenite, xenotime and various other minerals, including Au-bearing Cu,Ni,Zn mineral (Figure 3.19E – number 27).

Figure 3.18. The macroscopic (real size) image of the sample F65.1 – pitchblende vein.

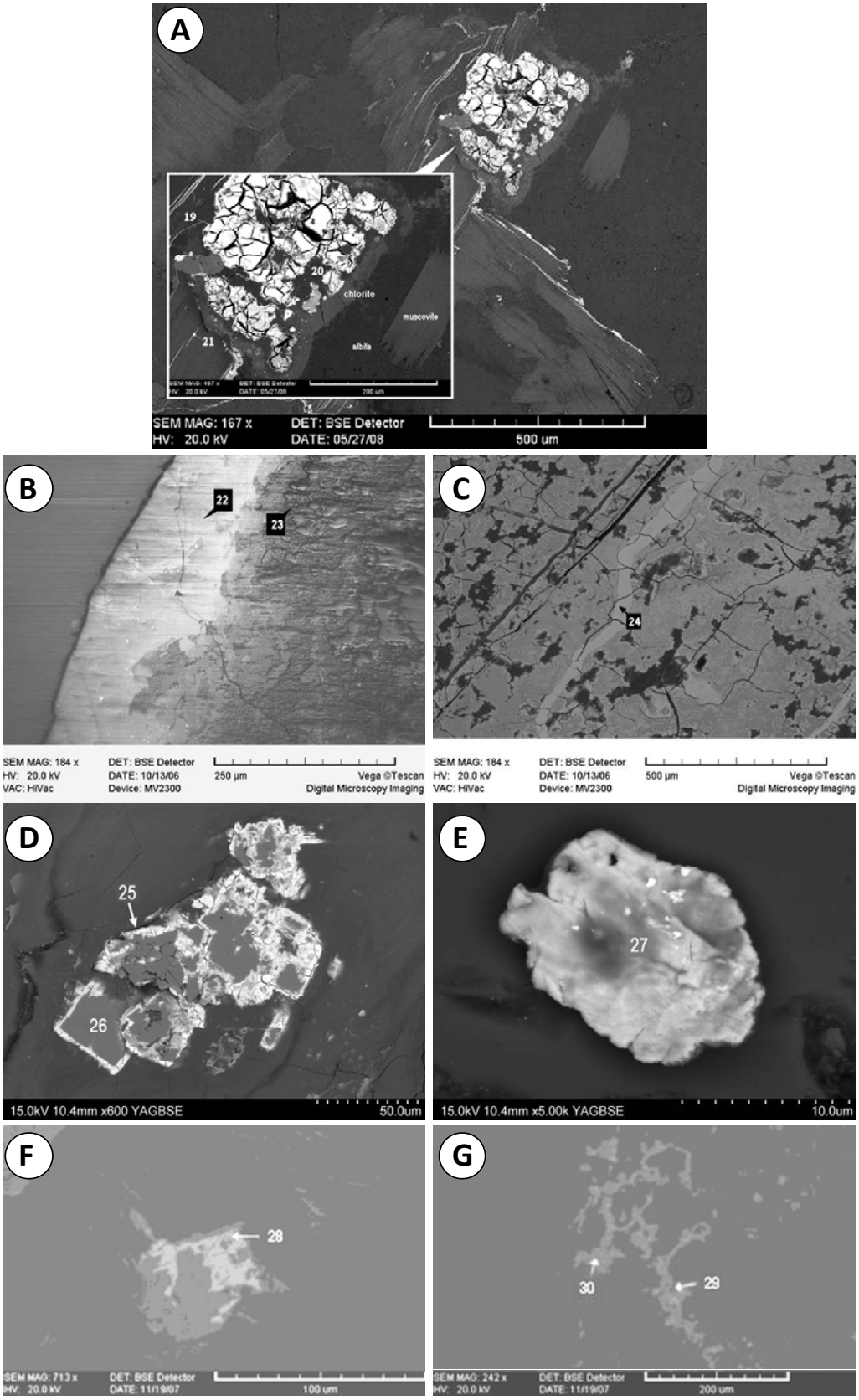

Figure 3.19. Radioactive and accessory minerals of the Litsevskoe ore-showing. *(BSEM images; the numbers correspond to semi quantitative SEM-EDS determinations).* **A.** Uraninite (19), hexavalent uranium minerals(20) and coffinite (21) [sample 64.1]; **B.** Pitchblende (22) and uranophane (23) [sample 65.1]; **C.** Uranophane-II (24); [sample 65.1]; **D.** Brannerite (25) and rutile (26) [sample 6520/4]; **E.** Cu,Ni,Zn Au-bearing mineral (27) [sample 6520/8]; **F.** Brannerite (28) with rutile in muscovite [sample 107.1]; **G.** REE and uranium bearing mineral (29,30) [sample 107.1].

3.3. REE distribution

The distribution of rare-earth elements for all the samples of each occurrence is presented in figure 3.20.

- Archean and Proterozoic occurrences have the highest REE content. The peraluminous rocks show enrichment in HREE and a strong Eu depletion. The basic rocks express different REE distribution with low HREE content.
- In the Paleozoic occurrences, the total REE content are lower, with a more marked Eu depletion. LREE are enriched in comparison with HREE.

Bea (1996) established that major minerals play a very subordinate role with respect to that of accessories (Gromet and Silver, 1983) in the REE repartition, especially in peraluminous systems (Figure 3.21). The accessory assemblage of peraluminous granites is composed of monazite, xenotime (restricted to low-Ca varieties), apatite, zircon, Th-orthosilicate, uraninite and betafite—pyrochlore minerals.

We can thus discuss about the observed REE distribution of REE in the Kola Peninsula occurrences with the accessory minerals that have been previously described in part 3.2.

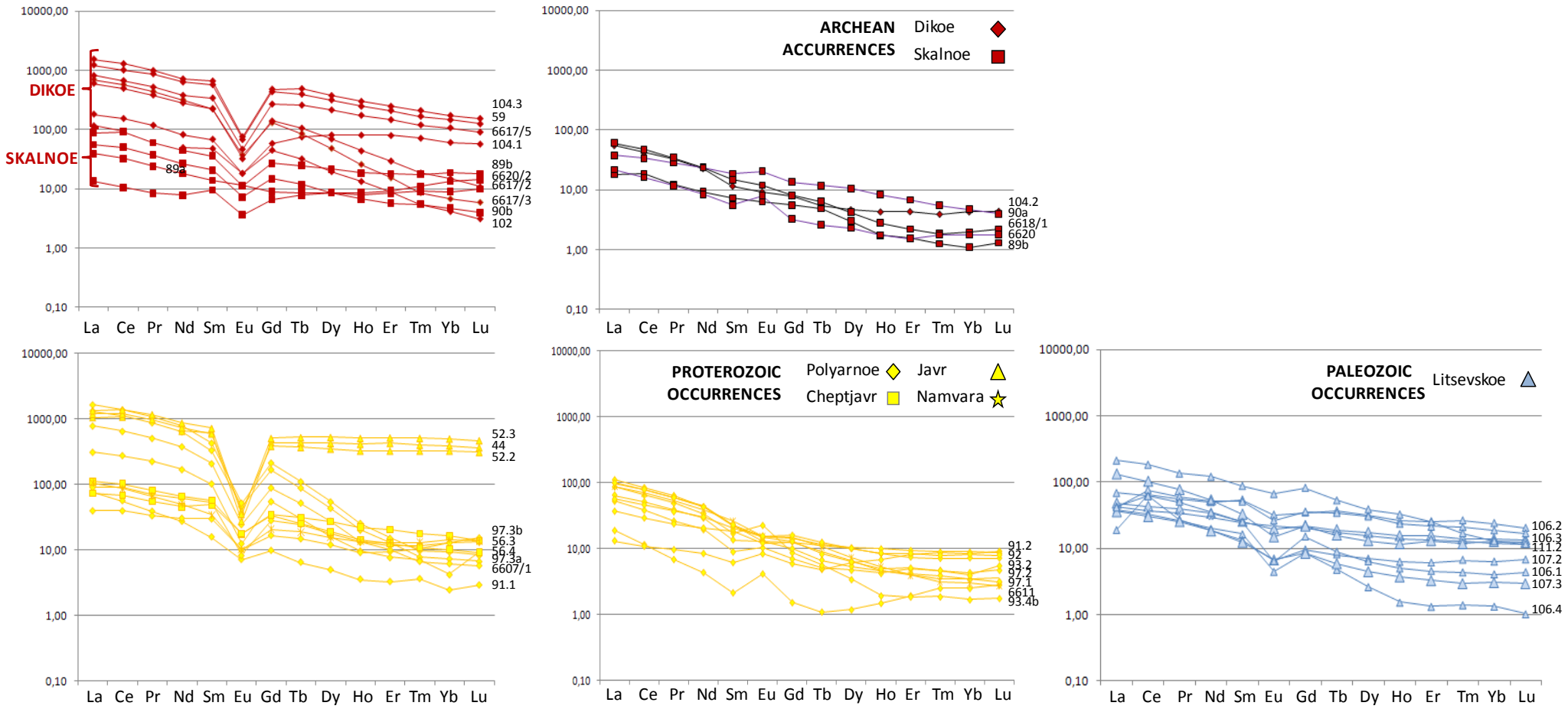

Figure 3.20. REE distribution diagram for the samples from the Archean (Dikoe and Skal'noe) occurrences (in red), the Paleoproterozoic occurrences (Polyarnoe, Namvara, Cheptjavr and Jevr) (in yellow) and form the Paleozoic ones (Litsvskoe) (in blue).

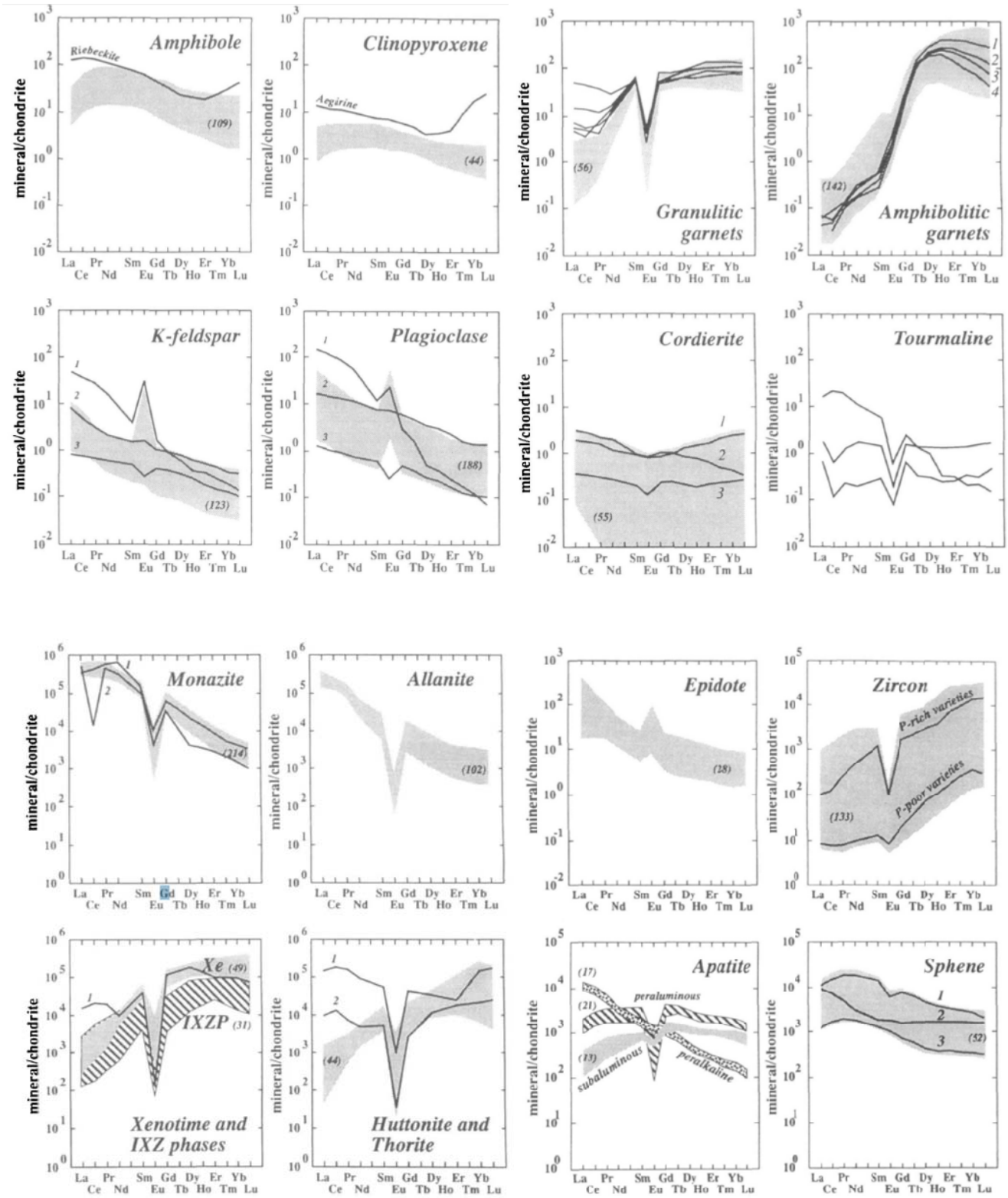

Figure 3.21. REE spectra of major and accessory minerals (Bea et al. 1996).

For Bea (1996), the textural position and small grain-size of REEYThU-rich accessories further complicates the partitioning of REE, Y, Th and U during melt segregation.
The behaviour of accessory minerals during partial melting depends on whether they are placed at major-phase grain boundaries or are included within major minerals (Watson *et al.,* 1989).

- In the first case, accessories are available for the melt and so react with it.
- In the second case, accessories may remain physically isolated from the melt, thus preventing any reaction, or may be entrained as inclusions if major minerals are incorporated into the melt as restitic crystals (Watt and Harley, 1993; Bea *et al.,* 1996).

However, this is not the situation for monazite, xenotime and zircon, because their grain-size is significantly smaller, usually <30 μm. Results of modal counting with SEM repeatedly indicate that the mass fraction of monazite, xenotime and zircon located at major-phase grain boundaries is <20 wt%, whereas >70 wt% of the mass of these minerals is included within biotite, which thus physically controls the behaviour of REE, Y, Th and U during melt segregation.

This fact has to be related with the field observations in the Kola Peninsula and on the thin section, where respectively biotite selvage always show an increase of radioactivity in comparison with the whole rock, and the fact that accessory minerals are always included in micas (biotite and/or muscovite) (see figures 3.12, 3.13, …).

In common peraluminous migmatites (Bea, 1996), the mass fraction of monazite, xenotime and zircon included within biotite is very high. Whether these inclusions are available for the melt during anatexis or stay within their host—either in restites or entrained within restitic crystals suspended in the melt—depends completely on the behavior of biotite. During crystallization, the small grain-size of newly formed accessories makes their separation from the melt physically impossible until a growing major mineral includes them. Biotite, which has near-zero contents of REE, Y, Th and U, is the mineral which shows the greatest tendency to include REE, Y, Th, U rich accessories, probably owing to the combined effects of local saturation adjacent to growing biotite crystals and heterogeneous nucleation.

The composition of the granitoids observed in the Kola Peninsula is mostly peraluminous (Figure 3.1). The geochemical behaviour of REE, Y, Th and U in differentiated granites changes with aluminium saturation. In general, the higher the aluminium saturation index [ASI = mol. Al2O3/(CaO + Na2O + K2O)], the stronger the depletion in REE (except Eu), Y, Th and U in leucocratic differentiates (Bea, 1993). A good example, which may have important consequences for the understanding of heat production in the crust, is the contrasting vertical distribution of REE, Y, Th and U (and K) in vertically zoned plutons: in I-type granitoids the concentrations of REE, Y, Th and U increase from the least to the most differentiated facies, accumulating upwards (Sawka & Chappell, 1988), whereas in S-type granitoids, in contrast, the concentrations of REE, Y, Th and U decrease from the least to the most differentiated facies, accumulating downwards (Bea *et al.,* 1994a). These differences are due to variations in the nature of the major and accessory minerals as a consequence of changes in the aluminium saturation, the key factor being the progressive replacement of allanite and sphene by monazite and xenotime with increasing ASI and decreasing CaO, which seems to occur in the following way.

REE distribution diagram have been also obtained directly on uraninite of the Archean Dikoe occurrence. This distribution shows the typical shape of a magmatic uraninite as demonstrated by Bonhoure (2007) and Mercadier et al. (2010) and confirms the magmatic uranium enrichment associated to Archean occurrence (Figures 22 and 23).

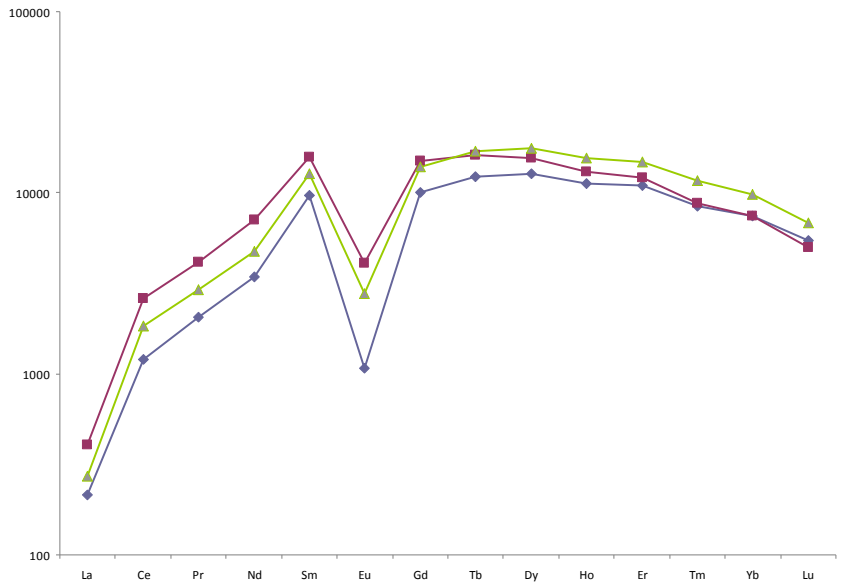

Figure 3.22. REE distribution diagram for the uraninite crystal of Dikoe *(by LA-ICP-MS, G2R, Nancy)*

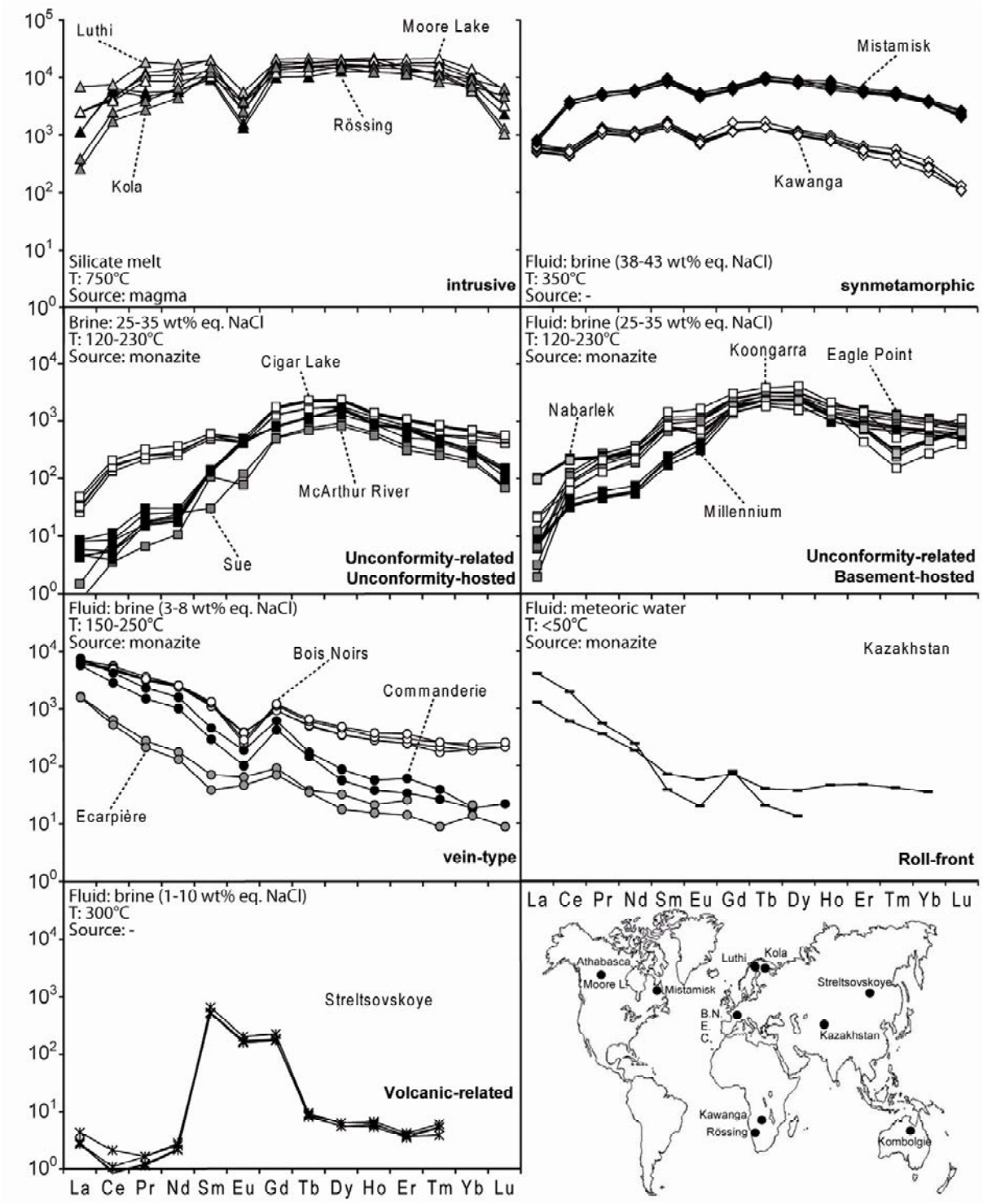

Figure 3.23. Spectres de terres rares spécifiques différents types de gisements (Mercadier et al., 2010)

3.4. Geochronological constraints

3.4.1. Archean occurrences

The less altered uraninite from the Dikoe ore-showing, the one from sample 59 was chosen for U-Pb isotopic dating. The Pb^{206}/U^{238} vs $Pb^{207}U^{235}$ and Pb^{207}/Pb^{204} vs Pb^{206}/Pb^{204} diagrams are presented on Figure 3.**24** A and B. The calculated ages 1825±20 and 1827±98 Ma don't correspond to the real age of the mineralization (U-Pb on uraninite: 2.7±50 Ga; *Anderson, 1990*) and could be possibly rejuvenated as a result of superimposed Svecofennian tectonothermal activation.

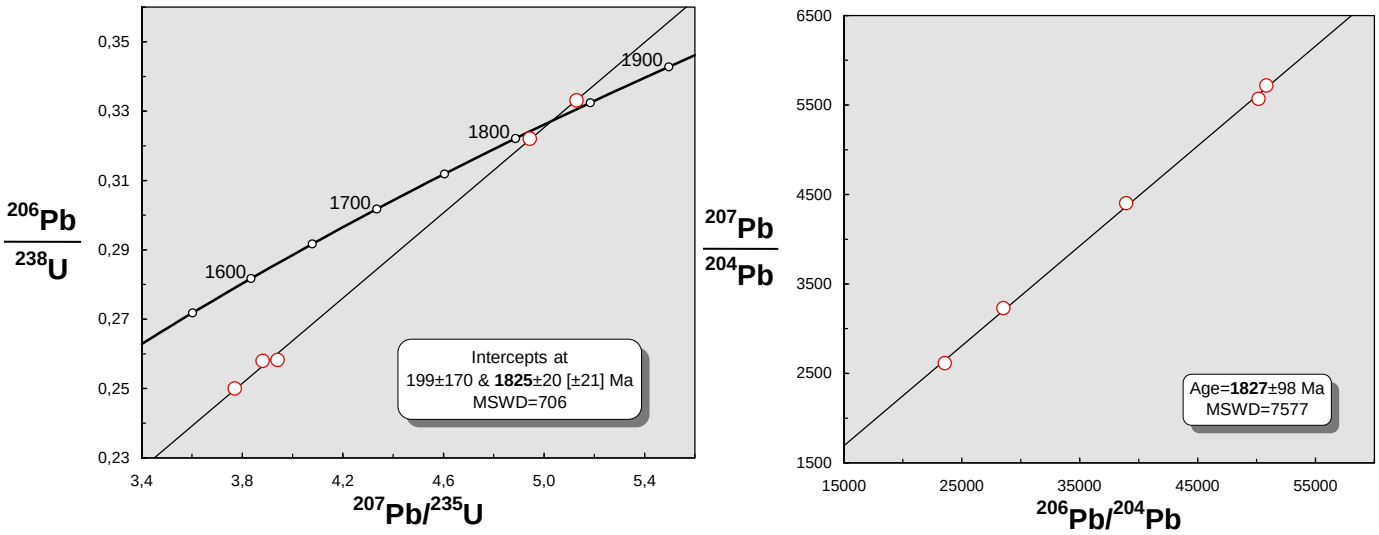

A. The Pb^{206}/U^{238} vs Pb^{207}/U^{235} concordia diagram; **B.** The Pb^{207}/Pb^{204} vs Pb^{206}/Pb^{204} discordia diagram;

Figure 3.24. U-Pb geochronological dating of the uraninite from the Dikoe ore-showing [sample 59].
(by SIMS SHRIMP-II – VSEGEI, St-Petersburg, Russia)

Geochronological dating was performed also for the well zoned zircons (Figure 3.25), separated from the granitoid hosting the Skal'noe ore-showing (sample 6618/1). The cores of the zircons give an age of 2465±130 Ma (Figure 3.26A), which correspond to the previously obtained ages. The zircon fringes give an age of 2115±56 Ma (Figure 3.26B), perhaps reflecting the Pb loss during metamorphic events. Also the ages of the cores most probably reflect inherited zircon from the source and the rims may reflect that of the granite crystallization. A resetting of Archean ages would give a Discordia with the point located between the Archean age and the age of the metamorphic event. Previous analyses were global zircon analyses which have most probably incorporated large fractions of inherited Archean zircons.

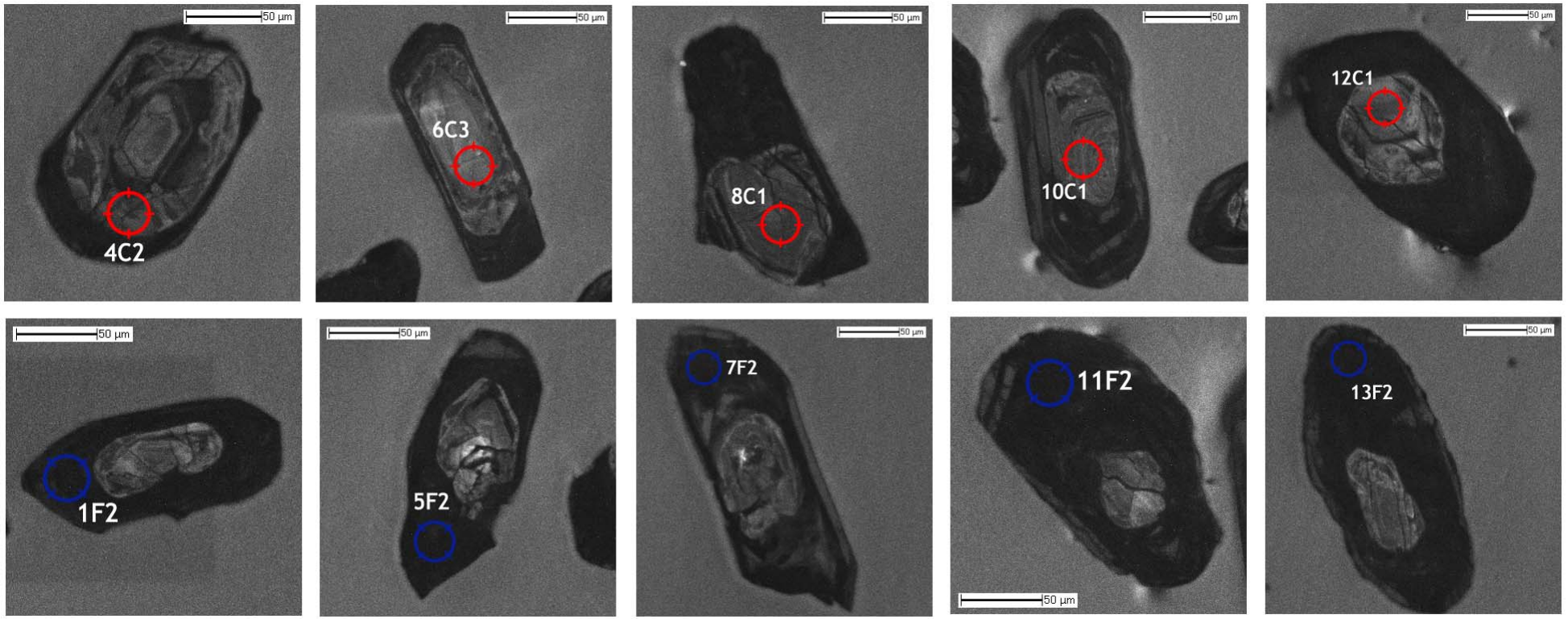

Figure 3.25. The CL (cathodoluminescent) images of the zircons from the Skalnoe ore-showing with the analytical points for U-Pb geochronological dating by SIMS [sample 6618/1].

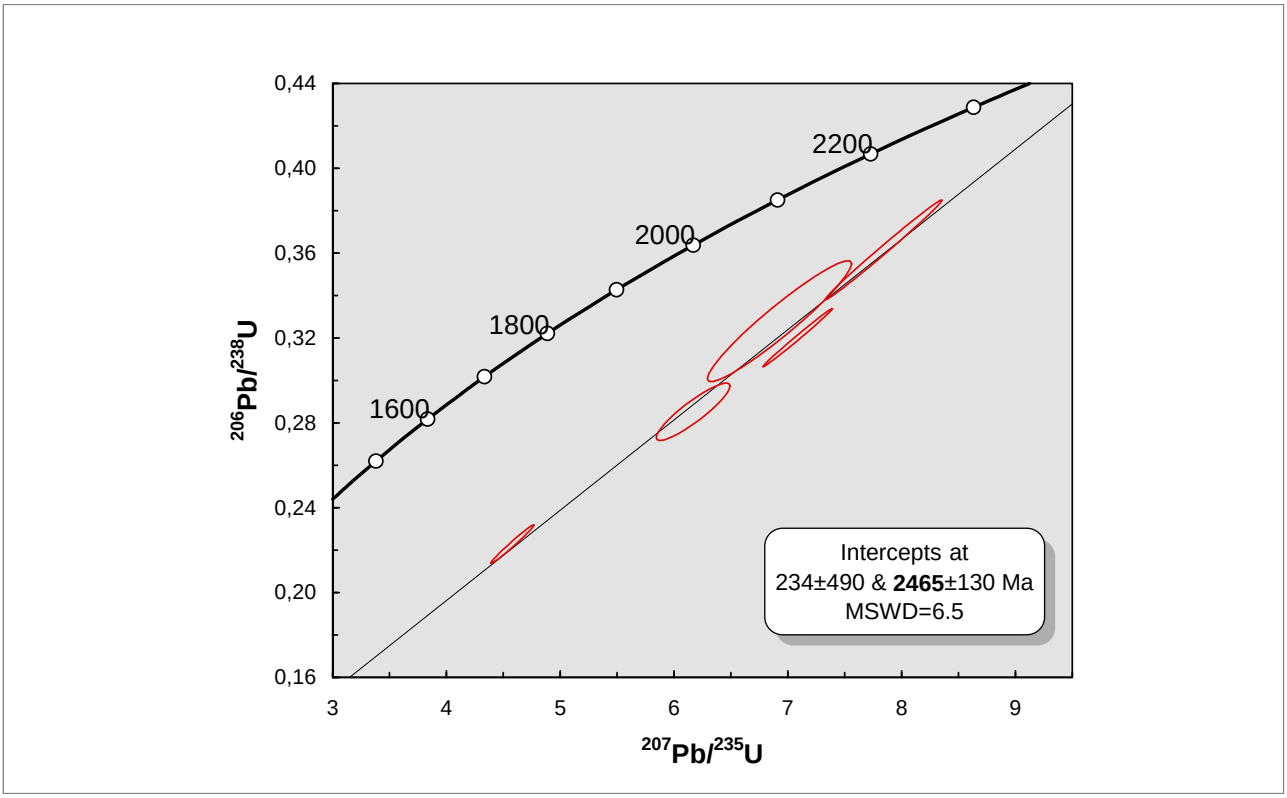

A. The Pb^{206}/U^{238} vs Pb^{207}/U^{235} discordia age for the cores of the zircons;

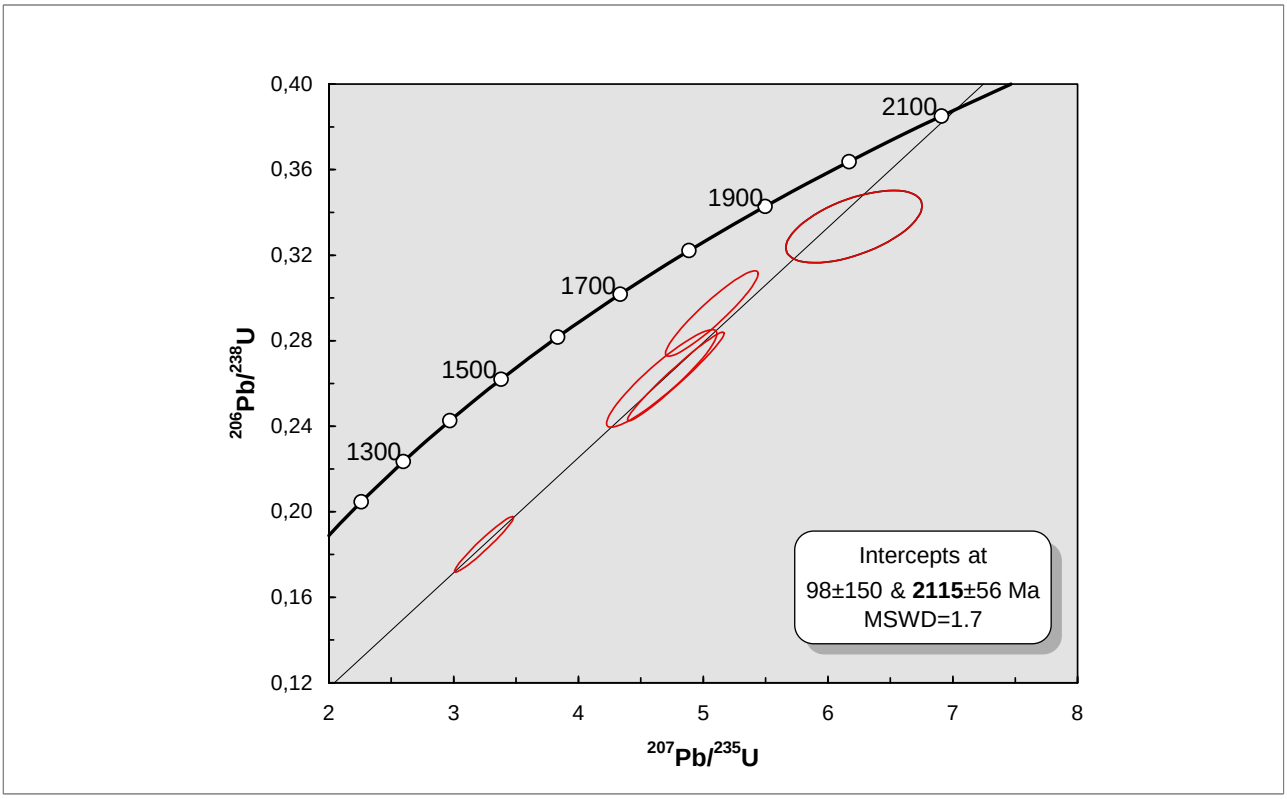

B. The Pb^{206}/U^{238} vs Pb^{207}/U^{235} discordia age for the fringes of the zircons;

Figure 3.26. U-Pb geochronological dating of the zircons from the Skal'noe ore-showing [sample 6618/1]. *(by SIMS CAMECA IMS 1270 - CRPG-CNRS, Nancy, France)*

3.4.2. Proterozoic occurrences

The sufficiently large size and relatively low rate of alteration of the uraninite crystals (Figure 3.27, Figure 3.29) have made possible in situ U-Pb isotopic dating with IMS-3F, the more so as Namvara and Cheptjavr occurrences have never been dated before. The results of these analyses are presented on Pb^{206}/U^{238} vs Pb^{207}/U^{235} diagrams (Figure 3.28 and Figure 3.30). For the Namvara uraninite an age of 2185±81 Ma is obtained, in agreement with the supposed Proterozoic age of the mineralization, while Cheptjavr's uraninite was dated at 1771±34 Ma, but the analytical data on the concordia diagram display unusually large error-ellipses. Uraninite from Cheptjavr ore-showing was studied with ICP and according to REE distribution is linked to magmatic source with a temperature > 700ºC.

As for Namvara and Cheptjavr, the dating has been performed on the uraninite from Polyarnoe ore-showing, but the results have too large analytic uncertainties and cannot be presented in a significant diagram.

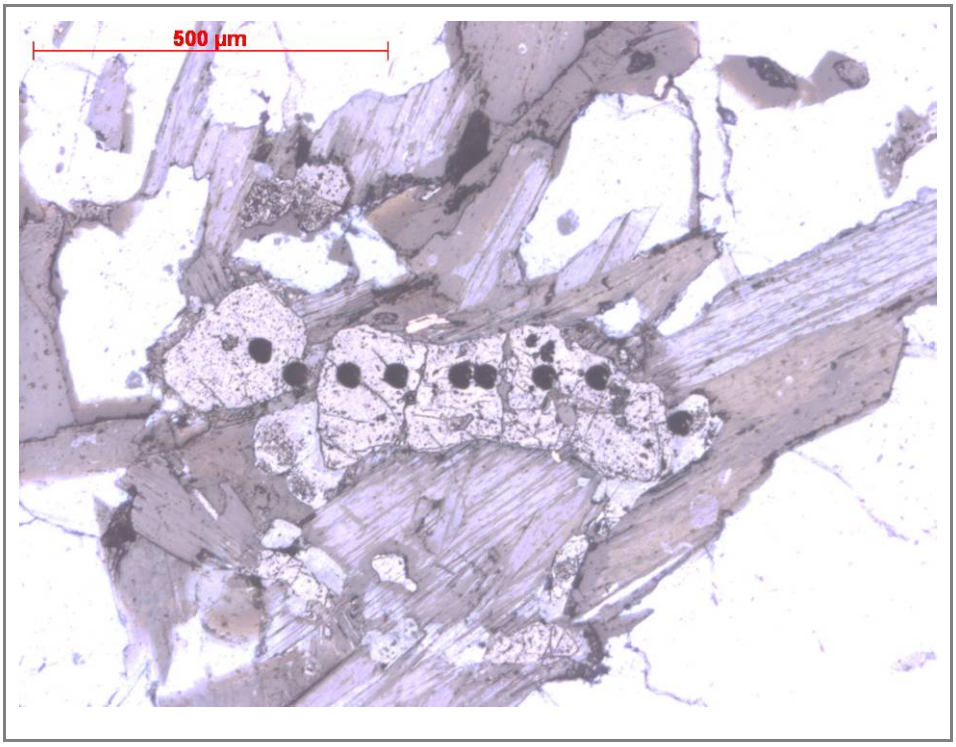

Figure 3.27. Reflected light image of an uraninite from the Namvara ore-showing with the analytical spots created during SIMS U-Pb geochronological dating [sample F134a].

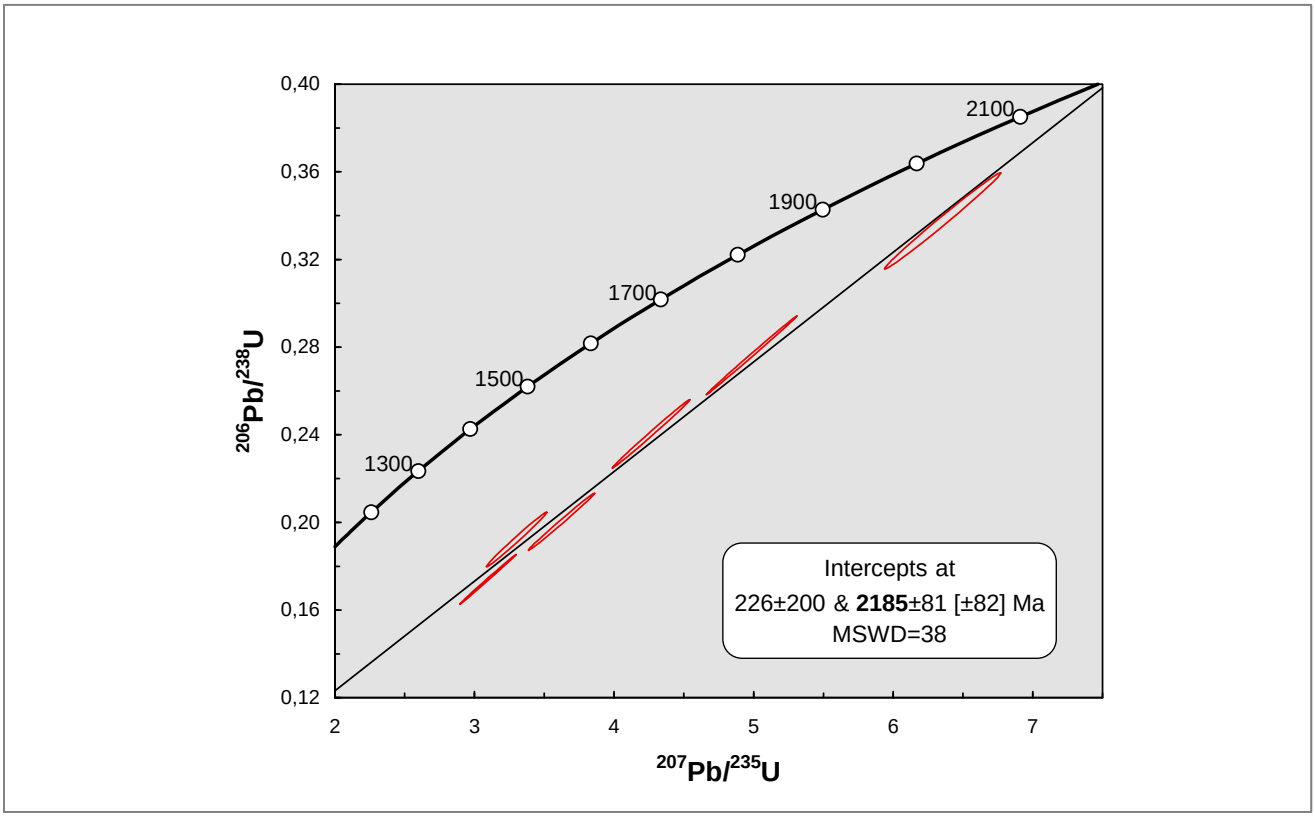

Figure 3.28. The Pb^{206}/U^{238} vs Pb^{207}/U^{235} concordia diagram for the uraninite from the Namvara ore-showing [sample 134a] *(by SIMS CAMECA IMS-3F - CRPG-CNRS, Nancy, France).*

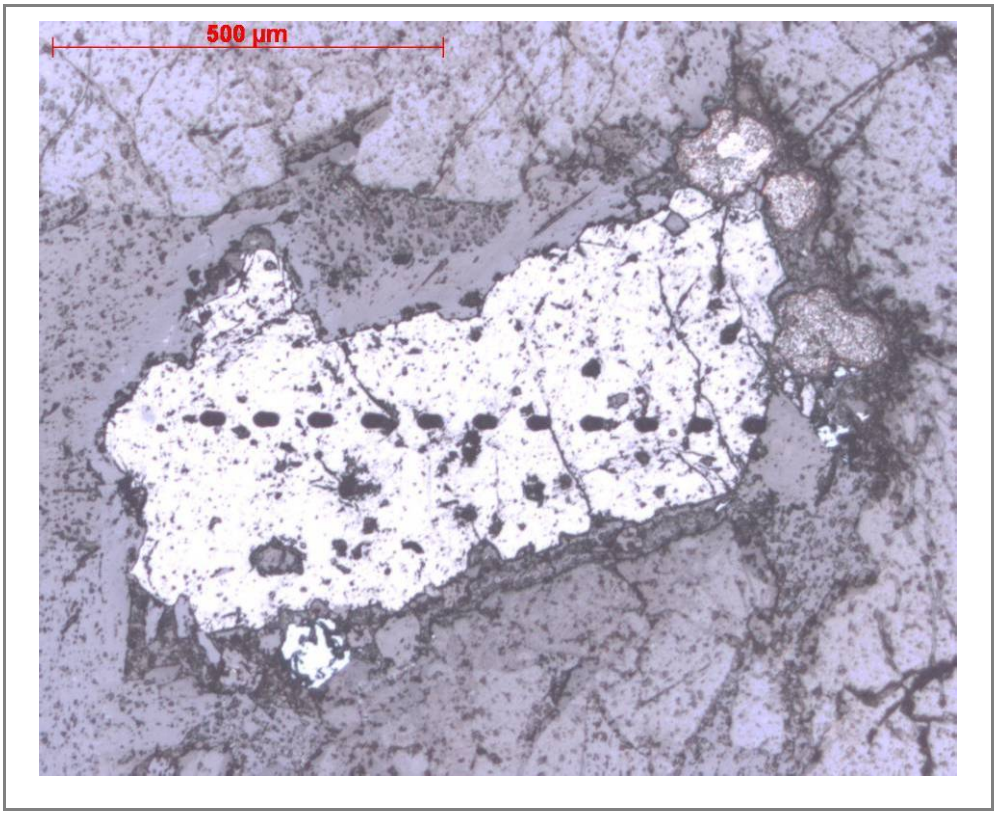

Figure 3.29. Uraninite from the Cheptjavr ore-showing [sample 56-3].

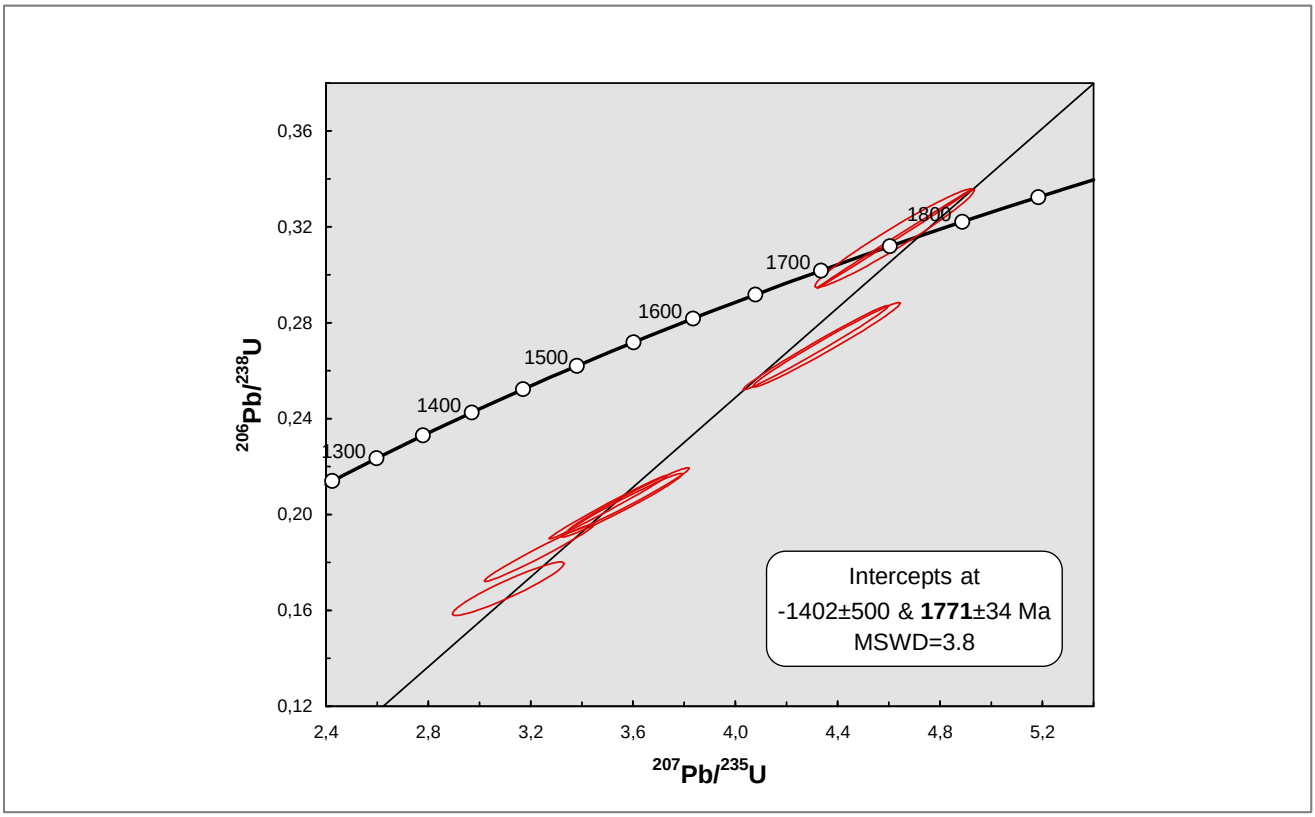

Figure 3.30. The Pb^{206}/U^{238} vs Pb^{207}/U^{235} concordia diagram for the uraninite from the Cheptjavr ore-showing [sample 56-3] *(by SIMS CAMECA IMS-3F - CRPG-CNRS, Nancy, France).*

3.4.3. Paleozoic occurrences

The U-Pb isotopic dating was performed on pitchblende (sample 65.1) – Pb^{206}/U^{238} vs Pb^{207}/U^{235} diagram is presented on Figure 3.31. The age of 455±6 Ma doesn't exactly correspond to the data of previous researchers (370±20 Ma - *Anderson; 1983*). The older age possibly results of radiogenic Pb abundance in the system, conditional on the presence of galena in the sample.

The Rb-Sr dating was performed for the sample F107.1 from the mafic dyke (Table 3.**2**), where muscovite has comparatively high contents of Rb^{87} and Sr^{86}. But at the same time the crystals are altered, and the low Rb^{87}/Sr^{86} ratio indicates the opening of the isotopic system, so the results have very high MSWD and are older, than the real age of the sample. Thus, the bulk-mica value seems to be the closest to the real age of the rock, which must be in fact less than 1000 Ma.

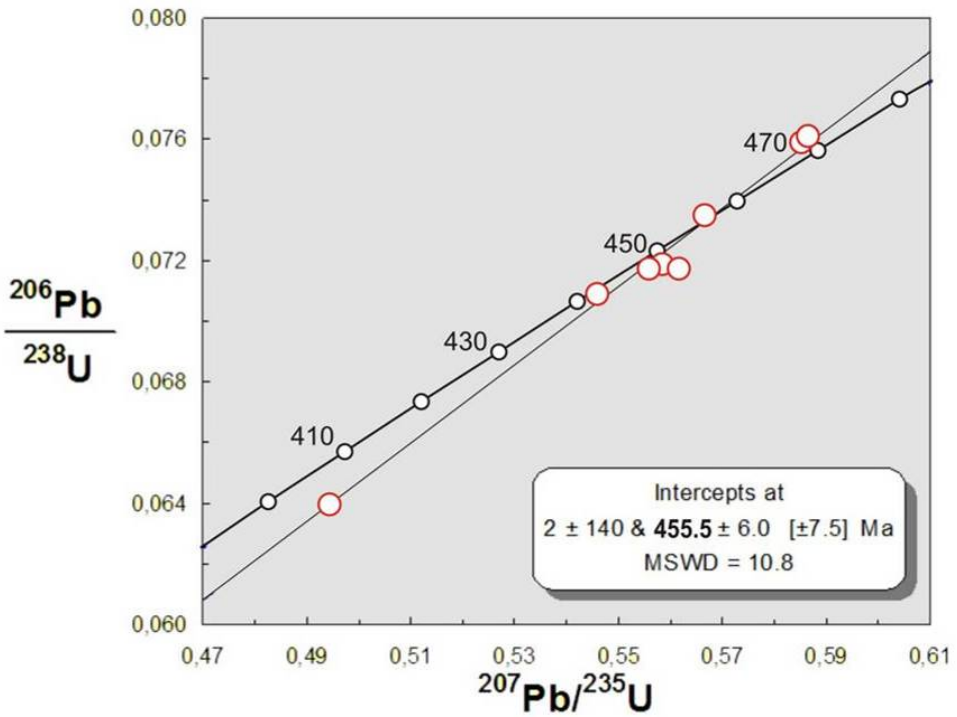

Figure 3.31. The Pb^{206}/U^{238} vs Pb^{207}/U^{235} diagram for the pitchblende from the Litsevskoe ore-showing [sample 65.1] *(by SIMS SHRIMP-II – VSEGEI, St-Petersburg, Russia).*

Table 3.2. Results of Rb-Sr analysis of the mafic dyke from the Litsevskoe ore-showing [sample 107.1]

1	107.1 bulk	12.94	6.913	5.4687	0.815700±10
2	107.1 apatite	1.044	137.6	0.0219	0.716075±10
3	107.1 mica	148.9	22.03	20.148	1.029850±28

(1,2,3) t = 1075±700 Ma IR = 0.72±0.12 **MSWD = 1700** (Model 3);
(1,2) t = 1276±8 Ma IR = 0.71567±0.00021;
(1,3) t = 1020±8 Ma IR = 0.73592±0.00083;
(2,3) t = 1090±6 Ma IR = 0.71573±0.00021;

Conclusions

Having endured several successive uranium enrichments from Archean to Paleozoic, the Litsa district presents numerous (over 30) uranium occurrences and manifestations of different type and age.

The oldest Archean (2.75-2.65 Ga) uranium with thorium and REE mineralization in the district is associated with Archean pegmatoidic rocks, most likely resulting from partial melting. The complex of provided geochemical, petrographical, mineralogical and geochronological studies revealed the specific features of these occurrences. Two major trends from the geochemical diagrams, corresponding to variable proportions of quartz-feldspars (probably a granitic melt) and biotite content in the rocks, were confirmed by optic observations. The uranium mineralization was studied with electronic microscopy and microprobe, and after dated by SIMS at 1825±20 and 1827±98 Ma, which is younger, than the expected age and could be rejuvenated as a result of superimposed processes. The age of the host rocks was dated on zircons, which an age of 2465±130 Ma (cores – reflecting inherited zircon from the source), and 2115±56 Ma (rims - reflecting the age of the crystallization).

The uranium occurrences of Paleoproterozoic age (2.2-2.1 Ga) are concentrated in the pegmatoidic granite veins in host gneisses, which after the data of previous researches had suffered superimposed chlorite-albite alterations. These alterations have not been observed with optic microscopy, whereas the geochemical diagrams display the decrease Na+Ca correlated with dequartzification, which is common for albitization, or also can represent a classical magmatic fractionation of plagioclase leading to an enrichment of the melt in Quartz and K-feldspar. The microprobe studies of uranium minerals revealed the sufficiently large and relatively low altered uraninite crystals for in situ U-Pb isotopic dating, the more so as some ore-showings (Namvara and Cheptjavr) have never been dated before. For the Namvara uraninite the obtained age of 2185±81 Ma is in agreement with the supposed Paloproterozoic, while Cheptjavr's uraninite dating displays unusually large error-ellipses on the concordia diagram and cannot be considered as a reliable result.

The uranium mineralization of the Litsevskoe occurrence is polychronic. The oldest one (1.75-1.65 Ga) is presented by uraninite, crystallized during migmatization of aluminous-rich metasediments, when uranium-rich peraluminous melts was formed. It is a preliminary uranium concentration of sedimentary origin, occurred during Late Paleoproterozoic. The disseminated radioactive mineralization from the mafic dyke, dated by Rb-Sr at about 1 Ga is represented by brannerite and REE-U minerals. The most abundant is Paleozoic mineralization, dated by SIMS at 455±6 Ma. From geochemical data, the host rocks display a high K-Na-Ca variability, presumably connected with albitization process, verified with thin sections, where microcline is partly replaced by albite with the chess-board texture. Besides there is a significant increase ferromagnesian and alumina components, induced by the presence of high alumina biotite, which is often replaced by chlorite and chamosite. Chloritization processes together with constant sericitization and hydromica alterations, observed in thin sections and revealed by X-ray analyses; compose the complex of middle to low temperature hydrothermal alterations of the host rocks in the occurrence.

PART 3. ANNEXE 1

from Brouand M. (BG Mines – AREVA)

USED ABBREVIATIONS AND SPECIFIC TERMS

ICP-AES and MS : **I**nductively **C**oupled **P**lasma (source) - **A**tomic **E**mission **S**pectroscopy (analytical method for major elements), and **M**ass **S**pectrometry (analytical method for trace elements).

A = Al-[Na+K-2Ca], chemical-mineralogical parameter (in millications) giving the excess of alumina not bound to the feldspars (similar to normative corundum, and A/CNK index.

B = Fe+Mg+Ti, chemical-mineralogical parameter (in millications) used as a differentiation index for igneous rocks.

Q=Si/3-[Na+K+2Ca/3), chemical-mineralogical parameter (in millications) estimating the quartz content of a rock by substracting silica bound to the feldspar to the total silica content of the rock.

P=K-[Na+Ca], chemical-mineralogical parameter (in millications) discriminating between K-feldspar (positive) and plagioclase (negative).

OBJECTIVES OF THE GEOCHEMICAL DIAGRAMS USED IN THIS REPORT

Several types of geochemical diagrams were used in this report:

• **Mineralogical-chemical diagrams** established by Debon and Le Fort (1983 & 1988) which intend to represent major element whole rock composition using chemical parameters (calculated in millications : $[M_{oxyde}/M_{atomique}]xNb_{atoms}x1000$) selected for their discriminating power of the major rock types according to their mineralogy. Specific diagrams have been established for sedimentary and for igneous rocks. The composition field of the main rock types and the main rock forming minerals are also plotted in these diagrams as references. Using these references, the global composition of the rocks can be compared with known rock compositions and their variation of composition can be discussed in term of mineral abundances or fractionation.

- **A = Al-[Na+K-2Ca] vs B = Fe+Mg+Ti** diagram used to discriminate the different granite types according to their source (A parameter) and differentiation index (B parameter), (Debon and Lefort, 1988). Most of the sediments (clay bearing sediments) and granites deriving from their partial melting plot in the peraluminous field (A>0). The metaluminous field (A<0) is typical for magmatic rocks derived from mantle partial melting or carbonate bearing sedimentary rock. The graywackes occupy most of the peraluminous field because of their large range of composition. The shales occupies a more restricted field with very high A parameter and high B parameter. Quartzo-feldspathic sediments are close to the origin of both axes.

- **Q=Si/3-[Na+K+2Ca/3) vs P=K-[Na+Ca]** diagram used to determine the main igneous rock types (Debon and Lefort). A reference grid with the average composition of the major rock types is used to determine the rock typology.

- **B=Fe+Mg+Ti vs Th** diagram allows to discriminate basic igneous rocks (low Th ~ 1 ppm) and high B from other rocks rich in femic minerals.

• Classical **binary diagrams** in which specific ratios or average compositions are used as references:

- **Th vs U**: used mainly to follow the behaviour of uranium with respect to Th which is a relatively stable element in most hydrothermal processes. Three reference ratios are used: (i) Th/U=4 for the average crust, Th/U=10 for granulitic rocks which have lost a large part of their uranium during metamorphism, Th/U=1 typical of U-enriched peraluminous leucogranites resulting from the partial melting of an U-enriched crustal source.

: A great care has to be taken in the interpretation of the data because alteration, which is very common in many of the studied samples, shift the plot location of these rocks in most of the diagrams and particularly in those involving Na, this element being the most readily leached during alteration and weathering.

PART 3. ANNEXE 2

Table 3.3. Chemical composition of the samples from the Archean (Dikoe and Skalnoe) occurrences

OCCURRENCES	LABORATORY	Sample description	Samples	SiO2	Al_2O_3	Fe_2O_3t	MnO	MgO	CaO	Na_2O	K_2O	TiO_2	P_2O_5	Pf	total
SKALNOE	SARM	pegmatite	88a	71,05	16,87	0,88	0,01	0,49	0,29	4,09	4,61	0,11	0,10	1,20	99,70
	VSEGEI	pegmatite	88b	77,10	13,10	0,70	0,01	0,42	0,50	2,78	4,28	0,08	0,12	0,92	100,01
	VSEGEI	pegmatite	89a	66,50	17,80	4,26	0,04	1,61	1,40	4,75	2,12	0,13	0,14	1,42	100,17
	SARM	qtz-fsp metasomatite with ms	89b	51,31	18,64	14,52	0,07	4,79	0,95	2,70	5,01	0,85	0,14	2,01	100,99
	SARM	pegmatite	90a	66,86	17,52	3,49	0,02	1,66	0,99	5,04	1,94	0,39	0,07	2,23	100,21
	SARM	pegmatite	90b	88,49	3,45	3,34	0,02	1,65	<D.L.	0,07	1,27	0,45	0,05	0,80	99,59
	SARM	pegmatite	6618/1	76,75	13,37	0,70	0,01	0,30	0,22	4,31	3,12	0,10	0,06	1,16	100,10
	SARM	pegmatite	6620	72,56	12,55	4,48	0,02	2,35	0,86	2,77	2,29	0,63	0,08	1,47	100,06
	SARM	pegmatite	6620/2	69,89	10,80	7,75	0,05	3,95	0,23	1,20	3,44	1,07	0,08	1,99	100,44
DIKOE	VSEGEI	granitoid	102	68,00	18,00	1,32	0,02	0,36	0,46	2,06	8,30	0,14	0,07	1,17	99,90
	VSEGEI	qtz-fsp metasomatite with ms	104.1	63,40	21,90	1,47	0,02	0,31	1,64	5,16	4,58	0,15	0,08	1,20	99,91
	VSEGEI	pegmatite	104.2	80,60	9,70	2,67	0,03	0,77	1,43	2,99	1,22	0,29	0,06	0,41	100,00
	SARM	qtz-fsp metasomatite with ms	104.3	54,63	29,24	1,55	0,01	0,42	1,06	3,77	6,12	0,15	0,20	3,21	100,36
	SARM	qtz-fsp metasomatite with ms	59	55,57	26,72	1,67	0,02	0,48	1,44	4,41	5,07	0,17	0,19	2,79	98,53
	SARM	qtz-fsp metasomatite with ms	6617/2	58,76	21,03	5,27	0,03	1,70	2,09	5,68	3,53	0,52	0,12	2,01	100,74
	SARM	pegmatite	6617/3	76,09	12,51	0,79	0,01	0,20	0,45	2,44	5,65	0,08	0,08	0,69	98,98
	SARM	pegmatite	6617/5	60,08	24,74	1,42	0,03	0,41	1,54	5,07	4,43	0,16	0,13	2,49	100,49

Table 3.3. Chemical composition of the samples from the Archean (Dikoe and Skalnoe) occurrences (suite).

Samples	Ba	Be	Co	Cr	Cs	Cu	Ga	Ge	Hf	In	Mo	Nb	Pb	Rb	Sb	Sn	Sr	Ta	Th	U	V	W	Y	Zn	Zr
88a	1929,00	<D.L.	1,53	33,07	<D.L.	7,45	23,72	1,18	5,64	<D.L.	3,61	2,30	33,23	69,53	<D.L.	1,03	172,10	0,25	49,79	38,67	33,38	1,63	8,54	13,78	172,80
88b	1530,00	0,66	1,15	38,10	0,23	5,31	17,20	1,78	1,32	<0.05	2,38	2,24	1,18	56,60	0,15	0,85	134,00	0,24	9,59	7,32	26,60	0,83	2,69	12,80	38,80
89a	347,00	1,25	6,86	69,60	1,10	13,90	18,70	2,15	2,94	<0.05	3,17	5,08	3,60	33,60	0,11	1,26	155,00	0,27	14,90	49,70	26,00	2,23	11,60	23,10	86,00
89b	473,00	1,67	21,84	137,10	6,39	5,90	29,58	2,51	10,48	<D.L.	1,43	20,30	40,71	143,60	<D.L.	2,22	126,00	1,72	28,96	59,32	99,40	2,27	31,90	87,97	334,70
90a	351,90	<D.L.	9,69	116,60	2,15	19,03	24,75	1,10	4,67	<D.L.	120,60	6,53	407,19	83,72	0,21	2,11	282,90	0,52	28,66	500,10	92,80	3,78	12,30	83,34	163,50
90b	134,40	<D.L.	10,60	205,10	2,63	20,29	11,04	0,98	7,77	<D.L.	175,70	8,80	348,64	67,61	<D.L.	1,80	5,02	0,73	53,45	610,60	100,50	2,91	7,12	90,80	256,20
6618/1	1402,00	0,00	1,60	71,51	0,00	9,02	15,99	1,06	3,96	<D.L.	3,56	26,63	28,10	45,28	0,23	1,27	146,20	1,56	8,77	32,00	17,13	0,97	3,48	17,57	171,70
6620	356,80	0,00	14,92	167,50	4,25	5,51	21,07	1,36	5,02	<D.L.	37,09	16,93	102,66	107,70	0,00	2,87	177,40	1,26	6,79	59,39	135,20	1,98	1,28	112,10	162,50
6620/2	394,00	1,56	27,77	288,20	7,71	21,55	30,18	1,33	14,06	<L.D.	141,60	65,47	209,64	177,80	0,25	4,98	78,63	4,75	28,80	239,30	232,90	3,06	15,22	193,00	448,60
102	1410,00	1,47	2,43	28,00	3,56	5,33	22,10	1,95	0,96	<0.05	69,40	9,02	11,30	197,00	0,13	3,76	243,00	0,83	52,80	399,00	26,30	4,30	16,30	20,40	23,30
104.1	731,00	1,68	3,40	27,30	2,60	8,79	25,00	0,95	1,70	<0.05	1,92	7,00	39,10	106,00	0,12	0,00	358,00	0,53	24,10	68,00	18,50	1,84	135,00	27,50	46,90
104.2	234,00	0,79	7,68	69,00	2,42	19,60	9,82	1,91	2,18	<0.05	2,56	4,47	3,14	56,50	0,29	0,68	252,00	0,37	4,42	4,01	39,90	<0.5	6,60	37,30	77,00
104.3	897,90	<D.L.	2,21	6,72	4,04	<D.L.	59,80	2,89	5,17	<D.L.	22,99	7,56	1014,50	174,50	<D.L.	5,23	237,00	0,49	390,30	2495,00	15,47	3,26	508,70	19,25	134,50
59	703,70	1,56	2,86	19,84	4,43	4,06	54,68	2,41	4,18	<D.L.	9,09	10,66	887,67	157,10	0,00	5,34	272,50	0,62	356,30	2288,00	15,50	2,90	366,70	19,01	111,80
6617/2	482,10	2,15	18,08	118,30	5,40	37,13	35,39	2,15	9,29	<D.L.	8,57	45,22	69,99	140,50	0,33	3,01	333,20	3,25	151,10	61,19	55,53	2,35	36,83	109,90	319,70
6617/3	1191,00	0,00	1,20	32,86	3,28	6,38	13,37	1,73	2,63	<D.L.	196,30	4,68	1060,89	135,40	0,00	1,87	237,30	0,45	183,90	1485,00	9,41	0,85	57,79	18,25	78,81
6617/5	548,30	0,00	2,42	15,96	3,25	0,00	44,19	2,06	3,88	< D.L.	10,80	9,86	677,96	127,20	0,00	4,42	294,50	0,61	215,20	1301,00	13,32	2,73	300,70	18,23	106,90

Samples	La	Ce	Pr	Nd	Sm	Eu	Gd	Tb	Dy	Ho	Er	Tm	Yb	Lu	□REE	$[Ce/Yb]_N$	Eu/Eu*	$[Gd/Yb]_N$	P	Q	B	A	Th/U
88a	10,67	32,34	3,46	12,91	4,14	0,70	3,55	0,56	2,52	0,30	0,64	0,08	0,50	0,09	72,46	16,74	0,56	5,74	-39,01	161,08	24,63	90,60	1,29
88b	4,47	11,70	1,18	4,40	1,12	0,37	1,13	0,18	0,76	0,10	0,26	0,03	0,18	0,03	25,91	16,82	1,01	5,07	-7,52	241,46	20,28	58,41	1,31
89a	13,50	32,10	3,60	12,60	3,16	0,42	3,01	0,44	2,19	0,44	1,39	0,23	1,48	0,25	74,81	5,61	0,42	1,64	-133,11	154,30	95,13	100,90	0,30
89b	21,65	58,64	5,79	21,08	5,54	0,64	5,50	0,92	5,43	1,04	3,00	0,45	3,08	0,45	133,21	4,93	0,35	1,44	2,55	79,93	311,88	138,08	0,49
90a	9,18	21,42	2,71	11,27	2,88	1,18	2,74	0,44	2,68	0,47	1,13	0,14	0,78	0,10	57,12	7,11	1,28	2,84	-138,97	155,65	90,00	104,53	0,06
90b	3,31	6,65	0,81	3,70	1,47	0,21	1,35	0,29	2,16	0,38	0,94	0,14	0,78	0,10	22,29	2,21	0,46	1,40			88,63		0,09
6618/1	14,73	30,16	3,33	11,09	2,26	0,69	1,64	0,24	1,07	0,16	0,36	0,05	0,32	0,06	66,14	24,17	1,10	4,10	-76,62	218,17	17,51	49,01	0,27
6620	5,28	10,27	1,13	3,99	0,85	0,46	0,66	0,10	0,58	0,10	0,25	0,05	0,29	0,05	24,04	9,20	1,89	1,85	-56,05	254,48	122,54	77,18	0,11
6620/2	9,50	20,67	2,30	8,54	2,14	0,66	1,83	0,32	2,15	0,49	1,54	0,28	2,20	0,36	52,98	2,44	1,02	0,67	30,31	273,50	208,89	91,72	0,12
102	44,20	97,40	11,30	38,80	10,50	1,05	9,10	1,19	4,93	0,75	1,44	0,14	0,68	0,08	221,56	37,07	0,33	10,81	101,96	129,08	27,25	93,66	0,13
104.1	28,60	59,20	-	23,50	7,31	1,04	11,90	2,81	20,60	4,57	13,20	1,83	10,00	1,44	186,00	1,53	0,34	0,96	-98,27	68,65	28,00	107,20	0,35
104.2	13,60	26,80	3,14	10,80	1,77	0,53	1,61	0,20	1,17	0,24	0,71	0,10	0,70	0,11	61,48	9,91	0,96	1,86	-96,02	308,16	56,25	16,83	1,10
104.3	375,10	819,30	95,11	337,90	101,30	4,43	97,95	18,30	95,23	16,97	41,01	5,38	28,68	3,91	2040,57	7,39	0,14	2,76	-10,30	38,92	31,75	283,99	0,16
59	298,30	639,70	83,70	299,50	87,83	3,96	88,21	14,78	80,20	13,99	34,73	4,30	24,12	3,18	1676,49	6,86	0,14	2,96	-59,97	41,28	34,91	222,70	0,16
6617/2	171,30	366,80	42,21	150,10	34,80	2,14	26,46	3,18	12,17	1,45	2,53	0,22	1,11	0,15	814,62	85,76	0,22	19,32	-145,23	43,19	114,88	79,83	2,47
6617/3	146,20	313,50	36,66	133,30	34,20	1,88	28,49	3,96	17,63	2,49	4,91	0,48	2,46	0,28	726,44	32,96	0,18	9,35	33,73	218,37	15,94	30,61	0,12
6617/5	199,70	427,90	50,16	179,50	52,60	2,69	54,80	9,66	54,29	9,84	24,21	3,06	17,62	2,29	1088,32	6,29	0,15	2,51	-96,79	57,55	29,95	172,70	0,17

Table 3.4. Chemical composition of the samples from the Paleoproterozoic occurrences.

OCCURRENCES	LABORATORY	Sample description	Samples	SiO2	Al_2O_3	Fe_2O_3t	MnO	MgO	CaO	Na_2O	K_2O	TiO_2	P_2O_5	Pf	total
POLYARNOE	VSEGEI	Orthogneiss	91.1	73,90	14,50	0,84	0,02	0,29	0,96	4,26	4,75	0,12	0,17	0,37	100,00
	VSEGEI	diabase	91.2	48,40	17,60	9,24	0,15	8,85	9,27	1,88	2,65	1,19	<.05	0,65	99,90
	VSEGEI	diabase with qtz-cb veins	91.3	53,30	16,60	10,60	0,16	4,98	8,79	3,56	0,69	0,77	0,13	0,46	100,00
	VSEGEI	gneiss	91.4	75,00	14,70	0,41	0,02	0,14	1,24	4,69	3,43	0,03	0,17	0,36	100,00
	VSEGEI	gneiss	92	63,80	16,50	7,45	0,07	3,11	1,20	2,43	2,03	0,73	0,05	2,61	100,00
	VSEGEI	qz-fsp granitoid	93.2	82,20	6,47	4,47	0,04	1,76	0,70	1,41	1,54	0,53	<.05	0,92	100,00
	VSEGEI	bt-rich fsp gneiss	93.3	66,60	15,20	5,37	0,05	2,31	1,97	4,53	2,33	0,57	0,06	1,02	100,00
	VSEGEI	leucogranite (plagioclase rich)	93.4	66,60	20,10	0,32	<.01	0,28	1,62	10,00	0,65	<.01	0,11	0,45	100,00
	VSEGEI	leucogranite (plagioclase rich)	93.4b	67,10	20,10	0,40	<.01	0,23	1,66	9,62	0,54	0,03	0,11	0,40	100,00
	VSEGEI	gneiss	97.1	67,80	15,00	4,61	0,04	2,09	2,23	4,23	2,32	0,60	0,12	1,00	100,00
	VSEGEI	bt-fsp rich gneiss	97.2	69,20	14,90	4,55	0,06	2,13	1,65	3,29	2,40	0,68	<.05	1,05	100,00
	VSEGEI	granitoid	97.3a	72,60	14,80	2,25	0,01	0,87	0,96	4,48	2,36	0,37	0,16	1,07	100,00
	VSEGEI	granitoid	97.3b	76,50	12,70	1,90	<.01	0,69	0,78	3,91	2,24	0,29	0,19	0,82	100,00
	VSEGEI	granitoid	97.3c	85,00	4,70	3,65	0,02	1,44	0,57	1,83	1,52	0,62	0,06	0,70	100,00
	SARM	qtz-fsp-bt gneiss	58-1	89,53	3,55	2,16	0,02	1,07	0,20	0,24	0,76	0,37	0,02	1,04	98,96
	SARM	qtz-fsp-bt gneiss	58-2	82,27	6,52	4,12	0,01	1,66	0,56	1,16	1,85	0,66	0,11	0,94	99,87
	SARM	cataclasite - pegmatoides	6607/1	79,30	6,90	5,52	0,03	1,97	0,21	1,32	2,14	0,75	0,09	1,46	99,68
	SARM	uraninite-rich pegmatoides	6607/5	97,14	0,74	0,28	0,01	0,06	0,04	0,00	0,09	0,04	0,02	0,43	98,83
CHEPTJAVR	SARM	bt rich qtz-fsp granite	56-3	65,19	15,84	5,25	0,05	1,19	1,87	4,48	3,67	0,48	0,07	0,62	98,71
	SARM	bt rich qtz-fsp granite	56-4	70,65	16,22	0,54	0,01	0,16	1,51	4,60	4,94	0,05	0,03	0,61	99,31
JAVR	VSEGEI	granite	114	53,40	15,50	13,80	0,11	6,05	1,18	2,29	1,29	1,78	0,23	4,26	99,90
	SARM	bt rich granite	52-2	60,85	18,79	4,63	0,05	2,03	1,81	5,34	2,85	0,62	0,19	1,97	99,12
	SARM	bt rich granite	52-3	57,50	16,94	8,79	0,06	3,49	1,85	4,10	1,28	1,02	0,25	3,20	98,47
PEREVAL	SARM	qtz-fsp pegmatoïdic granite	57-1	81,42	9,81	1,47	0,01	0,25	0,61	1,99	2,22	0,17	0,14	0,81	98,87
	SARM	qtz-fsp pegmatoïdic granite	57-2	83,40	8,84	0,50	0,01	0,12	0,16	1,26	4,51	0,07	0,00	0,74	99,60
NAMVARA	SARM	bt-gneiss	6611	73,77	15,38	1,57	0,01	0,57	0,93	3,61	2,71	0,20	0,08	1,42	100,25
	SARM	bt-gneiss with ky	6612/1	83,27	7,98	2,72	0,05	0,92	0,67	1,24	1,52	0,27	0,08	0,81	99,52
	SARM	bt-rich paragneiss	134.b	65,70	16,53	5,08	0,04	2,45	1,36	2,72	3,49	0,65	0,07	1,76	99,84

Table 3.4. Chemical composition of the samples from the Paleoproterozoic occurrences.

Samples	Ba	Be	Co	Cr	Cs	Cu	Ga	Ge	Hf	In	Mo	Nb	Pb	Rb	Sb	Sn	Sr	Ta	Th	U	V	W	Y	Zn	Zr
91.1	408,00	0,74	1,28	29,20	0,55	5,26	18,80	1,91	2,57	<0.05	3,37	5,23	3,69	124,00	0,12	1,73	127,00	0,29	11,40	7,47	9,04	<0.5	6,05	15,70	71,80
91.2	101,00	<0.5	47,00	202,00	3,29	14,20	12,30	2,05	0,70	<0.05	<1	2,86	0,92	147,00	<0.1	0,40	244,00	0,15	0,79	0,89	146,00	<0.5	10,70	74,10	22,60
91.3	181,00	0,70	37,30	25,50	0,71	22,40	18,20	1,97	2,43	0,06	2,15	4,94	3,54	20,80	<0.1	0,80	345,00	0,25	3,70	2,70	201,00	<0.5	15,20	77,70	87,10
91.4	223,00	<0.5	<1	30,80	0,37	5,37	16,00	2,33	0,98	<0.05	1,49	<1	0,66	61,10	0,11	0,80	114,00	<0.1	0,40	0,90	6,52	<0.5	2,43	11,80	22,20
92	529,00	1,75	28,90	170,00	0,99	43,90	20,70	2,22	4,17	0,05	2,45	8,26	5,62	65,90	<0.1	0,38	162,00	0,42	9,20	8,16	137,00	0,80	12,30	87,00	150,00
93.2	218,00	0,61	27,70	127,00	3,51	55,20	13,90	1,73	18,60	<0.05	3,14	16,60	2,30	112,00	0,10	3,28	90,60	0,68	39,90	391,00	85,60	0,75	10,40	76,10	579,00
93.3	580,00	1,91	23,50	133,00	2,96	14,90	19,00	1,97	2,66	<0.05	2,48	7,17	3,71	115,00	0,21	3,07	384,00	0,51	4,30	2,55	94,20	0,68	6,61	68,40	91,60
93.4	86,10	2,23	<1	28,50	0,27	83,00	16,80	1,73	2,33	<0.05	1,61	<1	4,63	24,60	<0.1	0,53	473,00	<0.1	13,90	6,21	11,90	<0.5	2,43	14,50	60,90
93.4b	85,40	2,89	<1	45,20	0,19	10,20	16,70	1,70	3,75	<0.05	2,49	1,08	4,71	19,30	<0.1	0,44	472,00	<0.1	16,40	9,87	9,97	<0.5	3,32	14,70	110,00
97.1	392,00	1,47	16,00	102,00	3,17	18,70	18,70	2,06	2,99	<0.05	2,53	7,70	2,52	137,00	0,20	1,24	271,00	0,59	6,46	5,02	99,90	<0.5	6,64	70,40	113,00
97.2	765,00	1,26	11,30	165,00	4,49	18,00	18,50	1,99	6,75	<0.05	2,50	9,09	6,14	112,00	0,11	0,46	306,00	0,48	12,70	2,89	94,80	0,52	8,21	58,60	253,00
97.3a	827,00	0,52	7,10	51,50	1,16	22,50	21,70	2,05	8,66	<0.05	10,40	9,66	82,80	88,40	<0.1	1,54	251,00	0,44	369,00	261,00	40,90	<0.5	28,00	42,60	248,00
97.3b	889,00	<0.5	5,70	46,40	0,88	15,70	19,30	2,18	13,20	<0.05	5,57	7,54	104,00	74,70	<0.1	1,34	226,00	0,37	478,00	365,00	32,00	<0.5	35,80	33,60	381,00
97.3c	229,00	<0.5	10,50	58,60	1,90	18,80	11,80	1,73	36,50	0,06	3,16	16,70	21,50	94,00	0,12	1,25	74,70	0,69	215,00	232,00	58,60	<0.5	12,60	62,70	1100,00
58-1	140,50	0,37	6,81	100,80	1,05	23,68	9,20	0,80	39,46	<D.L.	138,30	6,09	399,92	36,16	0,00	0,40	20,08	0,30	188,00	596,60	55,93	0,28	12,17	33,30	1195,00
58-2	388,40	0,21	14,72	89,79	2,34	60,35	18,66	1,83	19,90	<D.L.	6,24	16,77	288,18	117,70	0,00	1,64	107,10	0,92	389,00	299,40	65,22	0,26	27,43	82,36	562,00
6607/1	500,70	0,00	29,24	156,40	2,24	164,00	17,50	1,71	13,63	<D.L.	7,15	23,63	324,29	132,80	0,00	2,24	96,51	1,38	279,00	288,60	70,56	0,00	18,04	113,60	447,10
6607/5	70,04	0,00	0,93	95,50	0,00	9,21	1,67	0,91	27,30	< D.L.	342,10	5,30	461,56	6,70	4,70	4,76	8,69	0,40	216,40	529,80	3,84	0,36	15,23	8,36	850,40
56-3	214,30	1,79	8,82	155,80	3,24	12,06	30,18	0,98	5,47	<D.L.	17,17	28,18	352,18	173,00	0,00	2,53	198,20	1,13	98,22	957,10	45,48	0,59	30,82	89,71	157,60
56-4	440,40	1,62	0,96	20,36	0,94	4,14	20,91	0,95	3,12	< D.L.	3,63	3,60	210,17	139,90	0,00	0,37	228,00	0,20	102,10	251,70	2,64	0,00	19,81	11,25	74,64
114	93,40	2,36	32,60	211,00	0,85	34,00	43,50	2,57	176,00	0,10	388,00	136,00	83,70	81,20	<0.1	3,61	69,50	4,20	594,00	799,00	103,00	1,18	646,00	109,00	4490,00
52-2	303,30	2,68	11,42	136,10	1,42	24,19	40,95	2,77	83,12	0,08	242,30	43,99	333,33	122,50	0,00	2,28	179,70	2,30	502,50	767,60	50,17	0,77	508,20	59,09	1888,00
52-3	140,20	2,88	26,34	140,40	0,86	115,10	46,06	3,18	126,50	0,09	371,60	61,23	448,71	75,83	0,00	2,95	130,60	2,86	593,40	1224,00	72,75	1,07	807,80	67,94	2885,00
57-1	102,00	0,53	1,91	23,21	0,78	27,91	29,85	2,26	56,96	0,07	3,20	11,83	939,50	96,16	0,00	1,03	58,86	0,41	2662,00	1361,00	2,81	0,33	128,60	26,02	1263,00
57-2	181,90	0,00	0,72	62,88	0,87	5,70	14,66	0,99	6,97	< D.L.	3,61	16,16	200,70	140,80	0,00	0,71	60,91	0,74	650,80	168,00	2,32	0,00	17,42	9,59	154,40
6611	1006,00	0,00	4,57	77,23	0,75	12,11	15,57	1,06	3,47	<D.L.	19,52	5,22	78,20	89,97	0,00	1,65	339,70	0,29	13,92	51,61	23,86	0,00	6,99	50,01	117,70
6612/1	443,50	0,00	6,78	87,33	1,83	11,99	9,56	1,28	1,71	<D.L.	259,60	10,03	403,08	65,11	0,00	1,96	91,63	0,58	26,73	591,60	45,09	0,00	20,99	43,85	71,92
134.b	695,90	< L.D.	18,07	189,20	4,22	15,88	23,19	1,39	3,23	< D.L.	2,48	5,99	5,71	153,40	< L.D.	4,84	224,50	0,56	5,76	1,48	131,20	0,47	6,92	100,70	117,70

Table 3.4. Chemical composition of the samples from the Paleoproterozoic occurrences.

Samples	La	Ce	Pr	Nd	Sm	Eu	Gd	Tb	Dy	Ho	Er	Tm	Yb	Lu	ΣREE	$[Ce/Yb]_N$	Eu/Eu*	$[Gd/Yb]_N$	P	Q	B	A	Th/U
91.1	18,60	35,40	3,69	12,80	2,40	0,41	1,98	0,24	1,25	0,20	0,54	0,09	0,40	0,07	78,08	22,91	0,57	4,00	-53,48	160,47	19,25	11,71	1,53
91.2	3,19	6,87	0,92	3,96	0,94	0,48	1,20	0,18	1,53	0,38	1,33	0,22	1,37	0,23	22,80	1,30	1,38	0,71	-169,79	41,39	351,63	-102,79	0,89
91.3	13,90	29,80	3,54	14,50	3,09	0,88	2,94	0,44	2,65	0,57	1,58	0,23	1,48	0,22	75,82	5,21	0,89	1,61	-257,11	61,83	266,63	-117,75	1,37
91.4	4,60	7,34	0,66	2,06	0,33	0,24	0,31	0,04	0,30	0,08	0,32	0,06	0,41	0,07	16,83	4,63	2,29	0,61	-100,44	177,46	8,99	19,85	0,44
92	23,90	49,90	5,62	20,00	3,48	0,89	3,20	0,46	2,55	0,48	1,39	0,20	1,34	0,20	113,61	9,64	0,82	1,93	-56,61	218,43	180,00	159,29	1,13
93.2	9,10	18,70	2,30	9,77	2,85	0,70	2,58	0,42	2,51	0,47	1,22	0,18	1,18	0,18	52,16	4,10	0,79	1,77	-25,21	369,90	106,50	23,69	0,10
93.3	15,70	32,40	3,71	13,70	2,08	0,75	2,03	0,25	1,37	0,26	0,69	0,10	0,57	0,08	73,69	14,71	1,12	2,88	-131,72	150,69	132,00	32,16	1,69
93.4	21,70	41,30	4,63	16,50	2,43	1,32	1,95	0,19	0,72	0,10	0,21	0,03	0,15	0,03	91,25	71,26	1,85	10,51	-337,67	14,16	11,00	0,10	2,24
93.4b	21,10	41,30	4,71	16,00	2,63	1,31	1,78	0,21	0,87	0,11	0,31	0,05	0,28	0,05	90,70	38,18	1,85	5,14	-328,46	31,06	11,06	13,27	1,66
97.1	12,80	24,30	2,52	9,20	1,38	0,60	1,43	0,19	1,20	0,24	0,81	0,12	0,72	0,12	55,63	8,74	1,31	1,61	-126,90	164,15	117,38	28,84	1,29
97.2	27,00	53,60	6,14	20,60	3,35	0,86	2,64	0,31	1,61	0,28	0,85	0,12	0,65	0,14	118,15	21,34	0,88	3,28	-84,52	207,45	118,63	76,21	4,39
97.3a	318,00	703,00	82,80	296,00	50,50	2,65	34,00	3,29	11,00	1,14	2,12	0,20	1,21	0,17	1506,08	150,37	0,20	22,71	-111,43	197,01	54,50	61,36	1,41
97.3b	400,00	872,00	104,00	373,00	65,70	3,02	43,50	4,12	13,80	1,45	2,51	0,25	1,54	0,21	1885,10	146,55	0,17	22,83	-92,39	241,75	44,63	47,53	1,31
97.3c	75,30	175,00	21,50	79,60	15,70	0,73	11,20	1,13	4,05	0,55	1,28	0,18	0,70	0,24	387,16	64,70	0,17	12,93	-36,86	373,87	89,38	-19,52	0,93
58-1	9,72	25,31	3,22	14,50	4,60	0,58	3,42	0,56	3,06	0,52	1,56	0,27	2,14	0,39	69,83	3,06	0,45	1,29	5,11	470,98	58,34	38,71	0,32
58-2	259,30	552,60	71,86	265,10	45,46	1,87	25,14	2,67	9,66	1,09	2,28	0,23	1,42	0,22	1238,90	100,86	0,17	14,33	-8,07	373,31	101,11	30,97	1,30
6607/1	192,00	413,50	48,87	179,10	31,96	1,40	18,07	1,94	6,92	0,76	1,66	0,17	1,01	0,14	897,50	106,49	0,18	14,53	-0,66	349,87	127,64	39,89	0,97
6607/5	21,80	58,50	6,88	28,45	8,18	0,48	5,74	0,92	4,57	0,75	1,94	0,30	2,13	0,34	140,97	7,12	0,21	2,18	1,16	537,06	5,39	11,20	0,41
56-3	17,81	43,28	5,27	21,67	7,51	1,02	7,08	1,15	6,84	1,25	3,37	0,45	2,69	0,35	119,75	4,17	0,43	2,13	-99,80	117,10	101,30	21,41	0,10
56-4	27,04	64,38	7,80	31,16	8,75	1,03	6,88	0,94	4,74	0,81	2,09	0,28	1,68	0,23	157,80	9,94	0,40	3,32	-70,16	120,97	11,29	10,94	0,41
114	256,00	681,00	-	307,00	94,60	1,57	88,80	16,20	107,00	23,20	70,20	10,10	63,80	9,18	1728,65	2,76	0,05	1,12	-67,49	181,18	346,00	160,65	0,74
52-2	287,60	752,40	93,80	346,10	91,03	2,29	78,03	13,70	88,12	18,27	53,71	8,26	53,19	7,83	1894,33	3,66	0,08	1,19	-144,04	83,47	116,28	70,96	0,65
52-3	328,80	882,40	112,40	412,70	110,80	2,03	103,40	19,50	133,50	28,75	85,91	13,01	82,05	11,88	2327,13	2,78	0,06	1,02	-138,18	137,88	209,85	106,95	0,48
57-1	361,70	843,80	108,60	429,90	82,13	1,58	53,05	6,18	29,43	5,05	13,35	1,74	11,07	1,82	1949,40	19,73	0,07	3,87	-27,82	333,68	26,59	59,47	1,96
57-2	9,64	21,23	2,54	10,60	3,42	0,42	3,82	0,60	3,47	0,69	1,79	0,23	1,28	0,19	59,92	4,29	0,36	2,41	52,43	324,64	10,10	31,09	3,87
6611	21,53	44,35	5,11	18,41	4,01	0,88	3,01	0,40	1,86	0,30	0,66	0,08	0,49	0,07	101,16	23,38	0,77	4,96	-75,21	224,52	36,25	94,38	0,27
6612/1	25,84	54,87	6,42	23,41	5,26	0,58	4,23	0,71	3,97	0,77	2,17	0,33	2,37	0,35	131,27	5,99	0,38	1,44	-19,68	382,06	60,21	60,17	0,05
134.b	24,93	49,23	5,71	20,73	3,54	0,76	2,51	0,34	1,66	0,26	0,66	0,09	0,58	0,09	111,08	21,97	0,78	3,50	-37,64	186,89	132,96	114,04	3,88

Table 3.5. Chemical composition of the samples from the Litsa granite and Paleozoic uranium occurrences

OCCURRENCES	LABORATORY	Sample description	Samples	SiO2	Al_2O_3	Fe_2O_3t	MnO	MgO	CaO	Na_2O	K_2O	TiO_2	P_2O_5	Pf	total
LITSA GRANITE	SARM	granite	133.b	72,21	12,76	3,25	0,04	1,13	0,86	3,57	4,30	0,66	0,21	1,61	100,60
BEREGOVOE	SARM	bt-rich altered gneiss	6614	56,75	20,67	5,40	0,07	3,55	0,95	6,67	2,37	0,89	0,19	3,04	100,55
LITSEVSKOE	VSEGEI	migmatized biotite gneiss	62.1	63,44	16,76	6,10	0,04	2,79	1,47	3,72	2,50	0,65	0,08	2,45	100,00
	VSEGEI	fractured migmatite biotite gneiss	64.1	59,30	16,28	5,42	0,07	5,56	1,13	5,08	1,57	0,53	0,10	4,96	100,00
	VSEGEI	Pitchblende vein	65.1	55,04	15,28	5,94	0,11	2,37	1,37	2,72	2,04	0,51	0,20	0,00	85,58
	VSEGEI	altered gneiss	106.2	44,10	15,50	18,20	0,16	10,10	0,45	0,32	2,67	1,75	0,16	6,61	100,00
	VSEGEI	Mafic dyke	106.3	50,40	13,60	15,40	0,21	6,43	8,41	1,28	1,21	1,53	0,13	1,41	100,00
	VSEGEI	Mafic dyke	106.5	50,00	13,80	14,50	0,18	7,89	6,54	1,45	1,29	1,52	0,13	2,76	100,00
	VSEGEI	qtz-fsp-bt gneiss	106.1	73,40	14,50	1,18	0,01	0,45	0,51	3,92	5,43	0,18	0,09	0,50	100,00
	VSEGEI	qtz-fsp-bt gneiss	106.4	74,10	14,30	1,03	0,01	0,48	0,75	3,90	4,64	0,09	0,14	0,68	100,00
	VSEGEI	bt-rich gneiss	107.2	67,40	15,00	4,89	0,05	3,18	0,43	5,01	1,05	0,67	0,08	2,33	100,00
	VSEGEI	bt-rich gneiss	107.3	71,40	14,80	2,28	0,03	2,33	0,40	6,10	0,79	0,23	0,10	1,68	100,00
	VSEGEI	bt-rich gneiss	107.4	64,80	16,70	5,83	0,04	2,66	1,27	3,41	2,50	0,76	0,08	2,00	100,00
	VSEGEI	bt-rich gneiss	109.1	57,90	17,90	5,82	0,07	6,49	0,41	5,78	1,37	0,66	0,10	3,56	100,00
	VSEGEI	qtz-ms-pitchblende vein	111.2	70,30	14,60	3,29	0,06	1,55	0,63	5,03	2,17	0,38	0,08	2,12	100,00

Samples	Ba	Be	Co	Cr	Cs	Cu	Ga	Ge	Hf	In	Mo	Nb	Pb	Rb	Sb	Sn	Sr	Ta	Th	U	V	W	Y	Zn	Zr
133.b	1689,00	2,38	4,09	< D.L.	1,23	< D.L.	20,35	1,51	11,82	< D.L.	1,13	70,33	43,66	123,70	< D.L.	4,05	384,20	4,59	42,35	5,16	34,62	1,18	33,08	50,81	543,90
6614	376,60	2,62	15,39	67,29	3,03	8,63	39,89	2,58	13,87	< D.L.	2,37	21,31	44,36	128,00	2,10	5,03	297,40	1,25	337,60	14,80	95,97	1,79	19,89	89,82	540,60
62.1	8,07	4,47	20,82	179,10	0,20	31,51	22,74	1,63	2,98	3,63	7,75	144,10	12,99	209,20	1,17	0,10	149,10	0,88	9,08	2,64	132,20	0,32	0,84	97,62	14,94
64.1	2,55	4,64	17,83	117,00	0,20	73,04	24,15	1,29	3,81	1,44	15,16	105,10	61,60	104,50	1,28	0,08	209,00	1,83	11,57	546,90	97,53	0,40	1,43	70,53	33,63
65.1	1,97	32,69	47,92	146,70	1,64	431,70	41,79	4,98	3,81	7,42	45,74	127,00	4296,99	98,61	6,86	0,09	149,80	10,39	9,25	62960,00	278,60	15,28	51,34	48,39	1124,00
106.2	163,00	4,54	54,40	92,90	0,50	7,11	28,00	2,88	2,79	0,14	1,19	11,40	5,28	121,00	0,11	2,05	20,60	0,79	1,76	558,00	289,00	0,71	31,40	148,00	97,90
106.3	90,50	1,05	48,60	109,00	0,80	113,00	17,40	2,44	3,21	0,08	3,52	10,40	3,77	89,70	0,27	1,09	185,00	0,60	5,12	5,71	295,00	0,64	23,50	112,00	103,00
106.5	92,40	2,06	49,50	91,90	1,74	141,00	18,10	2,44	2,67	0,10	1,31	9,10	3,24	94,30	0,11	1,12	146,00	0,58	1,39	39,60	284,00	0,53	21,20	121,00	88,40
106.1	383,00	0,84	2,33	40,20	0,53	6,30	14,50	1,78	3,31	<0.05	2,23	8,87	4,85	147,00	0,13	0,82	69,10	0,38	14,30	6,64	7,54	<0.5	7,42	21,90	82,30
106.4	225,00	1,26	1,25	18,40	1,04	4,25	16,00	1,74	1,59	<0.05	1,25	3,02	2,55	152,00	<0.1	0,72	52,60	0,45	6,69	4,11	5,75	<0.5	2,64	25,40	39,60
107.2	57,70	2,07	12,20	118,00	0,74	12,10	22,40	1,60	3,92	<0.05	2,47	22,70	2,66	62,80	0,12	0,55	56,50	1,60	15,00	49,80	81,10	<0.5	9,41	59,70	126,00
107.3	57,10	2,11	6,72	47,40	0,40	13,70	15,90	1,72	1,28	<0.05	2,29	6,68	2,47	47,70	0,24	0,70	50,00	0,90	8,69	43,00	38,10	<0.5	7,47	36,10	36,40
107.4	272,00	5,31	18,20	169,00	6,85	41,60	24,40	2,02	4,24	0,08	2,87	19,10	7,39	204,00	0,23	0,89	136,00	2,16	12,60	11,20	126,00	0,63	19,20	71,70	149,00
109.1	137,00	3,82	21,80	109,00	2,71	37,60	25,50	2,01	3,62	0,06	1,14	20,10	5,82	101,00	<0.1	1,12	57,50	2,16	12,70	474,00	99,50	0,53	32,10	67,90	128,00
111.2	419,00	6,84	16,90	81,50	2,20	93,10	22,80	2,45	2,91	<0.05	10,70	22,70	13,00	98,80	0,37	0,99	89,10	3,13	12,70	528,00	71,30	0,76	102,00	28,60	96,20

Table 3.5. Chemical composition of the samples from the Litsa granite and Paleozoic uranium occurrences

Samples	La	Ce	Pr	Nd	Sm	Eu	Gd	Tb	Dy	Ho	Er	Tm	Yb	Lu	ΣREE	$[Ce/Yb]_N$	Eu/Eu*	$[Gd/Yb]_N$	P	Q	B	A	Th/U
133.b	207,40	407,60	43,66	147,30	20,25	3,14	10,57	1,37	6,90	1,17	3,53	0,52	3,65	0,54	857,60	28,88	0,66	2,34	-39,20	184,06	77,13	12,93	8,21
6614	404,90	882,60	-	393,30	62,91	2,83	32,51	2,68	8,18	0,77	0,91	0,16	0,97	0,13	1792,85	236,47	0,19	27,20	-181,71	38,20	167,48	106,13	22,81
62.1		29,25	58,75	6,82	25,00	4,63	3,43	0,49	2,73	0,52	1,53	0,24	1,64	0,25	135,28	4,62	1,53	1,69	-93,05	161,61	146,00	103,14	3,44
64.1		15,88	46,45	6,65	27,29	8,73	7,16	1,32	7,54	1,32	3,40	0,50	3,25	0,43	129,92	1,26	1,91	1,78	-150,63	118,59	206,75	81,78	0,02
65.1		392,40	917,70	138,50	588,30	187,50	206,40	27,77	143,90	24,23	55,18	6,32	33,49	4,54	2726,23	3,03	1,64	4,98	-68,79	158,20	133,50	119,72	0,00
106.2	4,54	41,80	5,28	23,30	8,37	1,86	7,07	1,39	7,98	1,46	4,20	0,67	3,92	0,51	112,35	2,76	0,74	1,46	38,46	172,41	501,88	220,90	0,00
106.3	11,70	27,30	3,77	15,90	3,89	1,13	4,47	0,71	4,37	0,87	2,58	0,35	2,25	0,34	79,63	3,14	0,83	1,61	-165,72	112,73	372,38	-100,56	0,90
106.5	10,50	23,70	3,24	13,80	3,67	1,27	4,18	0,65	4,00	0,79	2,17	0,33	1,98	0,29	70,57	3,10	0,99	1,71	-136,11	125,59	397,50	-37,04	0,00
106.1	16,70	39,00	4,85	16,50	3,86	0,37	3,07	0,33	1,61	0,28	0,75	0,11	0,66	0,11	88,20	15,29	0,33	3,76	-20,00	159,55	28,25	24,28	0,90
106.4	9,35	21,20	2,55	9,49	2,55	0,26	1,74	0,18	0,67	0,09	0,22	0,04	0,22	0,03	48,58	24,94	0,38	6,39	-40,46	178,03	26,04	29,24	0,04
107.2	10,50	39,30	2,66	8,97	2,04	0,38	1,95	0,30	1,76	0,35	1,00	0,17	1,03	0,17	70,58	9,88	0,58	1,53	-146,94	185,22	149,00	94,99	2,15
107.3	8,87	19,40	2,47	8,74	1,91	0,39	1,73	0,22	1,13	0,21	0,54	0,08	0,50	0,07	46,26	10,04	0,66	2,80	-187,10	178,17	89,63	62,51	1,63
107.4	32,40	65,40	7,39	25,50	5,04	0,86	4,40	0,59	3,30	0,66	2,16	0,30	2,08	0,31	150,39	8,14	0,56	1,71	-79,47	181,54	148,88	119,10	0,30
109.1	10,10	48,20	5,81	24,80	7,78	1,53	7,29	1,28	7,72	1,33	3,54	0,54	3,11	0,43	123,46	4,01	0,62	1,89	-164,61	101,06	243,25	120,96	0,20
111.2	52,00	117,00	13,00	57,30	13,50	3,84	16,80	1,98	9,84	1,83	4,16	0,43	2,10	0,29	294,07	14,42	0,78	6,47	-127,33	174,47	84,63	55,52	1,13

PART 3. ANNEXE 3

Table 3.6. Chemical composition of the radioactive and accessory minerals of the Archean (Dikoe and Skal'noe) occurrences. (SEM-EDS semi quantitative determinations).

(1) - uraninite						
Elmt	Spect. Type	Element %	Atomic %		Compound %	Nos. of ions
Si K	ED	1,37	3,74	SiO2	2,92	0,12
Ca K	ED	2,67	5,11	CaO	3,73	0,16
Pb M	ED	6,30	2,33	PbO	6,78	0,07
Th M	ED	4,83	1,60	ThO2	5,50	0,05
U M	ED	71,35	23,03	UO2	80,95	0,72
O		13,37	64,18			2,00
Total		99,88	100,00		99,88	
* = <2 Sigma					Cation sum	1,12

(2) - zircon						
Elmt	Spect. Type	Element %	Atomic %		Compound %	Nos. of ions
Al K	ED	2,84	3,07	Al2O3	5,38	0,19
Si K	ED	15,42	15,98	SiO2	32,99	0,97
Ca K	ED	1,36	0,99	CaO	1,90	0,06
Fe K	ED	0,72	0,37	FeO	0,92	0,02
Zr L	ED	43,54	13,89	ZrO2	58,81	0,85
O		36,12	65,70			4,00
Total		100,00	100,00		100,00	
* = <2 Sigma					Cation sum	2,09

(3) – monazite

Element	k-ratio (calc.)	ZAF	Atom %	Element Wt %	Wt % Err. (1-Sigma)	Compound Formula	Compound Wt %	No. of Cations
P -K	0.0954	1.827	19.29	17.43	+/- 0.26	P2O5	39.94	6.853
Ce-L	0.2357	1.257	7.25	29.63	+/- 0.79	Ce2O3	34.70	2.575
Ti-L	0.0000	1.587	0.00	0.00	+/- 0.00	TiO2	0.00	0.000
Th-M	0.0797	1.287	1.52	10.26	+/- 0.45	ThO2	11.67	0.538
Ca-K	0.0230	1.171	2.30	2.69	+/- 0.18	CaO	3.77	0.818
La-L	0.0663	1.274	2.08	8.45	+/- 0.97	La2O3	9.91	0.741
O -K	---	3.287	67.56	31.54 S	---	---	---	---
Total			100.00	100.00			100.00	11.525

(4) – Altered uraninite						
Elmt	Spect. Type	Element %	Atomic %		Compound %	Nos. of ions
Si K	ED	0.79	2.44	SiO2	1.70	0.07
Pb M	ED	9.41	3.93	PbO	10.13	0.12
Th M	ED	1.67	0.62	ThO2	1.90	0.02
U M	ED	76.05	27.65	UO2	86.27	0.85
O		12.08	65.36			2.00
Total		100.00	100.00		100.00	
* = <2 Sigma					Cation sum	1,06

Table 3.6. Chemical composition of the radioactive and accessory minerals of the Archean (Dikoe and Skal'noe) occurrences. (SEM-EDS semi quantitative determinations**).**

(5) – Altered uraninite						
Elmt	Spect. Type	Element %	Atomic %		Compound %	Nos. of ions
Si K	ED	1.79	4.92	SiO2	3.82	0.30
Fe K	ED	2.16	3.00	FeO	2.78	0.18
Pb M	ED	6.67	2.49	PbO	7.18	0.15
Th M	ED	3.75	1.25	ThO2	4.27	0.08
U M	ED	72.24	23.50	UO2	81.95	1.45
O		13.40	64.84			4.00
Total		100.00	100.00		100.00	
* = <2 Sigma					Cation sum	2,17

(6) – coffinite

Element	k-ratio (calc.)	ZAF	Atom %	Element Wt %	Wt % Err. (1-Sigma)	Compound Formula	Compound Wt %	No. of Cations
Si-K	0.0376	2.059	14.41	7.74	+/- 0.18	SiO2	16.57	5.349
U -M	0.6101	1.111	14.88	67.81	+/- 1.50	UO2	76.93	5.526
Ca-K	0.0367	1.266	6.06	4.65	+/- 0.26	CaO	6.51	2.251
O -K	---	4.901	64.65	19.80 S	---	---	---	---
Total			100.00	100.00			100.00	13.125

(7) – Xenotime						
Elmt	Spect. Type	Element %	Atomic %		Compound %	Nos. of ions
Al K	ED	0,97	1,18	Al2O3	1,84	0,07
P K	ED	15,87	16,73	P2O5	36,36	1,00
S K	ED	0,46	0,47	SO3	1,14	0,03
Se L	ED	2,35	0,97	SeO2	3,30	0,06
Sr L	ED	2,73	1,02	SrO	3,23	0,06
Y L	ED	31,41	11,54	Y2O3	39,89	0,69
Gd L	ED	1,62	0,34	Gd2O3	1,87	0,02
Er L	ED	3,01	0,59	Er2O3	3,44	0,04
U M	ED	1,32	0,18	UO2	1,50	0,01
O		32,83	67,00			4,00
Total		92,57	100,00		92,57	
* = <2 Sigma					Cation sum	1,97

Table 3.6. Chemical composition of the radioactive and accessory minerals of the Archean (Dikoe and Skal'noe) occurrences. (SEM-EDS semi quantitative determinations**).**

(8) – Nb-Ta-Ti-U oxide (pyrochlore type:$(Ca,U,REE)(Nb,Ta,Ti)_2O_6(O,OH,F)$						
Elmt	Spect. Type	Element %	Atomic %		Compound %	Nos. of ions
Al K	ED	0,30	0,59	Al2O3	0,57	0,04
Si K	ED	2,25	4,19	SiO2	4,81	0,25
P K	ED	0,96	1,63	P2O5	2,21	0,10
K K	ED	0,31	0,42	K2O	0,38	0,03
Ca K	ED	2,59	3,39	CaO	3,62	0,20
Ti K	ED	2,64	2,89	TiO2	4,40	0,17
Mn K	ED	0,52	0,49	MnO	0,67	0,03
Fe K	ED	1,91	1,79	FeO	2,46	0,11
Sr L	ED	1,05	0,63	SrO	1,24	0,04
Y L	ED	1,28	0,76	Y2O3	1,63	0,05
Nb L	ED	21,65	12,21	Nb2O5	30,97	0,74
Ta L	ED	3,66	1,06	Ta2O5	4,47	0,06
Pb M	ED	2,60	0,66	PbO	2,80	0,04
Th M	ED	2,86	0,65	ThO2	3,25	0,04
U M	ED	10,23	2,25	UO2	11,60	0,14
O		20,27	66,40			4,00
Total		75,08	100,00		75,08	
* = <2 Sigma					Cation sum	2,02

(9) - Nb-Ta-Ti-U oxide (pyrochlore type:$(Ca,U,REE)(Nb,Ta,Ti)_2O_6(O,OH,F)$						
Elmt	Spect. Type	Element %	Atomic %		Compound %	Nos. of ions
Al K	ED	0,53	0,78	Al2O3	1,00	0,05
Si K	ED	2,72	3,86	SiO2	5,81	0,23
P K	ED	1,07	1,37	P2O5	2,44	0,08
K K	ED	0,46	0,47	K2O	0,55	0,03
Ca K	ED	3,15	3,13	CaO	4,41	0,19
Ti K	ED	3,44	2,86	TiO2	5,74	0,17
Mn K	ED	0,52	0,38	MnO	0,67	0,02
Fe K	ED	2,96	2,12	FeO	3,81	0,13
Sr L	ED	1,28	0,58	SrO	1,51	0,04
Y L	ED	7,45	3,34	Y2O3	9,46	0,20
Nb L	ED	30,65	13,15	Nb2O5	43,85	0,80
Ta L	ED	2,47	0,54	Ta2O5	3,02	0,03
Pb M	ED	0,64*	0,12*	PbO	0,69*	0,01*
Th M	ED	4,23	0,73	ThO2	4,81	0,04
U M	ED	2,50	0,42	UO2	2,84	0,03
O		26,55	66,15			4,00
Total		90,61	100,00		90,61	
* = <2 Sigma					Cation sum	2,05

Table 3.7. The chemical composition of the radioactive and accessory minerals of the Paleoproterozoic (Polyarnoe, Namvara and Cheptjavr) occurrences (SEM-EDS semi quantitative determinations).

Element	k-ratio (calc.)	ZAF	Atom %	Element Wt %	Wt % Err. (1-Sigma)	Compound Formula	Compound Wt %	No. of Cations
Al-K	0.0009	1.926	0.53	0.17	+/- 0.05	Al2O3	0.31	0.197
Si-K	0.0040	1.493	1.83	0.59	+/- 0.04	SiO2	1.27	0.676
Pb-M	0.0913	1.190	4.54	10.86	+/- 0.30	PbO	11.69	1.674
U -M	0.6334	1.113	25.63	70.48	+/- 1.07	UO2	79.95	9.463
Fe-K	0.0025	0.897	0.34	0.22	+/- 0.15	Fe2O3	0.32	0.127
Th-M	0.0509	1.114	2.12	5.67	+/- 0.59	ThO2	6.45	0.781
O -K	---	3.418	65.01	12.01 S	---	---	---	---
Total			100.00	100.00			100.00	12.918

(11) – uraninite

Elt	Ligne	Int	Erreur	K	Kr	P%	A%	Formule	Ox%	Cat#
C	Ka	23.9	3.2781	0.0000	0.0000	0.00	0.00		0.00	0.00
O						12.10	62.55		0.00	0.00
Si	Ka	9.3	2.3376	0.0127	0.0090	1.60	4.72	SiO2	3.43	0.00
Fe	Ka	4.1	0.4151	0.0173	0.0123	1.22	1.81	FeO	1.57	0.00
Pb	Ma	62.0	2.3376	0.3126	0.2226	26.43	10.55	PbO	28.47	0.00
U	Ma	148.4	2.3376	0.6574	0.4682	58.65	20.38	UO2	66.53	0.00
Total				1.0000	0.7122	100.00	100.00		100.00	0.00

(12) – Yttrian uraninite (inclusion in zircon)

Element	k-ratio (calc.)	ZAF	Atom %	Element Wt %	Wt % Err. (1-Sigma)	Compound Formula	Compound Wt %	No. of Cations
Y -L	0.0282	1.609	4.46	4.54	+/- 0.29	Y2O3	5.77	1.670
Pb-L	0.1179	1.074	5.34	12.66	+/- 2.32	PbO	13.64	1.996
U -L	0.6328	1.123	26.06	71.04	+/-12.89	UO2	80.59	9.750
O -K	---	4.608	64.14	11.75 S	---	---	---	---
Total			100.00	100.00			100.00	13.416

(13) – uraninite

Element	k-ratio (calc.)	ZAF	Atom %	Element Wt %	Wt % Err. (1-Sigma)	Compound Formula	Compound Wt %	No. of Cations
Si-K	0.0030	1.990	1.89	0.60	+/- 0.07	SiO2	1.27	0.705
U -M	0.6082	1.175	26.74	71.44	+/- 0.82	UO2	81.04	9.979
Pb-L	0.1538	1.067	7.06	16.41	+/- 2.61	PbO	17.68	2.634
O -K	---	4.516	64.31	11.55 S	---	---	---	---
Total			100.00	100.00			100.00	13.317

(14) – brannerite

Element	k-ratio (calc.)	ZAF	Atom %	Element Wt %	Wt % Err. (1-Sigma)	Compound Formula	Compound Wt %	No. of Cations
Mg-K	0.0009	2.394	0.46	0.22	+/- 0.05	MgO	0.36	0.169
Al-K	0.0041	1.896	1.48	0.78	+/- 0.07	Al2O3	1.48	0.543
Si-K	0.0226	1.492	6.11	3.37	+/- 0.08	SiO2	7.22	2.245
Zr-L	0.0186	1.367	1.42	2.55	+/- 0.11	ZrO2	3.44	0.522
Pb-M	0.0595	1.284	1.87	7.64	+/- 0.26	PbO	8.23	0.689
U -M	0.4425	1.201	11.35	53.15	+/- 0.76	UO2	60.30	4.175
Ti-K	0.0770	1.150	9.39	8.85	+/- 0.18	TiO2	14.76	3.454
V -K	0.0017	1.102	0.18	0.18	+/- 0.09	V2O5	0.33	0.067
Fe-K	0.0276	0.987	2.48	2.72	+/- 0.15	Fe2O3	3.89	0.910
O -K	---	3.833	65.26	20.54 S	---	---	---	---
Total			100.00	100.00			100.00	12.776

Table 3.7. The chemical composition of the radioactive and accessory minerals of the Paleoproterozoic (Polyarnoe, Namvara and Cheptjavr) occurrences (SEM-EDS semi quantitative determinations**).**

(15) – ilmenite

Element	k-ratio (calc.)	ZAF	Atom %	Element Wt %	Wt % Err. (1-Sigma)	Compound Formula	Compound Wt %	No. of Cations
Ti-K	0.2830	1.066	18.33	30.17	+/- 0.27	TiO2	50.33	6.933
Mn-K	0.0175	1.164	1.08	2.04	+/- 0.28	MnO	2.63	0.408
Fe-K	0.2899	1.135	17.14	32.90	+/- 0.52	Fe2O3	47.04	6.484
O -K	---	3.948	63.45	34.89 S	---	---	---	---
Total			100.00	100.00			100.00	13.825

(16) – xenotime (phospho-thorite)

Element	k-ratio (calc.)	ZAF	Atom %	Element Wt %	Wt % Err. (1-Sigma)	Compound Formula	Compound Wt %	No. of Cations
Al-K	0.0030	1.884	1.01	0.56	+/- 0.05	Al2O3	1.07	0.366
Si-K	0.0482	1.487	12.33	7.17	+/- 0.12	SiO2	15.33	4.463
P -K	0.0151	1.378	3.25	2.08	+/- 0.13	P2O5	4.78	1.177
Th-M	0.2599	1.196	6.48	31.10	+/- 0.70	ThO2	35.39	2.344
U -M	0.2597	1.184	6.24	30.74	+/- 1.09	UO2	34.87	2.259
Fe-K	0.0283	0.989	2.42	2.80	+/- 0.19	Fe2O3	4.00	0.876
Y -L	0.0240	1.496	1.96	3.60	+/- 0.33	Y2O3	4.57	0.708
O -K	---	3.435	66.31	21.95 S	---	---	---	---
Total			100.00	100.00			100.00	12.193

(17) – monazite

Element	k-ratio (calc.)	ZAF	Atom %	Element Wt %	Wt % Err. (1-Sigma)	Compound Formula	Compound Wt %	No. of Cations
Si-K	0.0076	1.663	1.56	1.26	+/- 0.11	SiO2	2.71	0.561
P -K	0.1047	1.463	17.14	15.32	+/- 0.19	P2O5	35.11	6.163
Th-M	0.0752	1.324	1.49	9.96	+/- 0.52	ThO2	11.33	0.535
Ca-K	0.0394	1.051	3.58	4.14	+/- 0.15	CaO	5.80	1.288
La-L	0.0612	1.293	1.97	7.92	+/- 0.86	La2O3	9.28	0.710
Ce-L	0.1726	1.281	5.47	22.11	+/- 1.23	Ce2O3	25.90	1.966
Nd-L	0.0667	1.271	2.03	8.47	+/- 0.85	Nd2O3	9.88	0.732
O -K	---	2.672	66.75	30.82 S	---	---	---	---
Total			100.00	100.00			100.00	11.955

(18) – allanite

Element	k-ratio (calc.)	ZAF	Atom %	Element Wt %	Wt % Err. (1-Sigma)	Compound Formula	Compound Wt %	No. of Cations
Al-K	0.0639	1.735	10.21	11.09	+/- 0.09	Al2O3	20.96	3.962
Si-K	0.1095	1.587	15.37	17.37	+/- 0.11	SiO2	37.17	5.961
Ca-K	0.0887	1.093	6.01	9.70	+/- 0.10	CaO	13.57	2.332
La-L	0.0188	1.399	0.47	2.63	+/- 0.34	La2O3	3.09	0.183
Ce-L	0.0493	1.388	1.21	6.85	+/- 0.50	Ce2O3	8.02	0.471
Fe-K	0.0838	1.182	4.40	9.90	+/- 0.26	Fe2O3	14.16	1.709
Nd-L	0.0188	1.388	0.45	2.61	+/- 0.19	Nd2O3	3.04	0.174
O -K	---	3.142	61.87	39.85 S	---	---	---	---
Total			100.00	100.00			100.00	14.790

Table 3.8. The chemical composition of the radioactive and accessory minerals of the Litsevskoe ore-showing *(SEM-EDS semi quantitative determinations).*

(19) - uraninite						
Elmt	Spect. Type	Element %	Atomic %		Compound %	Nos. of ions
Mg K	ED	0.25	0.60	MgO	0.42	0.07
Al K	ED	1.12	2.38	Al2O3	2.12	0.30
Si K	ED	6.05	12.37	SiO2	12.94	1.54
Ca K	ED	2.99	4.29	CaO	4.19	0.53
Ti K	ED	0.25	0.30	TiO2	0.41	0.04
Fe K	ED	0.89	0.92	FeO	1.15	0.11
U M	ED	61.36	14.81	UO2	69.61	1.84
O		17.92	64.33		8.00	
Total		90.84	100.00		90.84	
* = <2 Sigma					Cation sum	4,44

(20) – boltwoodite (?)						
Elmt	Spect. Type	Element %	Atomic %		Compound %	Nos. of ions
Mg K	ED	0.16	0.19	MgO	0.27	0.04
Al K	ED	6.10	6.53	Al2O3	11.53	1.48
Si K	ED	20.63	21.20	SiO2	44.14	4.80
K K	ED	9.01	6.65	K2O	10.85	1.51
Ca K	ED	0.97	0.70	CaO	1.35	0.16
Fe K	ED	0.82	0.42	FeO	1.06	0.10
U M	ED	20.60	2.50	UO2	23.37	0.57
O		34.27	61.82		14.00	
Total		92.57	100.00		92.57	
* = <2 Sigma					Cation sum	8,65

(21) – coffinite (mixed with chlorite)						
Elmt	Spect. Type	Element %	Atomic %		Compound %	Nos. of ions
Mg K	ED	2.50	4.21	MgO	4.15	0.82
Al K	ED	3.86	5.85	Al2O3	7.30	1.14
Si K	ED	9.62	14.00	SiO2	20.58	2.72
K K	ED	1.70	1.78	K2O	2.05	0.34
Ti K	ED	0.57	0.49	TiO2	0.96	0.09
Mn K	ED	-0.27*	-0.20*	MnO	-0.35*	-0.04*
Fe K	ED	6.68	4.89	FeO	8.60	0.95
U M	ED	41.69	7.16	UO2	47.29	1.39
O		24.22	61.84		12.00	
Total		90.58	100.00		90.58	
* = <2 Sigma					Cation sum	7,41

Table 3.8. The chemical composition of the radioactive and accessory minerals of the Litsevskoe ore-showing *(SEM-EDS semi quantitative determinations).*

(22) – pitchblende						
Elmt	Spect. Type	Element %	Atomic %		Compound %	Nos. of ions
Si K	ED	3.37	7.93	SiO2	7.21	0.49
Ca K	ED	3.18	5.25	CaO	4.45	0.33
Fe K	ED	0.71	0.84	FeO	0.92	0.05
Y L	ED	0.31	0.23	Y2O3	0.39	0.01
Pb M	ED	3.25	1.04	PbO	3.50	0.06
Th M	ED	0.59	0.17	ThO2	0.67	0.01
U M	ED	73.04	20.29	UO2	82.86	1.26
O		15.55	64.25			4.00
Total		100.00	100.00		100.00	
* = <2 Sigma					Cation sum	2,23

(23) – uranophane						
Elmt	Spect. Type	Element %	Atomic %		Compound %	Nos. of ions
Si K	ED	6.78	13.20	SiO2	14.51	0.82
Ca K	ED	4.56	6.22	CaO	6.38	0.39
Pb M	ED	0.47	0.12	PbO	0.51	0.01
U M	ED	69.29	15.91	UO2	78.60	0.99
O		18.90	64.55			4.00
Total		100.00	100.00		100.00	
* = <2 Sigma					Cation sum	2,20

(24) – uranophane-II						
Elmt	Spect. Type	Element %	Atomic %		Compound %	Nos. of ions
Si K	ED	6.59	12.92	SiO2	14.11	0.80
Ca K	ED	4.54	6.23	CaO	6.35	0.39
Y L	ED	0.25*	0.15*	Y2O3	0.31*	0.01*
Pb M	ED	0.57	0.15	PbO	0.61	0.01
Th M	ED	0.44*	0.11*	ThO2	0.50*	0.01*
U M	ED	68.86	15.92	UO2	78.12	0.99
O		18.75	64.51			4.00
Total		100.00	100.00		100.00	
* = <2 Sigma					Cation sum	2,20

Table 3.8. The chemical composition of the radioactive and accessory minerals of the Litsevskoe ore-showing *(SEM-EDS semi quantitative determinations).*

(25) – branerite										
Elt	Ligne	Int	Erreur	K	Kr	P%	A%	Formule	Ox%	Cat#
C	Ka	67.1	4.0855	0.0000	0.0000	0.00	0.00		0.00	0.00
O	Ka	59.4	4.0855	0.1140	0.0801	27.00	74.66		0.00	0.00
Na	Ka	0.0	0.0000	0.0000	0.0000	0.00	0.00		0.00	0.00
Mg	Ka	0.0	0.0000	0.0000	0.0000	0.00	0.00		0.00	0.00
Al	Ka	4.2	4.0855	0.0029	0.0020	0.36	0.59		0.00	0.00
Si	Ka	13.1	4.0855	0.0095	0.0067	0.94	1.48		0.00	0.00
Ti	Ka	82.5	4.9027	0.1453	0.1021	11.47	10.60		0.00	0.00
Fe	Ka	8.2	0.3697	0.0279	0.0196	1.96	1.55		0.00	0.00
Zr	La	4.7	4.0855	0.0066	0.0046	0.60	0.29		0.00	0.00
Pb	Ma	18.5	4.0855	0.0450	0.0316	3.90	0.83		0.00	0.00
U	Ma	275.2	4.0855	0.6488	0.4556	53.77	9.99		0.00	0.00
				1.0000	0.7023	100.00	100.00		0.00	0.00

(26) – rutile										
Elt	Ligne	Int	Erreur	K	Kr	P%	A%	Formule	Ox%	Cat#
C	Ka	30.4	5.8773	0.0000	0.0000	0.00	0.00		0.00	0.00
O	Ka	59.6	5.8773	0.0884	0.0534	39.48	66.14		0.00	0.00
Ti	Ka	669.2	1.3283	0.9116	0.5503	60.52	33.86		0.00	0.00
				1.0000	0.6037	100.00	100.00		0.00	0.00

(27) – Au-bearing Cu,Ni,Zn, mineral (composite mixture)										
Elt	Ligne	Int	Erreur	K	Kr	P%	A%	Formule	Ox%	Cat#
C	Ka	108.1	15.7095	0.0000	0.0000	0.00	0.00		0.00	0.00
O	Ka	46.0	43.8180	0.0558	0.0475	12.79	44.11		0.00	0.00
Si	Ka	33.6	6.4265	0.0154	0.0131	1.95	3.82		0.00	0.00
Ni	Ka	21.7	0.7875	0.0730	0.0622	5.50	5.17		0.00	0.00
Cu	Ka	69.3	0.7875	0.3030	0.2579	24.43	21.22		0.00	0.00
Zn	Ka	38.3	0.7875	0.2257	0.1921	18.06	15.24		0.00	0.00
Au	La	6.8	0.7875	0.3271	0.2784	37.28	10.44		0.00	0.00
				1.0000	0.8511	100.00	100.00		0.00	0.00

(28) - branerite						
Elmt	Spect. Type	Element %	Atomic %		Compound %	Nos. of ions
Al K	ED	0,38	0,86	Al2O3	0,72	0,03
Si K	ED	0,62	1,33	SiO2	1,32	0,04
Ti K	ED	11,37	14,38	TiO2	18,96	0,44
Fe K	ED	1,59	1,72	FeO	2,04	0,05
Pb M	ED	3,79	1,11	PbO	4,08	0,03
U M	**ED**	**59,02**	15,03	UO2	66,96	0,46
O		17,32	65,58			2,00
Total		94,08	100,00		94,08	
* = <2 Sigma					Cation sum	1,05

Table 3.8. The chemical composition of the radioactive and accessory minerals of the Litsevskoe ore-showing *(SEM-EDS semi quantitative determinations).*

(29) – REE-U-mineral (composite mixture)						
Elmt	Spect. Type	Element %	Atomic %		Compound %	Nos. of ions
Si K	ED	5,25	9,91	SiO2	11,23	0,61
P K	ED	2,21	3,78	P2O5	5,06	0,23
Ca K	ED	0,66	0,88	CaO	0,93	0,05
Ti K	ED	1,91	2,12	TiO2	3,19	0,13
Fe K	ED	1,23	1,16	FeO	1,58	0,07
Y L	ED	6,18	3,69	Y2O3	7,85	0,23
Ce L	ED	16,71	6,33	Ce2O3	19,57	0,39
Nd L	ED	1,76	0,65	Nd2O3	2,05	0,04
Sm L	ED	1,77	0,63	Sm2O3	2,06	0,04
Gd L	ED	1,01	0,34	Gd2O3	1,17	0,02
Pb M	ED	1,39	0,36	PbO	1,50	0,02
U M	ED	**25,09**	5,59	UO2	28,46	0,35
O		19,47	64,56			4,00
Total		84,65	100,00		84,65	
* = <2 Sigma					Cation sum	2,20

(30) - REE-U-mineral (composite mixture)						
Elmt	Spect. Type	Element %	Atomic %		Compound %	Nos. of ions
Si K	ED	6,83	11,58	SiO2	14,60	0,72
P K	ED	2,45	3,77	P2O5	5,61	0,24
Ca K	ED	1,08	1,29	CaO	1,52	0,08
Ti K	ED	0,68	0,68	TiO2	1,13	0,04
Fe K	ED	0,56	0,48	FeO	0,72	0,03
Y L	ED	8,78	4,70	Y2O3	11,15	0,29
Ce L	ED	25,80	8,77	Ce2O3	30,22	0,55
Nd L	ED	3,19	1,05	Nd2O3	3,73	0,07
Sm L	ED	1,95	0,62	Sm2O3	2,27	0,04
Gd L	ED	2,40	0,73	Gd2O3	2,77	0,05
Pb M	ED	0,79	0,18	PbO	0,85	0,01
U M	ED	**10,80**	2,16	UO2	12,25	0,14
O		21,50	64,00			4,00
Total		86,81	100,00		86,81	
* = <2 Sigma					Cation sum	2,25

Table 3. 9. Microprobe limit detection presented in Figure 3.16 and Figure 3.17.

Uraninite											**Zircon**								
Sample 59					Sample 58-2			Sample 56-3				Sample 58-2							
D.L., ppm	A-1	A-2	B-1	B-2	A-1	A-2	A-3	B-1	B-2	B-3	D.L., ppm	A-1	A-2	A-3	A-4	B-1	B-2	B-3	B-4
Al	705	767	595	747	823	782	647	806	783	813	Al	306	322	305	327	305	329	314	317
Si	521	599	467	543	560	585	453	580	571	592	Na	1358	1347	1130	1207	1403	1328	1392	1404
K	1008	1415	866	1011	944	1489	948	971	1092	1110	Si	596	574	579	546	542	559	573	597
S	1068	1300	1185	1086	905	912	1191	1091	1193	1147	K	665	660	654	679	719	675	550	623
Ca	841	781	741	790	832	847	785	869	929	866	P	743	695	751	669	682	751	687	666
V	1467	1466	1338	1443	1425	1658	1520	1738	1587	1468	Ca	636	693	634	641	709	556	683	630
Fe	3159	2721	2612	2774	2338	3042	2378	2557	2755	3227	Fe	1324	1243	1329	1249	1464	1192	1185	1219
Zr	1722	2381	1393	1764	1678	1863	1496	1985	1921	1970	Y	850	837	827	822	851	839	856	857
Pb	1499	1464	1290	1390	1423	1596	1353	1546	1566	1614	Zr	1906	1932	2084	1870	1992	2041	2079	2088
U	5788	5838	4943	5696	5403	5855	5865	5741	5668	6106	Hf	694	706	765	703	690	725	699	697
Na	943	988	955	859	1016	1053	1078	1127	963	1196	Pb	1321	1357	1395	1284	1374	1311	1481	1425
Mg	713	780	566	690	830	893	641	794	844	806	U	1011	982	959	970	983	986	1023	1020
Ti	672	621	580	646	645	744	618	711	686	677	Th	903	889	913	842	892	882	858	904
Mo	1160	1362	1119	1255	1177	1278	1042	1196	1291	1327	Ti	352	355	352	358	346	346	341	350
La	998	947	822	969	956	1051	922	1049	1051	1054	Gd	1593	1621	1816	1547	1752	1631	1736	1727
Th	1484	1936	1229	1411	1544	1601	1488	1605	1608	1573	Dy	1523	1507	1512	1515	1649	1603	1568	1701
Mn	2630	2933	2324	2524	2808	2745	2599	2988	2695	2819	Er	2364	2331	2395	2529	2352	2392	2460	2481
Y	1189	1170	1086	1092	1085	1226	1040	1238	1217	1260	Yb	1525	1485	1605	1481	1578	1515	1567	1621
Ce	2833	2813	2445	2734	2771	2994	2630	2883	2937	3040	S	702	701	791	690	819	744	716	621
P	551	562	480	488	532	563	502	545	569	567									
Nd	5249	5243	4567	5178	4658	5496	4854	5560	5646	5465									
Dy	6585	6445	5591	6078	5984	6783	6180	6550	6663	6646									
Ta	1832	1752	1613	1738	1866	2020	1627	1957	1948	2030									
Se	1274	1394	1106	1384	1373	1544	1019	1569	1524	1528									
StdDev, wt%											StdDev, wt%								
Al	0,061	0,074	0,13	0,101	0,077	0,095	0,084	0,065	0,064	0,065	Al	0,031	0,037	0,04	0,042	0,033	0,042	0,032	0,03
Si	0,147	0,163	0,204	0,194	0,071	0,076	0,061	0,047	0,048	0,048	Na	0,108	0,113	0,09	0,101	0,109	0,13	0,103	0,107
K	0,134	0,111	0,104	0,132	0,089	0,123	0,093	0,096	0,102	0,105	Si	0,407	0,394	0,364	0,392	0,407	0,416	0,409	0,414
S	0,091	0,104	0,09	0,09	0,105	0,142	0,14	0,091	0,098	0,091	K	0,056	0,073	0,072	0,065	0,06	0,058	0,053	0,054
Ca	0,083	0,095	0,188	0,214	0,091	0,133	0,11	0,084	0,089	0,083	P	0,06	0,057	0,063	0,066	0,059	0,06	0,056	0,056
V	0,122	0,121	0,111	0,119	0,118	0,134	0,125	0,141	0,13	0,126	Ca	0,104	0,122	0,141	0,158	0,11	0,135	0,076	0,089
Fe	0,254	0,264	0,236	0,238	0,553	0,678	0,684	0,22	0,237	0,26	Fe	0,165	0,183	0,191	0,176	0,181	0,171	0,129	0,161
Zr	0,14	0,183	0,115	0,143	0,146	0,159	0,125	0,159	0,154	0,157	Y	0,066	0,068	0,073	0,07	0,066	0,068	0,072	0,066
Pb	0,82	0,179	0,117	0,156	0,368	0,374	0,329	0,578	0,582	0,589	Zr	1,372	1,24	1,088	1,211	1,37	1,267	1,436	1,429
U	2,68	1,061	2,649	3,566	3,08	3,281	2,521	3,506	3,565	3,546	Hf	0,096	0,091	0,093	0,087	0,092	0,097	0,084	0,09
Na	0,081	0,08	0,149	0,075	0,089	0,107	0,108	0,101	0,087	0,103	Pb	0,112	0,179	0,272	0,115	0,115	0,11	0,122	0,119
Mg	0,06	0,062	0,049	0,065	0,069	0,087	0,076	0,066	0,068	0,066	U	0,09	0,132	0,206	0,14	0,088	0,103	0,091	0,089
Ti	0,056	0,051	0,048	0,054	0,056	0,063	0,054	0,058	0,057	0,057	Th	0,075	0,073	0,076	0,071	0,074	0,075	0,074	0,075
Mo	0,097	0,109	0,09	0,101	0,098	0,105	0,087	0,099	0,105	0,108	Ti	0,029	0,03	0,03	0,03	0,029	0,03	0,03	0,029
La	0,083	0,08	0,068	0,08	0,079	0,087	0,076	0,087	0,087	0,087	Gd	0,134	0,141	0,156	0,136	0,143	0,138	0,145	0,144
Th	0,152	0,876	0,1	0,116	0,367	0,331	0,381	0,258	0,266	0,263	Dy	0,128	0,127	0,131	0,131	0,132	0,133	0,135	0,137
Mn	0,217	0,24	0,195	0,203	0,23	0,228	0,208	0,229	0,236	0,232	Er	0,197	0,199	0,202	0,207	0,198	0,192	0,203	0,204
Y	0,112	0,597	0,094	0,093	0,108	0,12	0,094	0,207	0,164	0,166	Yb	0,13	0,127	0,136	0,13	0,129	0,131	0,133	0,131
Ce	0,238	0,276	0,199	0,224	0,232	0,245	0,222	0,244	0,245	0,25	S	0,06	0,078	0,101	0,059	0,068	0,064	0,065	0,054
P	0,045	0,083	0,041	0,044	0,046	0,047	0,041	0,046	0,047	0,047									
Nd	0,436	0,477	0,38	0,425	0,428	0,457	0,412	0,464	0,473	0,462									
Dy	0,548	0,627	0,456	0,508	0,509	0,568	0,517	0,555	0,566	0,557									
Ta	0,152	0,146	0,14	0,145	0,152	0,166	0,135	0,162	0,16	0,166									
Se	0,108	0,115	0,091	0,114	0,118	0,127	0,087	0,128	0,128	0,125									

PART 4.

DISCUSSION ABOUT THE METALLOGENIC PROCESSES IN THE LITSA DISTRICT AND RELATION WITH THE GEODYNAMIC EVOLUTION OF THE FENNOSCANDIAN SHIELD

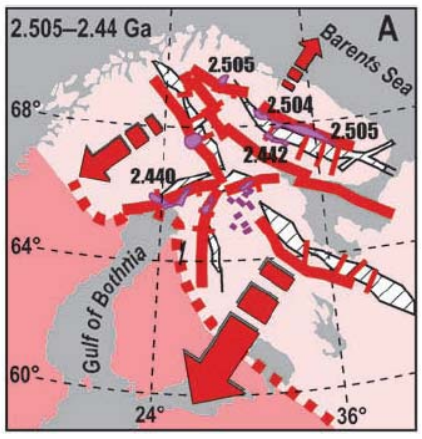

4.1. Geological processes leading to uranium enrichment in the Litsa district

The uranium metallogeny of the Litsa area has a protracted history, which started as early as the Archean, and lasted up to the Paleozoic. The Litsa area experienced several processes during which the uranium grade has increased, with two major types that should be considered: magmatic and epigenetic.

4.1.1. Magmatic processes:

Most of the Litsa area uranium occurrences result from the partial melting of country rock and subsequent uranium enrichment in magmatic melt (= migmatisation processes, which correspond to what Russian geologists call “feldspar metasomatism”). At least three episodes of partial melting occurred, during the Archean, Early and Late Paleoproterozoic.

- first enrichment in the Archean by partial melting processes of Archean host rocks and related granitoid injections (cf. Skalnoe and Dikoe occurrences)
- similar process during the Early Proterozoic i.e. partial melting of Late Archean or Early Paleoproterozoic aluminous gneisses (cf. Polarnoe and Koshkjavr occurrences)
- erosion and sedimentation of the aforementioned lithologies - already uranium enriched - and partial melting during the Late Paleoproterozoic (cf. Litsa and Beregovoe occurrences)

4.1.2. Epignetic processes

Epigenetic processes, leading to more local and rich uranium concentration comprise several types of middle and low temperature hydrothermal alteration, often accompanied by uranium deposition in pitchblende veins. Besides, the local uranium enrichment is connected with muscovite-bearing shearing and fluid-rock interaction along mafic dykes. The age of the processes is not much constrained, except pitchblende vein deposition, dated by U-Pb method.

- Paleozoic reactivation, in brittle conditions, associated with pitchblende deposition as vein (cf. Litsa occurrence, and possibly also Beregovoe and Polarnoe occurrences),
- fluid rock reaction along mafic dykes (cf. Litsa occurrence and possibly Polyarnoe),
- Uranium remobilisation associated with muscovite-bearing shearing (cf. Skalnoe, Dikoe and possibly also Polyarnoe occurrences),
- Uranium remobilisation associated with albite and chlorite hydrothermal alteration (cf. Polarnoe occurrence).

4.2. Evolution of geological structure and uranium abundance

In this paragraph, the principle stages of geodynamic evolution and relevant uranium enrichment are described. Traditionally, the certain stages in geodynamic evolution of the Fennoscandian shield are distinguished and called tectono-magmatic cycles (Table 3.2.1). Each of the cycle manifested in the set of geological events with the following reorganization of the earth crust: development of various magmatic complexes, regional metamorphism of the host rocks and tectonic deformations.

The contemporary tectonic aspect of the Kola province (and the whole Fennoscandian shield) was shaped in fact during Early Paleoproterozoic *(Scheglov; 1993)*. The continental crust was formed at 3.15 Ga, and each further period of its evolution was marked by development of mantle magmatism and relevant products of mantle-crust interaction, mainly connected with continental riftogenesis, and accompanied by a gradual enrichment in uranium.

Archean time

In Early Archean (Saamian) the oldest geological structures of the Fennoscandian shield were formed, they are known as cratonic nuclei and considered to be a reworked matter of the primary continental crust. Within the Litsa district they are presented by non-stratified TTG formations of the Barents Sea complex, with the age over 2.8-3.0 Ga *(Savitskii et al.; 1995)*. The oval domes built with these rocks almost entirely compose the Murmansk block and partly Central-Kola block, where they are dissected by Kola superdeep borehole SD-3 *(Glebovitsky; 2005)*. These formations are characterized by low uranium clarke value (below 0.5 ppm), but include monazite-bearing pegmatoidic granite with the signs of Th-U-REE mineralization *(Savitskii et al.; 1995)*.

The Late Archean (Lopian) is significant for the geodynamic events, which occurred within studied area. In the period of 3.1-3.0 Ga the upwelling of mantle plum brought to arc lifting of the crust without its rupture, so that complementary stretching and submergence took place in the adjacent margins. The arc uplifiting was a source of clastic matter for sedimentary basins in compensative depressions of its periphery, where the lowest terrigenous stratums of greenstone belt were accumulated.

With this period the sedimentation of supracrustal formations of Kola series in the Cental-Kola block is connected, forming the oldest within the Fennoscandian shield para-gneiss belt *(Glebovitsky; 2005)*.

Later, between 2.9 and 2.85 Ga, the installation of the Voron'ya-Kolomozero greenstone belt occurred with the relevant sequence of volcanic and sedimentary rocks. This structure on the early stages of its evolution developed like a rift - the through shape of depression and abundant mantle magmatism are typical for stretching conditions of riftogenesis *(Glebovitsky; 2005, Shcheglov; 1993)*. Besides, the petrogeochemical characteristics of komatiite volcanism display the high temperature and isotopic-geochemical «primitivism» of the mantle, which is correspondent to the axial part of the plum *(Glebovitsky; 2005)*. However, later the stretching processes switched to compression with folding, metamorphism and widespread granitization processes, which brought to the formations of the uranium bearing pegmatoidic granite with the oldest uranium occurrences (Dikoe and Skal'noe) in the district.

The age of these U-bearing rocks is 2750±50 Ma *(Anderson; 1990)* and their origin is debatable. Some researchers consider them to be a late kinematic intrusions or high-temperature K-Fsp metasomatites. The field observations provided in the framework of this thesis enabled to suppose the partial melting of Archean rocks with subsequent U enrichment in magmatic melt as major magmatic processes in these occurrences.

Economic valuable concentrations of uranium are not very typical for the Archean terrains *(De Vivo et al.; 1988)*, however within the Litsa district (and the whole Kola province) the first significant uranium enrichment corresponds to the age of 2.8-2.6 Ga, resulting from the Late Lopian (Rebolian) orogenic tectono-magmatic cycle, manifested in late and post collision intrusions. These occurrences could be compared to the Rössing deposit (Namibia), but the accumulation of uranium mineralized pegmatoid bodies is much smaller, more scattered and of too low grade to be considered as a deposit. Despite a good structural control of the emplacement of the mineralized sectors, the absence of carbonate lithologies prevented large accumulation of U-bearing magma, as did occur in Rössing *(Kister et al.; 2007)*.

On the whole, the Archean time of Fennoscandian shield evolution represent the stage of earth crust cratonization with the following differentiation on blocks. The first two cycles of regional and zonal metamorphism correspond to the ages of 2.88 Ga – granulite-amphibolite

facies of moderate pressure, and 2.76-2.0 Ga – progressive amphibolite (Andalusite-Sillimanite and Kyanite-Sillimanite facies) metamorphism *(Glebovitsky; 2005)*.

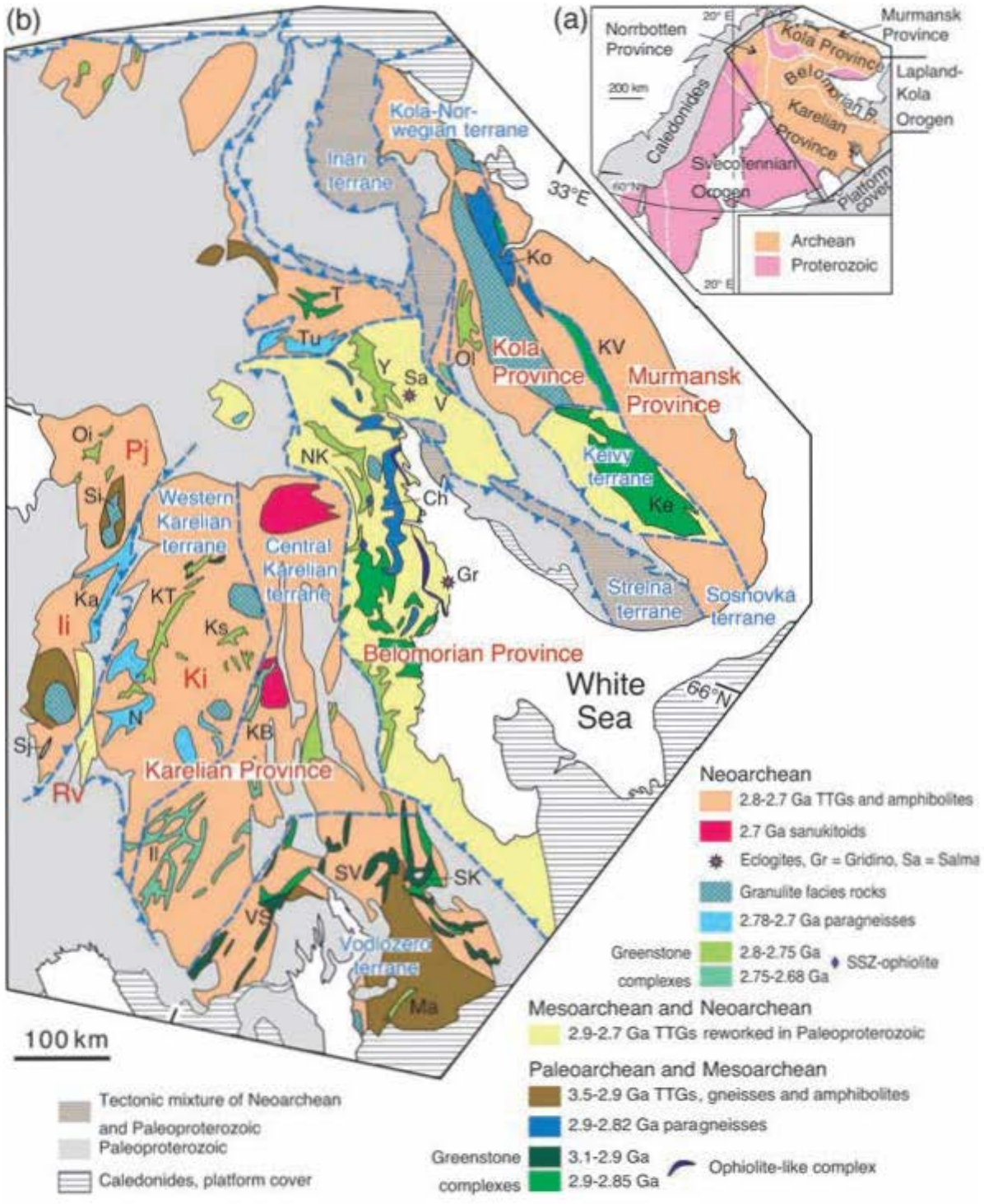

Figure 4.1. Geological scheme of the eastern Fennoscandian shield and representation of main Archean terranes and greenstone, schist and paragneiss belts. *(after Hölttä et al.; 2008)*

Ch = Chupa; Il = Ilomantsi; KB = Khedozero-Bolsheozero; Ke = Keivy; Ko = Kola; Ks = Kostomuksha; KT = Kuhmo-Suomussalmi-Tipasjärvi; KV = Kolmozero-Voronya; Ma = Matkalahta; N = Nurmes; NK = North Karelian; Ol = Olenegorsky; Oi = Oijärvi; SK = Sumozero-Kenozero; SV = South Vygozero; Tu = Tuntsa; T = Tulppio; V = Voche-Lambina; VS = Vedlozero-Segozero; Y = Yena. Complexes of the Western Karelian terrane: Ii = Iisalmi; Ki = Kianta; Pj = Pudasjärvi; Rv = Rautavaara; Sj = Siilinjärvi carbonatite; Si = Siurua gneiss.

Paleoproterozoic time

Paleoproterozoic time of the Fennoscandisn shield evolution manifested in progressive reorganization of the Archean crust. After protracted period of peneplenation, erosion and weathering the endogenic processes and tectonic motion had been activated, especially in the stretching zones along Archean blocks boundaries.

During 2.5-2.3 Ga the vigorous mantle upwelling and warming up the crust brought to the rupture of the arc uplifting and development of volcanic belts with the following transformation to the hollow. As mentioned in Part 1, the Pechenga zone inherited the Archean greenstone belt, where the stretching tectonic conditions continued during Proterozoic in comparison with switched to orogenic stage Voron'ya-Kolomozero belt *(Glebovitsky; 2005)*.

The complex interaction of mantle plum with the rocks of the lower crust resulted in formation of various volcanic and intrusive complexes. The variety of these complexes depended on total thickness of the crust, its permeability and maturity of mantle matter for melting. The basalt complex mark the initial stage of riftogenesis; andesite-rhyolithe complex is twice repeated in the sequence, coming from secondary magma pockets in the crust; intrusive pyroxenite-gabbro-norite complex is the most typical for the early stage of riftogenesis, forming large plutons mainly in the northern wing of the Pechenga zone. The posterior riftogenous stagewas marked by sequence of basalt-trachybasalt, Cu-Ni-bearing gabbro-wehrlite, nepheline-syenite complexes and finished with granitoid intrusions of Kaskel'javr complex.

With Early Paleoproterozoic associates the uranium mineralization in Polyarnoe ore-showing. Dated at 2150±50 Ma *(Anderson; 1990)* the Th-rich uraninite with molybdenite, zircon, xenotime, titanite and monazite presents typical for the Rössing or alaskite type of mineralization. Besides, the presence of mineralized albitized and chloritized apogranitoids (also called quartz-chlorite-albite metasomatite) could be compared with the regional Na-metasomatim, related to the uranium deposits of central Ukraine and Lagoa Real in Brazil *(Kister et al.; 2007)*.

The collision stage of riftogenesis is significant for the upwelling along the north-eastern deep faults (diagonal to the major axis of the rift) of the latite series mantle melt, which initiated the secondary palingenic melts and caused the multiphase Litsa-Araguba granitoid

complex formation. The latter intensively influenced the host rocks, forming migmatization fields around plutons.

These host rocks, presented by Kola series gneiss, were accumulated after erosion and sedimentation of Archean already uranium enriched lithologies. Thus, being additionaly uranium enriched peraluminous metasediments, they represent favorable protoliths for generating peraluminous melt with a high amount of a leachable uranium. This migmatization processes led to the formation of preliminary Late Paleoproterozoic uranium concentration in Litsevskoe and Beregovoe ore-showings (§2.5), where uraninite was dated at 1700±50 Ma *(Anderson; 1990).* The contribution of the Litsa-Araguba complex in metallogenesis of the Litsa district is a potential role as an additional source of uranium, being partly derived from the melting of preliminary uranium enriched lithologies *(Kister et al.; 2007)*.

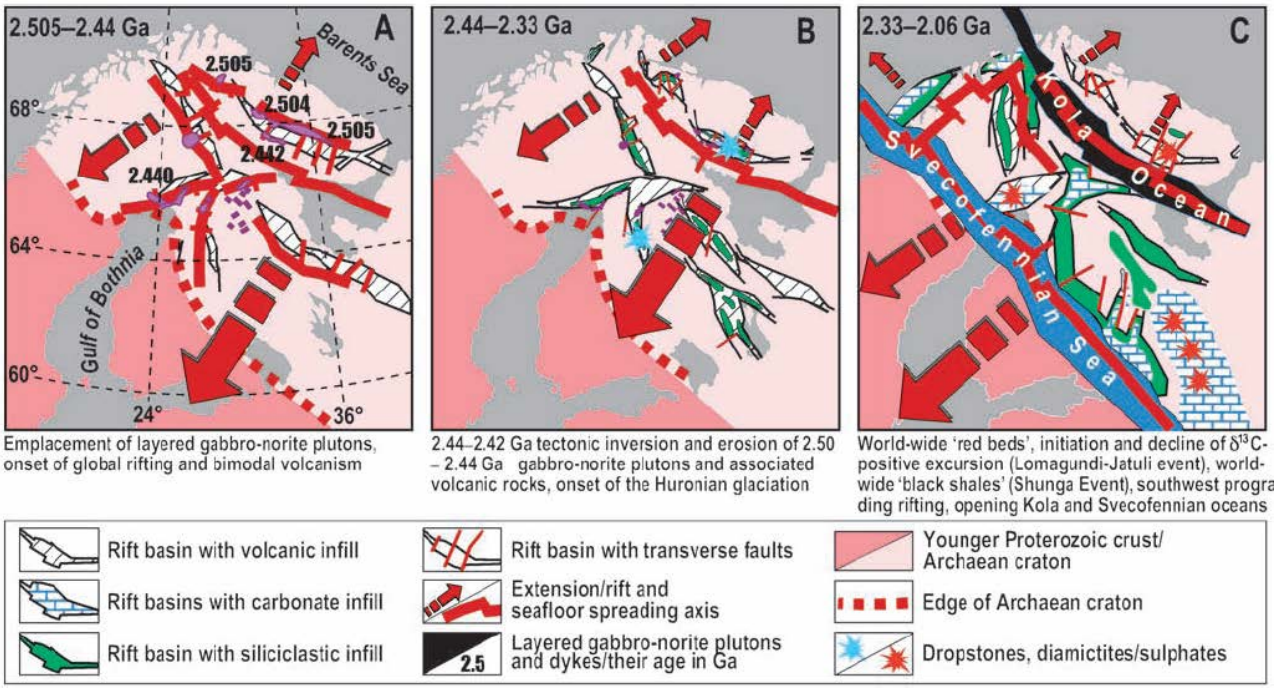

Figure 4.2. Rifting-related paleotectonic and paleogeographic evolution of the Fennoscandian Shield during the Early Paleoproterozoic. *(after Lahtinen at al., 2008)*

Mesoproterozoic – Neoproterozoic time

Later during the Mesoproterozoic (Riphean) intensive erosion, intercontinental sedimentation and a partial marine transgression in Kola province resulted in the formation of a terrigenous cover sequence, relicts of which are preserved on the Tersky coast of the White Sea, and on the Sredny and Rybachy peninsulas.

Riphean sediments in the Sredny and Ribachy peninsula are overall poorly radioactive, displaying only the presence of some syn-sedimentary (830±70 Ma) REE-P-U anomalies among the phosphate-bearing arkose sandstones of the Kil'din series.

The reduced and immature character of the Sredny-Rybachy sediments constitutes unfavorable conditions to generate oxidized acid brines able to leach and transport uranium, as found in the Athabasca Basin. While the Tersky basin appear more potential for the uranium metallogenesis, as it is comparatively much more mature and oxidized, with local evidence of hydrothermal activity and the presence of unconformity related uranium occurrences *(Afanasieva et al.; 2006)*. Two different geodynamic environments (Barents Sea vs. White Sea) may explain the strong difference in the nature of the Riphean sediments between the Tersky and Sredny-Rybachy areas.

The former extension of the Riphean basin around the Sredny-Ribachy peninsula is uncertain. It is therefore possible to speculate on a much wider extension with laterally more abundant oxidized facies, because of the presence of some breccia, containing angular fragments of arkose and conglomerate of hypothetical Riphean age, in the Litsa-Araguba tectonic zone *(Savitskii et al., 1995)*.

In Litsevskoe occurrence some radioactive anomalies are related to the mafic dykes, interpreted as being of syntectonic origin (fish-like structure) and playing a role of topochemical (reducing) trap for uranium during a later event of catalasis focused on their boundaries *(Kister et al.; 2007)*. The age of this dyke was estimated by Rb-Sr method as ~ 1000 Ma, but the precision is not much reliable, due to the opening of Rb-Sr system during alteration processes.

Also, a parallel could be done with the dyke of the Nyasyukk complex dated by Rb-Sr at 1860±30 Ma *(Sabotovich; 1987)*, which was observed in Polyarnoe occurrence, intersected the hosting rocks.

Paleozoic time

The Caledonian orogeny (530-380 Ma), when the Eastern part of the Fennoscandian shield collided with the Norwegian Caledonides, forming the Laurassia continent, was in fact the last significant tectonic event in the long process of formation of the Fennoscandian shield as a united continental crust domain; later reactivations have only had a minor influence on its structure.

Its contribution to the metallogenesis if the Litsa district is presented in Litsevskoe occurrence and consists of epigenetic uranium deposition in pitchblende veins, located within a quartz-muscovite pegmatoidic dyke-shaped body, probably related to a rather low temperature hydrothermal event in brittle conditions and dated by U-Pb at 370±20 Ma *(Anderson; 1990)* and 455±6 Ma *(this study)*.

Paleozoic reactivation occurred also in Polyarnoe occurrence, manifested as carbonate veinlets with galena, sphalerite, pyrite and chalcopyrite and pitchblende *(Savitskii et al.; 1995)*. The strike of such veinlets is N-E, i.e. identical to the pitchblende vein in Litsevskoe occurrence. The age of this event was dated by Pb-Pb on galena at 380±20 Ma *(Sabotovich; 1987*) and by U-Pb age on pitchblende at 375±18 Ma *(Anderson; 1990)*.

Undated events

Besides the abovementioned epigenetic processes, there are some, which can not be dated for the moment, only presumably by indirect features, like resemblances to the other dated objects.

Thus, the enhancement of the radioactivity was observed in cataclased or sheared zones of Archean granitoids, associated with muscovite filling along fractures in Dikoe occurrence. Such muscovite alteration has also been observed in shear zones crosscutting the host orthogneiss in the Polyarnoe occurrence, but no significant increase of the radioactivity has been detected in association with it. These muscovite-bearing sheared zones, observed at the regional scale, provide interesting evidence for later uranium hydrothermal remobilisation of the primary (magmatic) uranium pre-concentrations. Ages of this event is unknown and should be dated by K-Ar or Ar-Ar on the coarse-grained muscovite.

Tableau 4.1. Succession of the geological events in the Litsa district *(after: Scheglov, 1993; Glebovitsky, 2005; and others)*

Age, Ma		Tectono-magmatic cycle	Principal geological events			Uranium abundance
			Stage of geodynamic evolution		Related magmatism	
3600-3200	Saamian		continental crust formation (Barents Sea complex)			
3100	Lopian	***Lopian***	Voron'ya-Kolomozero greenstone belt formation	relief partitioning and sedimentation (Kola series)		
3000						
2900				crust rupture and rifting	komatiite-tholeite volcanism	
2800					baslat-andesite-dacite volcanism	*REE-Th-U mineralization (Dikoe and Skal'noe)*
2700				sedimentation (Tundra series) and collision	granitization (U-bearing pegmatoid)	
2600						
2500	Sumian	***Belomorian***	Pechenga riftogenesis	crust rupture and rifting	basalt, andesite-rhyolite volcanism; pyroxenite-gabbro-norite intrusions	
2400	Sariolian					
2300	Jatulian	***Karelian***		spreading and sedimentation	basalt-trachybasalt volcanism;	*U mineralization (Polyarnoe, Namvara, Javr, Chept'javr)*
2200						
2100	Ludicovian	***Svecofenian***				
1900	Kalevian			collision	gabbro-wehrlite (Cu-Ni); nepheline-syenite; mafyc dykes; granitoid intrusions (Kaskel'javr, Litsa-Araguba complexes)	*Preliminary U concentration (Litsevskoe, Beregovoe)*
1800	Vepsian					
1700						
1650-650	Riphean	***Dalslandian***	Barents Sea basin	uplifiting, erosion and sedimentation		*Mafyc dyke related U mineralization (Litsevskoe); REE-P-U mineralization (Sredny-Rybachy)*
650-540	Vendian					
540-290	Paleozoic	***Caledonian***	orogeny related reorganization (hydrothermal processes)			*U (vein-type) mineralization (Litsevskoe, Beregovoe); reactivation (Polyarnoe)*

Conclusions

Geodynamic evolution of the Litsa district, as a part of Kola province of the Fennoscandian shield, started in Late Archean and appeared in a sequence of tectono-magmatic cycles of the crust reorganization. Consecutive processes of syncline initiation, rifting, collision, peneplenation, erosion and sedimentation with related magmatism formed the present aspect of the area.

In the course of its geological history the Litsa district endured several successive uranium enrichments, presented by preliminary concentration, magmatic and epigenetic processes.

Magmatic processes started in the Archean as an evidenced by the uraninite-bearing Archean vein-like pegmatoids and continued during the Paleoproterozoic. They are similar to the uranium deposits of Namibia (Rössing), but also display unfavorable discrepancy. Erosion and sedimentation of such already uranium enriched lithologies led to the formation of uranium enriched peraluminous metasediments, which represented favorable protoliths for late Paleoproterozoic migmatisation processes, generating peraluminous melt with a high amount of U under a leachable form, like uraninite.

Then, epigenetic processes lead to local higher-grade uranium deposition. Paleozoic (Caledonian) reactivation, in brittle conditions, associated with pitchblende deposition as vein, is the only geochronologicaly constrained event. Fluid-rock interaction along mafic dykes is dated approximately as Riphean (Dalslandian). Uranium remobilization associated with muscovite-bearing shearing, with albite and chlorite hydrothermal alteration were not dated at all. The latter might recall Na-metasomatosis, occurring in large uraniferous provinces, as in Ukraine (Krivoi Rog) and Brazil (Lagoa Real).

The reduced and immature character of the Mesoproterozoic sediments displays unfavorable conditions for leaching and transporting large quantities of uranium, important for unconformity type deposition as in Canada (Athabasca), whereas they contain poor syn-sedimentary REE-P-U mineralization.

GENERAL CONCLUSION

The Litsa district is one of the most interesting areas of the Kola Peninsula in the aspect of its geological structure and the diversity of the uranium occurrences.

The protracted and complex history of its geodynamic evolution leads to the formation of various tectonic and geological units, which were formed as a response of tectono-magmatic cycles and control the localization of the uranium mineralization. Mantle plum related rifting and orogenic events were accompanied with diverse processes, which lead to preliminary concentrations and following remobilization and deposition of uranium, occurred in Archean, Paleoproterozoic and Paleozoic.

In spite the scarce scale of the uranium occurrences, Litsa district may present certain positive economic interest, considering its metallogenic potential with numerous and meaningful preconditions and features of uranium mineralization and developed infrastructure of the region with railroads and mining facilities.

Indeed the most potential zone seems to be located around the Litsa-Araguba granitoid complex, where favorable protoliths, structures and epigenetic processes are encountered.

Although in a whole the area was negatively estimated by «Nevskgeologia», which performed here abundant exploration in 1950-1980, there are some sectors, which had not been sufficiently explored, including the ones with utmost development of metallogenic preconditions and features. This results from political crisis of 1990, which interrupted most of exploration surveys in the country.

The weak glacial overburden and comparatively large portion of outcrops in the immediate area of the uranium occurrences favor additional exploration works in the most promising sectors with vein-type mineralization.

The principal aim of the study was to introduce the uranium metallogeny of the Litsa district. Its geological structure, metallogenic potential, uranium mineralization and its correlation with geodynamic evolution was presented in becoming parts. Nevertheless, several problems should be resolved by posterior researches for better understanding of uranium perspectives in the area.

Various uranium occurrences of the district, especially the Litsevskoe, which is in fact the most promising, deserve a special individual study with precise analyses, the more so as a number of problems could not be solved with the limits of present thesis. Besides more accurate isotopic dating of some units and alteration processes, the problem of uranium redistribution presents a pragmatic interest, due to the utmost uranium concentration in the vein-type occurrences.

Also the more certain correlation with the other occurrences in analogous geological environment, first of all with those in uraniferous provinces of the Fennoscandian shield could be an object of a special study.

Mesoproterozoic sediments with their poor mineralization and immature and reduced character present the least interest in the aspect of uranium potential, but could be studied else wise, for hydrocarbon or metallic resources.

GENERAL CONCLUSION

The Litsa district is one of the most interesting areas of the Kola Peninsula in the aspect of its geological structure and the diversity of the uranium occurrences.

The protracted and complex history of its geodynamic evolution leads to the formation of various tectonic and geological units, which were formed as a response of tectono-magmatic cycles and control the localization of the uranium mineralization. Mantle plum related rifting and orogenic events were accompanied with diverse processes, which lead to preliminary concentrations and following remobilization and deposition of uranium, occurred in Archean, Paleoproterozoic and Paleozoic.

In spite the scarce scale of the uranium occurrences, Litsa district may present certain positive economic interest, considering its metallogenic potential with numerous and meaningful preconditions and features of uranium mineralization and developed infrastructure of the region with railroads and mining facilities.

Indeed the most potential zone seems to be located around the Litsa-Araguba granitoid complex, where favorable protoliths, structures and epigenetic processes are encountered.

Although in a whole the area was negatively estimated by «Nevskgeologia», which performed here abundant exploration in 1950-1980, there are some sectors, which had not been sufficiently explored, including the ones with utmost development of metallogenic preconditions and features. This results from political crisis of 1990, which interrupted most of exploration surveys in the country.

The weak glacial overburden and comparatively large portion of outcrops in the immediate area of the uranium occurrences favor additional exploration works in the most promising sectors with vein-type mineralization.

The principal aim of the study was to introduce the uranium metallogeny of the Litsa district. Its geological structure, metallogenic potential, uranium mineralization and its correlation with geodynamic evolution was presented in becoming parts. Nevertheless, several problems should be resolved by posterior researches for better understanding of uranium perspectives in the area.

Various uranium occurrences of the district, especially the Litsevskoe, which is in fact the most promising, deserve a special individual study with precise analyses, the more so as a number of problems could not be solved with the limits of present thesis. Besides more accurate isotopic dating of some units and alteration processes, the problem of uranium redistribution presents a pragmatic interest, due to the utmost uranium concentration in the vein-type occurrences.

Also the more certain correlation with the other occurrences in analogous geological environment, first of all with those in uraniferous provinces of the Fennoscandian shield could be an object of a special study.

Mesoproterozoic sediments with their poor mineralization and immature and reduced character present the least interest in the aspect of uranium potential, but could be studied else wise, for hydrocarbon or metallic resources.

References

Anders E. and Grevesse N., 1989, Abundances of the elements: Meteoritic and solar. Geochimica and Cosmochimica Acta 57, 197-214.

Anderson E.B., Nikitin S.A., Zaslavsky V.G., Lobickov A.F., Markova T.A., Drozdov P.A., 1990. Isotopic dating of uranium occurrences of eastern part of the Baltic Shield. Abstracts of the all-Union meeting “Isotopic dating of endogen ore formations”, Kiev, pp. 174-176.

Afanasieva E.N. (responsible executor), Mikhailov V.A., Demicheva L.A., et al., 2004. Compilation of the uranium-bearing map of the Baltic shield, 1:2 500 000 scale. Report of COGEMA and VSEGEI collaboration (unpublished).

Afanasieva E.N. (responsible executor), Caillat C., Mironov Y.B., et al., 2006. Improvement of criteria of predicting uranium and complex (gold, copper, cobalt, uranium) mineralization. Report of VSEGEI (unpublished).

Afanasieva E.N. (responsible executor), Mikhailov V.A., Lipner A.A., et al., 2007. Assessment of the Kola Peninsula Uranium Potential. Report of AREVA NC and VSEGEI collaboration (unpublished).

Afanasieva E.N. (responsible executor), Lipner A.A., Serov L.V., et al., 2008. Assessment of the Kola Peninsula Uranium Potential. Report of VSEGEI (unpublished).

Amelin Y, U, Heaman, L.M. Semenov, V.S. 1995. U-Pb geochronology of layered mafic intrusions in the eastern Baltic Shield: implications for the timing and duration of Paleoproterozoic continental rifting. Precambrian Research, 75, 31-46.

Balagansky, V. V., M. J. Timmerman, N. Ye. Kozlova, and R. V. Kislitsyn, A 2.44 Ga syn-tectonic mafic dyke swarm in the Kolvitsa Belt, Kola Peninsula, Russia: implication for early Palaeoproterozoic tectonics in the north-eastern Fennoscandian Shield, Precam. Res., 105, 269-287, 2001.

Balashov Y.A., 1996. Geochronology of the Early Proterozoic rocks in the Pechenga-Varzuga structutre of the Kola Peninsula. Petrology, vol.4, No 1, pp. 3–25.

Bea, F., 1993. Aluminosity-dependent fractionation patterns in differentiated granite—leucogranite système, EOS, 74(16), 343.

Bea, F., Pereira, M. D., Corretge, L. G. & Ferstater, G. B., 1994a. Differentiation of strongly peraluminous, perphosphorous granite. The Pedrobernardo pluton, central Spain. Geochimica & Cosmochimca Acta, vol.5, 2609-2628

Bea, 1996. Residence of REE, Y5 Th and U inGranites and Grustal Protoliths; Implications for the Chemistry of Crustal Melts. Journal of Petrology, N°37, 512-552.

Belyaev O.A., Zagorodny V.G., Petrov V.P., et al., 1977. Facies of regional metamorphism of the Kola Peninsula. Leningrad, Nauka.

Bibikova, E., Skiöld, T., Bogdanova, S., Gorbatschev, R. and Slabunov, A., 2001, Titanite-rutile thermochronometry across the boundary between the Archean Craton in Karelia and the Belomorian Mobile Belt, eastern Baltic Shield, Precambrian Research, vol. 105, p. 315-330.

Bibikova, E. V., Bogdanova, S., Claesson, S. and Skiold, T., 1999, NORDSIM Ages on Provenance and Metamorphic Zircon Material in Belomorian Metasediments of the Baltic Shield, Journal of Conference Abstracts, Vol. 4, No. 1, Symposium A08, Early Evolution of the Continental Crust.

Bonhoure, J., Kister, P., Cuney, M. and Deloule, E., 2007, Methodology for Rare Earth Element Determinations of Uranium Oxides by Ion Microprobe, Geostandards and Geoanalytical Research 31, p. 209-225.

Carignan J., Hold, P., Mevelle, G. Morel, J. and Yeghichevan, D., 2001, Routine analysis of trace elements in geological samples using flow injection and low pressure on line liquid chromatography coupled to ICP-MS: a study of geochemical reference materials BR, DRN, UB-N, AN-G and GH, Geostandards Newsletter 25, p. 187-198.

Daly, J.S., Balagansky, V.V., Timmerman, M.J., Whitehouse, M.J., de Jong, K., Guise, P., Bogdanova, S., Gorbatschev, R., Bridgwater, D., 2001. Ion microprobe U-Pb zircon geochronology and isotopic evidence for a trans-crustal suture in the Lapland-Kola Orogen, northern Fennoscandian Shield. Precambrian Research, 105, pp.289-314.

Debon, F. and Le Fort, P., 1983, A chemical–mineralogical classification of common plutonic rocks and associations, Transactions of the Royal Society of Edinburgh, Earth Sciences 73, p. 135-149.

Debon, F. and Le Fort, P., 1988, A cationic classification of common plutonic rocks and their magmatic associations: principles, method, applications, Bulletin de Minéralogie 111, p. 493-510.

De Vivo B., Ippolito F., Capaldi G., Simpson P.R. (editors), 1988. Uranium geochemistry, mineralogy, geology, exploration and resources. Moscow, Mir.

Dobrzhinetskaya L.F., 1978. Structure-metamorphic evolution of the Kola series. Moscow, Leningrad ?

Glebovitsky V.A (editor), 2005. The Early Precambrian of the Baltic Shield. St-Petersburg, Nauka.

Glebovitsky V.A., Shemyakin V.M., 1996. Subdivision and correlation of the Early Precambrian. Regional geology and metallogeny, No 5, pp. 25-36.

Hölttä, P., Balagansky, V., Garde, A. A., Mertanen, S., Peltonen, P., Slabunov, A., Sorjonen-Ward, P. and Whitehouse, M., 2008, Archean of Greenland and Fennoscandia, Episodes, Vol. 31, No. 1, p. 13-19.

Kazansky V.I., 1988. Evolution of ore-bearing Precambrian structures. Moscow, Nedra.

Kister P., Cuney M., Andre-Mayer A.-S., 2007. Uranium potential of the Litsa area in the Kola Peninsula (Russia). BUM/DEX/PN – Field work report.

Kudryashov, N., 1999, Archean Kolmozero-Voronja Greenstone Belt: U-Pb Zircon and Sphene Data; Journal of Conference Abstracts, Vol. 4, No. 1, Symposium A08, Early Evolution of the Continental Crust.

Kudryashov, N., Gavrilenko, B., Apanasevich, E., 2003, Geochronology of the Archaean Kolmozero-Voron'ya Greenstone Belt: U-Pb dating of zircon, titanite, tourmaline and tantalite (Kola Region, North-Eastern BAltic Shield), EGS - AGU - EUG Joint Assembly, Geophysical Research Abstracts, Vol. 5, Abstract #398.

Lahtinen, R., Garde, A. A. and Melezhik, V. A., 2008, Paleoproterozoic evolution of Fennoscandia and Greenland, Episodes 31, p. 20-28.

Ledru P., Andre-Mayer A.-S., 2008. Uranium potential of the Kola and Karelian craton (Russia). BUM/DEX/PN – Field work report. Unpublished report AREVA, 48p.

Ludwig, K.R., 1999, Isoplot/Ex version 2.00 – A geochronological toolkit for Microsoft Excel, Berkeley Geochronology Center, Special Publication No. 2.

Mercadier J., Cuney M., Lach P., Boiron M-C., Bonhoure J., Richard A., Leisen M., Kister P. (2011) Origin of uranium deposits revealed by their rare earth element signature. Terra Nova, 23, 264-269.

Mikhailov V.A., Afanasieva E.N., Mironov Yu.B. Metallogenic uranium potential of the Northwestern region of the Russian Federation// Regional Geology and Metallogeny, N.32, St. Petersburg, 2007, p.20-28

Mitrofanov F.P., Negrutza V.Z. (editors), 2002. General stratigraphic scale of the Precambrian of Russia. Apatity, KSC of RAS.

Negrutsa, V.Z., 1984. Early Proterozoic Stages of Evolution of the Eastern Part of the Baltic Shield (in Russian). Nedra, Leningrad, 270 pp.

Negrutza V.Z., Basalaev A.A., Chikirev I.V., 1994. Barents sea phosphorite basin. Apatity, KSC of RAS.

«Nevskgeologia», 1957. Report about results of exploration works, carried out by Bolotnaya party in 1957. «Nevskgeologia» archive, unpublished.

Nevskgeologia», 1970. Report about results of complex airborne geophysical surveys, carried out by party №6 in 1970. «Nevskgeologia» archive, unpublished.

«Nevskgeologia», 1976. Report about results of complex airborne geophysical surveys, carried out by party №6 in 1974-1975. «Nevskgeologia» archive, unpublished.

Ovchinnikova, G.V., Lobach-Zhuchenko, S.B., Sergeev, S.A., Yakovleva, S.Z., Levchenkov, O.A., Neymark, L.A., Komarov, A.N., Gorokhovsky, B.M., Fedoseenko, A.M. and Krylov, I.N., 1991. Geochemical and isotope data on the dating and petrology of southeast Karelian late-kinematic granites. Geochem. Int., 28(6): 35-47.Pushkarev Y.D., 1995. Megacycles and evolution of the mantle-crust system. Leningrad, Nauka.

Pushkarev Y.D., Ryungen G.I., Shestakov G.I., 1978. Granitoids older than 2800 Ma of the Kola Peninsula. Oldest granitoids of the Baltic Shield, Apatity, pp. 18-43.

Savitskii A.V., Gromov A.Y., Mel'nikov E.K., et al., 1995. Uranium mineralization of the Litsk district of the Kola Peninsula, Russia. Geology of ore deposits, vol.37, No.5, pp. 403-416.

Sawka, W. N. & Chappell, B. W., 1988. Fractionation of uranium, thorium and rare earth elements in a vertically zoned granodiorite: implications for heat production distribution in the Sierra Nevada batholith, California, U.S.A. Géochimica & Cosmochimica Acta 52, 1131-1144.

Scheglov A.D., Moskaleva V.N., Markovsky B.A., 1993. Magmatism and metallogeny of riftogenic systems of eastern part of the Baltic Shield. St-Petersburg, Nedra.

Shurilov A., 2008. Uranium metallogeny of the Ladoga region (Karelia, Russia). PhD thesis, UHP, Nancy, 463p.

Timmerman M.J., Daly J.S., 1995. Sm-Nd evidence fro Late Archean crust formation in the Lapland – Kola Mobile Belt, Kola Peninsula, Russia and Norway. Precambrian Res., vol.72, pp. 97-107.

Vetrin V.R., 1984. Geological-geochemical features of the oldest granitoids of the Kola Peninsula. Nature accosiations of the grey Archean gneisses (geology and petrology), Leningrad, pp. 113-123.

Vetrin, V. R., Berezhnaya, N. G. and Rodionov, N. V., 2006, Petrology of Postorogenic Granitoids of the Northern Baltic Shield, Doklady Earth Sciences, 2006, Vol. 411A, No. 9, p. 1476-1479.

Vetrin V.R., Kamensky I.L., Bayanova T.B., Ikorsky S.V., 2000. Mantle component in Litsa-Araguba granitoids on the surface and in the section of Kola Superdeep Borehole: He isotopes in rocks and minerals. Results of Kola Superdeep Borehole section studies to the depth of 12 261 m, Apatity, pp. 5-8.

Vinogradov A.N., Vinogradova G.V., 1984. Evolution of ultrametamorphic and diaphtoric processes and associated U-Th and REE mineralization in the polymetamorphic complex of the Kola gneisses. Metamorphism and metamorphogenous ore formation of the Early Precambrian, Apatity, KSC of RAS, pp. 105-110.

Vrevsky A.B., Doctoral Dissertation in Geology and Mineralogy, St. Petersburg, 2000.

Watson, E. B., Vicenzi, E. P. & Rapp, R. P., 1989. Inclusion/host relations involving accessory minerals in high-grade metamorphic and anatectic rocks. Contributions to Mineralogy and Petrology 101, 220-231.

Watt, G. R. & Harley, S. L., 1993. Accessory phase controls on the geochemistry of crustal melts and restites produced during water-undersaturated partial melting. Contributions to Mineralogy and Petrology 114, 550-55